

# METHODS IN MOLECULAR BIOLOGY™

*Series Editor*  
**John M. Walker**  
School of Life Sciences  
University of Hertfordshire  
Hatfield, Hertfordshire, AL10 9AB, UK

For further volumes:  
<http://www.springer.com/series/7651>



# **Pain Research**

## **Methods and Protocols**

### **Second Edition**

Edited by

**Z. David Luo**

*Department of Anesthesiology & Perioperative Care, School of Medicine,  
University of California Irvine, Irvine, CA, USA;  
Department of Pharmacology, School of Medicine, University of California Irvine,  
Irvine, CA, USA*

*Editor*

Z. David Luo  
Department of Anesthesiology & Perioperative Care  
School of Medicine  
University of California Irvine  
Irvine, CA, USA

*and*

Department of Pharmacology  
School of Medicine  
University of California Irvine  
Irvine, CA, USA

ISSN 1064-3745                      e-ISSN 1940-6029  
ISBN 978-1-61779-560-2              e-ISBN 978-1-61779-561-9  
DOI 10.1007/978-1-61779-561-9  
Springer New York Dordrecht Heidelberg London

Library of Congress Control Number: 2012930385

© Springer Science+Business Media, LLC 2012

All rights reserved. This work may not be translated or copied in whole or in part without the written permission of the publisher (Humana Press, c/o Springer Science+Business Media, LLC, 233 Spring Street, New York, NY 10013, USA), except for brief excerpts in connection with reviews or scholarly analysis. Use in connection with any form of information storage and retrieval, electronic adaptation, computer software, or by similar or dissimilar methodology now known or hereafter developed is forbidden.

The use in this publication of trade names, trademarks, service marks, and similar terms, even if they are not identified as such, is not to be taken as an expression of opinion as to whether or not they are subject to proprietary rights.

Printed on acid-free paper

Humana Press is part of Springer Science+Business Media ([www.springer.com](http://www.springer.com))

---

## **Preface**

Since the first volume of this book was published in 2004, pain research has continued its rapid growth. This is primarily driven by the urgent need for better pain medications in health care. The advancements of medical technology, improvements in medical care, and increased patients' life span make pain research and related drug development high priorities for both the research community and pharmaceutical companies. Rapid development of basic science research tools, such as techniques of fluorometric labeling, genomic and proteomic high-throughput screening, and genetically modified animals, promotes the swift acceleration of pain research to a stage allowing integrated investigations of pain processing mechanisms at the single cell and/or molecule level, and in a spatially and temporally controlled manner. Using multidisciplinary approaches, we can dissect the complicity of the sensory circuits connecting peripheral stimulation to maladaptive changes in the sensory pathways as well as pain perceptions at the central nervous system. While similar pain syndromes from different etiologies may have similar behavioral endpoints, it is now believed that they are derived from distinct maladaptive changes in the sensory pathways that are mediated by unique mechanisms. Investigation of changes in sensory abnormalities thus relies on integrated studies that combine modern technologies with animal models mimicking pain-inducing pathological conditions in patients. Accordingly, it is my desire to assemble this Second Edition with more advanced techniques and animal models that are not made available in the First Edition, but are critical for integrated pain research. These methods and approaches are again written as easy to follow, step-by-step protocols. In combination with the First Edition, this book can be beneficial to novice pain researchers who may not have extensive experiences in the field, or to experienced pain researchers who would like to expand their research in new directions and/or to new mechanisms in different models. It was extremely rewarding and inspiring to learn from readers of the First Edition that the book became a useful handbook in their laboratories. I sincerely hope that this Second Edition will help increase the capacity of your research, and eventually help accelerate the drug discovery process, leading to better pain medications that will benefit our patients and society for decades to come.

Last but not least, I would like to dedicate this book to my lovely wife Jean. Her endless support, unconditional caring, and loving inspiration made this book possible.

*Irvine, CA, USA*

*Z. David Luo*



---

# Contents

<i>Preface</i> . . . . .	<i>v</i>
<i>Contributors</i> . . . . .	<i>ix</i>
1 Advancements in Pain Research. . . . . <i>Z. David Luo</i>	1
2 Genomic Methods for Clinical and Translational Pain Research . . . . . <i>Dan Wang, Hyungsuk Kim, Xiao-Min Wang, and Raymond Dionne</i>	9
3 Two-Dimensional Gel Electrophoresis: Discovering Neuropathic Pain-Associated Synaptic Biomarkers in Spinal Cord Dorsal Horn . . . . . <i>Om V. Singh and Yuan-Xiang Tao</i>	47
4 Whole-Cell Patch-Clamp Recordings on Spinal Cord Slices. . . . . <i>Ping Deng and Zao C. Xu</i>	65
5 Whole-Cell Recording in Isolated Primary Sensory Neurons . . . . . <i>Michael S. Gold</i>	73
6 Indwelling Supradural Catheters for Induction of Facial Allodynia: Surgical Procedures, Application of Inflammatory Stimuli, and Behavioral Testing . . . . . <i>Julie Wieseler, David Sprunger, Amanda Ellis, Steven F. Maier, and Linda R. Watkins</i>	99
7 An Experimental Model of Headache-Related Pain . . . . . <i>Rebecca M. Edelmayr, Michael H. Ossipov, and Frank Porreca</i>	109
8 A Rodent Model of Trigeminal Neuralgia . . . . . <i>David C. Yeomans and Mikhail Klukin</i>	121
9 New Models of Experimental Parotitis and Parotid Gland Distension in Rats . . . . . <i>Akiko Okada-Ogawa, Masamichi Shinoda, Kuniya Honda, and Koichi Iwata</i>	133
10 A Rat Pain Model of Facial Cancer . . . . . <i>Kentaro Ono, Nozomu Harano, Kiyotoshi Inenaga, and Osamu Nakanishi</i>	149
11 Orofacial Pain Models and Behavior Assessment . . . . . <i>Timothy K.Y. Kaan, Peter T. Ohara, and Luc Jasmin</i>	159
12 Unilateral T13 and L1 Dorsal Root Avulsion: Methods for a Novel Model of Central Neuropathic Pain. . . . . <i>Julie Wieseler, Amanda Ellis, Steven F. Maier, Linda R. Watkins, and Scott Falci</i>	171

13 A Lumbosacral Ventral Root Avulsion Injury and Repair Model  
for Studies of Neuropathic Pain in Rats . . . . . 185  
*Leif A. Havton*

14 A Rat Chronic Pain Model of Spinal Cord Contusion Injury . . . . . 195  
*Kelli Sharp, Amin Boroujerdi, Oswald Steward, and Z. David Luo*

15 The Spared Nerve Injury Model of Neuropathic Pain . . . . . 205  
*Marie Pertin, Romain-Daniel Gosselin, and Isabelle Decosterd*

16 A New Rat Pain Model of Thrombus-Induced Ischemia . . . . . 213  
*Jang-Hern Lee*

17 Rat Models of Pancreatitis Pain . . . . . 223  
*Karin N. Westlund and Louis Vera-Portocarrero*

18 The Monosodium Iodoacetate Model of Osteoarthritis  
Pain in the Rat . . . . . 239  
*Cheryl L. Marker and James D. Pomonis*

19 K/BxN Serum Transfer Arthritis as a Model of Inflammatory  
Joint Pain . . . . . 249  
*Christina A. Christianson, Maripat Corr, Tony L. Yaksh,  
and Camilla I. Svensson*

20 A New Rat Model of Bone Cancer Pain . . . . . 261  
*Ruixin Zhang and Lixing Lao*

21 Exposure of the Dorsal Root Ganglion to Pulsed Radiofrequency  
Current in a Neuropathic Pain Model of Peripheral Nerve Injury . . . . . 275  
*Danielle Perret, Doo-Sik Kim, Kang-Wu Li, and Z. David Luo*

*Index* . . . . . 285

---

## Contributors

- AMIN BOROUJERDI • *Department of Pharmacology, School of Medicine, University of California Irvine, Irvine, CA, USA*
- CHRISTINA A. CHRISTIANSON • *Department of Anesthesiology, University of California San Diego, San Diego, CA, USA*
- MARIPAT CORR • *Department of Medicine, University of California San Diego, San Diego, CA, USA*
- ISABELLE DECOSTERD • *Pain Research Unit, Department of Anesthesiology, University Hospital Center, University of Lausanne, Lausanne, Switzerland; Department of Cell Biology and Morphology, University of Lausanne, Lausanne, Switzerland*
- PING DENG • *Department of Anatomy & Cell Biology, Indiana University School of Medicine, Indianapolis, IN, USA*
- RAYMOND DIONNE • *National Institute of Nursing Research, National Institutes of Health, Bethesda, MD, USA*
- REBECCA M. EDELMAYER • *Department of Pharmacology, The University of Arizona, Tucson, AZ, USA*
- AMANDA ELLIS • *Department of Psychology and Neuroscience, University of Colorado at Boulder, Boulder, CO, USA*
- SCOTT FALCI • *Department of Psychology and Neuroscience, University of Colorado at Boulder, Boulder, CO, USA*
- MICHAEL S. GOLD • *Department of Anesthesiology, University of Pittsburgh, Pittsburgh, PA, USA*
- ROMAIN-DANIEL GOSSELIN • *Pain Research Unit, Department of Anesthesiology, University Hospital Center, University of Lausanne, Lausanne, Switzerland; Department of Cell Biology and Morphology, University of Lausanne, Lausanne, Switzerland*
- NOZOMU HARANO • *Department of Control of Physical Function, Kyushu Dental College, Kitakyushu, Fukuoka, Japan*
- LEIF A. HAVTON • *Departments of Anesthesiology & Perioperative Care, School of Medicine, University of California Irvine, Irvine, CA, USA*
- KARIN N. WESTLUND • *Department of Physiology, Chandler Medical Center, University of Kentucky, Lexington, KY, USA*
- KUNIYA HONDA • *Department of Physiology, School of Dentistry, Nihon University, Tokyo, Japan*
- KIYOTOSHI INENAGA • *Department of Biosciences, Kyushu Dental College, Kitakyushu, Fukuoka, Japan*
- KOICHI IWATA • *Department of Physiology, School of Dentistry, Nihon University, Tokyo, Japan*

- LUC JASMIN • *Department of Anatomy, University of California San Francisco, San Francisco, CA, USA; Los Angeles Neurosurgical Institute, Los Angeles, CA, USA*
- TIMOTHY K.Y. KAAH • *Department of Anatomy, University of California San Francisco, San Francisco, CA, USA*
- DOO-SIK KIM • *Department of Anesthesia and Pain Medicine, School of Medicine, Kosin University, Busan, Republic of Korea*
- HYUNGSUK KIM • *National Institute of Nursing Research, National Institutes of Health, Bethesda, MD, USA*
- MIKHAIL KLUKINOV • *Department of Anesthesia, Stanford University School of Medicine, Stanford, CA, USA*
- LIXING LAO • *Center For Integrative Medicine, School of Medicine, University of Maryland, Baltimore, MD, USA*
- JANG-HERN LEE • *Seoul National University, College of Veterinary Medicine and Research Institute for Veterinary Science, Seoul National University, Seoul, Republic of Korea*
- KANG-WU LI • *Department of Anesthesiology & Perioperative Care, School of Medicine, University of California Irvine, Irvine, CA, USA*
- Z. DAVID LUO • *Department of Anesthesiology & Perioperative Care, School of Medicine, University of California Irvine, Irvine, CA, USA; Department of Pharmacology, School of Medicine, University of California Irvine, Irvine, CA, USA*
- STEVEN F. MAIER • *Department of Psychology and Neuroscience, University of Colorado at Boulder, Boulder, CO, USA*
- CHERYL L. MARKER • *Algos Preclinical Services, St. Paul, MN, USA*
- OSAMU NAKANISHI • *Department of Control of Physical Function, Kyushu Dental College, Kitakyushu, Fukuoka, Japan*
- PETER T. OHARA • *Department of Anatomy, University of California San Francisco, San Francisco, CA, USA*
- AKIKO OKADA-OGAWA • *Department of Oral Diagnosis, School of Dentistry, Nihon University, Tokyo, Japan*
- KENTARO ONO • *Department of Biosciences, Kyushu Dental College, Kitakyushu, Fukuoka, Japan*
- MICHAEL H. OSSIPOV • *Department of Pharmacology, The University of Arizona, Tucson, AZ, USA*
- DANIELLE PERRET • *Department of Anesthesiology & Perioperative Care, School of Medicine, University of California Irvine, Irvine, CA, USA; Department of Physical Medicine & Rehabilitation, School of Medicine, University of California Irvine, Irvine, CA, USA*
- MARIE PERTIN • *Pain Research Unit, Department of Anesthesiology, University Hospital Center, University of Lausanne, Lausanne, Switzerland; Department of Cell Biology and Morphology, University of Lausanne, Lausanne, Switzerland*
- JAMES D. POMONIS • *Algos Preclinical Services, St. Paul, MN, USA*
- FRANK PORRECA • *Department of Pharmacology, The University of Arizona, Tucson, AZ, USA*

- KELLI SHARP • *Reeve-Irvine Research Center, School of Medicine,  
University of California Irvine, Irvine, CA, USA*
- MASAMICHI SHINODA • *Department of Physiology, School of Dentistry,  
Nihon University, Tokyo, Japan*
- OM V. SINGH • *Division of Biological and Health Science,  
University of Pittsburgh-Bradford, Pittsburgh, PA, USA*
- DAVID SPRUNGER • *Department of Psychology and Neuroscience,  
University of Colorado at Boulder, Boulder, CO, USA*
- OSWALD STEWARD • *Reeve-Irvine Research Center, School of Medicine,  
University of California Irvine, Irvine, CA, USA*
- CAMILLA I. SVENSSON • *Department of Physiology and Pharmacology,  
Karolinska Institutet, Stockholm, Sweden*
- YUAN-XIANG TAO • *Department of Anesthesiology and Critical Care Medicine,  
Johns Hopkins University School of Medicine, Baltimore, MD, USA*
- LOUIS VERA-PORTOCARRERO • *Neuromodulation Research, Medtronic, Inc.,  
Minneapolis, MN, USA*
- DAN WANG • *National Institute of Nursing Research, National Institutes of Health,  
Bethesda, MD, USA*
- XIAO-MIN WANG • *National Institute of Nursing Research,  
National Institutes of Health, Bethesda, MD, USA*
- LINDA R. WATKINS • *Department of Psychology and Neuroscience,  
University of Colorado at Boulder, Boulder, CO, USA*
- JULIE WIESELER • *Department of Psychology and Neuroscience, University of Colorado  
at Boulder, Boulder, CO, USA*
- ZAO C. XU • *Department of Anatomy & Cell Biology, Indiana University  
School of Medicine, Indianapolis, IN, USA*
- TONY L. YAKSH • *Department of Anesthesiology, University of California San Diego,  
San Diego, CA, USA*
- DAVID C. YEOMANS • *Department of Anesthesia, Stanford University  
School of Medicine, Stanford, CA, USA*
- RUIXIN ZHANG • *Center For Integrative Medicine, School of Medicine,  
University of Maryland, Baltimore, MD, USA*



# Chapter 1

## Advancements in Pain Research

Z. David Luo

**Key words:** Pain research, Mechanisms, Genotype–phenotype associations, Single-nucleotide polymorphisms, Genetically modified animals, Animal models

After the publication of the First Edition of this book in the series of *Methods in Molecular Medicine* (volume 99 in the series) in 2004, pain research continues its rapid acceleration until 2009, during which it experienced a plateau of growth that likely resulted from the economic downturn started in 2008 (Fig. 1). This rapid growth in pain research could be the driving force for an impressive 66% increase in new randomized, double-blind, placebo-control trials for neuropathic pain medications in the past 5 years compared with the last four decades. Unfortunately, little improvement in pain medications has been obtained (1) due to primarily our limited understanding of mechanisms mediating different pain states, especially that for chronic pain. It is highly possible that the growth in pain research will continue for decades to come due to three main reasons. First, there is an urgent need for more efficacious and safer pain medications that are necessary for better and individualized pain management. The increase in life expectancy of the general population and patients due to improvements in quality of health care and medicine is likely to increase the demand for better pain medications for improving the quality of daily life of those living with pain. It is estimated that the continuous increase in percentage of patients suffering from chronic pain (pain conditions lasting more than 6 months) arranges from 11 to 47% between 40 and 75 years of age (2), which will inevitably and continually increase the demand for better pain medications. Second, the cost of pain conditions to our society is high, estimated \$55 billion per year in loss of productivity from full-time workers alone (3), so better pain management can significantly help economic growth and stability. Third, the swift advancement in technologies and our better understanding of sensory circuitries and pain pathways serves as a driving force for timely

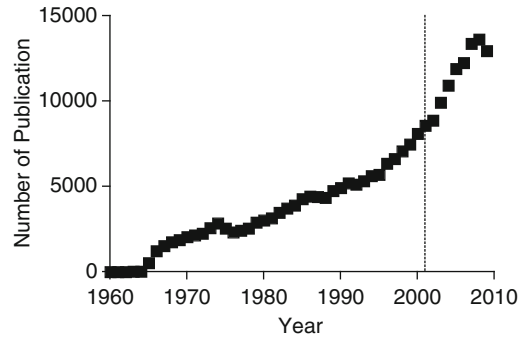


Fig. 1. Numbers of annual publications related to pain research from the last 50 years that were retrieved from PubMed using the keyword: pain. *Dotted line* indicates the time when similar data collection was performed for the First Edition of this book.

drug discovery research and development at an unprecedented pace to meet the demand for better pain medications.

One of the technologies that can speed up the discovery process in pain research is high-throughput screening, which can be accomplished at the genomic DNA, mRNA, or protein level. At the genomic DNA level, high-throughput screening technologies allow the identification of genetic variants that may mediate individual susceptibilities in pain development and sensitivities to pain medications, which can provide the genetic basis necessary for the development of individualized pain medications and management strategies. In addition, this approach allows the rapid transformation of basic research findings on target gene discovery to translational research by screening associations of pain phenotypes with human genetic variants that are associated with, and likely play important roles, in pain susceptibility and analgesic sensitivity. Using the approach of genotype–phenotype associations with single-nucleotide polymorphisms (SNP) in human volunteers, Neely et al. (4) have identified that the calcium channel alpha-2-delta-3 gene (*CACN-A2D3*) is associated with acute and chronic pain states in humans. Similar approaches have been used recently to identify SNP association with analgesic onset in oral surgery patients (5), opioid sensitivity in orofacial surgery patients (6), opioid usage in cancer pain patients (7), high pain sensitivity in chronic pain patients (8), breast cancer patients (9), and health volunteers (10). Several genetic loci are also identified through these approaches to play critical roles in migraine (11).

At the mRNA level, high-throughput screening using microarrays to detect global gene expression changes associated with pain-inducing conditions can lead to a rapid identification of candidate genes that may serve as potential targets for new drug development after validation. A recent review has summarized this discovery approach for identifying potential target genes that may play critical roles in pain transduction and mediating analgesic sensitivities (12).

Examples of these genes include, but are not limited to, the gene encoding the calcium channel alpha-2-delta-1 subunit protein (CACNA2D1) that has been shown to undergo upregulation in the sensory neurons and dorsal spinal cord post injuries in the central and peripheral nervous systems, which in turn plays a critical role in neuropathic pain initiation and maintenance (13–23); the gene encoding the alpha subunit of potassium channels (KCNS1), which is involved in sensory neuron excitability regulation and downregulated after peripheral nerve injuries (8); the gene encoding glial fibrillary acidic protein, a marker for injury-induced activation of astrocytes, that is upregulated in dorsal root ganglia and dorsal spinal cord post peripheral nerve injury and involved in maintenance of neuropathic pain (14); and genes encoding proteins related to inflammatory pain (24–26).

The application of these technologies and limitations associated with these technologies in pain research (12, 27) are described in details in Chapter 2 of this book. One of the potential pitfalls is that changes at the DNA/mRNA levels may not be always translated to similar changes in expression of encoded proteins that are ultimately the functional entities carrying out pathophysiological functions of genes. A complementary approach to this limitation is to apply proteomics to detect changes at the protein level under pain-inducing conditions.

Based on the strategy of detection, this approach can be used to detect changes of protein expression and post-translational modifications in experimental samples. Two detection methods can be utilized in this approach: Labeled-Probe or Label-Free methods (28). The Labeled-Probe method is mainly using labeled probes to detect immobilized targets, even though variations in detection methods are developed. These include (a) forward phase or antibody array using immobilized antibody to detect levels of labeled proteins, (b) reverse-phase or direct capture array using labeled antibody to detect levels of immobilized proteins, (c) Sandwich array capturing proteins of interest with immobilized antibodies followed by labeled secondary antibody detection of the captured proteins. For technical details, pros and cons of these detection methods, the reader is referred to a review article by Espina et al. (29). The Label-Free method includes (a) mass spectrometry, (b) surface plasmon resonance imaging, and (c) atomic force microscopy. Chapter 3 of this book describes in detail a method combining mass spectrometry with two-dimensional gel electrophoresis to identify changes in expression of proteins in dorsal spinal cord in a neuropathic pain model. In recent years, these approaches have been used to identify potential pain mediators/modulators that may play critical roles in pain processing, and serve as candidate targets for the development of pain medications (29–34).

Upon identification of dysregulated candidate genes/proteins under pain-inducing pathological conditions, functional validations

on whether changes in expression/modification of these genes/proteins contribute to sensory hyperexcitability and/or analgesic sensitivity is extremely critical because it is highly unlikely that all identified dysregulated-genes are mediators of pain processing. In this regard, electrophysiology recording for changes in pathophysiological activity/excitability of sensory neurons, spinal and supraspinal neurons, and sensory circuitries is widely used in combination with pharmacology and genetically modified animal approaches in mechanistic studies and target gene–protein validations. Based on the nature of questions that need to be addressed, electrophysiology studies can be performed at multiple levels, including (a) projection neurons or interneurons in spinal cord and supraspinal cord regions of anesthetized animals, (b) acutely isolated sensory fibers in anesthetized animals, (c) projection neurons or interneurons in slices of spinal cord or supraspinal cord regions, (d) cultured or acutely isolated sensory neurons. The methods, strengths, and limitations in detail for the last two approaches in pain research are included in Chapters 4 and 5, respectively, in this Edition that are complementary to the methods detailed for the first two approaches published in the First Edition of this book. Recently identified pain candidate targets and sensory circuits using electrophysiology recording in combination of other approaches include, but are not limited to, kainate receptors (35), calcium-stimulated adenylyl cyclase 1 (36), protein kinase M zeta (37), spinal cord NMDA-2B receptor (38). The recent development of automated-patch clamp systems made high-throughput electrophysiological recording feasible (39).

The final validation step in preclinical pain drug discovery relies on studies performed in animal models. In addition, since pain is a complex, multimechanism disorder, different mechanisms may underlie common pain states deriving from different pathological conditions. In this regard, it is hard to imagine that a single “magic drug” could be used some day to manage pain states induced by different disorders. Thus, understanding unique mechanisms mediating pain states from different etiologies becomes critical for the development of new pain medications and individualized pain management. To accomplish this task, pain researchers have recently developed various animal models mimicking pain-inducing pathological conditions that can be useful for studying pathways and mechanisms mediating unique pain states, and for validating new mechanism-based pain medications. For this reason, a large variety of newly developed rodent models mimicking behavioral hypersensitivity in human chronic pain disorders, such as headache-related pain, orofacial cancer, inflammatory and neuropathic pain, spinal cord injury-induced central pain, bone cancer pain, visceral pain with different origins, peripheral nerve injury and arthritis pain, are included in this volume. These animal models can also be used to validate procedures relevant to clinical pain management (40). One example of these studies is outlined in Chapter 21 of this book.

The power of target/pathway detection and validation in animal models can be further amplified by generating animal models with genetically modified mice, including (a) mice with fluorescently labeled target gene expression; and (b) mice with knock-in or knockout expression of the genes of interest. The former allows pain researchers to trace the expression and localization of potential target genes, label pathways and circuitry connections that are critical in pain processing. Recent discovery and characterization of pain circuits using this approach include those transmitting pain signals carried by nonpeptidergic nociceptors (41), by myelinated and unmyelinated sensory neurons (42), by a subset of nonnociceptive, myelinated primary afferents and PKC- $\gamma$  interneurons (43), and by serotonergic descending modulation pathways (44). The latter allows validation of contributory roles of genes/proteins of interest in pain processing and analgesic sensitivity. Recent identification and/or validation of potential mediators/modulators for pain processing/analgesic sensitivity using this approach include the calcium channel alpha-2-delta-1 subunit protein (45), the glial fibrillary acidic protein (14), the vasopressin-1A receptor (46), Ecto-5'-nucleotidase (47), sigma-1 receptor (48), acid-sensing ion channels 3 (49, 50) and transient receptor potential vanilloid 1 receptor (49, 51–53), and cannabinoid-CB<sub>1</sub> receptor (54).

In conclusion, the increasing demand for better pain medications and rapid advancement in research tools will drive the advancement in pain research and drug development toward a more mechanism-orientated and target-specific direction. This will in turn promote individualized pain management for improving the quality of daily life of those suffering from pain. Hopefully, the methods described in detail in this book will provide technical assistance for the acceleration of this process.

---

## Acknowledgments

Supported in part by grants from the National Institutes of Health (DE019298, NS064341) (Z.D. Luo).

## References

1. Finnerup, N. B., Sindrup, S. H., and Jensen, T. S. (2010) The evidence for pharmacological treatment of neuropathic pain. *Pain* 150, 573–81.
2. Kopf, A. (2010) Pain in Old Age and Dementia, in *Guide to Pain Management in Low-Resource Settings* (Kopf, A., and Patel, N. B., Eds.), pp 269–75, International Association for the Study of Pain, Seattle.
3. Katz, N. (2002) The impact of pain management on quality of life. *J Pain Symptom Manage* 24, S38–47.
4. Neely, G. G., Hess, A., Costigan, M., Keene, A. C., Goulas, S., Langeslag, M., Griffin, R. S., Belfer, I., Dai, F., Smith, S. B., Diatchenko, L., Gupta, V., Xia, C. P., Amann, S., Kreitz, S., Heindl-Erdmann, C., Wolz, S., Ly, C. V., Arora, S., Sarangi, R., Dan, D., Novatchkova,

- M., Rosenzweig, M., Gibson, D. G., Truong, D., Schramek, D., Zoranovic, T., Cronin, S. J., Angjeli, B., Brune, K., Dietzl, G., Maixner, W., Meixner, A., Thomas, W., Pospisilik, J. A., Alenius, M., Kress, M., Subramaniam, S., Garrity, P. A., Bellen, H. J., Woolf, C. J., and Penninger, J. M. (2010) A genome-wide Drosophila screen for heat nociception identifies alpha2delta3 as an evolutionarily conserved pain gene. *Cell* **143**, 628–38.
5. Kim, H., Ramsay, E., Lee, H., Wahl, S., and Dionne, R. A. (2009) Genome-wide association study of acute post-surgical pain in humans. *Pharmacogenomics* **10**, 171–9.
  6. Fukuda, K., Hayashida, M., Ide, S., Saita, N., Kokita, Y., Kasai, S., Nishizawa, D., Ogai, Y., Hasegawa, J., Nagashima, M., Tagami, M., Komatsu, H., Sora, I., Koga, H., Kaneko, Y., and Ikeda, K. (2009) Association between OPRM1 gene polymorphisms and fentanyl sensitivity in patients undergoing painful cosmetic surgery. *Pain* **147**, 194–201.
  7. Lotsch, J., Klepstad, P., Doehring, A., and Dale, O. (2010) A GTP cyclohydrolase 1 genetic variant delays cancer pain. *Pain* **148**, 103–6.
  8. Costigan, M., Belfer, I., Griffin, R. S., Dai, F., Barrett, L. B., Coppola, G., Wu, T., Kiselycznyk, C., Poddar, M., Lu, Y., Diatchenko, L., Smith, S., Cobos, E. J., Zaykin, D., Allchorne, A., Shen, P. H., Nikolajsen, L., Karppinen, J., Mannikko, M., Kelempisioti, A., Goldman, D., Maixner, W., Geschwind, D. H., Max, M. B., Seltzer, Z., and Woolf, C. J. (2010) Multiple chronic pain states are associated with a common amino acid-changing allele in KCNS1. *Brain* **133**, 2519–27.
  9. Nissenbaum, J., Devor, M., Seltzer, Z., Gebauer, M., Michaelis, M., Tal, M., Dorfman, R., Abitbul-Yarkoni, M., Lu, Y., Elahipanah, T., delCanho, S., Minert, A., Fried, K., Persson, A. K., Shpigler, H., Shabo, E., Yakir, B., Pisante, A., and Darvasi, A. (2010) Susceptibility to chronic pain following nerve injury is genetically affected by CACNG2. *Genome Res* **20**, 1180–90.
  10. Treister, R., Pud, D., Ebstein, R. P., Laiba, E., Gershon, E., Haddad, M., and Eisenberg, E. (2009) Associations between polymorphisms in dopamine neurotransmitter pathway genes and pain response in healthy humans. *Pain* **147**, 187–93.
  11. Estevez, M., and Gardner, K. L. (2004) Update on the genetics of migraine. *Hum Genet* **114**, 225–35.
  12. Luo, Z. D., and Figueroa, K. W. (2008) Multilevel genomic approach in pain research: basic science and clinical implications. *Rev. Analg.* **10**, 45–58.
  13. Wang, H., Sun, H., Della Penna, K., Benz, R. J., Xu, J., Gerhold, D. L., Holder, D. J., and Koblan, K. S. (2002) Chronic neuropathic pain is accompanied by global changes in gene expression and shares pathobiology with neurodegenerative diseases. *Neuroscience* **114**, 529–46.
  14. Kim, D. S., Figueroa, K. W., Li, K. W., Boroujerdi, A., Yolo, T., and David Luo, Z. (2009) Profiling of dynamically changed gene expression in dorsal root ganglia post peripheral nerve injury and a critical role of injury-induced glial fibrillary acidic protein in maintenance of pain behaviors [corrected]. *Pain* **143**, 114–22.
  15. Costigan, M., Befort, K., Karchewski, L., Griffin, R. S., D'Urso, D., Allchorne, A., Sitarski, J., Mannion, J. W., Pratt, R. E., and Woolf, C. J. (2002) Replicate high-density rat genome oligonucleotide microarrays reveal hundreds of regulated genes in the dorsal root ganglion after peripheral nerve injury. *BMC Neurosci* **3**, 16. Print 2002 Oct 25.
  16. Bauer, C. S., Nieto-Rostro, M., Rahman, W., Tran-Van-Minh, A., Ferron, L., Douglas, L., Kadurin, I., Sri Ranjan, Y., Fernandez-Alacid, L., Millar, N. S., Dickenson, A. H., Lujan, R., and Dolphin, A. C. (2009) The increased trafficking of the calcium channel subunit alpha2delta-1 to presynaptic terminals in neuropathic pain is inhibited by the alpha2delta ligand pregabalin. *J Neurosci* **29**, 4076–88.
  17. Boroujerdi, A., Kim, H. K., Lyu, Y. S., Kim, D. S., Figueroa, K. W., Chung, J. M., and Luo, Z. D. (2008) Injury discharges regulate calcium channel alpha-2-delta-1 subunit upregulation in the dorsal horn that contributes to initiation of neuropathic pain. *Pain* **139**, 358–66.
  18. Boroujerdi, A., Zeng, J., Sharp, K., Kim, D., Steward, O., and Luo, Z. D. (2011) Calcium channel alpha-2-delta-1 protein upregulation in dorsal spinal cord mediates spinal cord injury induced neuropathic pain states. *Pain* **152**, 649–55.
  19. Li, C. Y., Song, Y. H., Higuera, E. S., and Luo, Z. D. (2004) Spinal dorsal horn calcium channel alpha2delta-1 subunit upregulation contributes to peripheral nerve injury-induced tactile allodynia. *J Neurosci* **24**, 8494–9.
  20. Luo, Z. D., Calcutt, N. A., Higuera, E. S., Valder, C. R., Song, Y. H., Svensson, C. I., and Myers, R. R. (2002) Injury type-specific calcium channel alpha 2 delta-1 subunit up-regulation in rat neuropathic pain models correlates with antiallodynic effects of gabapentin. *J Pharmacol Exp Ther* **303**, 1199–205.
  21. Luo, Z. D., Chaplan, S. R., Higuera, E. S., Sorkin, L. S., Stauderman, K. A., Williams, M.

- E., and Yaksh, T. L. (2001) Upregulation of dorsal root ganglion (alpha)2(delta) calcium channel subunit and its correlation with allodynia in spinal nerve-injured rats. *J. Neurosci.* **21**, 1868–75.
22. Newton, R. A., Bingham, S., Case, P. C., Sanger, G. J., and Lawson, S. N. (2001) Dorsal root ganglion neurons show increased expression of the calcium channel alpha2delta-1 subunit following partial sciatic nerve injury. *Brain Res Mol Brain Res* **95**, 1–8.
  23. Valder, C. R., Liu, J. J., Song, Y. H., and Luo, Z. D. (2003) Coupling gene chip analyses and rat genetic variances in identifying potential target genes that may contribute to neuropathic allodynia development. *J Neurochem* **87**, 560–73.
  24. Wang, X. M., Wu, T. X., Hamza, M., Ramsay, E. S., Wahl, S. M., and Dionne, R. A. (2007) Rofecoxib modulates multiple gene expression pathways in a clinical model of acute inflammatory pain. *Pain* **128**, 136–47.
  25. Wang, X. M., Hamza, M., Gordon, S. M., Wahl, S. M., and Dionne, R. A. (2008) COX inhibitors downregulate PDE4D expression in a clinical model of inflammatory pain. *Clin Pharmacol Ther* **84**, 39–42.
  26. Wang, X. M., Hamza, M., Wu, T. X., and Dionne, R. A. (2009) Upregulation of IL-6, IL-8 and CCL2 gene expression after acute inflammation: Correlation to clinical pain. *Pain* **142**, 275–83.
  27. Kim, H., Clark, D., and Dionne, R. A. (2009) Genetic contributions to clinical pain and analgesia: avoiding pitfalls in genetic research. *J Pain* **10**, 663–93.
  28. Espina, V., Woodhouse, E. C., Wulfkuhle, J., Asmussen, H. D., Petricoin, E. F., 3rd, and Liotta, L. A. (2004) Protein microarray detection strategies: focus on direct detection technologies. *J Immunol Methods* **290**, 121–33.
  29. Sandoz, G., Thummler, S., Duprat, F., Feliciangeli, S., Vinh, J., Escoubas, P., Guy, N., Lazdunski, M., and Lesage, F. (2006) AKAP150, a switch to convert mechano-, pH- and arachidonic acid-sensitive TREK K(+) channels into open leak channels. *Embo J* **25**, 5864–72.
  30. Sung, H. J., Kim, Y. S., Kim, I. S., Jang, S. W., Kim, Y. R., Na, D. S., Han, K. H., Hwang, B. G., Park, D. S., and Ko, J. (2004) Proteomic analysis of differential protein expression in neuropathic pain and electroacupuncture treatment models. *Proteomics* **4**, 2805–13.
  31. Kunz, S., Tegeder, I., Coste, O., Marian, C., Pfenninger, A., Corvey, C., Karas, M., Geisslinger, G., and Niederberger, E. (2005) Comparative proteomic analysis of the rat spinal cord in inflammatory and neuropathic pain models. *Neurosci Lett* **381**, 289–93.
  32. Park, S., and Lee, J. (2009) Proteomic analysis to identify early molecular targets of pregabalin in C6 glial cells. *Cell Biol Int* **34**, 27–33.
  33. Riedl, M. S., Braun, P. D., Kitto, K. F., Roiko, S. A., Anderson, L. B., Honda, C. N., Fairbanks, C. A., and Vulchanova, L. (2009) Proteomic analysis uncovers novel actions of the neurosecretory protein VGF in nociceptive processing. *J Neurosci* **29**, 13377–88.
  34. Singh, O. V., Yaster, M., Xu, J. T., Guan, Y., Guan, X., Dharmarajan, A. M., Raja, S. N., Zeitlin, P. L., and Tao, Y. X. (2009) Proteome of synaptosome-associated proteins in spinal cord dorsal horn after peripheral nerve injury. *Proteomics* **9**, 1241–53.
  35. Wu, L. J., Ko, S. W., and Zhuo, M. (2007) Kainate receptors and pain: from dorsal root ganglion to the anterior cingulate cortex. *Curr Pharm Des* **13**, 1597–605.
  36. Xu, H., Wu, L. J., Wang, H., Zhang, X., Vadakkan, K. I., Kim, S. S., Steenland, H. W., and Zhuo, M. (2008) Presynaptic and postsynaptic amplifications of neuropathic pain in the anterior cingulate cortex. *J Neurosci* **28**, 7445–53.
  37. Li, X. Y., Ko, H. G., Chen, T., Descalzi, G., Koga, K., Wang, H., Kim, S. S., Shang, Y., Kwak, C., Park, S. W., Shim, J., Lee, K., Collingridge, G. L., Kaang, B. K., and Zhuo, M. (2010) Alleviating neuropathic pain hypersensitivity by inhibiting PKMzeta in the anterior cingulate cortex. *Science* **330**, 1400–4.
  38. Qu, X. X., Cai, J., Li, M. J., Chi, Y. N., Liao, F. F., Liu, F. Y., Wan, Y., Han, J. S., and Xing, G. G. (2009) Role of the spinal cord NR2B-containing NMDA receptors in the development of neuropathic pain. *Exp Neurol* **215**, 298–307.
  39. Sunesen, M., and Jacobsen, R. B. (2011) Study of TRP Channels by Automated Patch Clamp Systems. *Adv Exp Med Biol* **704**, 107–23.
  40. Perret, D. M., Kim, D.-S., Li, K.-W., Sinavsky, K., Newcomb, R. L., Miller, J. M., and Luo, Z. D. (2011) Application of Pulsed Radiofrequency Currents to Rat Dorsal Root Ganglia Modulates Nerve Injury-Induced Tactile Allodynia. *Anesthesia & Analgesia* **113**, 610–6.
  41. Braz, J. M., Nassar, M. A., Wood, J. N., and Basbaum, A. I. (2005) Parallel “pain” pathways arise from subpopulations of primary afferent nociceptor. *Neuron* **47**, 787–93.
  42. Braz, J. M., and Basbaum, A. I. (2009) Triggering genetically-expressed transneuronal tracers by peripheral axotomy reveals convergent

- and segregated sensory neuron-spinal cord connectivity. *Neuroscience* **163**, 1220–32.
43. Neumann, S., Braz, J. M., Skinner, K., Llewellyn-Smith, I. J., and Basbaum, A. I. (2008) Innocuous, not noxious, input activates PKC $\gamma$  interneurons of the spinal dorsal horn via myelinated afferent fibers. *J Neurosci* **28**, 7936–44.
  44. Braz, J. M., and Basbaum, A. I. (2008) Genetically expressed transneuronal tracer reveals direct and indirect serotonergic descending control circuits. *J Comp Neurol* **507**, 1990–2003.
  45. Li, C. Y., Zhang, X. L., Matthews, E. A., Li, K. W., Kurwa, A., Boroujerdi, A., Gross, J., Gold, M. S., Dickenson, A. H., Feng, G., and Luo, Z. D. (2006) Calcium channel  $\alpha_2\delta_1$  subunit mediates spinal hyperexcitability in pain modulation. *Pain* **125**, 20–34.
  46. Schorscher-Petcu, A., Sotocinal, S., Ciura, S., Dupre, A., Ritchie, J., Sorge, R. E., Crawley, J. N., Hu, S. B., Nishimori, K., Young, L. J., Tribollet, E., Quirion, R., and Mogil, J. S. (2010) Oxytocin-induced analgesia and scratching are mediated by the vasopressin-1A receptor in the mouse. *J Neurosci* **30**, 8274–84.
  47. Sowa, N. A., Taylor-Blake, B., and Zylka, M. J. (2010) Ecto-5'-nucleotidase (CD73) inhibits nociception by hydrolyzing AMP to adenosine in nociceptive circuits. *J Neurosci* **30**, 2235–44.
  48. Diaz, J. L., Zamanillo, D., Corbera, J., Baeyens, J. M., Maldonado, R., Pericas, M. A., Vela, J. M., and Torrens, A. (2009) Selective sigma-1 ( $\sigma_1$ ) receptor antagonists: emerging target for the treatment of neuropathic pain. *Cent Nerv Syst Agents Med Chem* **9**, 172–83.
  49. Jones, R. C., 3rd, Xu, L., and Gebhart, G. F. (2005) The mechanosensitivity of mouse colon afferent fibers and their sensitization by inflammatory mediators require transient receptor potential vanilloid 1 and acid-sensing ion channel 3. *J Neurosci* **25**, 10981–9.
  50. Yuan, F. L., Chen, F. H., Lu, W. G., and Li, X. (2009) Acid-sensing ion channels 3: a potential therapeutic target for pain treatment in arthritis. *Mol Biol Rep* **37**, 3233–8.
  51. Vardanyan, A., Wang, R., Vanderah, T. W., Ossipov, M. H., Lai, J., Porreca, F., and King, T. (2009) TRPV1 receptor in expression of opioid-induced hyperalgesia. *J Pain* **10**, 243–52.
  52. Wang, Z. Y., Wang, P., Merriam, F. V., and Bjorling, D. E. (2008) Lack of TRPV1 inhibits cystitis-induced increased mechanical sensitivity in mice. *Pain* **139**, 158–67.
  53. Kim, H. Y., Kim, K., Li, H. Y., Chung, G., Park, C. K., Kim, J. S., Jung, S. J., Lee, M. K., Ahn, D. K., Hwang, S. J., Kang, Y., Binshtok, A. M., Bean, B. P., Woolf, C. J., and Oh, S. B. (2010) Selectively targeting pain in the trigeminal system. *Pain* **150**, 29–40.
  54. Fioravanti, B., De Felice, M., Stucky, C. L., Medler, K. A., Luo, M. C., Gardell, L. R., Ibrahim, M., Malan, T. P., Jr., Yamamura, H. I., Ossipov, M. H., King, T., Lai, J., Porreca, F., and Vanderah, T. W. (2008) Constitutive activity at the cannabinoid CB1 receptor is required for behavioral response to noxious chemical stimulation of TRPV1: antinociceptive actions of CB1 inverse agonists. *J Neurosci* **28**, 11593–602.

## Genomic Methods for Clinical and Translational Pain Research

Dan Wang, Hyungsuk Kim, Xiao-Min Wang, and Raymond Dionne

### Abstract

Pain is a complex sensory experience for which the molecular mechanisms are yet to be fully elucidated. Individual differences in pain sensitivity are mediated by a complex network of multiple gene polymorphisms, physiological and psychological processes, and environmental factors. Here, we present the methods for applying unbiased molecular-genetic approaches, genome-wide association study (GWAS), and global gene expression analysis, to help better understand the molecular basis of pain sensitivity in humans and variable responses to analgesic drugs.

**Key words:** Pain, Genome-wide association study, Single nucleotide polymorphism, Whole-genome sampling analysis, Copy number variation, Global gene expression analysis, Microarray

---

### 1. Introduction

Human pain sensitivity varies widely among different individuals. Understanding the genetic contribution to molecular processes that contribute to variation in pain is critical for elucidating the mechanism of variable responses to analgesic drugs and may contribute to better prevention, medical diagnosis, and individualized treatment. Candidate gene studies have identified several genetic variations that produce interindividual difference in pain sensitivity and analgesic drug responses (1–8). However, like many other “hypothesis-driven” genetic approaches, the significant findings are sometimes difficult to replicate when followed up in subsequent association studies (9–11). This is not surprising considering our imperfect understating of the complexity of pain biology and the size of human genome. Inconsistent outcomes are often caused by

variable study designs, sample heterogeneity, small samples sizes, phenotype complexity, and alternative statistical approaches. Therefore, it is critical to use appropriate methodologies to gain insight into genetic mechanisms of pain and eventually to apply this knowledge to pain treatment.

Genome-wide association studies (GWAS) catalog human genetic variation and correlate it with phenotypic difference by scanning millions of single nucleotide polymorphism (SNP) across the whole genome, and overcome the limitation of candidate gene association studies. GWAS published to date use various commercial genotyping platforms to assess differences in allele frequencies between cases and controls. Though rare variants are often overlooked, GWAS have successfully uncovered hundreds of genetic loci associated with many common diseases, such as obesity (12), diabetes (13), rheumatoid arthritis (14), and Crohn's disease (15). Our recent report (16) suggests that GWAS are also powerful and unbiased for identifying novel genes implicated in a complex phenotype such as pain and responses to analgesic drugs.

Comprehensive analysis of global gene expression using DNA microarray is another hypothesis-free method to identify disease-related genetic variations and has become a widespread technology in genomics research. Thousands of transcripts can be assayed simultaneously, therefore providing data on a large and unbiased set of traits (17). Over the past few years, we have successfully applied this method to the field of clinical pain research and identified genes with dynamic changes in expression that appear to be functionally associated with acute inflammatory pain and inflammation (18–21).

While these powerful methods hold great promise for elucidating novel targets for intervention and may provide greater understanding of the molecular-genetic pathways associated with pain, inflammation and the transition for acute to chronic pain, they are fraught with significant pitfalls in their application to clinical and translational research. In Subheading 4, we suggest a systematic approach to reporting important variables associated with conducting genetic studies in humans that permit evaluation of the strength of the findings based on considerations considered axiomatic since the adoption of the Consolidated Standards of Reporting Trials (CONSORT) recommendations for reporting the results of clinical trials.

---

## 2. Materials

### 2.1. Genome-Wide Association Study

#### 2.1.1. Genomic DNA Preparation

1. Reduced EDTA TE buffer (10 mM Tris-HCL, 0.1 mM EDTA, pH 8.0, TEKnova), stored at room temperature.
2. AccuGENE water, molecular biology grade (Cambrex), kept at 4°C.

3. Purified genomic DNA, stored at  $-20^{\circ}\text{C}$ .
4. Reference Genomic DNA 103, included in Affymetrix Genome-Wide Human SNP Nsp/Sty Assay kit 5.0/6.0 (kit 1, see Note 1).

*2.1.2. Sty Restriction  
Enzyme Digestion,  
Ligation, and PCR*

1. Sty I (10 U/ $\mu\text{l}$ ), NE Buffer 3 (10 $\times$ ), and BSA (100 $\times$ ; 10 mg/ml) from New England Biolabs (NEB), stored at  $-20^{\circ}\text{C}$ .
2. T4 DNA Ligase (400 U/ $\mu\text{l}$ ) and T4 DNA Ligase Buffer (10 $\times$ ) from NEB, stored  $-20^{\circ}\text{C}$  (see Note 2).
3. Adaptor, Sty (50  $\mu\text{M}$ ) and PCR primer 002 (100  $\mu\text{M}$ ) included in kit 1, stored at  $-20^{\circ}\text{C}$ .
4. Clontech TITANIUM DNA Amplification kit (kit 2) stored at  $-20^{\circ}\text{C}$ :
  - dNTPs (2.5 mM each).
  - GC-Melt (5 M).
  - TITANIUM™ Taq DNA Polymerase (50 $\times$ ).
  - TITANIUM™ Taq PCR Buffer (10 $\times$ ).
5. All Purpose Hi-Lo DNA Marker (Bionexus), stored at room temperature.
6. Gel, Reliant® Gel System, precast agarose gel (2% Seakem Gold, TBE, Cambrex), stored at room temperature (see Note 3).
7. Gel Loading Buffer, 2 $\times$  (Sigma-Aldrich), stored at room temperature.
8. Cooling chambers, single and double gold block (Diversified Biotech).
9. Thermal cyclers (pre-PCR lab and main lab).

*2.1.3. Nsp Restriction  
Enzyme Digestion,  
Ligation, and PCR*

1. Nsp I (10 U/ $\mu\text{l}$ ), NE Buffer 2 (10 $\times$ ), and BSA (100 $\times$ ; 10 mg/ml) from NEB, stored at  $-20^{\circ}\text{C}$ .
2. Adaptor, Nsp I (50  $\mu\text{M}$ ), included in kit 1 and stored at  $-20^{\circ}\text{C}$ .

*2.1.4. PCR Product  
Pooling, Purification,  
and Quantitation*

1. 75% Ethanol (ACS grade ethanol diluted to 75% using AccuGENE water), kept at room temperature.
2. Elution Buffer (Buffer EB, Qiagen), kept at room temperature.
3. Magnetic Beads (Agencourt), kept at  $4^{\circ}\text{C}$ .
4. Deep-Well Storage Plate, 2.4 ml (pooling plate) (E&K Scientific).
5. Plate holders (USA Scientific).
6. Jitterbug Microplate Incubator Shaker.
7. Vacuum Manifold, MultiScreenHTS (Millipore).
8. Plate, 2 ml, 96-Well Format Filterplate (PES 0.45  $\mu\text{m}$ ), Hydrophilic, Long Drip Director (E&K Scientific).

9. Elution catch plate, 96-well, conical bottom.
10. Spectrophotometer, high-throughput microplate spectrophotometer or NanoDrop.

#### *2.1.5. Fragmentation and Labeling*

1. Fragmentation Buffer (10×) and Fragmentation Reagent (DNase I), included in kit 1, and stored at  $-20^{\circ}\text{C}$ .
2. DNA labeling Reagent (30 mM), Terminal Deoxynucleotidyl Transferase (TdT; 30 U/ $\mu\text{l}$ ) and Terminal Deoxynucleotidyl Transferase Buffer (TdT Buffer; 5×), included in kit 1 and stored at  $-20^{\circ}\text{C}$ .
3. 4% NuSieve 3:1 Plus gel (Cambrex).

#### *2.1.6. Target Hybridization*

1. Denhardt's Solution (50×) (Sigma-Aldrich), stored at  $-20^{\circ}\text{C}$ .
2. DMSO (100%), stored at room temperature in dark area. Toxic, handle with care.
3. EDTA (0.5 M), stored at room temperature.
4. Herring Sperm DNA (HSDNA; 10 mg/ml, Promega), stored at  $-20^{\circ}\text{C}$ .
5. Human Cot-1 DNA (1 mg/ml) (Invitrogen), stored at  $-20^{\circ}\text{C}$ .
6. 12× MES Stock solution (1 L): 70.4 g of MES hydrate (Sigma-Aldrich), 193.3 g MES sodium salt (Sigma-Aldrich) dissolved in AccuGENE water, pH 6.5–6.7, filter-sterilized, and stored at  $4^{\circ}\text{C}$ .
7. Tetramethylammonium Chloride (TMACL; 5 M, Sigma-Aldrich), stored at room temperature. Toxic, handle with care.
8. Tween-20, 10%, stored at room temperature.
9. Oligo Control Reagent (OCR), 0100, included in kit 1 and stored at  $-20^{\circ}\text{C}$ .
10. Genome-Wide Human SNP Array 6.0 (Affymetrix), stored at  $4^{\circ}\text{C}$ .
11. GeneChip Hybridization Oven 640 (Affymetrix).
12. Tough-Spots (1/2 and 3/8 in.).

#### *2.1.7. Washing, Staining, and Scanning Arrays*

1. 20× SSPE (3 M NaCl, 0.2 M  $\text{NaH}_2\text{PO}_4$ , 0.02 M EDTA; Cambrex).
2. Wash A (Nonstringent Wash Buffer): for 1 L, mix 300 ml of 20× SSPE, 1.0 ml 10% Tween-20 and 699 ml of water, filtered through a 0.2- $\mu\text{m}$  filter and stored at room temperature.
3. Wash B (Stringent Wash Buffer): for 1 L, mix 30 ml of 20× SSPE, 1.0 ml of 10% Tween-20, and 969 ml of water, filtered through a 0.2- $\mu\text{m}$  filter and stored at room temperature.

4. Stain Buffer: Add 360  $\mu\text{l}$  of 20 $\times$  SSPE, 3.96  $\mu\text{l}$  of Tween-20 (3%), and 24  $\mu\text{l}$  of Denhardt's Solution (50 $\times$ ) to 800.04  $\mu\text{l}$  of  $\text{H}_2\text{O}$  to make 1,188  $\mu\text{l}$  of stain solution. Prepare the solution right before use.
5. SAPE stain solution: Remove Streptavidin Phycoerythrin (SAPE) from 4 $^\circ\text{C}$  and tap the tube to mix well. Add 6  $\mu\text{l}$  of 1 mg/ml SAPE to 594  $\mu\text{l}$  of Stain buffer. Make fresh solution right before use.
6. Anti-streptavidin antibody (0.5 mg/ml): resuspend 0.5 mg antibody (goat, biotinylated from Vector laboratories) in 1 ml water and store at 4 $^\circ\text{C}$ .
7. Array Holding Buffer (1 $\times$ ): Mix 8.3 ml of 12 $\times$  MES Stock Buffer, 18.5 ml of 5 M NaCl (RNase-free and DNase-free), 0.1 ml of 10% Tween-20, and 73.1 ml of water. Store at 2–8 $^\circ\text{C}$  and shield from light.
8. Distilled water.
9. Affymetrix GeneChip Fluidics Station 450.
10. Affymetrix GeneChip Scanner 3000 7G.

## **2.2. Global Gene Expression Analysis**

### *2.2.1. Preparation of Total RNA*

1. Purified total RNA sample.
2. Spectrophotometer (NanoDrop UV–vis Spectrophotometer).
3. Bioanalyzer (Agilent Technologies).

### *2.2.2. First-Strand cDNA Synthesis*

1. First-strand Enzyme mix, included in GeneChip 3' In Vitro Transcription Express Kit (Kit 3, Affymetrix), and stored at –20 $^\circ\text{C}$ .
2. First-strand Buffer mix (Kit 3, –20 $^\circ\text{C}$ ).
3. Poly-A Control stock and Poly-A Control Dilution Buffer (Kit 3, –20 $^\circ\text{C}$ ).
4. Thermal Cycler with heated lid (capable of holding 0.2-ml tubes for reaction incubation).
5. DNase and RNase-free water (Kit 3, –20 $^\circ\text{C}$ ).

### *2.2.3. Second-Strand cDNA Synthesis*

1. Second-Strand Buffer mix (Kit 3, –20 $^\circ\text{C}$ ).
2. Second-Strand Enzyme mix (Kit 3, –20 $^\circ\text{C}$ ).

### *2.2.4. In Vitro Transcription to Synthesize Biotin-Labeled aRNA*

1. IVT Biotin label (Kit 3, –20 $^\circ\text{C}$ ).
2. IVT Enzyme Mix (Kit 3, –20 $^\circ\text{C}$ ).
3. IVT Labeling Buffer (Kit 3, –20 $^\circ\text{C}$ ).

### *2.2.5. aRNA Purification*

1. RNA binding beads (Kit 3, 4 $^\circ\text{C}$ ).
2. Magnetic Stand for 96-well plates (Ambion).
3. aRNA binding buffer concentrate (Kit 3, room temperature).

4. aRNA wash solution concentrate (Kit 3, room temperature).
5. 100% Ethanol, ACS reagent grade.
6. aRNA elution buffer (Kit 3, room temperature).
7. Orbital shaker for 96-well plates (or Jitterbug Microplate Incubator Shaker).

*2.2.6. Evaluation and Fragmentation of aRNA*

1. RNA 6000 Nano chip kit (Agilent Technologies).
2. 5× Array Fragmentation Buffer (Kit 3, room temperature).

*2.2.7. Target Hybridization*

1. Control oligo B2 (3 nM, Kit 3, -20°C).
2. 20× Hybridization Controls (Kit 3, -20°C).
3. 2× Hybridization Mix (GeneChip Hybridization, Wash and Stain Kit, Affymetrix, Kit 4, kept at 4°C).
4. Prehybridization mix (Kit 4, 4°C).
5. DMSO (Kit 4, room temperature).
6. Nuclease-free water (Kit 4, 4°C).
7. GeneChip Human Genome U133 Plus 2.0 Array (Affymetrix), stored at 4°C.
8. GeneChip Hybridization Oven 640 (Affymetrix).

*2.2.8. Washing, Staining and Scanning Arrays*

1. Stain Cocktail 1 (Kit 4, stored at 4°C).
2. Stain Cocktail 2 (Kit 4, 4°C).
3. Array Holding Buffer (Kit 4, 4°C).
4. Wash Buffer A (Kit 4, 4°C).
5. Wash Buffer B (Kit 4, 4°C).
6. GeneChip Fluidics Station 450.
7. Tough-Spots, label dots.
8. Affymetrix GeneChip Scanner 3000 7G.

---

## 3. Methods

### **3.1. Genome-Wide Association Study**

GWAS use high-throughput genotyping technologies to assay at least 100,000 SNPs representing nearly 12 million unique human SNPs and relate them to clinical conditions and measurable traits (22). The method described here is based on the whole-genome sampling analysis (WGSA) for large-scale genotyping of complex DNA (23). The procedure uses restriction digestion to fractionate the genome, followed by PCR amplification of a selected subset of the genome, resulting reduction in genome complexity. The assay includes restriction digestion, ligation of adaptor, one primer PCR amplification in selected size range, fragmentation and labeling prior to hybridization to the oligo-nucleotide array.

The Affymetrix Genome-Wide Human SNP 6.0 is the sixth-generation product in genotyping SNPs based on the WGSa assay. A single array interrogates 906,600 SNPs by combining the Sty I and Nsp I PCR fractions and through reducing the absolute number of features associated with each SNP on the array. This array also contains more than 945,000 probes for the detection of copy number variations (CNVs) in the genome.

The following protocol is for processing 48 genomic DNA samples using the Affymetrix Genome-Wide Human SNP 6.0 Array and the recommended workflow is shown in Fig. 1. However, the actual workflow can be determined empirically with each possible stopping point presented in italics. To minimize possible cross-contamination, it is highly recommended to handle genomic DNA, perform restriction enzyme digestions and ligation, and set up PCR reactions in a separate room (pre-PCR room) from the rest of the procedures (main lab).

### 3.1.1. Genomic DNA Preparation

1. Dilute high quality genomic DNA from human peripheral blood or tissue to 50 ng/ $\mu$ l using reduced EDTA TE buffer (see Note 4).
2. Aliquot 5  $\mu$ l of each DNA to the corresponding wells of two 96-well plates (first four rows). Use Reference Genomic DNA 103 as positive control and water as negative control.
3. Seal the plate and the *diluted genomic DNA can be stored at  $-20^{\circ}\text{C}$ .*

### 3.1.2. Sty Restriction Enzyme Digestion, Ligation, and PCR

In this stage, the human genomic DNA will be first digested with Sty I restriction enzyme. The digested samples will be ligated to the Sty adaptor and finally the DNA will be amplified using the adaptor-specific primers. The PCR condition is optimized to preferentially amplify restriction fragments that are between 250 and 1,000 bp. PCR products will be confirmed by running 3  $\mu$ l of the sample on a 2% TBE gel.

1. Take one genomic DNA plate out and keep it in a cooling chamber on ice (see Note 5).
2. Make Sty I digestion master mix in an Eppendorf tube (see Note 6):

	Per sample, $\mu$ l	48 Samples (15% extra), $\mu$ l
AccuGene Water	11.55	637.6
NE Buffer 3 (10 $\times$ )	2	110.4
BSA (100 $\times$ , 10 mg/ml)	0.2	11
Sty I (10 U/ $\mu$ l)	1	55.2
Total	14.75	814.2

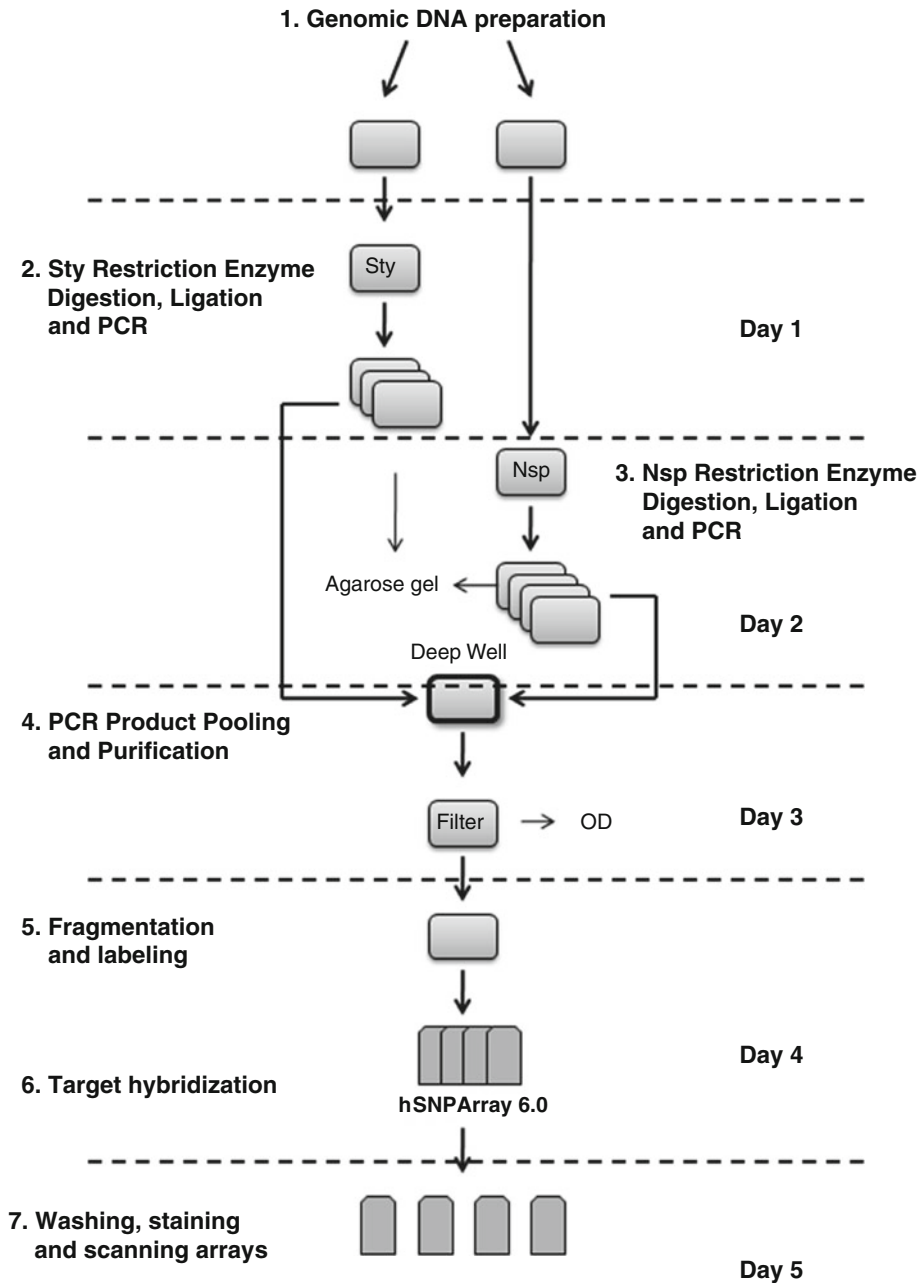


Fig. 1. Recommended workflow for Affymetrix Genome-Wide Human SNP 6.0 Array.

3. Aliquot 67  $\mu$ l of Sty I digestion master mix to each tube of the 12-strip tubes.
4. Add 14.75  $\mu$ l of Sty I digestion master mix to each DNA samples using a 12-channel P20 pipette. The total volume in each well is now 19.75  $\mu$ l.

5. Seal the plate with adhesive film, mix thoroughly by vortexing the plate at high speed for 3 s (see Note 7) and centrifugation at  $800 \times g$  for 30 s.
6. Incubate the plate on a thermal cycler (with preheated lid) and run the Digest program (see Note 8).

37°C	120 min
65°C	20 min
4°C	Hold

7. Remove the plate and centrifuge at  $800 \times g$  for 30 s.
8. *If not proceeding directly to the next step, store the plate at  $-20^{\circ}\text{C}$ .*
9. Make Sty I ligation master mix in an Eppendorf tube (see Note 9):

	Per sample, $\mu\text{l}$	48 Samples (25% extra), $\mu\text{l}$
T4 Ligase Buffer (10 $\times$ )	2.5	150
Adaptor Sty I (50 $\mu\text{M}$ )	0.75	45
T4 DNA Ligase (400 U/ $\mu\text{l}$ )	2	120
Total	5.25	315

10. Aliquot 25  $\mu\text{l}$  of Sty I ligation master mix to each tube of the 12-strip tubes.
11. Adding 5.25  $\mu\text{l}$  of Sty I ligation master mix to each DNA samples using a 12-channel P20 pipette. The total volume in each well is now 25  $\mu\text{l}$ .
12. Seal the plate with adhesive film, mix thoroughly by vortexing the plate at high speed for 3 s and centrifugation at  $800 \times g$  for 30 s.
13. Incubate the plate on a thermal cycler (with preheated lid) and run the Ligation program:

16°C	180 min
70°C	20 min
4°C	Hold

14. Remove the plate and spin it down at  $800 \times g$  for 30 s. Place the plate in a cooling chamber.
15. Pour ~10 ml of precooled AccuGENE water into a solution basin and add 75  $\mu\text{l}$  of the water to each reaction using a 12-channel P200 pipette. The total volume in each well is now 100  $\mu\text{l}$ .

16. Seal the plate with adhesive film, mix thoroughly by vortexing the plate at high speed for 3 s and centrifugation at  $800 \times g$  for 30 s. Label the plate as StyLig.
17. *If not proceeding directly to the next step, store the plate at  $-20^{\circ}\text{C}$ .*
18. Take three 96-well reaction plates and label them StyP1, StyP2, and StyP3. Place the plates in two double cooling chambers on ice.
19. Transfer 10  $\mu\text{l}$  of each Sty ligated sample to the corresponding well of each PCR plate. Seal the plates with adhesive films and leave them in cooling chambers on ice. Keep the StyLig plate (70  $\mu\text{l}$  left) at  $-20^{\circ}\text{C}$ .
20. Prepare the Sty PCR master mix in a 50-ml Falcon tube (see Note 10):

	Each reaction, $\mu\text{l}$	48 Samples $\times$ 3 (15% extra), ml
AccuGENE water	39.5	6.541
TITANIUM buffer (10 $\times$ )	10	1.656
GC-Melt (5 M)	20	3.312
dNTP (2.5 mM each)	14	2.318
PCR primer 002 (100 $\mu\text{M}$ )	4.5	0.745
TITANIUM Taq DNA		
Polymerase (50 $\times$ )	2	0.331
Total	90	14.903

21. Vortex the master mix at high speed three times, 1 s each time.
22. Pour the mix into a solution basin on ice.
23. Add 90  $\mu\text{l}$  of Sty PCR master mix to each sample using a 12-channel P200 pipette (see Note 11). The total volume in each well is 100  $\mu\text{l}$ .
24. Seal the plates tightly with adhesive films. Mix thoroughly by vortexing and centrifugation at  $800 \times g$  for 30 s.
25. Transfer the plates to the main lab and incubate in a thermal cycler with preheated lid. Run the PCR program. The program varies depending on the thermal cyclers used in the lab.  
For the GeneAmp PCR System 9700 (silver or gold-plated silver blocks)

94°C	3 min	1×
94°C	30 s	} 30×
60°C	45 s	
68°C	15 s	
68°C	7 min	
4°C	<i>Hold (or overnight)</i>	
Volume	100 µl	

For the Bio-Rad thermal cyclers (MJ Tetrad PTC-225)

94°C	3 min	1×
94°C	30 s	} 30×
60°C	30 s	
68°C	15 s	
68°C	7 min	
4°C	<i>Hold (or overnight)</i>	
Volume	100 µl	

26. Remove the plates from the thermal cycler and spin down at  $800 \times g$  for 20 s. Keep the plates in the coolers on ice or at 4°C.
27. Take one fresh 96-well plate and aliquot 3 µl of Gel Loading Dye to each well in row A through D using a 12-channel P20 pipette. Label the plate “Pgel”.
28. Transfer the first row of the amplified DNA in StyP1 plate (3 µl) to the corresponding wells in Pgel plate.
29. Transfer the second row of the amplified DNA in StyP1 plate (3 µl) to the corresponding wells in Pgel plate.
30. Transfer the third row of the amplified DNA in StyP2 plate (3 µl) to the corresponding wells in Pgel plate.
31. Transfer the fourth row of the amplified DNA in StyP3 plate (3 µl) to the corresponding wells in Pgel plate.
32. Seal the Pgel plate. Vortex for 3 s and spin down at  $800 \times g$  for 30 s.
33. Load the total volume from each well of the Pgel plate onto 2% TBE gels along with the all purpose Hi-Lo DNA marker (see Note 12).
34. Run the gels at 120 V for 40–60 min. Verify that the PCR products are between ~250 and 1,100 bp.
35. Seal the Sty PCR plates (StyP1, StyP2, and StyP3) and store them at -20°C.

3.1.3. *Nsp* Restriction  
Enzyme Digestion,  
Ligation, and PCR

During this stage, the human genomic DNA will be first digested with *Nsp* I restriction enzyme. The digested samples will be ligated to the *Nsp* adaptor and the DNA will be amplified using the adaptor-specific primers. The PCR condition is optimized to preferentially amplify restriction fragments between 250 and 1,000 bp. PCR products will be confirmed by running 3  $\mu$ l of the sample on a 2% TBE gel.

1. Take the second genomic DNA plate out and keep it in a cooling chamber on ice.
2. Make *Nsp* I digestion master mix in an Eppendorf tube:

	Per sample, $\mu$ l	48 Samples (15% extra), $\mu$ l
AccuGene Water	11.55	637.6
NE Buffer 2 (10 $\times$ )	2	110.4
BSA (100 $\times$ , 10 mg/ml)	0.2	11
<i>Nsp</i> I (10 U/ $\mu$ l)	1	55.2
Total	14.75	814.2

3. Aliquot 67  $\mu$ l of *Nsp* I digestion master mix to each tube of the 12-strip tubes.
4. Add 14.75  $\mu$ l of *Nsp* I digestions master mix to each DNA samples using a 12-channel P20 pipette. The total volume in each well is now 19.75  $\mu$ l.
5. Seal the plate with adhesive film, mix thoroughly by vortexing the plate for 3 s and centrifugation at 800  $\times g$  for 30 s.
6. Incubate the plate on a thermal cycler (with preheated lid) and run the Digest program:

37°C	120 min
65°C	20 min
4°C	Hold

7. Remove the plate and spin it down at 800  $\times g$  for 30 s.
8. *If not proceeding directly to the next step, store the plate at -20°C.*
9. Make *Nsp* I ligation master mix in an Eppendorf tube:

	Per sample, $\mu$ l	48 Samples (25% extra), $\mu$ l
T4 Ligase buffer (10 $\times$ )	2.5	150
Adaptor <i>Nsp</i> I (50 $\mu$ M)	0.75	45
T4 DNA Ligase (400 U/ $\mu$ l)	2	120
Total	5.25	315

10. Aliquot 25  $\mu$ l of Nsp I ligation master mix to each tube of the 12-strip tubes.
11. Add 5.25  $\mu$ l of Nsp I ligation master mix to each DNA samples using a 12-channel P20 pipette. The total volume in each well is now 25  $\mu$ l.
12. Seal the plate with adhesive film, mix thoroughly by vortexing the plate for 3 s and centrifugation at 800  $\times g$  for 30 s.
13. Incubate the plate on a thermal cycler (with preheated lid) and run the Ligation program:

16°C	180 min
70°C	20 min
4°C	Hold

14. Remove the plate and spin it down at 800  $\times g$  for 30 s. Place the plate in a cooling chamber.
15. Pour ~10 ml of precooled AccuGENE water into a solution basin and add 75  $\mu$ l of the water to each reaction using a 12-channel P200 pipette. The total volume in each well is now 100  $\mu$ l.
16. Seal the plate with adhesive film, mix thoroughly by vortexing the plate at high speed for 3 s and centrifugation at 800  $\times g$  for 30 s. Label the plate as NspLig.
17. *If not proceeding directly to the next step, store the plate at -20°C.*
18. Take four 96-well reaction plates and label them NspP1, NspP2, NspP3, and NspP4. Place the plates in three double cooling chambers on ice.
19. Transfer 10  $\mu$ l of each Nsp ligated sample to the corresponding well of each PCR plate. Seal the plates with adhesive films and leave them in cooling chambers on ice. Keep the NspLig plate (60  $\mu$ l left) at -20°C.
20. Prepare the Nsp PCR master mix in a 50 ml Falcon tube:

	Each reaction, $\mu$ l	48 Samples $\times$ 4 (15% extra), ml
AccuGENE water	39.5	8.722
TITANIUM buffer (10 $\times$ )	10	2.208
GC-Melt (5 M)	20	4.416
dNTP (2.5 mM each)	14	3.091
PCR primer 002 (100 $\mu$ M)	4.5	0.994
TITANIUM Taq DNA Polymerase (50 $\times$ )	2	0.442
Total	90	19.873

21. Vortex the master mix at high speed three times, 1 s each time.
22. Pour the mix into a solution basin on ice.
23. Adding 90  $\mu\text{l}$  of Nsp PCR master mix to each sample in four PCR plates using a 12-channel P200 pipette. The total volume in each well is 100  $\mu\text{l}$ .
24. Seal the plates tightly with adhesive films. Mix thoroughly by vortexing and centrifugation at  $800\times g$  for 30 s.
25. Transfer the plates to the main lab and incubate in a thermal cycler with preheated lid. Run the PCR program.
26. Remove the plates from the thermal cycler and spin down at  $800\times g$  for 30 s. Keep them in the coolers on ice or at  $4^{\circ}\text{C}$ .
27. Take one fresh 96-well plate and aliquot 3  $\mu\text{l}$  of Gel Loading Dye to each well in row A through D using a 12-channel P20 pipette. Label the plate "Pgel".
28. Transfer the first row of the amplified DNA in NspP1 plate (3  $\mu\text{l}$ ) to the corresponding wells in Pgel plate.
29. Transfer the second row of the amplified DNA in NspP2 plate (3  $\mu\text{l}$ ) to the corresponding wells in Pgel plate.
30. Transfer the third row of the amplified DNA in NspP3 plate (3  $\mu\text{l}$ ) to the corresponding wells in Pgel plate.
31. Transfer the fourth row of the amplified DNA in NspP4 plate (3  $\mu\text{l}$ ) to the corresponding wells in Pgel plate.
32. Seal the Pgel plate. Vortex for 3 s and spin down at  $800\times g$  for 30 s.
33. Load the total volume from each well of the Pgel plate onto 2% TBE gels.
34. Run the gels at 120 V for 40–60 min. Verify that the PCR products are between ~250 and 1,100 bp.
35. *Seal the Nsp PCR plates (NspP1, NspP2, NspP3, and NspP4) and store them at  $-20^{\circ}\text{C}$ .*

#### 3.1.4. PCR Product Pooling, Purification and Quantitation

During this stage, the Sty and Nsp PCR products will be pooled and purified using magnetic beads in a deep well 96-well plate. The PCR products will be washed and eluted using a filter plate connected to a vacuum manifold. Finally, the purified PCR products will be quantitated using NanoDrop or spectrophotometer plate reader.

1. Thaw all the frozen PCR products (three Sty PCR plates and four Nsp PCR plates) to room temperature on the bench top.
2. Vortex each plate at high speed for 3 s and spin down at  $800\times g$  for 30 s. Cut the seal between each row so that it can be removed one row at a time.
3. Place a deep-well pooling plate on the bench top.

4. Remove the seal to expose row A on each PCR plate. Transfer the reactions from row A of each plate to the corresponding wells of row A on the pooling plate.
5. Remove the seal from each PCR plate to expose the next row.
6. Repeat step 4 and finish transferring the reactions from rows B to D.
7. When finished, the total volume of each well of pooling plate should be about 700  $\mu$ l.
8. Take the magnetic beads stock from the refrigerator and mix well by shaking the bottle gently but thoroughly.
9. Pipette ~50 ml of magnetic beads to a solution basin and add 1 ml of the beads to each well of pooled PCR product using a 12 channel P1200 pipette.
10. Mix well by pipetting up and down five times. To avoid overflow, move pipette up and down during the pipetting. Visually check each well. Change tips for each row.
11. Cover the plate to avoid contamination and incubate at room temperature for 10 min.
12. Set up the vacuum apparatus and connect the gauge and the pressure controller to the Millipore vacuum manifold. Place a filter plate in the Millipore vacuum manifold.
13. Transfer each reaction of the pooling plate to the corresponding wells of the filter plate using a 12-channel P1200 pipette.
14. Seal the unused wells with an adhesive film and turn on the vacuum to 20–24 in Hg (do not exceed 24 in Hg). If the vacuum power does not increase, press the plate against the manifold to secure the seal.
15. Cover the plate and allow the liquid to completely dry (~40–60 min).
16. Inspect each well using a flashlight to confirm complete dry (see Note 13) and turn off the vacuum.
17. Immediately add 0.9 ml of 75% ethanol to each well using a 12-channel P1200 pipette and turn the vacuum back on to 20–24 in Hg.
18. After the ethanol level is down, add another 0.9 ml of 75% ethanol to each well.
19. Allow the liquid to completely dry (10–20 min). Check with a flashlight.
20. Turn off the vacuum and remove the manifold from the apparatus.
21. Tap off excess ethanol from the bottom of the manifold on a large Kimwipe.

22. Return the manifold to the vacuum apparatus, turn on the vacuum to 20–24 in Hg and allow the plate to dry for additional 8 min.
23. Turn off the vacuum, remove the filter plate, and blot the bottom of the plate with Kimwipes to remove excess liquid. Take off the adhesive film.
24. Attach the elution plate to the bottom of the filter plate using two strips of tape (see Note 14). This assembly is now referred to as the plate stack.
25. Pipette 3 ml of Buffer EB to a solution basin and add 55  $\mu$ l of Buffer EB to each well using a 12-channel P200 pipette (see Note 15).
26. Tap the plate stack to move all the Buffer EB to the bottom of the wells.
27. Tightly seal the filter plate with an adhesive film.
28. Place the plate stack on Jitterbug for 10 min at setting 5. Inspect each well to make sure that the beads are thoroughly resuspended. Remove the adhesive film.
29. Put the plate stack on the vacuum manifold. Seal the empty wells with an adhesive film.
30. Place the deep well collar over the plate stack.
31. Turn the vacuum on to 20–24 mmHg and ensure that a seal is formed between the collar and the base of the manifold (see Note 16).
32. Leave the plate stack on the manifold for 5–15 min. Closely monitor the filter plate to ensure that the wells are completely dry.
33. Remove the plate and seal it with an adhesive film. Spin the plate down for 5 min at  $1400\times g$  in room temperature.
34. *Transfer 45  $\mu$ l of the eluate to a fresh PCR plate for fragmentation. Seal the plate and keep it at  $-20^{\circ}\text{C}$ .*
35. For the rest of the eluate, check OD of each sample using NanoDrop or:
  - Add 198 AccuGENE water to rows A to D in an optical plate.
  - Transfer 2  $\mu$ l of the eluate to the corresponding wells of the optical plate.
  - Set a 12-channel P200 pipette to 180  $\mu$ l and mix each sample by pipetting up and down three times.
  - Add 200  $\mu$ l of AccuGENE water to row E (blank control).
  - Measure the OD of each PCR product at 260, 280 and 320 nm using a microplate spectrophotometer.

36. A final PCR product concentration should be between 4.0 and 6.0  $\mu\text{g}/\mu\text{l}$  and the OD260/OD280 ratio should be between 1.8 and 2.0 (see Note 17).

### 3.1.5. Fragmentation and Labeling

During this stage, the purified PCR products will be fragmented using Fragmentation reagent (DNase I), and the results will be confirmed by running 1.5  $\mu\text{l}$  of each reaction on a 4% TBE gel. The fragmented samples are then end-labeled with biotin using the DNA labeling Reagent.

1. Take out the PCR plate with the purified DNA from  $-20^{\circ}\text{C}$  and leave it on the cooling chamber on ice to thaw.
2. Thaw fragmentation buffer on ice (see Note 18).
3. Vortex and spin the Fragmentation buffer to mix thoroughly. Add 28  $\mu\text{l}$  to each tube of the 12-strip tubes.
4. Add 5  $\mu\text{l}$  of the Fragmentation Buffer to each of the purified DNA in the PCR plate. The total volume in each well is now 50  $\mu\text{l}$ .
5. In an Eppendorf tube, add 309.6  $\mu\text{l}$  of AccuGENE water (if the Fragmentation reagent is 2.5 U/ $\mu\text{l}$ , see Note 19) and 36  $\mu\text{l}$  of the Fragmentation Buffer.
6. Spin down the Fragmentation Reagent (do not vortex) and add 14.4  $\mu\text{l}$  of the reagent to tube to make fragmentation master mix (see Note 20).
7. Vortex the tube and spin down.
8. Add 28  $\mu\text{l}$  of the fragmentation master mix to each well of the 12-strip tubes.
9. Add 5  $\mu\text{l}$  of the fragmentation master mix to each of the four rows of the PCR plate. Change tips after each dispense. The total volume in each well is now 55  $\mu\text{l}$ .
10. Seal the plate with an adhesive film. Vortex thoroughly but quickly. Spin down at  $4^{\circ}\text{C}$  at  $800\times g$  for 30 s.
11. Immediately load the plate onto the preheated block of the thermal cycler (preheat to  $37^{\circ}\text{C}$  for at least 10 min) and run the Fragment program:

37°C	35 min
95°C	15 min
4°C	Hold

12. While waiting, take out a standard non-PCR 96-well plate.
13. Add loading dye into a solution basin. Using a 12-channel P10 pipette, add 4  $\mu\text{l}$  of the loading dye to the four rows of the 96-well plate.

14. Remove the PCR plate from the thermal cycler and spin down the plate at  $800 \times g$  for 30 s.
15. Add 1.5  $\mu\text{l}$  of each fragmented PCR product into 4  $\mu\text{l}$  of loading dye in the standard 96-well plate.
16. Run on 4% TBE Gel with the BioNexus All purpose Hi-L ladder at 120 V for 30–60 min. Inspect the gel to verify that the average fragment size is  $<180$  bp (see Note 21).
17. Thaw  $5\times$  TdT Buffer and DNA Labeling Reagent on ice, and prepare Labeling master mix in an Eppendorf tube:

	<b>Each sample, <math>\mu\text{l}</math></b>	<b>48 Sample (15% extra), <math>\mu\text{l}</math></b>
TdT buffer ( $5\times$ )	14	772.8
DNA Labeling Reagent (30 mM)	2	110.4
TdT enzyme (30 U/ $\mu\text{l}$ )	3.5	193.2
Total	19.5	1,076.4

18. Aliquot 89  $\mu\text{l}$  of the Labeling master mix to each well of 12-strip tubes.
19. Add 19.5  $\mu\text{l}$  of Labeling master mix to each sample of the fragmented DNA. The total volume is now 73  $\mu\text{l}$ .
20. Seal the plate with adhesive film. Vortex for 3 s and spin down at  $800 \times g$  for 30 s.
21. Place the plate onto the preheated block of the thermal cycler ( $37^\circ\text{C}$ , at least 10 min) and run the Label program:

$37^\circ\text{C}$	4 h
$95^\circ\text{C}$	15 min
$4^\circ\text{C}$	Hold

22. Freeze the samples at  $-20^\circ\text{C}$ .

### 3.1.6. Target Hybridization

During this stage, a Hybridization master mix will be added to each sample. After being denatured on a thermal cycler, each sample will be loaded onto a Genome-Wide Human SNP Array 6.0. The arrays are then placed into a hybridization oven and the samples are left to hybridize at  $50^\circ\text{C}$  for 16–18 h.

1. Turn on the thermal cycler to preheat the lid. Leave the block at room temperature.
2. Turn on the hybridization oven and set the temperature to  $50^\circ\text{C}$  with 60 rpm rotation. Preheat for at least 1 h.
3. Unwrap the arrays and place them on bench top, septa side up.
4. Thaw the label plate in cooling chamber on ice.

5. In a 50-ml centrifuge tube, make the Hybridization master mix (see Note 22):

	One array, $\mu\text{l}$	48 Arrays (15% extra), $\mu\text{l}$
MES (12 $\times$ ; 1.25 M)	12	660
Denhardt's solution (50 $\times$ )	13	715
EDTA (0.5 M)	3	165
HSDNA (10 mg/ml)	3	165
OCR, 0100	2	110
H Cot-1 DNA (1 mg/ml)	3	165
Tween-20 (3%)	1	55
DMSO (100%)	13	715
TMACL (5 M)	140	7,700
Total	190	10,450

6. Vortex the Hybridization master mix until no precipitates (up to 5 min) and pulse-spin for 3 s.
7. Pour 1 l ml of Hybridization master mix into a solution basin.
8. Using 12-channel P200 pipette, add 190  $\mu\text{l}$  of the hybridization master mix to each sample on the label plate. The total volume in each well is now 263  $\mu\text{l}$ .
9. Seal the plate tightly with adhesive film and vortex the center of the plate for at least 10 s.
10. Spin down the plate at  $800 \times g$  for 30 s.
11. Cut the adhesive film between each row of samples. Do not remove the film.
12. Place the plate onto the thermal cycler and close the lid. Run the Hybridization program:

95°C	10 min
49°C	Hold

13. Turn on the computer and register all the samples in Affymetrix GeneChip Console (AGCC):
  - Click on Affymetrix Launcher and start the AGCC portal.
  - Select “Quick registration” and enter the number of samples.
  - Assign the samples to an existing project or name a new project.
  - Select the array type (SNP6.0) and put the array in a barcode reader to enter the barcode automatically.
  - Enter the sample file name for each array.
  - Turn off the computer.

14. During the denaturation, prepare the arrays: label each array and allow the arrays to warm to room temperature for 10–15 min. Attach two Tough-Spots to each array. Insert a 200  $\mu$ l pipette tip into the upper right septum of each array for ventilation.
15. When the thermal cycler block reaches 49°C, slide back the lid to expose the first row of the samples only.
16. Remove the film from the first row.
17. Using P200 pipette, mix the denatured sample by pipetting up and down once, and remove 200  $\mu$ l from the first well.
18. Immediately inject the sample into an Array from the lower left septum. Cover the septa with the Tough-Spots (1/2 in., see Note 23).
19. Repeat the process on next sample. Put two arrays at a time into the oven and make sure that the oven is balanced (see Note 24).
20. After the entire row is loaded, place a fresh adhesive film over the completed row.
21. Repeat steps 15–20 with the next row of samples.
22. Store the remaining samples and *any samples not yet hybridized in a tightly sealed plate at –20°C.*
23. Allow the Arrays to rotate at 50°C, 60 rpm for 16–18 h.

### 3.1.7. Washing, Staining, and Scanning Arrays

During this step, the hybridized arrays will be washed and stained with streptavidin–phycoerythrin conjugate (SAPE) using an automated protocol on the GeneChip Fluidics Station 450 which has been primed. Once stained, each array is filled with Array Holding Buffer before being scanned with the GeneChip Scanner 3700 7G.

1. Turn on the Fluidics Station. In the AGCC Launcher, click the AGCC Fluidics Control Icon.
2. Prime the Fluidics Station (see Note 25):
  - Select protocol Prime\_450 for each module.
  - Fill the intake buffer reservoir with Wash buffer A.
  - Fill the intake buffer reservoir B with Wash buffer B.
  - Empty the waste bottle and fill the water reservoir with deionized water.
  - Place three empty 1.5 ml tubes into the stain holder positions 1, 2, and 3.
  - Place the washblock lever into the engaged/closed position. Push the needle lever into the down position.
  - Run the Prime\_450 maintenance protocol.

3. Remove the arrays from the oven. Take off the Tough Spots.
4. Insert a 200  $\mu$ l pipette tip into the upper right septum of each array for ventilation.
5. Extract the hybridization cocktail from each array through lower left septum and transfer it to the corresponding well of the hybridization plate. Store on ice or at  $-20^{\circ}\text{C}$  for long term storage.
6. Fill each array completely with  $\sim 270$   $\mu$ l of  $1\times$  Array Holding Buffer (see Note 26). Allow the arrays to equilibrate to room temperature. Pipetting back and forth may be needed to remove bubbles.
7. Start the AGCC Fluidics Control software.
8. Select the correct sample file name.
9. Select the protocol GenomeWideSNP6\_450.
10. Start the protocol and follow the instructions in the LCD on the fluidics station.
11. Insert an array into the designated module of the fluidics station.
12. When “Load Vials 1–2–3” is shown on the LCD of the fluidics station, place the three vials into the sample holders 1, 2 and 3:
  - Place one vial (600  $\mu$ l) of SAPE stain solution in sample holder 1.
  - Place one vial (600  $\mu$ l) of anti-streptavidin biotinylated antibody stain solution in sample holder 2.
  - Place one vial (1 ml) of Array holding buffer in sample holder 3.
13. Press down on the needle lever to start the run. The dialog box at the workstation terminal and LCD of the fluidics station will display the status of the washing and staining steps.
14. When staining is finished, remove the three vials containing stain and replace with three empty Eppendorf tubes as prompted.
15. Remove the array from the fluidics station.
16. Check the array window to make sure that there is no bubbles or air pockets (see Note 27).
17. If the array has no large bubble, it is ready for scanning. Arrays can be stored at  $4^{\circ}\text{C}$  in the dark for up to 24 h. Allow them to warm up to room temperature before scanning to avoid breakage.
18. After all the arrays have been stained, shut down the Fluidics station:
  - When the last array is removed, gently lift up the cartridge lever to engage the washblock. The instrument automatically performs a Cleanout procedure.

- When REMOVE VIALS is shown in the LCD, remove the Eppendorf tubes from the sample holders.
  - Place the wash lines into a bottle filled with dH<sub>2</sub>O.
  - Using AGCC, choose the Shutdown\_450 protocol for all modules and run the protocol.
  - Turn off the Fluidics Station.
  - Place the wash lines in a different bottle of dH<sub>2</sub>O than the one used for the shutdown protocol.
19. If necessary, clean the glass surface of the array with Kimwipe. On the back of the array, clean excess fluid around the septa.
  20. Cover both septa with Tough Spots (3/8 in., see Note 28).
  21. Turn on the scanner for at least 10 min before use. Click the AGCC Scan Control icon in the Affymetric Launcher.
  22. Insert an array into the scanner.
  23. Follow AGCC instructions and begin the scan.

### **3.2. Global Gene Expression Analysis**

This protocol is based on the linear RNA amplification using T7 in vitro transcription technology with as little as 50 ng of total RNA. Total RNA first undergoes reverse transcription to synthesize first-strand cDNA. This cDNA is then converted to a double-stranded cDNA which is used as template for in vitro transcription. In vitro transcription synthesizes biotin-labeled aRNA when biotin-labeled ribonucleotides are included in the reaction. After purification and fragmentation, biotin labeled aRNA is hybridized to a probe array. The hybridized probe array is stained with streptavidin–phycoerythrin conjugate and scanned by the GeneChip Scanner 3000 7G. The amount of light emitted at 570 nm is proportional to the bound target at each location on the probe array.

We use Human Genome U133 Plus 2.0 Array which provides comprehensive analysis of the relative expression level of more than 47,000 transcripts and variants, representing more than 38,500 well-characterized human genes.

This protocol is written for processing 16 samples using 100 ng of total RNA and the recommended workflow is shown in Fig. 2. Actual sample number, total RNA amount and stopping point (presented in italics) can be determined empirically.

#### **3.2.1. Preparation of Total RNA**

RNA quality is the most important factor affecting the outcome of the experiment. The purified total RNA (see Note 29) is quantitated using a NanoDrop spectrophotometer. The ratio of A<sub>260</sub>–280 values should fall in the range of 1.9–2.1. It is highly recommended to check RNA integrity using the Agilent 2100 bioanalyzer with an RNA LabChip kit, following manufacturer's guide.

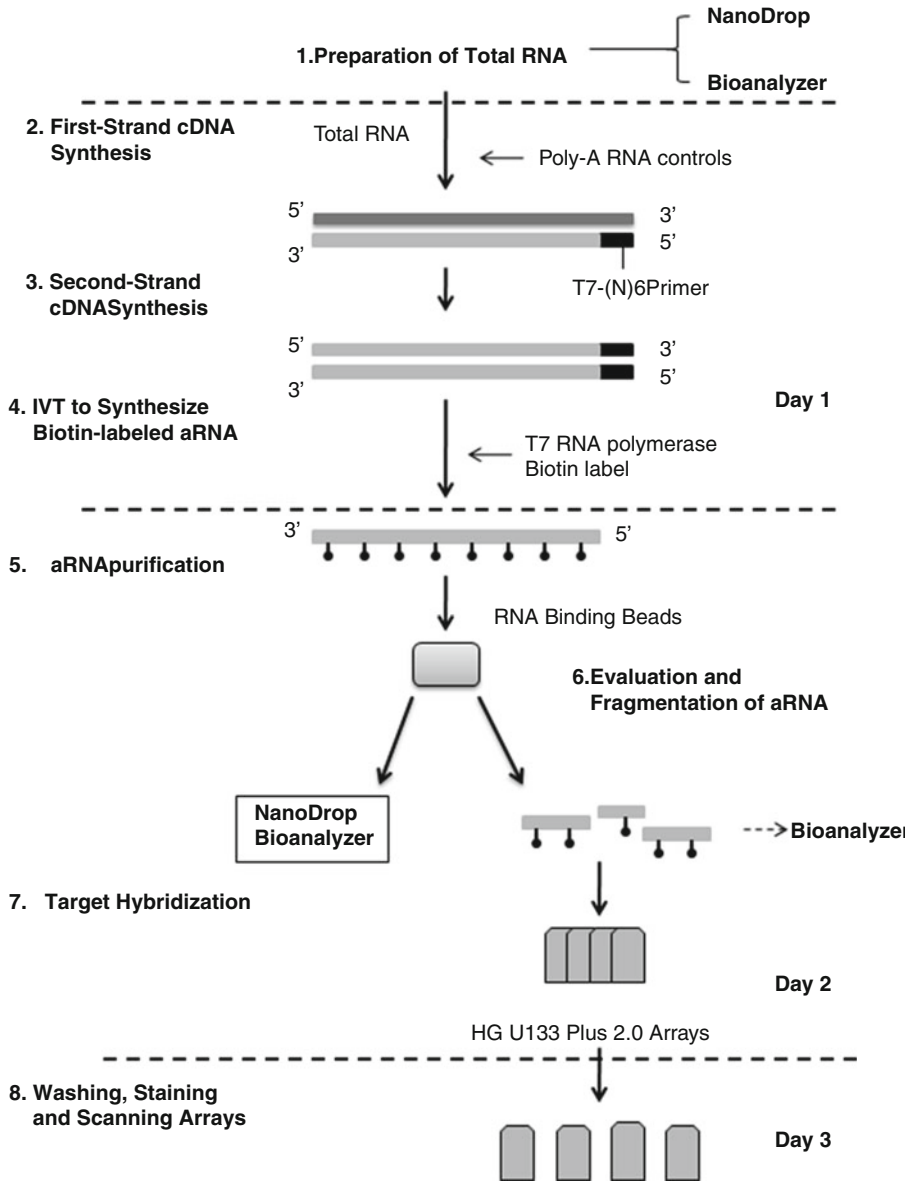


Fig. 2. Recommended workflow for GeneChip Expression Analysis.

3.2.2. First-Strand cDNA Synthesis

During this step, total RNA is primed with engineered primers containing a T7 promoter sequence. The reaction synthesizes single-stranded cDNA containing a T7 promoter sequence using SuperScript reverse transcriptase. The poly-A RNA controls is diluted and added to the starting samples so that the whole processes can be monitored independently from the quality of the starting total RNA.

1. Prepare Poly-A control RNA (*Bacillus subtilis* genes *lys*, *phe*, *thr*, and *dap*) dilution:
  - Add 2  $\mu$ l of the Poly-A Control stock to 38  $\mu$ l of Poly-A Control Dilution Buffer to make the first dilution (1:20). Mix thoroughly.
  - Add 2  $\mu$ l of the first dilution to 98  $\mu$ l of Poly-A Control Dilution Buffer to make the second dilution (1:50). Mix thoroughly.
  - Add 2  $\mu$ l of the second dilution to 98  $\mu$ l of Poly-A Control Dilution Buffer to make the third dilution (1:50). Mix thoroughly.
  - Add 2  $\mu$ l of the third dilution to 18  $\mu$ l of Poly-A Control Dilution Buffer to make the fourth dilution (1:10). Mix thoroughly.
2. Place the supplied PCR tubes on ice. Add 2  $\mu$ l of the fourth dilution and 100 ng of total RNA to the tubes (see Note 30):

Total RNA sample (100 ng)	Variable
Diluted Poly-A RNA controls	2 $\mu$ l (fourth dilution)
Nuclease-free water	To 5 $\mu$ l

3. Thaw first-strand synthesis reagents on ice. Mix the reagents well by vortexing and pulse spin.
4. Make first-strand master mix in a nuclease-free microfuge tube on ice (see Note 31):

	Per sample, $\mu$ l	16 Samples (10% extra), $\mu$ l
First-Strand Buffer mix	4	70.4
First-Strand Enzyme mix	1	17.6
Total Volume	5	88

5. Mix well by gently vortexing and pulse-spin for 3 s.
6. Add 5  $\mu$ l first-strand master mix to each of the total RNA/Poly-A control mixture for a final volume of 10  $\mu$ l.
7. Mix thoroughly by gently vortexing. Spin the tubes down for 3 s.
8. Place the tubes on a thermal cycler and run the First-strand cDNA synthesis program (see Note 32):

42°C	2 h
4°C	Hold

9. Centrifuge for 5 s to collect the samples at the bottom of the tubes. Place the tubes on ice and immediately proceed to next step.

### 3.2.3. Second-Strand cDNA Synthesis

During this step, single-stranded cDNA is converted to double-stranded cDNA, which will be used later as template for transcription. The reaction uses DNA polymerase I and RNaseH to simultaneously synthesize second-strand cDNA and degrade the RNA.

1. Thaw second-strand synthesis reagents on ice. Mix the reagents well by vortexing and pulse spin.
2. Make second-strand master mix on ice:

	Per sample, $\mu\text{l}$	16 Samples (10% extra), $\mu\text{l}$
Nuclease-free water	13	228.8
Second-strand buffer mix	5	88
Second-strand enzyme mix	2	35.2
Total	20	352

3. Mix well by gently vortexing and pulse-spin for 3 s.
4. Add 20  $\mu\text{l}$  of Second-strand master mix to each First-strand cDNA sample. Mix thoroughly by flicking the tubes 3–4 times. Centrifuge briefly to collect the reaction at the bottom of the tubes. The total volume is now 30  $\mu\text{l}$ . Place the tubes on ice.
5. Precool the thermal cycler block to 16°C (see Note 33). Place the tubes on the thermal cycler and run the second-strand cDNA synthesis program:

16°C	1 h
65°C	10 min
4°C	Hold

6. After the reaction, centrifuge briefly and place the tubes on ice.
7. Immediately proceed to Subheading 3.2.4 or store the samples at  $-20^{\circ}\text{C}$ .

### 3.2.4. In Vitro Transcription (IVT) to Synthesize Biotin-Labeled aRNA

During this step, antisense biotin-labeled aRNA is synthesized and amplified by in vitro transcription of the second-strand cDNA template using T7 RNA polymerase and biotin-labeled ribonucleotides.

1. Thaw the IVT reagents on ice. Mix the reagents well by vortexing and pulse spin.

- At room temperature, prepare IVT master mix in a nuclease-free tube:

	Per sample, $\mu\text{l}$	16 Samples (10% extra), $\mu\text{l}$
IVT Biotin Label	4	70.4
IVT Labeling Buffer	20	352
IVT Enzyme Mix	6	105.6
Total	30	528

- Mix well by gently vortexing and pulse-spin for 3 s.
- Add 30  $\mu\text{l}$  of the IVT master mix to each double-stranded cDNA sample. Mix thoroughly by gently vortexing. Centrifuge briefly to collect the reaction at the bottom of the tubes. The total volume in each tube is now 60  $\mu\text{l}$ .
- Place the tubes on a thermal cycler and run the IVT program (see Note 34)

40°C	16 h
4°C	Hold

- Place the tubes on ice briefly and proceed to the aRNA purification or *immediately freeze at  $-20^{\circ}\text{C}$  for overnight storage.*

### 3.2.5. aRNA Purification

In this procedure, aRNA will be mixed with and bind to RNA Binding Beads. Enzymes, salt, inorganic phosphate, and unincorporated NTPs will be removed. After wash, purified aRNA will be eluted in aRNA Elution solution to improve its stability.

- Preheat the bottle of aRNA Elution Solution to 50–60°C for at least 10 min.
- Make sure to add 100% ethanol to the bottle of aRNA Wash Solution.
- Vortex the RNA Binding beads and prepare aRNA Binding Mix in a nuclease-free tube:

	Per sample, $\mu\text{l}$	16 Samples (10% extra), $\mu\text{l}$
RNA Binding beads	10	176
aRNA Binding Buffer concentrate	50	880
Total	60	1,056

- Add 60  $\mu\text{l}$  of aRNA Binding Mix to each sample and transfer each sample to a well of a U-Bottom plate. Mix well by pipetting up and down several times.

5. Using an 8-channel P200 pipette, add 120  $\mu$ l of 100% ethanol to each sample. Mix by pipetting up and down several times.
6. Put the plate on an orbital shaker and shake gently (300–500 rpm, see Note 35) for at least 2 min.
7. Move the plate to a magnetic stand and capture the magnetic beads for about 5 min (see Note 36).
8. Carefully aspirate the supernatant without disturbing the beads.
9. Remove the plate from the magnetic stand. Add 100  $\mu$ l of aRNA Wash Solution to each sample and shake the plate at moderate speed (700–900 rpm, see Note 37) for 1 min.
10. Capture the beads on the magnetic stand for 5 min.
11. Carefully aspirate the supernatant without disturbing the beads.
12. Repeat steps 9–11 to do another wash.
13. Move the plate to the shaker and shake the plate vigorously (1,000–1,200 rpm, see Note 38) for 1 min to evaporate residual ethanol from the beads.
14. Add 50  $\mu$ l of preheated aRNA Elution Solution to each sample.
15. Vigorously shake (1,000–1,200 rpm) for 3 min (see Note 39).
16. Move the plate to the magnetic stand and capture the beads for 5 min.
17. Carefully transfer the supernatant to nuclease-free PCR tubes.
18. Place the tubes on ice to proceed with quantitation and fragmentation. *Alternatively, store aRNA at  $-20$  or  $-80^{\circ}\text{C}$  (see Note 40).*

### 3.2.6. Evaluation and Fragmentation of aRNA

During this step, the yield of the purified aRNA will be assessed by UV absorbance and the sizes of the unfragmented aRNA will be assessed using an Agilent bioanalyzer. aRNA will then be fragmented by incubating in Fragmentation buffer at  $94^{\circ}\text{C}$ .

1. Measure 1.5  $\mu$ l of the aRNA sample on NanoDrop Spectrophotometer using aRNA Elution Solution as blank (see Note 41).
2. Determine the yield of aRNA (see Note 42).
3. Analyzing aRNA size distribution using an Agilent bioanalyzer and RNA 6000 Nano chip kit following the manufacturer's instructions. Unfragmented aRNA should distribute between 250 and 5,500 nt with most between 600 and 1,200 nt.
4. Add 15  $\mu$ g of each aRNA to fresh nuclease-free tubes. Add Nuclease-free water to each tube so that the sample volume is 32  $\mu$ l.

5. Add 8  $\mu\text{l}$  of 5 $\times$  Array Fragmentation Buffer to each tube. Mixing thoroughly by vortexing and pulse spin. The total volume of each reaction is now 40  $\mu\text{l}$ .
6. Place the tubes on the thermal cycler and run the Fragmentation program:

94°C	35 min
4°C	Hold

7. Place the tubes on ice (see Note 43). Use fragmented aRNA immediately or *store at*  $-20^{\circ}\text{C}$ .

### 3.2.7. Target Hybridization

During this step, the fragmented aRNA will be diluted with a Hybridization mix. After being denatured on a thermal cycler, each sample will be loaded onto a Human Genome UI33 Plus 2.0 Array. The arrays are then placed into a hybridization oven and the samples are left to hybridize at  $45^{\circ}\text{C}$  for 16 h.

1. Thaw Control oligo B2 and 20 $\times$  Hybridization controls on ice. Heat the 20 $\times$  Hybridization controls to  $65^{\circ}\text{C}$  for 5 min to completely resuspend the aRNA. Take other hybridization reagents from the refrigerator.
2. Equilibrate the arrays to room temperature immediately before use. Label the arrays with corresponding sample names.
3. Turn on the hybridization oven and set the temperature to  $45^{\circ}\text{C}$  (see Note 44). Preheat for at least 1 h.
4. Prepare Hybridization master mix in a nuclease-free bottle provided in Kit 4 (see Note 45):

	Per sample, $\mu\text{l}$	16 Samples (10% extra), $\mu\text{l}$
Control oligo B2 (3 nM)	4.2	73.9
20 $\times$ Hybridization controls ( <i>bioB</i> , <i>bioC</i> , <i>bioD</i> , and <i>cre</i> )	12.5	220
2 $\times$ Hybridization mix	125	2,200
DMSO	25	440
Nuclease-free water	50	880
Total	216.7	3,813.9

5. Vortex the tube and centrifuge at  $1000\times g$  for 30 s.
6. Aliquot 216.7  $\mu\text{l}$  Hybridization master mix to each of 16 nuclease-free tubes. Add 33.3  $\mu\text{l}$  (12.5  $\mu\text{g}$ ) of each fragmented aRNA to the tubes. Mix thoroughly. The total volume of each reaction is now 250  $\mu\text{l}$ .
7. Turn on the computer and register all the samples in AGCC (project name, array name, barcode, and sample name) as detailed in Subheading 3.1 Turn off the computer.

8. Load the hybridization cocktails (fragmented aRNA + Hybridization master mix) to the arrays:
  - Heat the hybridization cocktails to 99°C for 5 min in a heat block.
  - While waiting, insert a 200 µl pipette tip into the upper right septum of each array. Wet the arrays with 200 µl of prehybridization mix by filling it through the lower left septum.
  - Incubate the arrays in the hybridization oven at 45°C for 10 min. Rotate at 60 rpm.
  - Transfer the hybridization cocktails from 99°C heat block to 45°C heat block. Keep at 45°C for 5 min.
  - Spin the hybridization cocktails at maximum speed for 10 min to precipitate any insoluble material.
  - Remove the arrays from the hybridization oven. Vent the array with a clean P200 pipette tip and extract the prehybridization mix from the array with a micropipettor. Refill the array with 200 µl of the clarified hybridization cocktail.
  - Cover the septa with the Tough-Spots (1/2 in.).
9. Put the arrays into the oven and make sure that the oven is balanced.
10. Allow the arrays to rotate at 45°C, 60 rpm for 16 h.

### 3.2.8. Washing, Staining, and Scanning Arrays

In this procedure, hybridized arrays are washed and stained with streptavidin–phycoerythrin conjugate using an automated protocol on the GeneChip Fluidics Station 450, followed by scanning on GeneChip Scanner 3000 7G.

1. Turn on the Fluidics Station and the computer.
2. Prime the station as in Subheading 3.1. Use Wash Buffer A and B in kit 4.
3. Remove the arrays from the hybridization oven. Vent the array by inserting a clean pipette tip into top right septum and extract the hybridization cocktail with a micropipettor through the remaining septum (see Note 46).
4. Refill the arrays with 250 µl of Wash Buffer A (see Note 47).
5. Take Stain Cocktail 1, Stain Cocktail 2, and Array Holding Buffer from kit 4 at 4°C.
6. Gently tap the bottles to mix well.
7. Add 600 µl of Stain Cocktail 1 into a 1.5-ml amber microfuge tube (see Note 48).
8. Add 600 µl of Stain Cocktail 2 into a 1.5-ml microfuge tube.
9. Add 800 µl of Array Holding Buffer into a 1.5-ml microfuge tube.
10. Spin down all vials to get rid of air bubbles.
11. Start the AGCC Fluidics Control Software.

12. Select the correct sample name. Select the protocol FS 450\_0001.
13. Start the protocol and follow the instructions in the LCD on the fluidics station.
14. Insert an array into the designated module of the fluidics station.
15. When “Load Vials 1–2–3” is shown on the LCD of the fluidics station, place the three vials into the sample holders 1, 2, and 3:
  - Place one vial containing 600  $\mu$ l Stain Cocktail 1 in sample holder 1.
  - Place one vial containing 600  $\mu$ l Stain Cocktail 2 in sample holder 2.
  - Place one vial containing 800  $\mu$ l Array holding buffer in sample holder 3.
16. Press down on the needle lever to start the run. The dialog box at the workstation terminal and LCD of the fluidics station will display the status of the washing and staining steps.
17. When staining is finished, removed the three vials containing stain and replace with three empty 1.5 ml tubes as prompted.
18. Remove the array from the fluidics stain.
19. Check the array window to make sure that there is no bubbles or air pockets.
20. If the array has no large bubble, it is ready for scanning. Arrays can be stored at 4°C in the dark for up to 24 h. Allow them warm up to room temperature before scanning.
21. After all the arrays have been stained, shut down the Fluidics station as detailed in Subheading 3.1.
22. If necessary, clean the glass surface of the array with Kimwipe. On the back of the array, clean excess fluid around the septa.
23. Cover both septa with Tough Spots (3/8 in.).
24. Turn on the scanner for 30 min before use. Click the AGCC Scan Control icon in the Affymetric Launcher.
25. Insert an array into the scanner.
26. Follow AGCC instructions and begin the scan.

---

## **4. Clinical Protocols for Genetic Pain Research**

### ***4.1. Limitations and Pitfalls of Genetic Association Studies***

The molecular methods described above are powerful means for identifying common variants influencing complex traits, genome wide screening to identifying SNPs that may be associated with a trait, or evaluating changes in the expression of these genes that may differ over time, across diseases and symptoms or contribute

to interindividual variability. Candidate gene association studies (CGAS) rely heavily on choosing genes on the basis of already-revealed biological processes. Owing to this limitation, CGAS can only identify genetic risk factors in which the pathophysiology is relatively well understood. However, most published CGAS for pain and analgesic responses show only weak associations and often fail to replicate in subsequent studies (11). This suggests that either the rationale for choosing the genes of interest or the particular SNPs has been biased by this prior knowledge of the pathophysiology, that the total number of comparisons made in performing the statistical analyses was not taken into account and resulted in a false positive association or other pitfalls inherent in association studies have biased the outcome (for discussion, see ref. 11).

The availability of high-throughput genotyping technology, as described in Subheading 3, allows whole-genome screening in GWAS. Currently available platforms allow the genotyping of more than one million SNPs, rapidly assessing a very large percentage of the genetic differences between individual samples. The sample sizes required are increased by the large number of hypotheses that are tested and create additional pressure to loosen criteria for subject enrollment but possibly confound the genetic association due to population stratification and enrollment of subjects who may not be fully comparable to others in the same phenotypic classification. Even if multistage association studies are done to narrow down the candidate genomic regions, a few thousand cases and controls may be needed, but collecting several thousand patients diagnosed with a single painful condition to result in a homogeneous population is very challenging.

Despite these powerful techniques, the availability of high-quality human reference genome and the ability to carefully characterize a clinical pain phenotype with quantitative sensory testing, there are still many potential pitfalls. Even for highly heritable phenotypes such as height, estimated as approximately 80%, the contribution of genetic variability for phenotypic expression of the characteristic suggests that phenotypic expression stems from multiple genetic and environmental factors. Pain has a lower degree of heritability and is likely a more complex phenomenon than height, making it unlikely that the influence of a single SNP on a pain phenotype may be extremely small. Statistical approaches vary highly across published studies (11) based on the nature of the outcome measured and reporting of corrections for multiple-test corrections. Population stratification can also produce false associations since the pattern of genetic variations and the rating of pain may not be uniform between ethnic populations. The potential for multiple factors that may produce spurious results and misleading conclusions in genetic studies of pain in humans suggests that only studies with careful designs followed by replication from independent groups and supportive laboratory data can be considered as well validated.

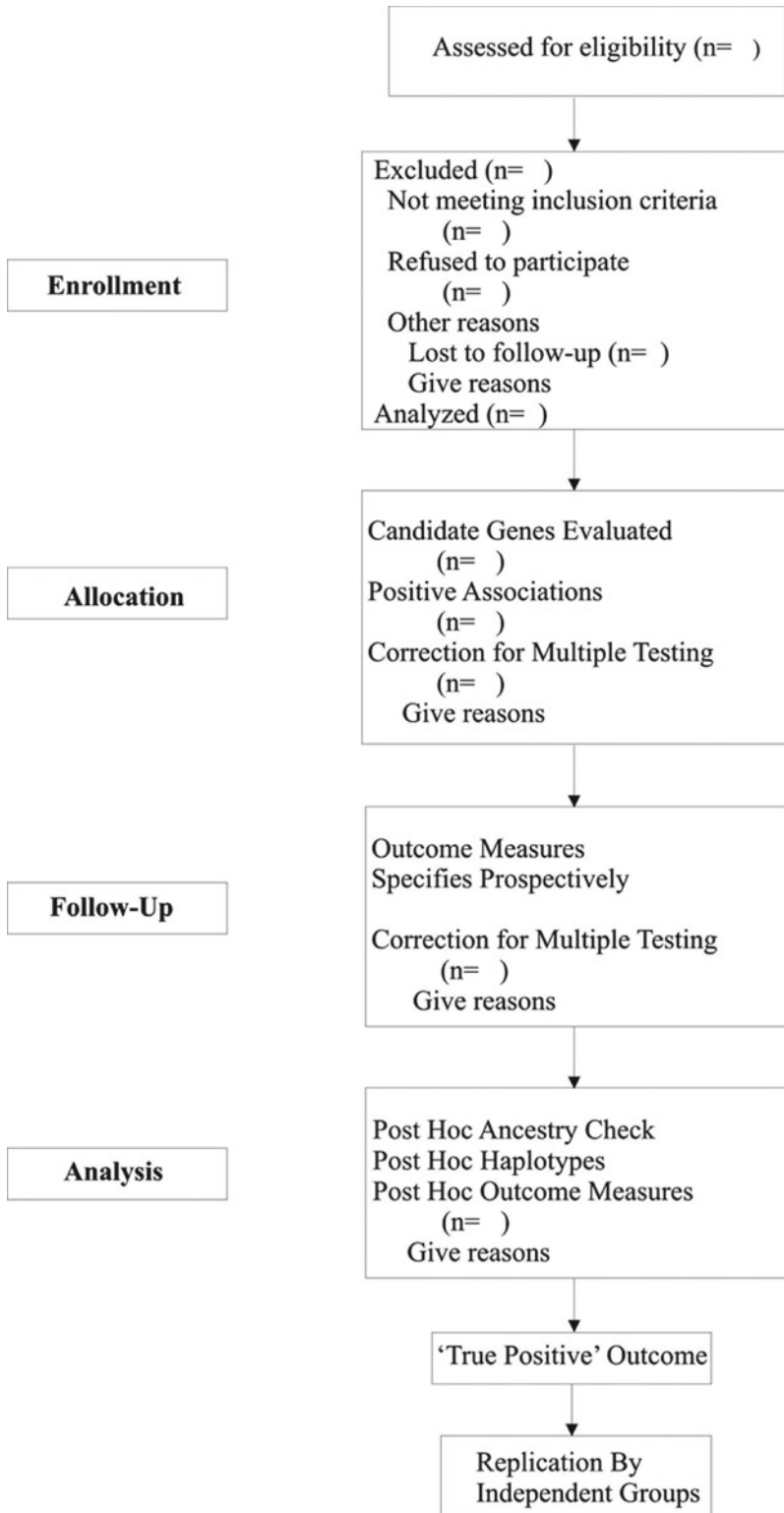


Fig. 3. CONSORT-like guideline for reporting genetic association data. Reproduced from ref. 11 with permission from Elsevier Inc.

*4.1.1. Recommendations  
for Reporting Clinical  
Genetic Pain Research  
Findings*

Population stratification, lack of adequate sample size, inappropriate choice of genetic variations, inevitable type 1 and 2 errors, and problematic statistical analysis along with publication bias are recognized problems in genetics research. The heterogeneity of pain and the interpretation of pain models also add complexity to study design and interpretation. Figure 3 presents a schematic approach to reporting possible sources of error in conducting genetic studies of pain modified from the CONSORT guidelines for reporting clinical trials data. Special attention to the steps unique to genetic studies that should be considered in evaluating genetic findings in clinical pain research includes the following:

- Size of the sample relative to the expected genetic effect.
- Definition of the phenotype and genotype (SNP versus haplotype).
- Stratification, Hardy–Weinberg equilibrium, and other sample population characteristics.
- Plausibility of the genes under study affecting the phenotype.
- Replication studies.
- Statistical issues associated with multiple comparisons.

---

## 5. Notes

1. The kits used in this protocol:
  - Kit 1: Genome-Wide Human SNP Nsp/Sty Assay kit 5.0/6.0 (Affymetrix).
  - Kit 2: TITANIUM DNA Amplification kit (Clontech).
  - Kit 3: GeneChip 3' IVT Express Kit (Affymetrix).
  - Kit 4: GeneChip Hybridization, Wash, and Stain Kit (Affymetrix).
2. Materials and reagents are listed when first required.
3. The gel contains ethidium bromide and should be placed in biohazard box after use.
4. DNA must be double-stranded and free of PCR inhibitors. We isolate human genomic DNA from white blood cells using the Puregene™ DNA isolation kit (Gentra Systems Inc.). Genomic DNA extracted with QIAamp DNA Blood Maxi kit (Qiagen) has also been tested successfully with the Assay.
5. Always place 96-well plate in a cooling chamber (single or double based on the number of plate handled in the same time) on ice.
6. When making master mix, keep all reagents (except enzymes) in a cooling chamber on ice and mix each component thoroughly

by vortexing for 3 s and pulse-spin before adding to the tube. Leave the enzyme at  $-20^{\circ}\text{C}$  until ready to use. Enzymes must not be vortexed. They should be spun down immediately before use. Mix the master mix thoroughly by vortexing and centrifugation. Always transport enzymes (and other reagents) in a Benchtop StrataCooler (Stratagene).

7. When vortex a 96-well plate, always seal the plate tightly with adhesive film and vortex the plate at three different places for 1 s each.
8. Preset all the programs for convenience.
9. Aliquot the T4 DNA ligase Buffer (10 $\times$ ) after thawing on ice for the first time to avoid multiple freeze–thaw cycle.
10. Do not add TITANIUM Taq DNA Polymerase until ready to aliquot the master mix to ligated samples.
11. Change the pipette tips after each dispense when adding the PCR master mix to avoid cross-contamination.
12. PCR products can also be verified using E-gel 48 2% agarose gel (Invitrogen).
13. The surface changes from shiny to matte when dry. There should be no standing liquid in any of the wells.
14. Do not completely seal the plate with tape.
15. Dispense as close to the beads as possible without touching them. If using Rainin tips, rest the ridge of the pipette tip on the lip of the plate when pipetting. Buffer EB should be applied directly on top of the beads.
16. This process may take several tries before the pressure catches on.
17. Do not proceed if the number falls outside of the range.
18. Do not take out the fragmentation reagent. It is extremely temperature sensitive. Handle the tube by the cap only. Dilute immediately prior to use. Transport and hold in a  $-20^{\circ}\text{C}$  cooler.
19. The concentration of the Fragmentation Reagent varies. Check the tube label before diluting the reagent to 0.1 U/ $\mu\text{l}$ .
20. The reagent is viscous. Pipette slowly and avoid excess solution on the outside of the pipette tip.
21. The success of fragmentation is confirmed by the presence of a smear of less than 200 bp in size.
22. Add TMCAL first. Pipette DMSO to the solution to avoid touching the side wall of the tube. Hybridization master mix can be made ahead of time in a larger volume, aliquoted out 11 ml and stored for up to 1 week at  $-20^{\circ}\text{C}$ .
23. Slightly cover the middle window to make it easy for later removal.

24. Do not allow loaded arrays to sit at room temperature for more than 1.5 min. Load no more than 32 Arrays in one hybridization oven at a time. Do not place arrays next to each other without spacing at least one section.
25. Priming ensures the lines of the fluidics station are filled with the appropriate buffers and should be done:
  - When the fluidics station is first started.
  - When wash solutions are changed.
  - Before washing, if a shutdown has been performed.
  - If the LCD window instructs to do so.
26. Arrays can be stored in the Array Holding Buffer at 4°C for up to 3 h before washing and staining.
27. If a bubble is present, do not return the array to array holder. Manually fill the array with Array Holding Buffer.
28. The Tough Spots used here are smaller than the previous ones so that they will not interfere with the scanning process.
29. Total RNA can be isolated from tissues or blood samples using Trizol Reagent (Invitrogen), RNeasy Mini kit (Qiagen), or PAXgene Blood RNA kit (Qiagen).
30. Use 50–500 ng of total RNA. If necessary, concentrate the total RNA by vacuum centrifugation.
31. First-Strand cDNA Synthesis mix includes T7-(N)<sub>6</sub> primers and SuperScript reverse transcriptase which can also be purchased separately (Affymetrix and Invitrogen).
32. Do not use water bath or heat block. Incubate all reactions in a thermal cycler. Preset all the programs for convenience.
33. Subjecting the reaction to temperatures over 16°C will affect aRNA yield. Disable the heated lid or keep the lid off during the second-strand cDNA synthesis.
34. Optimal IVT incubation time is sample-type and RNA-amount dependent, and should be determined empirically. Overnight IVT reaction time has been shown to maximize the labeled cRNA yield. If a shorter incubation time (4 h) is desired, 1 μl (200 U) of T7 RNA polymerase (Ambion) can be added to each reaction.
35. Setting 4 on the Barnstead/Lab-line Titer Plate Shaker (Model # 4625) or setting 1 on Boekel “Jitterbug” Plate Shaker (Model # 130000).
36. When capture is complete, the mixture becomes transparent and the RNA Binding Beads will form pellets.
37. Setting 7 on the Barnstead/Lab-line Titer Plate Shaker or setting 4 on Boekel Jitterbug Plate Shaker.

38. Setting 10 on the Barnstead/Lab-line Titer Plate Shaker or setting 7 on Boekel Jitterbug Plate Shaker.
39. Check to make sure that the RNA Binding Beads are fully dispersed.
40. Purified aRNA can be stored at  $\leq -20^{\circ}\text{C}$  for up to 1 year, but the number of freeze–thaw cycles should be minimized to maintain aRNA integrity.
41. We use NanoDrop for its convenience. No dilutions or cuvettes are needed. aRNA concentration can also be determined by using traditional spectrophotometer (reading at 260 nm) or by using RiboGreen (Invitrogen). Follow the manufacturer’s instructions for using RiboGreen.
42. aRNA yield from equal amounts of total RNA from different sources may vary considerably. If necessary, concentrate the aRNA by vacuum centrifugation using medium or low heating setting.
43. The success of the fragmentation can be confirmed by assessing 300 ng of fragmented aRNA using an Agilent bioanalyzer and RNA 6000 Nano chip kit. The reaction should produce a distribution of 35–200 nt aRNA fragment with a peak at approximately 100–120 nt.
44. The hybridization temperature is  $45^{\circ}\text{C}$  instead of  $50^{\circ}\text{C}$  which is used in GWAS SNP array.
45. This is the standard format. For midi, mini or micro array format, please refer to manufacturer’s guide. Make sure that DMSO is completely thawed when first used. Store DMSO at room temperature after the first use.
46. The used hybridization cocktails can be rehybridized on another array if necessary. Store the cocktail at  $-20^{\circ}\text{C}$ .
47. The arrays in Wash Buffer A can be store at  $4^{\circ}\text{C}$  for up to 3 h before proceeding to washing and staining. Equilibrate the arrays to room temperature before washing and staining.
48. Stain Cocktail 1 is light-sensitive.

## References

1. Zubieta, J. K., Heitzeg, M. M., Smith, Y. R., Bueller, J. A., Xu, K., Xu, Y., Koeppe, R. A., Stohler, C. S., and Goldman, D. (2003) COMT val158met genotype affects mu-opioid neurotransmitter responses to a pain stressor, *Science* **299**, 1240–1243.
2. Klepstad, P., Rakvag, T. T., Kaasa, S., Holthe, M., Dale, O., Borchgrevink, P. C., Baar, C., Vikan, T., Krokan, H. E., and Skorpen, F. (2004) The 118 A > G polymorphism in the human mu-opioid receptor gene may increase morphine requirements in patients with pain caused by malignant disease, *Acta Anaesthesiol Scand* **48**, 1232–1239.
3. Mogil, J. S., Ritchie, J., Smith, S. B., Strasburg, K., Kaplan, L., Wallace, M. R., Romberg, R. R., Bijl, H., Sarton, E. Y., Fillingim, R. B., and Dahan, A. (2005) Melanocortin-1 receptor gene variants affect pain and mu-opioid analgesia in mice and humans, *J Med Genet* **42**, 583–587.

4. Janicki, P. K., Schuler, G., Francis, D., Bohr, A., Gordin, V., Jarzembowski, T., Ruiz-Velasco, V., and Mets, B. (2006) A genetic association study of the functional A118G polymorphism of the human mu-opioid receptor gene in patients with acute and chronic pain, *Anesth Analg* **103**, 1011–1017.
5. Tegeder, I., Costigan, M., Griffin, R. S., Abele, A., Belfer, I., Schmidt, H., Ehner, C., Nejm, J., Marian, C., Scholz, J., Wu, T., Allchorne, A., Diatchenko, L., Binshtok, A. M., Goldman, D., Adolph, J., Sama, S., Atlas, S. J., Carlezon, W. A., Parsegian, A., Lotsch, J., Fillingim, R. B., Maixner, W., Geisslinger, G., Max, M. B., and Woolf, C. J. (2006) GTP cyclohydrolase and tetrahydrobiopterin regulate pain sensitivity and persistence, *Nat Med* **12**, 1269–1277.
6. Diatchenko, L., Nackley, A. G., Slade, G. D., Bhalang, K., Belfer, I., Max, M. B., Goldman, D., and Maixner, W. (2006) Catechol-O-methyltransferase gene polymorphisms are associated with multiple pain-evoking stimuli, *Pain* **125**, 216–224.
7. Lee, Y. S., Kim, H., Wu, T. X., Wang, X. M., and Dionne, R. A. (2006) Genetically mediated interindividual variation in analgesic responses to cyclooxygenase inhibitory drugs, *Clin Pharmacol Ther* **79**, 407–418.
8. Reyes-Gibby, C. C., Shete, S., Ravvag, T., Bhat, S. V., Skorpen, F., Bruera, E., Kaasa, S., and Klepstad, P. (2007) Exploring joint effects of genes and the clinical efficacy of morphine for cancer pain: OPRM1 and COMT gene, *Pain* **130**, 25–30.
9. Tabor, H. K., Risch, N. J., and Myers, R. M. (2002) Candidate-gene approaches for studying complex genetic traits: practical considerations, *Nat Rev Genet* **3**, 391–397.
10. Kim, H., and Dionne, R. A. (2007) Lack of influence of GTP cyclohydrolase gene (GCH1) variations on pain sensitivity in humans, *Mol Pain* **3**, 6.
11. Kim, H., Clark, D., and Dionne, R. A. (2009) Genetic contributions to clinical pain and analgesia: avoiding pitfalls in genetic research, *J Pain* **10**, 663–693.
12. Scuteri, A., Sanna, S., Chen, W. M., Uda, M., Albai, G., Strait, J., Najjar, S., Nagaraja, R., Orru, M., Usala, G., Dei, M., Lai, S., Maschio, A., Busonero, F., Mulas, A., Ehret, G. B., Fink, A. A., Weder, A. B., Cooper, R. S., Galan, P., Chakravarti, A., Schlessinger, D., Cao, A., Lakatta, E., and Abecasis, G. R. (2007) Genome-wide association scan shows genetic variants in the FTO gene are associated with obesity-related traits, *PLoS Genet* **3**, e115.
13. Salonen, J. T., Uimari, P., Aalto, J. M., Pirskanen, M., Kaikkonen, J., Todorova, B., Hypponen, J., Korhonen, V. P., Asikainen, J., Devine, C., Tuomainen, T. P., Luedemann, J., Nauck, M., Kerner, W., Stephens, R. H., New, J. P., Ollier, W. E., Gibson, J. M., Payton, A., Horan, M. A., Pendleton, N., Mahoney, W., Meyre, D., Delplanque, J., Froguel, P., Luzzatto, O., Yakir, B., and Darvasi, A. (2007) Type 2 diabetes whole-genome association study in four populations: the DiaGen consortium, *Am J Hum Genet* **81**, 338–345.
14. Plenge, R. M., Seielstad, M., Padyukov, L., Lee, A. T., Remmers, E. F., Ding, B., Liew, A., Khalili, H., Chandrasekaran, A., Davies, L. R., Li, W., Tan, A. K., Bonnard, C., Ong, R. T., Thalamuthu, A., Pettersson, S., Liu, C., Tian, C., Chen, W. V., Carulli, J. P., Beckman, E. M., Altschuler, D., Alfredsson, L., Criswell, L. A., Amos, C. I., Seldin, M. F., Kastner, D. L., Klareskog, L., and Gregersen, P. K. (2007) TRAF1-C5 as a risk locus for rheumatoid arthritis – a genomewide study, *N Engl J Med* **357**, 1199–1209.
15. Duerr, R. H., Taylor, K. D., Brant, S. R., Rioux, J. D., Silverberg, M. S., Daly, M. J., Steinhardt, A. H., Abraham, C., Regueiro, M., Griffiths, A., Dassopoulos, T., Bitton, A., Yang, H., Targan, S., Datta, L. W., Kistner, E. O., Schumm, L. P., Lee, A. T., Gregersen, P. K., Barmada, M. M., Rotter, J. I., Nicolae, D. L., and Cho, J. H. (2006) A genome-wide association study identifies IL23R as an inflammatory bowel disease gene, *Science* **314**, 1461–1463.
16. Kim, H., Ramsay, E., Lee, H., Wahl, S., and Dionne, R. A. (2009) Genome-wide association study of acute post-surgical pain in humans, *Pharmacogenomics* **10**, 171–179.
17. Rockman, M. V., and Kruglyak, L. (2006) Genetics of global gene expression, *Nat Rev Genet* **7**, 862–872.
18. Wang, X. M., Wu, T. X., Lee, Y. S., and Dionne, R. A. (2006) Rofecoxib regulates the expression of genes related to the matrix metalloproteinase pathway in humans: implication for the adverse effects of cyclooxygenase-2 inhibitors, *Clin Pharmacol Ther* **79**, 303–315.
19. Wang, X. M., Wu, T. X., Hamza, M., Ramsay, E. S., Wahl, S. M., and Dionne, R. A. (2007) Rofecoxib modulates multiple gene expression pathways in a clinical model of acute inflammatory pain, *Pain* **128**, 136–147.
20. Wang, X. M., Hamza, M., Gordon, S. M., Wahl, S. M., and Dionne, R. A. (2008) COX inhibitors downregulate PDE4D expression in a clinical model of inflammatory pain, *Clin Pharmacol Ther* **84**, 39–42.

21. Wang, X. M., Hamza, M., Wu, T. X., and Dionne, R. A. (2009) Upregulation of IL-6, IL-8 and CCL2 gene expression after acute inflammation: Correlation to clinical pain, *Pain* **142**, 275–283.
22. Pearson, T. A., and Manolio, T. A. (2008) How to interpret a genome-wide association study, *JAMA* **299**, 1335–1344.
23. Kennedy, G. C., Matsuzaki, H., Dong, S., Liu, W. M., Huang, J., Liu, G., Su, X., Cao, M., Chen, W., Zhang, J., Liu, W., Yang, G., Di, X., Ryder, T., He, Z., Surti, U., Phillips, M. S., Boyce-Jacino, M. T., Fodor, S. P., and Jones, K. W. (2003) Large-scale genotyping of complex DNA, *Nat Biotechnol* **21**, 1233–1237.

## Two-Dimensional Gel Electrophoresis: Discovering Neuropathic Pain-Associated Synaptic Biomarkers in Spinal Cord Dorsal Horn

Om V. Singh and Yuan-Xiang Tao

### Abstract

Nerve injury-induced neuropathic pain is a major public health problem worldwide. Current treatment for neuropathic pain has had limited success because the mechanisms that underlie the induction and maintenance of neuropathic pain are incompletely understood. However, recent advances in proteomics may allow us to uncover complicated biological mechanisms that occur under neuropathic pain conditions. Here, we introduce a combined approach of two-dimensional gel electrophoresis (2-DE) with mass spectrometry (MS) to identify the expression changes in synaptosome-associated proteins in spinal cord dorsal horn after unilateral fifth spinal nerve injury. In 2-DE, a set of highly abundant synaptic proteins with a *pI* range of 4–7 are separated and compared by size fractionation (25–100 kDa). Then, the differentially expressed proteins are identified and validated by MS, and their potential involvement in physiological and pathological processes is searched. Thus, proteomic analysis can provide expression profiles of synaptic proteins and their posttranslational modifications in cells, tissues, and organs of the nervous system under neuropathic pain conditions.

**Key words:** Proteomics, Two-dimensional gel electrophoresis, Spinal cord dorsal horn, Spinal nerve injury, Synaptosomal fraction

---

### 1. Introduction

Neuropathic pain is a major clinical syndrome that results from disease or dysfunction in the nervous system, such as from peripheral nerve injury or spinal cord injury (1). Current treatment for this disorder has had limited success because our understanding of the mechanisms that underlie the induction and maintenance of neuropathic pain is still incomplete. Peripheral nerve insult-induced pre- and posttranslational changes in expression and function of receptors, enzymes, and voltage-dependent ion channels in primary

afferent neurons of the dorsal root ganglion and at synapses in the pathway for nociception in the central nervous system might contribute to pain hypersensitivity in neuropathic pain (2–7). Changes in the expression of some genes and their translational protein products in pain-related regions after peripheral nerve injury have been reported (6, 7). However, these studies have shown changes related to selected genes and proteins of interest. The global changes in pain-related regions remain to be explored under neuropathic pain conditions.

Proteomic analysis can provide expression profiles of proteins and their posttranslational modifications in cells, tissues, and organs. Recently, we combined the approaches of two-dimensional gel electrophoresis (2-DE) and mass spectrometry (MS) to report that peripheral nerve injury produced changes not only in synaptic protein expression but also in synaptic protein trafficking in dorsal horn neurons (5). These changes might participate in the central mechanism that underlies the maintenance of neuropathic pain. Here, we introduce the method to identify changes in the expression of synaptosome-associated proteins in spinal cord dorsal horn after unilateral fifth spinal nerve injury (SNI). We first present how to prepare the SNI model and isolate the crude synaptosomal fraction derived from spinal dorsal horn of rats. Then, we describe how to carry out 2-DE in combination with MS to examine the global changes of synaptosome-associated proteins in dorsal horn. Finally, we briefly describe the use of Western blot analysis to further validate the proteomic analysis.

---

## 2. Materials

### 2.1. Animals

Male Sprague–Dawley Rats (250–350 g).

### 2.2. Buffer for Synaptosomal Membrane Fractionation

1. Buffer A: 10 mM Tris–HCl (pH 7.4), 250 mM sucrose, 2 mM EGTA, 1 mM PMSF, 1 mM benzamidine, and 40  $\mu$ M leupeptin.
2. Modified 2-DE lysis buffer: 9 M urea, 4% CHAPS, 20 mM Tris–HCl (pH 8.8).

### 2.3. Sample Preparation for 2-DE

1. Protein analysis and sample cleanup kits: RC-DC protein analysis kit (Bio-Rad, Hercules, CA, USA), and 2-D cleanup kit (GE Healthcare, Piscataway, NJ, USA).
2. Rehydration buffer: 8 M urea, 2 M thiourea, 4% CHAPS, 40 mM dithiothreitol (DTT), 0.5% carrier ampholyte (pH 4–7), 0.002% bromophenol blue (*w/v*). Buffer should be stored at  $-20^{\circ}\text{C}$  and thawed at room temperature before use.
3. Protein rehydration: passive rehydration in disposable rehydration/equilibration trays (Bio-Rad) and active rehydration in PROTEAN<sup>®</sup> isoelectric focusing (IEF) trays (Bio-Rad).

4. Immobilized pH gradient (IPG) strips: ReadyStrip™, 17 cm, pH 4–7 (Bio-Rad). IPG strips must be stored at  $-20^{\circ}\text{C}$  or as recommended by the manufacturer.
5. First-dimension IEF: PROTEAN® IEF cell (Bio-Rad). Make paper wicks 5–6 mm in length using Whatman #1 filter paper (Millipore, Billerica, MA, USA); mineral oil (Sigma, St. Louis, MO, USA).
6. Equilibration buffer:
  - (a) Buffer I: 6 M urea, 2% SDS, 0.375 M Tris–HCl (pH 8.8), 20% glycerol. Add fresh 130 mM DTT before each use. Store at  $-20^{\circ}\text{C}$ , and thaw at room temperature before use.
  - (b) Buffer II: 6 M urea, 2% SDS, 0.375 M Tris–HCl (pH 8.8), 20% glycerol. Add fresh 135 mM iodoacetamide (IAA) before each use. Store at  $-20^{\circ}\text{C}$  and thaw at room temperature before use.
7. TGS buffer (1×): 25 mM Tris–HCl (pH 8.3), 192 mM glycine, and 0.1% (*w/v*) SDS. 1× TGS can be stored at room temperature.
8. Overlay agarose: 0.5% agarose (low melting grade) in 1× TGS.
9. Second-dimension SDS–PAGE:
  - (a) 30% Acrylamide/bis solution (37.5:1) (this is a neurotoxin when unpolymerized—care should be taken to avoid exposure).
  - (b) *N,N,N',N'*-tetramethylethylenediamine (TEMED, Bio-Rad). TEMED can be stored at room temperature.
10. Ammonium persulfate: prepare 10% solution in water (see Note 1) and immediately freeze in single-use aliquots of 1 ml at  $-20^{\circ}\text{C}$ .
11. Water-saturated isobutanol: shake equal volumes of water and isobutanol in a glass bottle and allow to separate; use top layer. Solution can be stored at room temperature.
12. Running buffer: 1× TGS as described in step 7 above.
13. Second-dimension gel electrophoresis: Ettan™ DALT six large Vertical System (GE Healthcare).
14. 2-DE gel image development: SilverQuest™ silver staining kit (Invitrogen, Carlsbad, CA, USA).
15. Image acquisition: Molecular Imager FX (Bio-Rad).
16. Spot pattern analysis: Progenesis Nonlinear Dynamics software version 2005.

#### **2.4. Protein In-Gel Digestion and Peptide Extraction**

1. Protein spot excision: Spot Picker, 1.5 mm (The Gel Company, San Francisco, CA, USA).
2. Destaining solutions (see Note 2):
  - (a) Solution I: 30 mM potassium ferrocyanide.
  - (b) Solution II: 100 mM sodium thiosulfate.

3. Protein digestion solution: sequencing-grade modified trypsin (Promega, Madison, WI, USA). Stock solution: prepare 500 ng/ $\mu$ l by adding 40  $\mu$ l 1% acetic acid solution to one vial of 20  $\mu$ g trypsin. Divide into eight tubes with 5  $\mu$ l in each tube and store at  $-20^{\circ}\text{C}$ . Working solution: dilute stock solution into 10 ng/ $\mu$ l immediately before use by adding 2.5–122.5  $\mu$ l of 10 mM ammonium bicarbonate ( $\text{NH}_4\text{HCO}_3$ ).
4. Peptide extraction: 0.1% trifluoroacetic acid (TFA) in 60% acetonitrile (ACN).
5. Peptide purification: ZipTip C18, P10 tip size (Millipore).
6. Wetting solution: 50% ACN in 0.1% TFA solution in water.
7. Equilibration and washing solution: 0.1% TFA in water.
8. Wash solution: 5% methanol in 0.1% TFA in water.
9. Matrix solution: 10 mg matrix  $\alpha$ -cyano-4-hydroxy-cinnamic acid (CHCA) (Sigma) in 60% ACN.
10. Centrifugal vacuum concentrator such as the Vacufuge by Eppendorf (Eppendorf, Brinkman Instr. Inc., NY, USA).

**2.5. Mass Spectrometry and Peptide Mass Fingerprinting**

1. Peptide standards (Sigma): prepare by adding 1.5  $\mu$ l bradykinin, 0.5  $\mu$ l ACTH, 2.0  $\mu$ l insulin from 10 pmol/ $\mu$ l stock solutions to 6  $\mu$ l matrix solution. All peptide stock solutions should be stored at  $-20^{\circ}\text{C}$ .
2. Matrix-assisted laser desorption ionization (MALDI)–time of flight (TOF) mass spectrometer (Voyager DE-STR, Applied-Biosystems, Inc., Framingham, MA, USA).
3. Peptide-loading platform: MALDI plate (Applied-Biosystems, Inc.).
4. Peptide Mass Fingerprinting (PMF) Online peptide search engines:
  - (a) ProFound-peptide mapping.
  - (b) MS-Fit.
  - (c) MASCOT Peptide Mass Fingerprint equipped with NCBItr and Swiss-Prot databases.

---

## 3. Methods

### 3.1. SNI-Induced Neuropathic Pain Model

1. Sterilize all surgical instruments.
2. The surgeon should wash his hands before performing surgery, and wear a cap, gown, mask, and gloves.
3. Induction of anesthesia is with 3% isoflurane, and anesthesia is maintained with 1.5% isoflurane.
4. Place the rat in a prone position.

5. Clean the rat's skin with Betadine solution and ethanol and then make a dorsolateral incision into the skin of the lower back.
6. Identify the transverse process of L6, free it from its muscle attachments, and then remove it.
7. Isolate the underlying L5 nerve root, ligate it with a 6-0 silk suture, and transect it just distal to the ligation.
8. After appropriate hemostasis, close the muscle layer with chromic gut, and suture the skin with either silk suture or surgical staples.
9. In a control group, repeat the surgical procedure as described above, but do not ligate or transect the spinal nerve.
10. After surgery, return the rat to its cage and observe it for any signs of motor deficits.
11. Any animal that shows signs of paralysis should be euthanized.
12. At 14 days post-surgery, the animals are decapitated, and spinal cord is collected and stored at  $-80^{\circ}\text{C}$ .

### **3.2. Fractionation of Synaptosome- Associated Proteins**

1. Place the tissue in 0.4–1.0 ml Buffer A in 15-ml tubes. Homogenize it with a Polytron tissue grinder four times for 30 s each time, resting 30 s between each time.
2. Centrifuge the homogenate at  $900 \times g$  for 15 min at  $4^{\circ}\text{C}$ . The supernatant (S1; total soluble protein) is collected and the pellet (P1; nuclei fraction) discarded.
3. Centrifuge the supernatant in an ultracentrifuge at  $10,000 \times g$  for 20 min at  $4^{\circ}\text{C}$ .
4. After the centrifugation, the supernatant (S2, crude cytosolic fraction) and pellet (P2, crude synaptosomal membrane) are collected.
5. Lyse the P2 hypo-osmotically in 500  $\mu\text{l}$  of  $\text{dH}_2\text{O}$  for 1 min on ice and then centrifuge it at  $25,000 \times g$  for 30 min at  $4^{\circ}\text{C}$ .
6. After the centrifugation, the pellet (P3, synaptosomal fraction) is collected, and the supernatant (S3) is discarded.
7. P3 is considered the synaptosomal membrane fraction and is stored at  $-80^{\circ}\text{C}$  for later use.

### **3.3. Sample Preparation for 2-DE**

1. Dissolve the synaptosomal membrane fraction (P3) in 2-DE lysis buffer. Measure the protein concentration in the P3 fraction with the Bio-Rad RC-DC kit as recommended in the manufacturer's protocol. Because urea interferes in the Lowery method of protein measurement, it should be removed first (see Note 3).
2. Clean approximately 50  $\mu\text{g}$  of protein with the 2-D cleanup kit. Follow the directions for protein purification as described in the manufacturer's recommended protocol.

3. Dissolve the pellet in 300  $\mu$ l IEF rehydration buffer (see Note 4). Centrifuge the dissolved protein solution at  $12,000 \times g$  for 10 min at room temperature to settle the impurities.

### **3.4. First-Dimension Gel Electrophoresis**

1. Using forceps, place the paper wicks at both ends of the PROTEAN IEF focusing tray. Wet the paper wicks by pipetting 10  $\mu$ l of deionized water onto each wick. Then load the sample in rehydration buffer (300  $\mu$ l) onto the rehydration tray (see Note 5).
2. Using forceps, place the precast ReadyStrip IPG strip (17 cm, pH 4–7) in the PROTEAN IEF focusing tray for active rehydration. Place the strip gel-side down onto the sample (see Note 6). Cover each strip with 2 ml of mineral oil to prevent evaporation during the rehydration process. Cover the tray with a plastic lid (see Note 7).
3. Rehydrate the IPG strip for 12 h at 35°C at 50 V followed by isoelectric focusing of proteins using following sequential conditions: (a) 250 V for 20 min on linear ramp, (b) 10,000 V for 2 h on linear ramp, (c) 10,000 V at 45,000 V/h on rapid ramp, and (d) hold at 500 V on rapid ramp until IPG strips are removed from the first dimension (see Note 8).
4. After completion of the first dimension, carefully remove the strips and hold them vertically for 10–15 s to remove the excess mineral oil. Rinse the IPG strips in running water, place them onto a piece of dry filter paper, and blot them with a second piece of wet filter paper (see Note 9).
5. Before beginning the second dimension of gel electrophoresis, equilibrate the focused proteins on the IPG strips by placing the strips in the equilibration tray in 5 ml of equilibration buffer I with freshly added 130 mM DTT. Keep them oriented with the gel side facing upward. Shake them gently for 10 min on an orbital shaker at room temperature.
6. Decant the equilibration buffer I and add buffer II (with fresh 135 mM IAA). Gently shake the IPG strips for 10 min on the orbital shaker at room temperature.
7. During the second equilibration step, melt the overlay agarose in a microwave oven.

### **3.5. Preparation of Molecular Weight Marker for Second Dimension Gel Electrophoresis**

1. Regardless of the specified pH, rehydrate the IPG strips (7 cm) under passive conditions in disposable rehydration/equilibration trays with 75  $\mu$ l Precision Plus Protein Standards marker for 12 h at room temperature. Store the rehydrated IPG strips at 4°C (see Note 10).
2. Before beginning the second dimension gel electrophoresis, cut the IPG strips to 4–8 mm in size and place them on the second dimension SDS-PAGE.

**3.6. Protein Separation  
by Second Dimension  
Gel Electrophoresis  
on SDS-PAGE**

1. The protocol given here uses the Ettan™ DALT six-large-vertical-gel system, but the instructions can be adapted to other formats of gel systems. The glass plates for the 2-DE gels should be cleaned with laboratory-grade detergent after use and rinsed extensively with distilled water.
2. Prepare a 1.0-mm thick, 10% gel by mixing 16.6 ml 30% acrylamide/bis solution (37.5:1) with 20 ml sterile deionized water, 12.5 ml of 1.5 M Tris-HCl (pH 8.8), 0.5 ml of 10% SDS solution, 0.5 ml of 10% ammonium persulfate solution, and 20  $\mu$ l of TEMED.
3. Pour the gel, leaving about 1.0 cm of space for the IPG strips, and overlay with 1 ml distilled water. The total time for polymerization of a 24-cm gel is approximately 2–3 h longer than for the minigel (7 cm) (see Note 11).
4. During the gel polymerization, prepare 1 $\times$  running buffer by diluting 500 ml 10 $\times$  TGS buffer with 4,500 ml of water in a measuring cylinder and pouring into the assembly chamber up to the designated mark. The attached circulatory pump is then turned on to mix the buffer.
5. Fill a 100-ml graduated cylinder or tube the same length or longer than the IPG strips with 1 $\times$  TGS buffer. Remove bubbles on the surface of the buffer with a Pasteur pipette. Grasp the IPG strips with forceps and wash them by immersing them in the 1 $\times$  TGS buffer to rinse off the extra equilibration buffer.
6. Fill the empty space on the top of the SDS gel with 1 $\times$  TGS buffer. Place the IPG strips on one side of the glass plate on top of the gel and push them slightly into the solution with forceps and a spatula (see Note 12). The forceps and spatula should push on the plastic backing of the strip and not the gel matrix.
7. Once the IPG strips are set on the top of the gel, excess 1 $\times$  TGS can be poured off by inclining the gel on one side. Load a pre-rehydrated piece of molecular weight marker toward the acidic end (+ve) (see Note 13). Overlay the IPG strips with melted agarose covering solution.
8. Fill the gel unit assembly with 1 $\times$  TGS up to the mark as recommended by manufacturer. Connect the unit to a power supply and run at 50 V for 30 min. Adjust to 100 W and run until the blue dye front arrives at the bottom of the gel (~5–6 h) (see Note 14).

**3.7. Image Acquisition  
and 2-DE Gel Spot  
Pattern Analysis**

1. After completion of the second dimension, remove the 2-DE gels from the glass plates under flowing water.
2. Stain the 2-DE gels with the MS-compatible SilverQuest™ Silver staining kit as described in the manufacturer's manual. Obtain images of the silver-stained gel with the Molecular

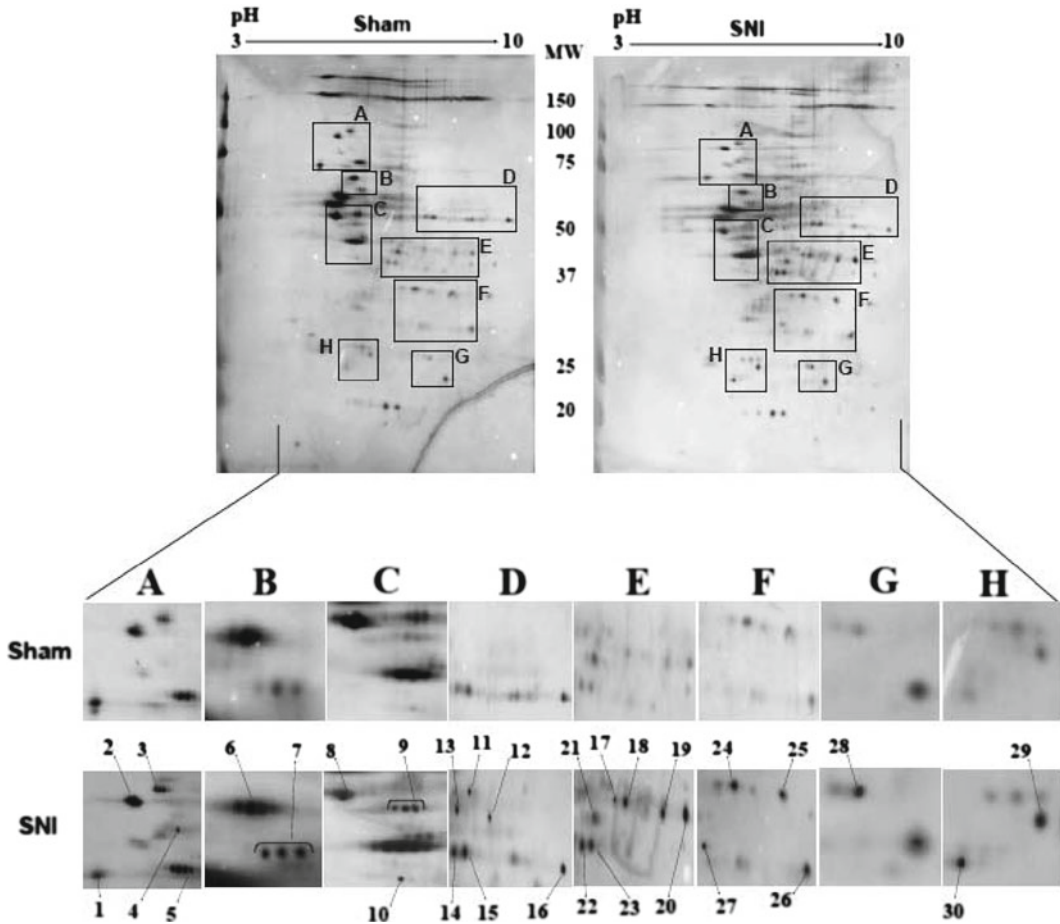


Fig. 1. A comparison of the proteome maps of silver-stained 2-DE gels shows expression of synaptosome-associated proteins in the ipsilateral dorsal horns of the fifth lumbar spinal cord segments derived from sham-operated and SNI rats. Protein lysate was prepared as described in the Subheading 3. Total protein (50  $\mu$ g) underwent isoelectric focusing onto an IPG strip (pH 3–10 nonlinear) and was separated on a 10% SDS–PAGE gel. Proteins were visualized by MS-compatible silver staining. The images were scanned and analyzed for protein differential expression using Progenesis Nonlinear Dynamic software (version 2005). The zoomed areas A through H from two gels show informative regions that were identified to have a high number (protein spots 1–30) of >2-fold differentially expressed proteins/enzymes (e.g., protein spot 7, neuronal acetylcholine receptor protein; protein spot 12, GABA(A) receptor; protein spot 14, serotonin receptor 2A) and molecular chaperones (e.g., protein spot 2, HSP 90- $\beta$ ; protein spot 4, HSP70; and protein spot 29, HSP  $\beta$ -8) in sham (*left*) versus SNI (*right*) represented by *arrows*. The corresponding protein gel spots were excised, trypsinized, and analyzed by MALDI-TOF MS. The proteins were then subsequently identified by peptide mass fingerprints as shown in Table 1.

Imager FX. Figure 1 shows consistently reproducible images of the total protein profile of sham-operated and SNI rats.

3. After being stained, gels can be stored in 30% ethanol at room temperature until punched for protein spots.
4. Any sets of experiments that will be compared directly should be run and silver stained in parallel. The images are further processed for spot detection, gel alignment, and spot quantification by match ratio using Progenesis Nonlinear Dynamics

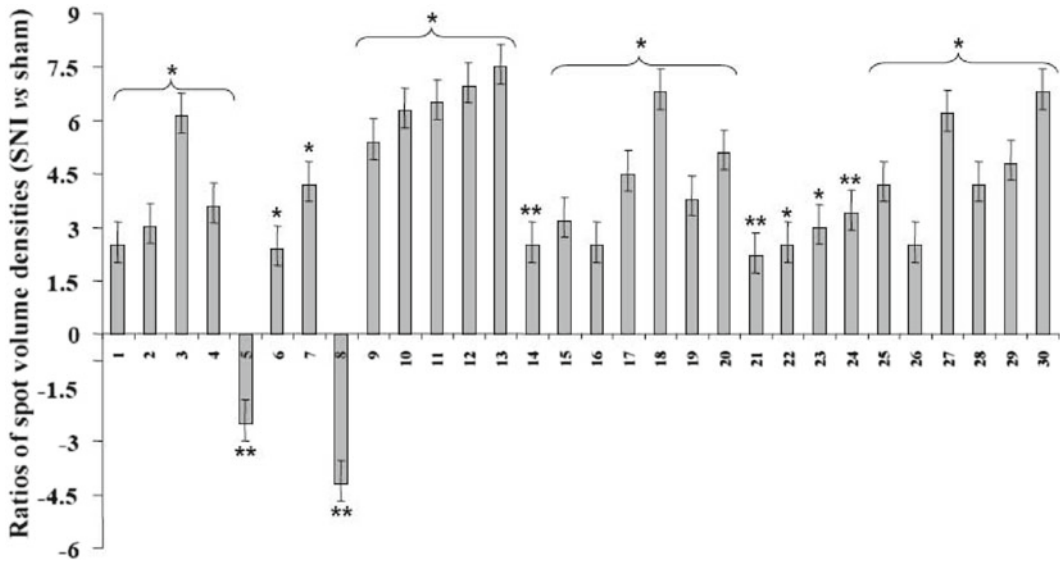


Fig. 2. Relative protein spot intensities of identified and unidentified proteins. The *x* axis refers to the spot's location (1–30) in Fig. 1, and the *y* axis represents the ratios of protein spot volume densities. The protein spot volume densities were calculated by software by dividing the values of individual spot volume densities from the SNI group by the values of the corresponding spot volume densities from the sham group.  $n=3$  repeats (total nine rats)/group. \* $p<0.05$  and \*\* $p<0.01$  versus the sham group.

software. Once software-based automatic warping and matching is complete, three replicate gels can be averaged with the average gel command.

5. After normalization for background silver staining, the software is used to detect the spot volume from the average gel image. Progenesis software automatically calculates and reports the variation or error of all 2-DE spots represented in a digitally constructed average gel. Figure 2 shows the quantification of relative spot densities of differentially modulated protein spots.

### 3.8. In-Gel Digestion of Protein

1. Excise the software-analyzed selective protein spots of interest with a plastic plunger (The Gel Company, San Francisco, CA, USA) digest them in parallel with a blank gel as control in triplicate (see Note 15).
2. Place the protein-containing gel pieces in 1.5- $\mu$ l microcentrifuge tubes prerinsed with ACN. Wash the gel pieces twice with 50% methanol for 10 min. At this point they can then be stored at  $-20^{\circ}\text{C}$ .
3. Destain the gel pieces by adding a 1:1 mix (100  $\mu$ l + 100  $\mu$ l) of destaining solution I and solution II until the gel pieces are no longer brown ( $\sim 10$ – $15$  min) (see Note 16).
4. Discard the destaining solutions and wash the gel pieces three times with 200  $\mu$ l water for 10 min each (depending on the clarity of the gel pieces, they can be washed additional times).

5. Wash the gel pieces with 20 mM  $\text{NH}_4\text{HCO}_3$  (100  $\mu\text{l}$ ) and dehydrate them with ACN (100  $\mu\text{l}$ ), twice for 10 min each.
6. Completely dry the dehydrated gel pieces in a vacuum concentrator at room temperature until they look like dry rice grains (~15–20 min).
7. Place the gel pieces in 25–30  $\mu\text{l}$  of protein digestion solution (10 ng/ $\mu\text{l}$  trypsin in 20 mM  $\text{NH}_4\text{HCO}_3$ ) and incubate on ice for 45 min.
8. Remove the excess trypsin solution around the gel pieces and replace it with 25  $\mu\text{l}$  of 10 mM  $\text{NH}_4\text{HCO}_3$  (see Note 17).
9. Incubate the gel pieces in 10 mM  $\text{NH}_4\text{HCO}_3$  overnight at 37°C in a water bath.
10. Rinse another 1.5-ml microcentrifuge tube with ACN.
11. After incubation in step 9, briefly centrifuge tube at higher speed.
12. Collect the supernatant into 1.5-ml microcentrifuge tubes from step 10.
13. Extract the peptides from the gel pieces by adding 200  $\mu\text{l}$  of 0.1% TFA in 60% ACN. Shake vigorously for 60 min at 30°C (see Note 18).
14. Collect the supernatants and dry them in a vacuum concentrator. Solubilize the resulting peptides in 10  $\mu\text{l}$  of 0.1% TFA. They can be stored at –20°C before purification by ZipTip.

### **3.9. Peptide Purification and MS**

1. Prior to peptide purification, wash the MALDI plate in four steps: (1) deionized water; (2) 50% methanol; (3) 100% methanol; and (4) 100% ACN. Repeat each step twice and then allow the MALDI plate to dry completely.
2. Thaw the frozen peptides at room temperature and centrifuge them briefly at high speed. Wet the ZipTip C18 reverse phase column four times in wetting solution. Equilibrate the ZipTip by washing it four times in washing solution. Bind the dissolved peptides to the column by filling the ZipTip with peptide solution 10–15 times. Wash the bound peptides in wash solution four times and release them by rinsing the ZipTip with 2  $\mu\text{l}$  CHCA matrix solution. Spot the eluate directly onto the MALDI plate (see Note 19).
3. Prepare a standard solution of peptides in a 500  $\mu\text{l}$  centrifuge tube by adding 1.5  $\mu\text{l}$  bradykinin, 0.5  $\mu\text{l}$  ACTH, and 2.0  $\mu\text{l}$  insulin from 10 pmol/ $\mu\text{l}$  stock solutions in 6  $\mu\text{l}$  matrix solution. Spot the standard on the same plate to calibrate the MALDI instrument.
4. Mass analyses are performed on the MALDI-TOF MS (Voyager DE-STR, Applied-Biosystems, Inc.) equipped with a 337 nm nitrogen laser.

5. Mass spectra are automatically calibrated upon acquisition by two-point residual porcine trypsin autolytic fragments (842.51 and 2210.10 [M+H<sup>+</sup>] ions) and matrix-added standard bradykinin and ACTH peaks (757.39 and 2,465.19 [M+H<sup>+</sup>] ions). Raw spectra are baseline-corrected and noise-filtered (correlation factor = 7).
6. Deisotope the spectra and automatically collect the peaks by using the “copy peak list” feature of the software. Keratin- and trypsin-derived extra peaks must be removed manually from monoisotopic standard peak lists. All the submitted masses are accurate to the level of 25–50 ppm.

### **3.10. Identification of Proteins**

1. Monoisotopic masses of each spectrum in triplicate are searched in the NCBIInr databases (NCBIInr 2005.01.03) by using the MS-Fit search engine (The Rockefeller University Edition, version 2005.02.14). Identified proteins are further confirmed by searching in ProFound-Peptide Mapping and MASCOT Peptide Mass Fingerprint search engines using the NCBIInr and Swiss-Prot 07.05.2006 databases.
2. The unmatched peptides and miscleavage sites are disregarded. All mass searches are performed under all bacterial taxonomic categories in a pre-assumed experimental mass and pI range and cross-checked with other available search engines.
3. The search parameters are allowed complete modification with iodoacetamide (Cys). Peptides are matched with the theoretical peptide masses of all proteins against all bacterial entries in the NCBIInr database with these parameters: (1) peptide tolerance limit of 20–50 ppm or better mass accuracy; (2) number of peptides matched averaging more than 15 (minimum = 6); (3) matched peptides covering at least 25% of the whole protein sequence with a significant Z score (>90% probability) and higher Mowse score; and (4) each identified protein cross-referenced to the comparable pI and molecular weight (kDa) obtained from experimental image analysis on the 2-DE gel (see Note 20).
4. Table 1 shows the identified proteins, the total number of hit peptides, and the coverage value of differentially expressed protein spots in sham-operated and SNI groups.

### **3.11. Western Blot Analysis**

1. Validate the changes in protein expression shown by proteomic analysis in the total soluble fraction (S1) and synaptosomal membrane fraction (P3) by Western blot analysis.
2. Heat the samples for 5 min at 95°C and then load them onto 4% stacking/10% separating SDS–polyacrylamide gels (20 µg protein/lane).
3. Electrophoretically transfer the proteins onto a nitrocellulose membrane.

**Table 1**  
**Differentially expressed protein spots with in-gel digestion and MALDI-TOF MS analysis**

Spot no.	Accession no.	Protein name	Theoretical Mr (kDa)/pI	Observed Mr (kDa)/pI	Matching peptides (n)	Unmatched peptides (n)	Sequence coverage (%)	Expression
<i>Proteins involved in transmission and modulation of noxious information</i>								
SNI 7	P12389	Neuronal acetylcholine receptor protein, alpha-2 subunit precursor	58.61/5.2	57.8/5.1	15	21	25	↑
SNI 12	P47742	Gamma-aminobutyric-acid receptor rho-2 subunit precursor (GABA(A) receptor)	54.29/9.1	54.5/7.0	24	10	25	↑
SNI 14	P14842	5-Hydroxytryptamine 2A receptor (5-HT-2A) (serotonin receptor 2A) (5-HT-2)	52.85/7.0	50.8/6.7	15	21	38	↑
SNI 15	P10860	Glutamate dehydrogenase 1, mitochondrial precursor (GDH)	61.41/8.1	50.9/6.9	15	28	30	↑
SNI 17	P09606	Glutamine synthetase (glutamate-ammonia ligase) (GS)	42.26/6.6	41.8/6.7	8	26	22	↑
<i>Proteins involved in cellular metabolism</i>								
SNI 8	P10719	ATP synthase beta chain, mitochondrial precursor	56.35/5.2	51.2/4.9	15	17	45	↓
SNI 9	P07323	Gamma-enolase (2-phospho-d-glycerate hydro-lyase) (neural enolase) (neuron-specific enolase) (NSE) (enolase 2)	47.14/5.0	58.4/5.1	27	5	56	↑
SNI 11	P11980	Pyruvate kinase isozymes M1/M2 (pyruvate kinase muscle isozyme)	57.81/6.6	59.4/6.7	10	29	15	↑
SNI 16	P15999	ATP synthase alpha chain, mitochondrial precursor	59.75/9.2	51.3/9.1	12	38	28	↑
SNI 19	P09605	Creatine kinase, sarcomeric mitochondrial precursor (S-MtCK) (Mib-CK) (basic-type mitochondrial creatine kinase)	47.38/8.8	43.7/7.1	23	18	26	↑

SNI 25	Q64591	2,4-Dienoyl-CoA reductase, mitochondrial precursor (4-enoyl-CoA reductase (NADPH))	36.13.85/9.1	36.5/7.7	7	21	24	↑
SNI 26	Q91ZW1	Transcription factor A, mitochondrial precursor (mtTFA)	28.18/9.8	29.5/7.5	9	25	37	↑
<i>Proteins involved in plasma membrane receptor trafficking</i>								
SNI 1	P46462	Transitional endoplasmic reticulum ATPase (TER ATPase) (15S Mg(2+)-ATPase p97 subunit (Valosin-containing protein) (VCP))	89.35/5.1	88.5/5.2	62	15	47	↑
SNI 3	Q05764	Beta-adducin (erythrocyte adducin beta subunit) (adducin 63)	80.59/5.7	82.7/5.6	60	37	41	↑
SNI 22	O35964	SH3-containing GRB2-like protein 1 (SH3domain protein 2B) (SH3p8)	41.49/5.4	41.5/5.6	40	15	52	↑
SNI 23	Q9JIM9	Septin-5 (peanut-like protein 1) (cell division control-related protein 1)	42.85/6.3	41.8/5.8	30	23	44	↑
SNI 27	PI6446	Phosphatidylinositol transfer protein alpha isoform (PtdIns transfer protein alpha) PtdInsTP) (PI-TP-alpha)	31.90/6.0	30.5/6.0	28	31	69	↑
<i>Proteins involved in oxidative stress, apoptosis, and degeneration</i>								
SNI 2	P34058	Heat-shock protein HSP 90-beta (HSP 84)	83.31/5.1	83.5/5.0	24	18	29	↑
SNI 4	P63017	Heat-shock cognate 71 kDa protein (heat-shock 70-kDa protein 8)	70.8/5.4	70.5/5.3	24	20	36	↑
SNI 5	P19527	Neurofilament triplet L protein (68-kDa neurofilament protein) (neurofilament light polypeptide) (NF-L)	61.33/4.6	60.6/4.7	16	26	20	↓
SNI 6	P23565	Alpha-internexin (alpha-Inx)	56.11/5.2	57.5/5.1	13	32	37	↑

(continued)

**Table 1**  
**(continued)**

Spot no.	Accession no.	Protein name	Theoretical Mr (kDa)/pI	Observed Mr (kDa)/pI	Matching peptides (n)	Unmatched peptides (n)	Sequence coverage (%)	Expression
SNI 10	P59215	Guanine nucleotide-binding protein G(o), alpha subunit 1	40.06/5.3	39.7/5.2	9	18	29	↑
SNI 13	Q641X3	Beta-hexosaminidase alpha chain precursor (N-acetyl-beta-glucosaminidase) (beta-N-acetyl-hexosaminidase) (hexosaminidase A)	60.53/6.8	59.7/6.7	6	24	12	↑
SNI 18	P13233	2',3'-Cyclic-nucleotide 3'-phosphodiesterase (CNP) (CNPase)	47.26/9.0	42.6/6.8	11	18	26	↑
SNI 20	Q9JLS4	Secreted frizzled-related protein 4 precursor (sFRP-4)	39.76/9.0	40.5/7.5	19	25	31	↑
SNI 28	P21816	Cysteine dioxygenase type I (cysteine dioxygenase type I) (CDO) (CDO-1)	23.02/6.0	24.6/6.0	5	11	20	↑
SNI 29	Q9EPIX	Heat-shock protein beta-8 (HspB8) (alpha crystallin C chain) (small stress protein-like protein HSP22)	21.59/4.9	23.5/4.7	15	14	30	↑
<i>Unidentified (UI) proteins</i>								
SNI 21	UI		UI	44.5/6.2	UI	66	UI	↑
SNI 24	UI		UI	55.2/6.8	UI	38	UI	↑
SNI 30	UI		UI	22.5/4.5	UI	45	UI	↑

Spinal nerve injury-induced changes in expression of the proteins as indicated by *up arrows* (increase) and *down arrows* (decrease)

4. Block the blotting membranes with 5% non-fat dry milk dissolved in Tris-HCl buffer (pH 7.4) for 1 h.
5. Incubate the membranes overnight at 4°C with primary antibodies in blocking buffer.
6. Detect the proteins with appropriate secondary antibody and visualize with chemiluminescence reagents provided with the ECL kit (Amersham Pharmacia Biotech, Piscataway, NJ, USA) and exposure to film.
7. Quantify the intensity of the blots with densitometry.

---

## 4. Notes

1. All solutions should be prepared in deionized water, unless stated otherwise. This standard is referred to as “water” in the text.
2. Unless stated otherwise, all solutions should be stored at 4°C.
3. Protein samples must be thawed on ice. Briefly centrifuge at higher speed whenever the protein is thawed on ice from -80°C.
4. If the protein pellet does not dissolve, vortex for 10–15 min at room temperature. To help ensure that the protein pellet dissolves easily, do not over dry the pellet in step 2. Overly dried pellets might be dissolved by repeated freezing and thawing.
5. Avoid trapping air bubbles in the solution.
6. Make sure that the acidic end (marked + on the IPG strip) is at the anode (red/+).
7. Before protein samples are loaded for active rehydration, the frozen ReadyStrip IPG strips should be removed from -20°C and left at room temperature for 5–10 min. Carefully peel the plastic cover sheets from the ReadyStrip IPG strips using with forceps. Load the IPG strips into the solution facing gel-side down onto the protein sample, making sure not to trap any air bubbles underneath the strips. Trapped air bubbles can be removed by holding one end of the IPG strip with forceps and moving it back and forth slowly until the bubble moves to the edge of the strip. Slowly overlay IPG strips with mineral oil.
8. Refer to the PROTEAN IEF cell manual from Bio-Rad to program the machine. During IEF, the current should not reach or exceed 50  $\mu\text{A}/\text{gel}$ . If the current reaches the maximum limit, it indicates that the protein sample has salt impurities. The salt impurities may cause horizontal lines in the second dimensional gel image. Salt impurities can be removed by washing twice with the wash buffer in the 2-D cleanup kit system under Subheading 2.3 step 1.

9. Excess mineral oil must be removed from the IPG strips. The presence of mineral oil may cause horizontal lines in the 2-DE gel.
10. During storage, the IPG strip gels should not be allowed to dry out. To ensure that the strips remain hydrated, wrap them with plastic wrap.
11. The polymerization efficiency of the gel can be examined by checking the leftover gel solution in the beaker. The polymerized gel inside the assembly should not be left at room temperature overnight because the gel might dry out.
12. Adding 1× TGS on top of the gel makes it easier to slide the IPG strips down to the gel.
13. It is good practice to place a molecular weight marker at one end (either acidic, +/, or basic, -) to verify the polarity of the IPG strips and the orientation of the gel.
14. While the gel is running, overheating in the assembly can be avoided by attaching a water circulatory pump at 10°C. The second dimension gel electrophoresis can be performed overnight at 100 V until the blue dye front arrives at the bottom of the gel.
15. The protein spot must be punched with extra care to avoid possible contamination of keratin and overlapping of other spots, and to excise sufficient numbers of blank gel pieces from each parallel gel.
16. Reagent A and Reagent B, available in the Invitrogen SilverQuest silver staining kit, can be used.
17. Add extra 10 mM  $\text{NH}_4\text{HCO}_3$  if necessary; gel pieces should not dry out during incubation.
18. The sample tubes are centrifuged briefly and the supernatants are mixed together. Then step 10 is repeated.
19. Creating a replica of the MALDI plate on paper with the exact position of each spot helps in the recognition of the spotted samples.
20. The protein selection should be made based on the maximum coverage. A peptide error of  $\pm 25$  or less is preferred; otherwise the search may hit multiple false positives. Always consider the peptide sequence that has proline (P), which is an uncharged residue and travels faster in the MALDI-TOF tube; if it is not included in the search, then the bulky charged residue inside sequence should have alanine (A) or lysine (K).

---

## Acknowledgments

This work was supported by National Institutes of Health Grants NS 058886 and NS 072206 and the Blaustein Pain Research Fund (Y.-X. T). The authors thank Claire Levine, MS, for her editorial assistance.

## References

1. Campbell, J. N. and Meyer, R. A. (2006) Mechanisms of neuropathic pain. *Neuron* **52**, 77–92.
2. Latremoliere, A. and Woolf, C. J. (2009) Central sensitization: a generator of pain hypersensitivity by central neural plasticity. *J. Pain* **10**, 895–926.
3. Price, T. J. and Geranton, S. M. (2009) Translating nociceptor sensitivity: the role of axonal protein synthesis in nociceptor physiology. *Eur. J. Neurosci.*, **29**, 2253–2263.
4. Guan, X., Zhu, X. and Tao, Y. X. (2009) Peripheral nerve injury up-regulates expression of interactor protein for cytohesin exchange factor 1 (IPCEF1) mRNA in rat dorsal root ganglion. *Naunyn Schmiedeberg's Arch. Pharmacol.*, **380**, 459–463.
5. Singh, O. V., Yaster, M., Xu, J. T., Guan, Y., Guan, X., Dharmarajan, A. M., Raja, S. N., Zeitlin, P. L. and Tao, Y. X. (2009) Proteome of synaptosome-associated proteins in spinal cord dorsal horn after peripheral nerve injury. *Proteomics* **9**, 1241–1253.
6. Yang, L., Zhang, F. X., Huang, F., Lu, Y. J., Li, G. D., Bao, L., Xiao, H. S. and Zhang, X. (2004) Peripheral nerve injury induces trans-synaptic modification of channels, receptors and signal pathways in rat dorsal spinal cord. *Eur. J. Neurosci.*, **19**, 871–883.
7. Coyle, D. E. (2007) Spinal cord transcriptional profile analysis reveals protein trafficking and RNA processing as prominent processes regulated by tactile allodynia. *Neuroscience* **144**, 144–156.

## Whole-Cell Patch-Clamp Recordings on Spinal Cord Slices

Ping Deng and Zao C. Xu

### Abstract

Whole-cell patch-clamp recording technique is a powerful tool to study intrinsic membrane properties and synaptic interactions in the spinal cord. Spinal cord slice is an ideal preparation for electrophysiological studies under physiological and pharmacological manipulation that is difficult to perform in an *in vivo* preparation. Depending on experimental purposes, the extracellular and intracellular environment of neurons can be easily controlled during whole-cell recording to isolate membrane conductance of interest and to manipulate its modulation, which is important for addressing cellular mechanisms under particular physiological and pathological conditions. Several methods for preparing spinal cord slices have been developed for whole-cell patch-clamp recordings. Here we describe practical procedures for preparing spinal cord slices from adult rats and whole-cell recording from neurons in the spinal dorsal horn.

**Key words:** Spinal cord, Dorsal horn, Neuronal excitability, Synaptic transmission, Voltage-clamp, Current-clamp

---

### 1. Introduction

Early electrophysiological studies of the spinal cord rely largely on *in vivo* intracellular recordings in intact animals, especially for spinal dorsal horn neurons (1, 2). However, it is difficult to maintain stable *in vivo* intracellular recordings for small neurons, such as substantia gelatinosa neurons (3), limiting the examination of electrophysiological characteristics (e.g., membrane properties and synaptic inputs) in superficial neurons of the spinal dorsal horn. Thus, methods have been developed to prepare *in vitro* spinal cord slices for intracellular or extracellular recordings. Neonatal or immature rats are the favorite animals in initial studies to yield satisfactory results (4, 5). It is now possible to prepare spinal cord slices from adult rats (6, 7). Basically, two major steps are involved

in the preparation of spinal cord slices, including the removal of the spinal cord from the vertebral canal and the incubation of slices. Several methods or modifications are available in each step. For example, the spinal cord can be removed from the vertebral canal by either hydraulic extrusion (8–10) or laminectomy (5, 6, 11, 12). For cutting slices, transverse and longitudinal (parasagittal and horizontal) slices have been reported (8, 11, 13–15). It is worthy to mention that each method has its advantages and limitations. Transverse slices (usually with one root) may be more suitable for examining neurons within a single spinal cord segment. On the contrary, longitudinal cutting may yield a slice attached with multiple roots or nerves (6, 16). In addition, it may be easier to identify the superficial laminae (I and II) of spinal dorsal horn on parasagittal slices (6, 8). It has also been shown that horizontal slices may significantly reduce disruption of white matter axons and preserve the integrity of glial-axonal interactions (12). Therefore, the adoption of each method depends on the goal of the experiment.

Since the first demonstration (17) and the subsequent improvement, whole-cell patch-clamp recording on spinal cord slices has been widely applied for electrophysiological studies of the spinal cord, including pain research (18). This technique is capable of detecting transmembrane currents under voltage-clamp configuration, or measuring membrane voltages under current-clamp configuration. Whole-cell recordings include several techniques, such as visualization of neurons in slices under infrared differential interference contrast (IR-DIC) microscope, obtaining a tight seal between the recording electrode and cell membrane, accessing to the inside of the cell, and measuring ionic currents or membrane voltages based on experimental design. In this chapter, we briefly describe basic protocols for whole-cell patch-clamp recordings on transverse spinal cord slices.

---

## 2. Materials

### 2.1. Equipments

#### 2.1.1. Preparation of Spinal Cord Slice

1. Isoflurane mixer (VIP 3000, Matrix).
2. Dissecting microscope (ASZ30L3, Bausch & Lomb).
3. Vibratome (VT1000S, Leica).
4. Other surgical tools: bone rongeur, microforceps, microscissors, a syringe (20 ml) with an 18-gauge needle.

#### 2.1.2. Whole-Cell Patch-Clamp Recording

1. Patch-clamp recording setup: amplifier (Axopatch 200B, Molecular Devices), stimulator (Master 8, A.M.P.I.), computer A/D interface (ITC-16, Instrutech), oscilloscope (V-552, Hitachi), vibration isolated workstation (LW3048B-OPT, Newport),

micromanipulator (MC1000e-R, SD Instruments), IR-DIC microscope with 40× water immersion objective (BX51WI, Olympus), video camera (OLY-150IR/DIC, Olympus America), video monitor (PVM-137, Sony).

2. Electrode puller (P-97, Sutter Instruments).
3. Borosilicate glass (TW150-3, World Precision Instruments).
4. Bipolar tungsten electrode (5 M $\Omega$ , MicroProbes).
5. Perfusion system (Valve Driver II, Parker).
6. Computer and data-acquisition program (AxoGraph 4.9 or pCLAMP, Molecular Devices).

## 2.2. Solutions

1. Solution for cutting slices: 230 mM sucrose, 26 mM NaHCO<sub>3</sub>, 2.5 mM KCl, 1.25 mM NaH<sub>2</sub>PO<sub>4</sub>, 0.5 mM CaCl<sub>2</sub>, 10 mM MgSO<sub>4</sub>, and 10 mM glucose, pH 7.4, 290–305 mOsm/L, equilibrated with 95% O<sub>2</sub> and 5% CO<sub>2</sub> (see Note 1).
2. Artificial CSF (aCSF): 130 mM NaCl, 3 mM KCl, 2 mM CaCl<sub>2</sub>, 2 mM MgCl<sub>2</sub>, 1.25 mM NaH<sub>2</sub>PO<sub>4</sub>, 26 mM NaHCO<sub>3</sub>, and 10 mM glucose, pH 7.4, 295–305 mOsm/L, equilibrated with 95% O<sub>2</sub> and 5% CO<sub>2</sub> (see Note 2).
3. Intracellular solution I: 120 mM KMeSO<sub>4</sub>, 12 mM KCl, 1 mM MgCl<sub>2</sub>, 1 mM EGTA, 0.2 mM CaCl<sub>2</sub>, 10 mM HEPES, 2 mM Mg-ATP, and 0.4 mM Na-GTP, pH 7.4 (adjust with 1 N KOH), 295–300 mOsm/L. Store in aliquots (0.5–1.0 ml) at –20°C. We usually use this solution to study the passive and active membrane properties of neurons.
4. Intracellular solution II: 92 mM CsMeSO<sub>4</sub>, 43 mM CsCl, 5 mM TEA, 2 mM EGTA, 1 mM MgCl<sub>2</sub>, 3 mM QX314, 10 mM HEPES, and 2 mM Mg-ATP, pH 7.4 (adjust with Tris-base), 295–300 mOsm/L. Store in aliquots (0.5–1.0 ml) at –20°C. We usually use this solution to record the excitatory or inhibitory postsynaptic currents.

## 2.3. Drugs

1. Ion channel blockers: tetrodotoxin (0.5–1.0  $\mu$ M) for blocking voltage-dependent Na<sup>+</sup> channels, 4-aminopyridine (2–5 mM) and tetraethylammonium (5 mM) for blocking voltage-dependent K<sup>+</sup> channels, CdCl<sub>2</sub> (0.1–0.3 mM) for blocking voltage-dependent Ca<sup>2+</sup> channels.
2. Antagonists for excitatory synaptic transmission: 6-cyano-7-nitroquinoxaline-2,3-dione (CNQX, 10  $\mu$ M) for AMPA receptors, (–)-2-amino-5-phosphonopentanoic acid (APV, 50  $\mu$ M) for NMDA receptors.
3. Antagonists for inhibitory synaptic transmission: (–)-bicuculline methiodide (30  $\mu$ M) for GABA<sub>A</sub> receptors, strychnine (1  $\mu$ M) for glycine receptors.

### 3. Methods

#### 3.1. Preparation of Spinal Cord Slice

In this section, we describe general protocols for preparing spinal cord slices. In brief, the spinal cord is removed by hydraulic extrusion, and slices are cut by using a vibratome. Some modifications may exist between different laboratories.

1. The adult rat (Sprague–Dawley, 200–250 g) is anesthetized with a mixture of 2–3% isoflurane, 33% O<sub>2</sub>, and 65% N<sub>2</sub> (by using an isoflurane mixer).
2. The spinal cord is quickly removed from the vertebral canal by hydraulic extrusion (for laminectomy, see Note 3). First, a midline longitudinal back skin incision is made to expose the vertebrarium. Then, after decapitation, the caudal end of the vertebral canal is opened by a transverse cutting (at the fifth lumbar vertebra). A syringe is filled with ice-cold cutting solution (1–4°C, 10–20 ml) and mounted with an 18-gauge needle (the sharp tip has been cut). The needle is inserted into the caudal end of the vertebral canal, and the spinal cord is extruded from the cervical end by applying pressure on the syringe.
3. The removed spinal cord is immersed in the cutting solution (4°C). Under dissecting microscope, the dura matter is removed. Dorsal and ventral roots, except the root(s) of interest, are then carefully cut with microscissors and microforceps. After the removal of pia-arachnoid membrane, the spinal cord is cut manually into a 5-mm block that contains the spinal segments for subsequent recordings (e.g., the lumbar enlargement).
4. The spinal cord block is fixed on a specimen plate with cyanoacrylic glue, which is then mounted in the buffer tray of a vibratome (see Note 4). The buffer tray is filled with cutting solution (4°C, equilibrated continuously with 95% O<sub>2</sub> and 5% CO<sub>2</sub>). The tissue block is immersed in the cutting solution.
5. Spinal cord slices (300–450 μm) are prepared by using a vibratome, with very low forward speed (1–4 mm/min) and high vibrating frequency (7–8 Hz) to avoid pushing the tissue.
6. The spinal cord slices are incubated in oxygenated aCSF (equilibrated continuously with 95% O<sub>2</sub> and 5% CO<sub>2</sub>) at room temperature (~24°C) and allowed to recover for >1 h before recording.

#### 3.2. Whole-Cell Patch-Clamp Recording

Basic experimental procedures for whole-cell patch-clamp recording are summarized in this section. Before whole-cell recording, we assume that the patch-clamp recording setup has been perfectly assembled.

1. After incubation (recovery), a spinal cord slice is transferred to the recording chamber, which is continuously perfused with oxygenated aCSF at a flow rate of 2–3 ml/min. The slice is immersed and secured firmly on the bottom of the recording chamber by using nylon mesh (see Note 5).
2. Using IR-DIC microscope combined with video camera and monitor, a spinal cord region (e.g., superficial laminae) is located with a low magnifying objective (2.5×). Then, the neuron of interest is visually identified with 40× water immersion objective (see Note 6).
3. A recording electrode is pulled using an electrode puller, and then filled with an appropriate intracellular solution. Fire polished electrodes are always better than unpolished ones to get tight seal. We usually use electrodes with resistance of 2–5 M $\Omega$  when filled with intracellular solution.
4. The filled electrode is mounted on the holder that is connected to the headstage. During electrode placement, a positive pressure is applied by a small syringe (1 ml, connected with the holder through a silicon tube). When the electrode is lowered into the bath, the liquid junction potential is zeroed by adjusting the pipette offset. At the same time, electrode resistance is continuously monitored under voltage-clamp mode by applying a hyperpolarizing voltage step (5 mV, 10 ms).
5. As the electrode is lowered onto the neuron, a small dimple appears on the cell surface due to the positive pressure. Meanwhile, the electrode resistance increases approximately by 10–50%.
6. The positive pressure is quickly removed and a gentle negative pressure is applied by a small syringe. This may form a stable gigaseal (>1 G $\Omega$ ) between the electrode and the cell membrane (see Note 7).
7. The electrode capacitance transients are eliminated by using the fast and slow compensation adjustment on the amplifier (see Note 8).
8. At a potential of –60 mV, a gentle suction is applied by mouth to rupture the membrane patch and access to the inside of the neuron. The formation of whole-cell configuration is indicated by a large membrane capacitance current.
9. Immediately after the formation of whole-cell configuration, the resting membrane potential is directly read from the amplifier under current-clamp ( $I=0$ ) mode. Otherwise, the dialysis of cell cytoplasm by intracellular solution may result in a change of membrane potential.

10. After reaching a stable whole-cell configuration (see Note 9), the series resistance and capacitance are compensated by adjusting corresponding compensation on the amplifier.
11. Recordings (data acquisition) are performed based on experimental design, with voltage-clamp or current-clamp mode (see Note 10). For some experiments, drugs (e.g., channel blocker or receptor agonist and antagonist) may be added in extracellular solution to isolate current or voltage responses.
12. Finally, the data are stored in a computer for offline analysis.

---

## 4. Notes

1. All solutions should be prepared with distilled water ( $>18 \text{ M}\Omega\text{-cm}$ ). We always add  $\text{CaCl}_2$  last to prevent precipitation of calcium.
2. We usually prepare 1,000 $\times$  stock solution for the following: 3 M KCl, 1.25 M  $\text{NaH}_2\text{PO}_4$ , 2 M  $\text{MgCl}_2$ , 2 M  $\text{CaCl}_2$ . These stock solutions can be stored at  $4^\circ\text{C}$  for up to 4 weeks. The aCSF is made fresh daily.
3. To remove the spinal cord from the vertebral canal with laminectomy, the rat is deeply anesthetized and the body temperature is kept at  $\sim 37^\circ\text{C}$ . After a back skin incision, the vertebrarium (including the spinose processes, transverse processes, and bilateral vertebral foramina) is exposed, and laminectomy is carefully performed with rongeurs. A fragment of spinal cord (1.0–2.0 cm) with attached roots is excised and then quickly immersed in the ice-cold cutting solution. During the surgery, one should avoid to squeeze or to stretch the spinal cord.
4. The orientation of block is dependent on experimental design. For cutting transverse slices, the spinal cord is perpendicular to the cutting blade and one of the ends is fixed on the specimen plate. For parasagittal cutting, the long axis of the dorsal or ventral surface is facing the cutting blade, with one lateral side fixed. For horizontal cutting, the long axis of one lateral side is facing the cutting blade, usually with ventral surface fixed. In addition, a chilled block of 2–3% agar (with a shallow groove) is necessary for supporting the spinal cord block during cutting.
5. To make the nylon mesh, a piece of platinum wire is bent into a U-shaped frame. Then, 3–5 single strands of nylon stocking are tightly stretched and glued (with cyanocrylate) across the two arms of the U-shaped platinum frame. The strands are paralleled about 0.3–0.5 mm apart. The size of nylon mesh can be adjusted according to the recording chamber.

6. It is important to select healthy neurons for patch-clamp recordings. In the slices, healthy neurons exhibit a smooth and bright cell surface, and their nuclei are invisible. In contrast, unhealthy neurons have visible nuclei, with swollen or shrunken cell bodies. All unhealthy neurons are not patchable, or cannot maintain stable recordings. In addition, the depth of neurons in slices should be considered. Generally, neurons located deeper in the slices have better integrity of cellular structure and neuronal connections.
7. During the formation of gigaseal, the electrode is usually held at a hyperpolarizing potential (e.g.,  $-40$  mV), which may improve the quality of tight seal.
8. To reduce the electrode capacitance transients, the extracellular solution in the recording chamber should be consistently kept at a low level. In addition, coating the electrode with Sylgard is also helpful.
9. We usually wait  $>5$  min after the formation of whole-cell configuration, to allow steady-state dialysis between the cytoplasm and intracellular solution.
10. During recording, the series resistance should be periodically monitored. It is common that partial or complete resealing may occur during experiment. Application of gentle suction(s) may reduce series resistance; however, cells with  $>15\%$  change of series resistance should be excluded from analysis. For Axopatch 200B amplifier, only fast I-clamp mode is used for current-clamp recordings to reduce voltage error of fast signals. In addition, with voltage-clamp recording, the space-clamp issue should be considered, especially for currents with fast kinetics (e.g., voltage-dependent  $\text{Na}^+$  currents and fast A-type  $\text{K}^+$  currents).

## References

1. Eccles, J. C., Eccles, R. M., and Lundberg, A. (1960) Types of neurone in and around the intermediate nucleus of the lumbosacral cord, *J Physiol* **154**, 89–114.
2. Hongo, T., Jankowska, E., and Lundberg, A. (1966) Convergence of excitatory and inhibitory action on interneurons in the lumbosacral cord, *Exp Brain Res* **1**, 338–358.
3. Cervero, F., Molony, V., and Iggo, A. (1977) Extracellular and intracellular recordings from neurones in the substantia gelatinosa Rolandi, *Brain Res* **136**, 565–569.
4. Miletic, V., and Randic, M. (1981) Neonatal rat spinal cord slice preparation: postsynaptic effects of neuropeptides on dorsal horn neurons, *Brain Res* **254**, 432–438.
5. Murase, K., and Randic, M. (1983) Electrophysiological properties of rat spinal dorsal horn neurones in vitro: calcium-dependent action potentials, *J Physiol* **334**, 141–153.
6. Bentley, G. N., and Gent, J. P. (1994) Electrophysiological properties of substantia gelatinosa neurones in a novel adult spinal slice preparation, *J Neurosci Methods* **53**, 157–162.
7. Magnuson, D. S., Johnson, R., Peet, M. J., Curry, K., and McLennan, H. (1987) A novel spinal cord slice preparation from the rat, *J Neurosci Methods* **19**, 141–145.
8. Chery, N., Yu, X. H., and de Koninck, Y. (2000) Visualization of lamina I of the dorsal horn in live adult rat spinal cord slices, *J Neurosci Methods* **96**, 133–142.

9. Meikle, A. D., and Martin, A. H. (1981) A rapid method for removal of the spinal cord, *Stain Technol* **56**, 235–237.
10. Moghaddasi, M., Velumian, A. A., Zhang, L., and Fehlings, M. G. (2007) An ex vivo preparation of mature mice spinal cord to study synaptic transmission on motoneurons, *J Neurosci Methods* **159**, 1–7.
11. Keller, A. F., Coull, J. A., Chery, N., Poisbeau, P., and De Koninck, Y. (2001) Region-specific developmental specialization of GABA-glycine cosynapses in laminae I-II of the rat spinal dorsal horn, *J Neurosci* **21**, 7871–7880.
12. Nashmi, R., Velumian, A. A., Chung, I., Zhang, L., Agrawal, S. K., and Fehlings, M. G. (2002) Patch-clamp recordings from white matter glia in thin longitudinal slices of adult rat spinal cord, *J Neurosci Methods* **117**, 159–166.
13. Phelan, K. D., and Newton, B. W. (2000) Intracellular recording of lamina X neurons in a horizontal slice preparation of rat lumbar spinal cord, *J Neurosci Methods* **100**, 145–150.
14. Randic, M., Jiang, M. C., and Cerne, R. (1993) Long-term potentiation and long-term depression of primary afferent neurotransmission in the rat spinal cord, *J Neurosci* **13**, 5228–5241.
15. Yoshimura, M., and Jessell, T. M. (1989) Primary afferent-evoked synaptic responses and slow potential generation in rat substantia gelatinosa neurons in vitro, *J Neurophysiol* **62**, 96–108.
16. Lu, Y., Inokuchi, H., Tanaka, E., Li, J. S., and Higashi, H. (2000) A spinal cord slice preparation for analyzing synaptic responses to stimulation of pelvic and pudendal nerves in mature rats, *J Neurosci Methods* **100**, 71–78.
17. Edwards, F. A., Konnerth, A., Sakmann, B., and Takahashi, T. (1989) A thin slice preparation for patch clamp recordings from neurones of the mammalian central nervous system, *Pflugers Arch* **414**, 600–612.
18. Nguyen, D., Deng, P., Matthews, E. A., Kim, D. S., Feng, G., Dickenson, A. H., Xu, Z. C., and Luo, Z. D. (2009) Enhanced pre-synaptic glutamate release in deep-dorsal horn contributes to calcium channel alpha-2-delta-1 protein-mediated spinal sensitization and behavioral hypersensitivity, *Mol Pain* **5**:6.

## Whole-Cell Recording in Isolated Primary Sensory Neurons

Michael S. Gold

### Abstract

The isolated sensory neuron in vitro is a powerful model with which to address a number of important neurobiological questions. Isolated neurons are relatively easy to prepare from both neonatal and adult animals and can be studied both acutely and after considerable time on culture. Intracellular recording is one of the most powerful ways to study these neurons. Methods are described for both the preparation of isolated sensory neurons in vitro as well as for recording major classes of ionic currents ( $\text{Na}^+$ ,  $\text{K}^+$ , and  $\text{Ca}^{2+}$ ) from these neurons with whole cell voltage-clamp techniques. Methods are also provided for an initial characterization of active and passive electrophysiological properties of these neurons in current clamp as well as the use of perforated patch recording as a means to mitigate some of the limitations associated with conventional whole cell patch recording. The reader should be aware that the regulation of ion channels in sensory neurons may very subtle, requiring considerably more sophisticated protocols than have been provided here. The reader should also be aware that there is a tremendous heterogeneity among sensory neurons, which is both a curse and a blessing for those who wish to study them. Thus, the methods provided here should only be considered the starting point for a more detailed analysis of sensory neurons.

**Key words:** Primary afferent, Somatosensory, Voltage-gated ion channels, Patch clamp

---

### 1. Introduction

Dissociated sensory neurons are an excellent model system with which to address an array of neurobiological questions. The presence of a wide variety of ion channels and receptors facilitates the biophysical analysis of ion channel properties and the study of cell signaling pathways. Acutely dissociated neurons are particularly amenable to the former as these neurons are devoid of processes and therefore possess an ideal geometry for rapid and complete control over the membrane potential. Furthermore, dissociated neurons are completely isolated from one another making it possible to obtain virtually complete control of the extracellular

milieu where fast perfusion systems can be used to enable the study of even the most rapidly desensitizing ligand gated channels. While not addressed in this chapter, patch-clamp techniques employed for electrophysiological recording make it possible to not only control the intracellular milieu but also extract the intracellular contents for analysis of genes and gene products. Given the function of sensory neurons *in vivo*, the study of isolated sensory neurons *in vitro* is also an excellent model system for the mechanistic analysis of somatosensation. In particular, many if not all of the channels necessary for sensory transduction are present and functional in isolated sensory neurons *in vitro* including mechanoreceptors (1), thermoreceptors (for both heating (2) and cooling (3)), as well as a wide variety of chemoreceptors (4). Furthermore, comparing properties of isolated sensory neurons from naïve animals and those exposed to an array of manipulations makes it possible to determine whether an injury-induced change in neuronal excitability reflects a direct change in the neuron studied as well as the identification of mechanisms that may contribute to the changes in excitability (5–7). While the advantages of the study of isolated sensory neurons *in vitro* are numerous, readers should be aware of the disadvantages of this preparation before deciding whether or not it is the most appropriate way to address the experimental questions at hand. These include the following: (1) the inability to unequivocally identify the afferent subpopulation in the absence of axon conduction velocity or receptive field properties, (2) the potential for damage to membrane properties associated with the use of enzymes required for dissociation, (3) a neuron in culture is by definition injured, (4) the impact of unknowns such as the components of serum used in culture that may alter neuronal properties, and (5) the impact of removing neurons from the influence of other neurons and support cells. Nevertheless, because the advantages of this preparation far outweigh the disadvantages in addressing a wide array of experimental questions, this chapter details methods for the preparation of isolated sensory neurons *in vitro* as well as the electrophysiological characterization of the major classes of voltage-gated ion channels in these neurons.

---

## 2. Materials

### **2.1. Tissue Collection and Preparation**

1. Short acting (i.e., isoflurane to be used in hood or with scavenging system) and longer acting (i.e., pentobarbital) anesthetic.
2. Hair clippers.
3. Surgical supplies including (a) scalpel hold and blades (#10 for skin, #11 for dural incision), (b) syringes (1 cc) and needles (25 G), (c) boning scissors or guillotine, (d) forceps (toothed),

- (e) Rongeurs, (f) fine forceps for tissue collection, (g) fine scissors (Spring scissors) for tissue collection, (h) Jewelers forceps, and (i) alcohol wipes.
4. Coated coverslips (see Note 1): prepared prior to anesthetizing animal.
  5. Culture media: minimal essential media (MEM) complete: prepared prior to anesthetizing animal, consisting of MEM (see Note 2), MEM vitamins, antibiotics, and 10% fetal bovine serum (see Note 3).
  6. Enzyme solution: MEM with MEM vitamins and Pen–Strep to which collagenase (see Note 4) has been added. Prepared prior to anesthetizing animal.
  7. Shaking water bath (heated to 37°C).
  8. Centrifuge.
  9. Laminar flow hood.
  10. Sterile pipette tips (100 µl to 10 ml).
  11. Sterile Pasteur pipettes.
  12. Vacuum attached to waste bottle.
  13. Source of flame (i.e., Bunsen burner).
  14. Inverted microscope.
  15. Balance for weighing animals.

## **2.2. Recording Chambers and Perfusion Systems**

### **2.2.1. Recording Chambers**

The protocol for tissue dissociation involves plating dissociated neurons on glass coverslips. While it is certainly possible to plate cells directly in culture dishes and use the culture dish as a recording chamber, there are several reasons to consider an alternative approach. First, adequate isolation of ionic currents may require relatively tight control over the contents of the extracellular solution. One of the best ways to achieve this is by continuously perfusing neurons with fresh extracellular solution. Recording chambers with a trough or channel design facilitate a unidirectional flow of solution across the neurons. Relatively rapid and complete extracellular solution changes are often necessary if several different ionic currents are to be studied in the same neuron. It has also been demonstrated that transmitters are released from sensory neuron cell bodies (8) and that these neurons express autoreceptors (4). Continuous fluid exchange can minimize the impact of autoreceptor activation. Second, for pharmacological studies, it is often desirable to study responses to test compounds in neurons that have not been previously exposed to the test compound. The easiest way to achieve this is to study a single neuron on each coverslip. Plating neurons on multiple coverslips facilitates the study of multiple neurons from the same animal. Third, it is often desirable to minimize the volume of extracellular solution used. This can be

particularly important for expensive or rare test compounds, although minimizing the volume of the extracellular solution is also important for increasing the fidelity of electrical recordings. Finally, if fluorescent markers are used to identify the neurons of interest and the signal to noise ratio for the marker employed is relatively low, a chamber that enables visualizing neurons through a single piece of lightweight cover glass can minimize loss of fluorescent signal. For all of these reasons, we routinely plate neurons on small (5 mm) round coverslips that fit into custom 5 mm wide channel type recording chambers.

### 2.2.2. Perfusions Systems

While a gravity-fed inflow and vacuum-assisted outflow is the easiest solution to a continuous perfusion system, it is often necessary to have better control over the rate of solution changes. This is particularly true for rapidly desensitizing receptor/ion channels, where responses can be significantly attenuated if the receptors are desensitized faster than they are activated with a relatively slow solution exchange system. There are a number of commercially available systems that enable relatively rapid and complete solution exchanges. Given the size of sensory neurons, the systems that are associated with a “flush” where drug-free solution is used to wash the drug from the cell after termination of the application, are essential if relatively short application periods are required (see Note 5).

### 2.3. Voltage-Clamp: Isolation of Na<sup>+</sup>, K<sup>+</sup>, and Ca<sup>2+</sup> Currents

1. Patch electrodes pulled from borosilicate or comparable glass fire polished to a tip resistance of 1–2 MΩ when filled with electrode solution (see below). Low-resistance electrodes should be used to minimize voltage-errors.

2. Solutions to record Na<sup>+</sup> currents in relative isolation (see Note 6):

Intracellular solution (mM): Cs-methanesulfonate 100, tetraethylammonium (TEA)-Cl 40, NaCl 5, CaCl<sub>2</sub> 1, MgCl<sub>2</sub> 2, HEPES 10, EGTA 11, Mg-ATP 2, and Li-GTP 1.

Extracellular solution (mM): Na-methanesulfonate 35, Choline-Cl 65, TEA-Cl 30, CaCl<sub>2</sub> 2.5, MgCl<sub>2</sub> 5, CdCl<sub>2</sub> 0.05, HEPES 10, glucose 10.

To minimize changes in the concentration of permeable cations, the pH of both solutions is adjusted with Tris base. Osmolality of both solutions is adjusted with sucrose to 310 and 320 for electrode and extracellular solutions, respectively.

3. Solutions to record K<sup>+</sup> currents in relative isolation:

Electrode solution (mM): K-methanesulfonate 110, KCl 30, NaCl 5, CaCl<sub>2</sub> 1, MgCl<sub>2</sub> 2, HEPES 10, EGTA 11, Mg-ATP 2, and Li-GTP 1.

Extracellular solution (mM) KCl 3, Choline-Cl 130, CaCl<sub>2</sub> 2.5, MgCl<sub>2</sub> 0.6, HEPES 10, glucose 10. Fifty micromolar Cd<sup>2+</sup> can be used to block voltage-gated Ca<sup>2+</sup> currents. We have also used a solution in which Ca<sup>2+</sup> was replaced with Co<sup>2+</sup>.

To minimize changes in the concentration of permeable cations, the pH of both solutions is adjusted with Tris base. Osmolality of both solutions is adjusted with sucrose to 310 and 320 for electrode and extracellular solutions, respectively.

4. Solutions used to record voltage-gated  $\text{Ca}^{2+}$  currents in relative isolation:

Electrode solution (mM): Cs-methanesulfonate 100, Na-methane-sulfonate 5, TEA-Cl 40,  $\text{CaCl}_2$  1,  $\text{MgCl}_2$  2, EGTA 11, and HEPES 10.

Bath solution contained Choline-Cl 100, TEA-Cl 30,  $\text{CaCl}_2$  2.5,  $\text{MgCl}_2$  0.6, NFA 0.1, HEPES 10, and glucose 10.

To minimize changes in the concentration of permeable cations, the pH of both solutions is adjusted with Tris base. Osmolality of both solutions is adjusted with sucrose to 310 and 320 for electrode and extracellular solutions, respectively.

#### **2.4. Current Clamp Recording**

1. Patch electrodes pulled from borosilicate or comparable glass fire polished to a tip resistance of  $\sim 1.5\text{--}3\text{ M}\Omega$  when filled with electrode solution (see below).

2. Solutions for current clamp recording:

Electrode solution (mM): K-methanesulfonate 110, KCl 30, NaCl 5,  $\text{CaCl}_2$  1,  $\text{MgCl}_2$  2, HEPES 10, EGTA 11, Mg-ATP 2, and Li-GTP 1

Extracellular solution (mM): KCl 3, NaCl 130,  $\text{CaCl}_2$  2.5,  $\text{MgCl}_2$  0.6, HEPES 10, and glucose 10.

To minimize changes in the concentration of permeable cations, the pH of both solutions is adjusted with Tris base. Osmolality of both solutions is adjusted with sucrose to 310 and 320 for electrode and extracellular solutions, respectively.

#### **2.5. Perforated Patch Recording**

1. Patch electrodes pulled from borosilicate or comparable glass fire polished to a tip resistance of  $2\text{--}4\text{ M}\Omega$  when filled with electrode solution (see below). Slightly smaller tip opening may help prevent rupture of the membrane patch.
2. Fungicide such as nystatin, amphotericin B, or gramicidin. Purchased and stored in powder form until the day of use. A stock solution of fungicide is prepared in DMSO. We use a stock solution of 90 mg/ml for nystatin and amphotericin B and a stock solution of 15 mg/ml for gramicidin, where the former stock solutions are diluted to a final concentration of 600  $\mu\text{g}/\text{ml}$ , while that for gramicidin is diluted to a final concentration of 50  $\mu\text{g}/\text{ml}$  (see Note 7).
3. Solutions for perforated patch recording.

Electrode solution (in mM): K-methansulfonate, 110; KCl, 30, Na-methansulfonate, 5; CaCl<sub>2</sub>, 1; MgCl<sub>2</sub>, 2; EGTA, 11; and HEPES, 10. As with the solutions described above, pH is adjusted with Tris-base, and osmolality adjusted to 310 with sucrose. To suppress K<sup>+</sup> currents, K<sup>+</sup> can be replaced with Cs<sup>+</sup>.

Extracellular solution: any of the solutions described above will work and the most appropriate for the experimental question should be employed.

To minimize changes in the concentration of permeable cations, the pH of both solutions is adjusted with Tris base. Osmolality of both solutions is adjusted with sucrose to 310 and 320 for electrode and extracellular solutions, respectively.

---

## 3. Methods

### **3.1. Harvest, Dissociation, and Culture of Isolated Sensory Neurons**

#### *3.1.1. Harvest*

The following methods are employed for the collection of dorsal root and trigeminal ganglia from the adult rodent. Tissue collection does not need to be performed in a laminar flow hood.

1. Weigh animal to administer proper anesthesia (see Note 8).
2. Inject pentobarbital (60 mg/kg) or rodent cocktail [1 ml/kg of ketamine 55 mg/ml, xylazine 5.5 mg/ml, and acepromazine 1.1 mg/ml, to obtain surgical plane of anesthesia (i.e., animals are areflexic to noxious stimulation)].
3. Surgical exposure.
  - (a) Dorsal root ganglia:
    - Shave the back.
    - Clean surgical area with alcohol wipes.
    - Make midline incision through skin. Free skin from connective tissue and reflect at least 3 cm laterally in the rat and 1 cm in the mouse. Make two additional incisions lateral to the transverse processes of the vertebrae. Use rongeurs to remove muscle and connective tissue from vertebrae. Clear at least two segments above and below the region of interest.
    - Perform a laminectomy with rongeurs by carefully removing dorsal lamina, exposing the spinal cord. In the mouse, this is most easily done by cutting through the lamina with relatively sturdy fine scissors.
    - By carefully removing the pedicle with rongeurs, it is possible to expose the dorsal root ganglion.
    - Free spinal nerve of muscle and connective tissue, grasp with forceps, and cut the nerve distal to the forceps. Pulling up on the ganglia while gently clearing

connective tissue with fine scissors, each ganglion is finally harvested by cutting the central process.

- Place ganglia in 35-mm culture dish filled with ice-cold MEM-complete.
- With fine jewelers forceps, gently remove connective tissue (capsule) from around the ganglion.
- Place cleaned ganglia in enzyme solution and proceed to isolation steps.

(b) Trigeminal ganglia:

- Decapitate rat or mouse with guillotine or boning scissors.
- Make an incision through the skin over the top of the skull and free the bone of the skin, muscle, and connective tissue with the rongeurs.
- Working from the back of the head with the rongeurs, expose the brainstem and cerebellum by removing most rostral vertebrae and the occipital bone. Parietal bones can then be removed. Scooping from rostral to caudal, remove the brain to expose the trigeminal ganglia lying beneath it.
- Remove additional bone over the central nerve. With a #11 scalpel blade, cut through dura overlaying the ganglia with incisions medial and lateral to ganglia. The mandibular branch is readily identified leaving the ganglia laterally just above the widest margin of the ganglia.
- Grasping the central nerve with forceps, gently lift the ganglia while carefully freeing connective tissue. The ganglia are completely removed following cuts to the spinal nerves leaving the mandibular, maxillary, and ophthalmic divisions (although the latter two will not be distinguishable).
- Place ganglia in 35-mm culture dish filled with ice-cold MEM-complete.
- Remove excess nerve, keeping in mind that the cell bodies are widely distributed throughout the full length of the ganglia. Remove any large pieces of connective tissue. Ganglia are then cut into small pieces with fine scissors and the pieces placed in MEM containing collagenase.

*3.1.2. Dissociation*

The following protocol is optimized for dissociation of DRG or TG neurons from the adult rat. Tissue from other species (mouse, guinea pig, rabbit, etc.) or younger animals will require modifications. As a general rule, the amount of connective tissue should be used to determine the activity of the enzymes employed and the duration of incubation: less connective tissue, such as that in

younger animals or mice, will require lower enzyme activity and/or shorter incubation times.

1. Coat coverslips. Prepare laminin (Mouse) (1 mg/ml)+ornithine (1 mg/ml) (poly-L-ornithine). Thaw Laminin slowly. Add 10  $\mu$ l laminin to 2 ml aliquot of ornithine.

Soak the coverslips (chamber slides may be used for this step to facilitate microscopy) for 5–30 min, drain, and dry.

2. Prepare culture media: minimal essential media supplemented with vitamins and antibiotics: MEM-Complete (MEM-COMP).

We use our cell culture facility MEM with Earle's balanced salt solution (BSS).

To 45 ml Fresh MEM, add the following:

500  $\mu$ l 100 $\times$  MEM vitamins.

500  $\mu$ l 100 $\times$  penicillin–streptomycin.

5 ml heat-inactivated fetal bovine serum. We heat-inactivate the serum ourselves by placing serum in 56°C for 34 min.

3. Prepare MEM+0.125% collagenase. We use Collagenase P from Roche Bioscience. We make aliquots with 625 mg/200  $\mu$ l of collagenase in distilled water. This aliquot is added to 4.8 ml of MEM with vitamins and antibiotics but with no FBS. Enzymatic activity may vary between lots of collagenase. Consequently, the concentration of enzyme and/or the incubation time may have to be adjusted with each new lot.

4. Dissect DRGs (see above) and place them in MEM-COMP on ice.

5. Desheath DRGs on ice (see Note 9).

This is most easily done under a dissecting microscope with fine jewelers forceps (i.e., Dumont #5).

6. Transfer DRGs to 5 ml MEM-Collagenase solution.

Incubate at 37°C in shaker bath 1 $\times$  45 min (see Note 10).

7. Prepare Hanks (Mg<sup>2+</sup>, Ca<sup>2+</sup> Free) with 0.25% trypsin ( $\geq$ 180 U/mg protein, but see Note 11) and 0.002% EDTA.

Trypsin and EDTA are in aliquots made so that when added to the appropriate volume of Hanks solution, the final volume is 2.5 ml and the final concentrations are as indicated. A 0.02% EDTA solution is used for the stock of EDTA which is diluted 1:10. We generally make up trypsin in 100  $\mu$ l aliquots.

8. Aspirate collagenase solution—being careful to avoid sucking up the DRG and then add the trypsin solution. If cells have been bubbled with carbogen during the collagenase treatment, they should be centrifuged ( $\sim$ 450 $\times g$  for 4 min) prior to aspiration.

9. Triturate DRGs in 2.5 ml Trypsin Hanks with fire-polished Pasteur pipette.

This is the most critical step. If it takes too many passes through the pipette (indicating insufficient digestion of connective tissue), your yield of cells drops precipitously. If the ganglia break up too easily (indicating overdigestion) your yield of cells will also decrease (see Note 12).

10. Quench Trypsin by adding 2.5 ml MEM-COMP containing.
  - 80  $\mu\text{g}/\text{ml}$  DNase (Type 1) (optional).
  - 100  $\mu\text{g}/\text{ml}$  soybean trypsin inhibitor (optional).
  - 2.5 mg/ml  $\text{MgSO}_4$ .These reagents are also made as stock solutions stored as aliquots where the aliquot and concentration of stock solution is determined so as to yield the final concentrations indicated in 2.5 ml of solution. The  $\text{Mg}^{2+}$  added to the MEM-COMP and the  $\text{Ca}^{2+}$  already present should attenuated most trypsin activity.
11. Centrifuge cells at  $\sim 450 \times g$  for 4 min.
12. Aspirate quenched trypsin solution and resuspend cells in fresh MEM-COMP. The volume in which cells are resuspended will be determined by the number of ganglia prepared at a given time and the plating density desired (see Note 13).
13. Incubate at  $37^\circ\text{C}$ , 3%  $\text{CO}_2$ , 90% humidity. (Note that adult cells seem to prefer 3%  $\text{CO}_2$ , while neonates seem to prefer 5%.) To enable neurons to attach to coverslips, we incubate for 2 h prior to flooding to culture dish with  $\sim 2$  ml of culture media (see below).
14. Flood culture dishes with the appropriate culture media with or without trophic factors (see Note 14). If neurons are to be cultured, a bicarbonate buffered media should be used. We use MEM-COMP for this purpose.
15. Change culture media (MEM-COMP) the next day and feed every 2 days thereafter with a half change of fresh culture media.
16. To limit neuritic outgrowth—neurons can be kept at room temperature in a HEPES buffered culture media. We routinely use L-15 to which the following are added to obtain the final concentrations indicated: 5 mM Na-HEPES (pH 7.4), 5 mM glucose, 1  $\times$  pen/strep, 5% fetal bovine serum.
17. The following two strategies can be employed to limit the number of nonneural cells in culture. Employing these strategies are particularly important for cultured neurons as they will be quickly overgrown with nonneural cells if nothing is done to address this issue.
  - (a) For short-term culture, it is possible to “purify” the neurons by preplating dissociated cells for 2–4 h on dishes coated with ornithine only. The nonneural cells adhere to

coverslips more tightly than neurons so that the neurons can be washed from the dishes and replated on ornithine–laminin coated coverslips.

- (b) For longer-term culture, mitotic inhibitors should be employed. 5-Fluorouridine added to the culture media for 2–4 days should be sufficient to eliminate the majority of nonneuronal cells. Based on the evidence that Cytosine  $\beta$ -D-arabinofuranoside can block the actions of NGF (9), it may be necessary to avoid use of this inhibitor.

### **3.2. Characterization of Voltage-Gated Currents in Isolated Sensory Neurons**

A detailed discussion of the theory and practice of electrophysiological recording techniques is beyond the scope of the present chapter. For such a discussion, the reader is referred elsewhere (10, 11). The two general approaches that have been widely used for intracellular recording involve the use of either sharp electrodes or patch electrodes. As with all experimental techniques, there are strengths and weakness associated with either approach; whether or not either is more appropriate for the study of isolated sensory neurons depends on the nature of the question being addressed. As a general rule, because of the nature of the recording configuration, sharp electrodes are more appropriate for the study of large diameter neurons, where clamp control can be a real problem with patch recording. Conversely, because neurons are actually “impaled” for intracellular recording with sharp electrodes and small diameter neurons are easily damaged in this process, patch electrodes are more appropriate for the study of small diameter neurons. Furthermore, because of the relatively low-resistance access to the cell cytosol associated with conventional whole cell patch recording, it is possible to control both intracellular and extracellular milieu of the cell, facilitating isolation of ion channels under study as well as the delivery of membrane impermeable test compounds. While it was generally necessary to use different amplifiers for sharp- and patch-electrode recording, it is now possible to purchase hybrid amplifiers that can be used with either approach. Because we have been most interested in the study of nociceptive afferents and the characterization of ion channels, the focus of the following discussion is on the use of patch clamp techniques for these purposes.

#### **3.2.1. Voltage-Gated $\text{Na}^+$ Currents**

While differentially distributed among subpopulations of sensory neurons (12) and developmentally regulated (at least  $\text{Na}_v1.3$  (13) and  $\text{Na}_v1.5$  (14)), there is evidence that eight of the nine known alpha-subunits encoding voltage-gated  $\text{Na}^+$  channels are present in sensory neurons. These generally underlie three major types of  $\text{Na}^+$  current defined by the sensitivity to tetrodotoxin (TTX) and/or biophysical properties: low threshold rapidly activating and inactivating TTX sensitive currents, high threshold slowly activating and inactivating TTX-resistant currents, and low threshold persistent

TTX-resistant currents. Approaches to further differentiate TTX-sensitive currents with additional toxins (15) or voltage-clamp protocols are not discussed further here.

Protocol for the Isolation of Tetrodotoxin Sensitive and TTX Resistant Na<sup>+</sup> Currents (see Note 15)

Please note, different protocols are needed for the study of low-threshold persistent Na<sup>+</sup> currents:

1. Start with a steady-state inactivation protocol. A holding potential of  $-70$  mV, should be sufficient. While the prepulse potential duration can influence transitions between fast, slow, and ultraslow inactivated states, a 100 ms duration prepulse is a reasonable place to start for the characterization of fast inactivation on current availability. Prepulse voltage steps from  $-120$  to  $0$  mV should be sufficient to inactivate both TTX-sensitive and TTX-resistant current, where current availability is monitored with a 15 ms test pulse to  $-15$  mV or so (see Note 16). A test pulse of  $-15$  mV is suggested to enable monitoring both fast (TTX-sensitive) and slow (TTX-resistant) components of the evoked current. A 15-ms test pulse is suggested so as to enable inspection of tail currents (those associated with the hyperpolarizing voltage-step at the end of the test potential): poorly isolated currents will be associated with large slowly inactivating tail currents. Because TTX-resistant current is subject to slow inactivation in some cells, an interstep interval of 5–10 s should be employed. Changes in evoked current should be monitored closely to determine when and if there is a prepulse potential at which the fast component of the current is completely inactivated and the slow-component is fully available for activation. This can be used as a prepulse potential to inactivate the fast component leaving the slow component intact. And while we describe the use of this potential in the generation of current activation data below, this potential can be used to isolated fast and slow components in the characterization of a range of other biophysical properties such as onset and recovery from inactivation.
2. Current activation data is then collected with two different protocols. The first protocol should involve a 100 ms prepulse to  $-120$  mV or the prepulse potential at which fast currents are fully available for activation followed by a series of 15 ms voltage steps from  $-60$  to  $+40$  mV. Again, for a rough estimate of current activation properties, a 10 mV voltage step should be sufficient. Smaller voltage steps will yield higher resolution estimates. Again, a 5-s interstep interval should be employed. Voltage steps through  $+40$  mV are useful to enable the determination of the current reversal potential to be used in converting current to conductance. The second protocol should be identical to the first, accept that the prepulse is to the potential at which the fast current was fully inactivated. Digitally subtracting

the second family of currents from the first will yield the fast current in isolation. Please note however, that current separation with voltage is not always possible as there is overlap between the inactivation curves of these two current types. In this case, TTX should be used to isolate currents where the first protocol is before and then after application of TTX.

3. Isolation of the persistent current can be achieved with solutions comparable to those used for the TTX-sensitive and slow TTX-resistant currents (16) (but see Note 17). While not necessary, it is easiest to apply TTX to block TTX-sensitive currents so that a voltage protocol can be used to isolate persistent current from slowly inactivating current. The reader should be aware that the persistent current is readily subject to the development of irreversible slow inactivation (17). Consequently, if the purpose of the experiment is simply to determine whether the persistent current is present in the neuron in question, it may be more appropriate to start with an activation protocol from a holding potential of  $-120$  mV or so with at least 100 ms voltage steps ranging from  $-100$  to  $+30$  mV. However, if more detailed analysis is desired, a strategy comparable to that described above for separating fast from slow currents should be employed with the exceptions being that the test potential should be considerable longer ( $>100$  ms) and to a considerably more hyperpolarized potential (i.e.,  $-50$  mV) so that only the inactivation of the persistent current will be monitored. This first inactivation protocol is used to determine whether the prepulse potential/holding potential is sufficient to ensure full availability of persistent current. Current activation data is again generated with two protocols. The first being from a holding potential at which persistent current is fully available for activation and the second being from  $-60$  mV, a potential at which persistent current should be inactivated.

### 3.2.2. Voltage-Gated $K^+$ Currents

Voltage-gated  $K^+$  channels constitute the largest family of voltage-gated ion channels, many members of which are present in sensory neurons. Summarizing protocols to isolate all of the currents present in sensory neurons is beyond the scope of the present chapter given the range of different channels that have been described and the unique protocols that must be used to study these currents in isolation. The most unique types of currents, such as those associated with the Kv6 (inward rectifying) and Kv7 (M-type) channels, generally require a combination of voltage-protocols and pharmacological approaches. Rather, because they are the most widely studied and ubiquitously expressed among sensory neurons (18), I focus on the typical transient (A-type) and persistent (delayed rectifier type) currents. While the complexity of even these two current types can often preclude “clean” isolation of current types, it would be a mistake to ignore the complexity of the currents

in these neurons by using a “generic” protocol, as conclusions drawn from currents characterized with such an approach may be misleading. The strategy described below has been our approach to address the complexity of currents in sensory neurons. The following recording solutions suggested for isolation of  $K^+$  currents are designed to minimize not only the impact of  $Na^+$  and  $Ca^{2+}$  currents but also the impact of  $Ca^{2+}$ -modulated  $K^+$  currents that are present at relatively high densities in at least some subpopulations of sensory neurons (19).

Protocol to Record  
Voltage-Gated  
 $K^+$  Currents

1. Start with a steady-state inactivation protocol. As with  $Na^+$  currents, a steady-state inactivation protocol is useful to assessing the general types of currents present in a neuron as well as whether any prepulse potential can be used to “isolate” one component from another. A holding potential of  $-70$  mV is sufficient to enable detection of most current types in sensory neurons. A 500 ms prepulse to  $-120$  mV should also be sufficient to remove most channels from an inactivated state. Again, however, readers should use prepulse potentials sufficiently hyperpolarized to clearly demonstrate that the current is fully available for activation. A 100 ms test potential of  $+20$  mV should be sufficient to activate even the highest threshold currents, while still enabling resolution of even rapidly inactivating currents. As with  $Na^+$  currents, a series of prepulse potentials ranging from  $-120$  to  $0$  mV at 10 mV increments should be sufficient to broadly define the populations of currents present, although smaller voltage-steps may be necessary to more accurately identify prepulse potentials that can be used to isolate current types (see Note 18).
2. Generate activation curves. As with voltage-gated  $Na^+$  currents, steady-state inactivation data should be used to pick the most appropriate prepulse potential to enable isolation of different current types (see Note 19).

3.2.3. Voltage-Gated  
 $Ca^{2+}$  Currents

Unlike voltage-gated  $Na^+$  and  $K^+$  currents in sensory neurons, there are only two major types of voltage-gated  $Ca^{2+}$  currents, generally referred to as high-threshold activating (HVA) or low threshold activating (LVA) currents. And while voltage protocols such as those described for both  $Na^+$  and  $K^+$  currents can be used to isolated LVA from HVA currents, the HVA currents are a mix of at least three, and more commonly four different channel types including L ( $CaV1$ ), N ( $CaV2.2$ ), P/Q ( $CaV2.1$ ), and R-type currents (20), the first three of which require the use of pharmacological tools for isolation. Fortunately, there are relatively selective tools available for these purposes which include dihydropyridines,  $\omega$ -conotoxin GVIA, and  $\omega$ -agatoxin TK for L, N, and P/Q types, respectively.

Protocol to Record  
Voltage-Gated Ca<sup>2+</sup>  
Currents

1. Generate current activation data to assess the presence of LVA current. A 100 ms prepulse to  $-120$  mV is more than enough to relieve LVA current of inactivation. A series of 50-ms test pulses from  $-70$  to  $+40$  mV in 10 mV steps should be enough to enable both the detection of the presence of LVA current (which should begin to activate between  $-50$  and  $-40$  mV), as well as assess the voltage dependence of HVA current activation (see Note 20).
2. If LVA current is present, and readers wish to assess the voltage-dependence of inactivation of the LVA current, a protocol comparable to the inactivation protocols described for both Na<sup>+</sup> and K<sup>+</sup> currents can be employed. The prepulse potential should start close to  $-120$  mV. A 100 ms test pulse to  $-30$  mV enables activation of LVA current in the relative absence of HVA current. A longer test pulse should be used to confirm the absence of HVA current, as the LVA current should completely inactivate over this time.

**3.3. Current Clamp  
Recording**

Current clamp recording is a powerful way of assessing whether an experimental manipulation results in a change in excitability. Monitoring changes in both passive and active properties also provides a sensitive approach with which to identify ion channels that may contribute to the changes in excitability. We routinely use current clamp recording to assess both acute (21) and persistent (7) changes in excitability. And while we routinely use patch-clamp amplifiers for this purpose, it is important to point out that the circuitry of a patch-clamp amplifier is not designed for current clamp. Newer amplifiers have been modified to minimize the deleterious impact of using these amplifiers in current clamp, but significant errors in the voltage traces can be introduced when older models are used (22). The solutions used in current clamp should be as close to physiological as possible.

*3.3.1. A Time Locked  
Protocol for Current Clamp  
Analysis (see Note 21)*

1. Determination of passive electrophysiological properties: resting membrane potential, input resistance and membrane capacitance. Membrane capacitance is determined in voltage clamp prior to switching to current clamp with a 20 mV hyperpolarizing voltage step. Input resistance is determined with a series of 5–6 small (2 pA) hyperpolarizing current injection applied from the resting membrane potential (see Note 22).
2. Determine the presence of spontaneous activity. We monitor neurons for 1–2 min following completion of the input resistance protocol.
3. Determine active electrophysiological properties: A brief ( $\leq 4$  ms) depolarizing current injection is used to evoke an action potential. Depolarizing current injection is increased by 50 pA steps until an action potential is evoked. Voltage data

should be sampled at least 2 kHz, and at least 500 ms of data should be acquired with each sweep so as to be able to monitor the complete decay of the after-hyperpolarization (AHP) (see Note 23).

4. Determine neuronal excitability (see Note 24): The primary measures of excitability that we have used include the following.
  - (a) Action potential threshold, which corresponds to the potential at which the regenerative depolarization of the membrane potential occurs. This can often be determined as a positive change in the first derivative of the action potential waveform.
  - (b) Current threshold, which corresponds to the amount of current injected at the time corresponding to the action potential threshold. This is generally obtained with a protocol involving a ramp depolarization.
  - (c) Rheobase, which we define as the smallest current injection necessary to evoke an action potential. Readers should be aware that this is slightly different from the original definition which was the greatest amount of current that failed to evoke an action potential. Critical to both definitions is the time domain, where sufficiently long pulses need to be used to determine “smallest” or “greatest” amount of current injected. We use a current injection of at least 500 ms.
  - (d) Accommodation/adaptation, either of which is used to describe the extent to which neurons generate multiple action potentials during sustained depolarization. The number of action potentials evoked during the sustained depolarization is generally used to quantify this parameter.
  - (e) The response to suprathreshold stimulation, which is generally measured by counting the number of action potentials evoked during current injection greater than current threshold or greater than rheobase. We routinely used multiples of rheobase to assess the response to suprathreshold stimulation (21).

Three general protocols are used to determine excitability:

- (a) Ramp. Nicol et al. (23) have used a 1 s ramp of 150–300 pA/s to assess excitability in sensory neurons. While the number of action potentials evoked during the current injection is used as the primary dependent measure, current threshold and action potential threshold can be assessed as well with this protocol.
- (b) Ramp and hold. Because we found that many neurons did not tolerate the 1 s ramp well, we have employed a protocol consisting of a 250 ms ramp to a plateau (hold) that is maintained for another 500 ms. The current injection used for each neuron is determined by increasing the amplitude of the current injection by 50 pA steps until an action potential is evoked during the ramp phase of the protocol. This is important to enable determination of action potential threshold and current threshold.

The “hold” component of the protocol is used to facilitate assessing changes in accommodation (see Note 25).

- (c) “Square” pulse (see Note 26). A step depolarization is the most common stimulus employed. And while often referred to as a square pulse, we generally employ a step  $\geq 500$  ms. We use incrementally increasing steps until an action potential is evoked (see Note 27).

### **3.4. Perforated-Patch Recording**

As mentioned earlier, one of the advantages to the use of whole-cell patch recording is the ability to control both intracellular and extracellular milieu. A problem with this configuration, however, is that with dialysis of the intracellular milieu, there can be changes and/or loss of mediators necessary to maintain channels in their “native” state. Voltage-gated  $\text{Ca}^{2+}$  channels are notoriously sensitive to changes in the intracellular milieu that may decrease with time after establishing whole cell access, a process referred to as “run-down”. While we have not observed consistent changes in voltage-gated  $\text{Ca}^{2+}$  current amplitude in sensory neurons with conventional whole cell patch recording (20), we have observed other labile currents in DRG neurons (24). “Sharp” electrode recording is one way to minimize the impact of cell dialysis. However, as noted above, this technique is difficult to employ for the study of small diameter neurons. Another approach to mitigate this problem is with perforated patch recording. In this configuration, a fungicide such as nystatin is added to the electrode solution. This class of drugs has the unique feature of forming ion channels in cell membranes which can be relatively selective for monovalent ions. This feature enables electrical access while minimizing disruption of cellular contents. A high resistance seal is formed as with convention patch recording, except rather than rupturing the membrane with a voltage pulse of suction, the fungicide will slowly form ion channels enabling whole cell access (see Note 28).

#### **3.4.1. Obtaining Whole Cell Access Via the Perforated Patch**

Stock solutions of fungicides are diluted into fresh electrode solution for each electrode. Back-filling the electrode solution devoid of fungicide can help seal formation, but can also delay the perforation process. Establish a high resistance seal on the isolated cell as well conventional whole-cell patch recording. However, less suction should be employed to avoid spontaneous rupture of the cell membrane. Seal resistance should be monitored with a test pulse as with conventional patch recording. As whole cell access is established over time (min), the capacitive transient associated with the entire membrane will begin to emerge. This process should stabilize with a time constant of decay for the capacitive transient well under 5 ms.

---

## 4. Notes

1. We have described the use of laminin–ornithine coated coverslips for plating neurons because it is often useful to have neurons adhere to the bottom of a recording chamber if one wishes to study several neurons in a single field of view under conditions where the extracellular solution is continually exchanged. Ornithine, a charged molecule, is used to facilitate neuronal adhesion. Poly-D-lysine is even more commonly used than ornithine, where the plating surface is soaked in a 0.1 mg/ml solution for tens of minutes to hours. Due to poly-lysine toxicity, care must be taken to thoroughly wash excess poly-lysine from the slip prior to drying. Surfaces coated with poly-L-ornithine which does not have the toxicity of lysine need only be air-dried. We add laminin (10  $\mu\text{g}/\text{ml}$ ), an extracellular matrix protein to the poly-L-ornithine prior to coating, to further promote adhesion to poly-L-ornithine coated surfaces. However, the drawback of the laminin is that it promotes neurite extension, thereby limiting the time during which neurons may be adequately voltage-clamped after plating. Other charged molecules such as concanavalin-A are also employed with success (25).
2. We describe the use of MEM, but the choice of media depends on the nature of the specific questions to be addressed and the nature of the experimental protocol. Trophic factors (see below) are just one of many factors that can influence the properties of the neurons to be studied. The specific needs of the neurons will depend on the age of the animal from which the cells were obtained and the time period over which the neurons will be studied after they are harvested. The longer the neurons are to be maintained in culture, the more important the choice of media becomes. For short-term culture, investigators have been successful with Ham's F-12, F-14, or a combination of MEM and F-12. Even more restrictive media will work for short-term culture, as several groups routinely maintain neurons in a physiological saline solution with glucose prior to recording (26, 27). Finally, as suggested above, to further limit the possibility of phenotypic changes associated with dissociation, sensory neurons may be stored at room temperature or lower (28, 29).
3. Many cell types are maintained in culture in a medium containing 10% serum and sensory neurons will also thrive in such a medium. Our own experience is that if it is necessary to maintain sensory neurons in culture for longer than 24 h, the use of serum or a serum substitute becomes increasingly important to keep the cells healthy. We have described the use of fetal bovine serum,

but we and others have successfully employed horse and rat serum as well. We have also touched on the limitations associated with the use of serum, the most problematic of which are variability from lot to lot and the lack of control over what is actually in the serum. Readers should also be aware that even brief exposure of sensory neurons to serum profoundly influences the properties of sensory neurons maintained in culture (30). To mitigate at least some of the impact of variability between lots of serum, we routinely use heat-inactivated serum, but this is clearly not a perfect solution. Consequently, investigators have turned to serum substitutes. Several of these are commercially available and appear to enable the maintenance of healthy sensory neurons (31). The other two solutions that have been employed to address the serum “problem” is the use of a completely defined medium (see ref. 30), or to omit serum and maintain neurons for a short period of time in serum free media (see ref. 25).

4. We have focused on enzymatic approaches for the dissociation of sensory neurons because this is a strategy we have successfully employed. Readers should be aware, however, that there are investigators who employ a nonenzymatic approach to obtaining isolated neurons. Nevertheless, an enzyme based strategy entails a trade-off between speed (minimizing the time between tissue harvest and recording) and preservation of plasma membrane proteins. More aggressive enzymatic treatments that produce more rapid dissociation require shorter exposure time, but they increase the likelihood that plasma membrane proteins (i.e., the ion channels to be studied) may be altered or destroyed. A number of different enzyme preparations are available that are prepared within a range of specific activity and to varying degrees of homogeneity. Ranges in activity are useful in narrowing the choice of enzyme. However, there may be a lot of variability between preparations of the same enzyme, so it is necessary to test the enzyme under the specific conditions in which it will be used. Thus, it may be helpful to order several small aliquots of an enzyme with different lot numbers, test them, and then order a large quantity of the lot that gave the best results.
5. While much of the recording we have done has been at room temperature, perfusion systems can also be used to control the temperature of the neuron being studied, largely to slow the kinetics of rapidly activating/inactivating currents. A combination of temperature regulated recording chamber and perfusion system provides the most effective control over the recording environment.
6.  $\text{Na}^+$  currents are normally inward and as a result voltage errors are depolarizing. These two features coupled to the rapid

activation kinetics can make clamp control difficult. Two general approaches to address this issue include the following: (1) minimizing the size of the evoked currents and (2) minimizing series resistance. The former is readily achieved by reducing the concentration of  $\text{Na}^+$  in the bath solution by replacing it with a nonpermeable, nonblocking cation. We use TEA for this purpose. The latter can be minimized by using low-resistance electrodes ( $<2 \text{ M}\Omega$ ) and maximizing series resistance compensation on the amplifier.

7. The primary reason to use gramicidin instead of nystatin or amphotericin B is because of the differences in the ion selectivity of the channels formed by these compounds. That is, because gramicidin channels are selective for cations, the intracellular  $\text{Cl}^-$  concentration is left relatively intact (32). This enables estimation of the intracellular  $\text{Cl}^-$  concentration and consequently, the impact of activating  $\text{Cl}^-$  channels in the excitability of sensory neurons (33). Given the recent interest in the regulation of intracellular  $\text{Cl}^-$  concentration in sensory neurons and the impact of changes in  $\text{Cl}^-$  regulation on injury-induced changes in  $\text{GABA}_A$ -receptor signaling (34), gramicidin perforated patch recording is increasing in popularity.
8. Tissue harvesting protocol can be adapted to the neonate and/or other species with relative ease. With practice, ganglia can be removed very quickly, minimizing the concerns about anoxia. If collection times under 10 min are achieved, it is no longer necessary to rely on vascular perfusion for tissue oxygenation, making it possible to eliminate contamination with blood products by transcardially perfusing rodents with ice cold oxygenated Krebs's solution prior to tissue collection.
9. If a little peripheral nerve is left when removing ganglia, this can be used to gain leverage as connective tissue surrounding the ganglia is removed. If rats have not been exsanguinated, blood sticking to ganglia can help visualize the connective tissue during removal. This is a tricky step. However, if the collagenous sheath is not removed, mechanical dissociation of neurons is difficult. DRG are minced with fine scissors by some investigators, to avoid the difficulty of desheathing—although we are always concerned about destroying cells that might be needed with mincing.
10. Incubation time can vary depending on activity of collagenase! Shaking is a key step here and to facilitate, it does not hurt to swirl the ganglia/collagenase solution every 15 min or so. To facilitate tissue oxygenation, maintenance of pH during this enzyme treatment step and gentle agitation of ganglia, we slowly bubble this solution with carbogen (5%  $\text{CO}_2$ /95%  $\text{O}_2$ ) via a piece of PE-50 tubing inserted through a hole cut in the cap of the tube used for this incubation step. If tissue is not

bubbled during this step, MEM-COMP can be used for the collagenase solution. However, the presence of serum in MEM-COMP will result in a frothy solution with bubbling and the loss of neurons.

11. If the focus of the study is receptors that are particularly labile to trypsin cleavage, the trypsin can be omitted and/or trypsin activity quenched with trypsin inhibitor. If a large number of ganglia are prepared at once, it may be necessary to include DNase to mitigate the impact of DNA liberated from cells ruptured during the dissociation step.
12. Six passes total through an incrementally smaller tip is about right. The final tip opening should be just small enough to occlude the passage of air (that is you can feel the resistance of air passing through the tip). The total time in trypsin, including the trituration steps, should be 5 min.
13. There is a relatively wide range of plating densities that do not appear to be detrimental to the health of sensory neurons ranging from less than one neuron per  $100 \mu\text{m}^2$  to over ten neurons per  $100 \mu\text{m}^2$ . However, overdiluting and overplating will both result in a loss of neurons. We plate at  $\sim 2$  DRG per 35-mm culture dish. To increase cell density, we resuspend cell in a small volume ( $\sim 100 \mu\text{l}/\text{DRG}$ ) and plate ganglia as drops ( $\sim 15\text{--}30 \mu\text{l}$ ) onto the coverslips.
14. Many people also add neurotrophic factors when plating neurons and/or at the time of flooding. The most commonly used is nerve growth factor (NGF, 2.5S)  $10\text{--}20 \text{ ng/ml}$ . Whether or not to use trophic factors, however, is as much an experimental question as is one of basic cell culture. The phenotype of adult sensory neurons is maintained by access to a variety of different trophic factors from the NGF family (NGF, BDNF, neurotrophin-3 and neurotrophin-4) and from the glial cell line derived family of ligands (GDNF, neurturin, artemin, and persephin), with different subpopulations of sensory neurons expressing the receptors for different trophic factors and therefore regulated by the presence or absence of the receptor ligand. Because both increases and decreases in access to neurotrophic factors appear to be important for the sensory neuron response to injury, the choice of what to include or exclude should be made with care.
15. The literature is now full of data on the biophysical properties of voltage-gated  $\text{Na}^+$  currents in sensory neurons. Careful inspection of the published values for parameters such as the potential at which half the total current is activated ( $V_{0.5}$  for activation) or inactivated ( $V_{0.5}$  for inactivation) reveals considerable variability, even for currents such as the slowly-activating and inactivating TTX-resistant current, that should reflect activity in a single channel type (i.e.,  $\text{Na}_v 1.8$ ). There are

a number of potential explanations for this variability including the impact of ancillary subunits (35), phosphorylation (36) and/or genetic variability (37), in addition to potential problems associated with clamp control. Thus, using standard protocols to “isolate” current types may not always be justified, particularly if one is studying a unique population of afferents. What is described is a general strategy for mitigating the impact of poorly isolated current types and developing a voltage-clamp protocol that will enable characterization of Na<sup>+</sup> current properties.

16. Approximate voltages are given here for resting membrane potential and test potential because the actual values must be determined empirically for the neurons under study. If it is not possible to achieve full current availability from a holding potential of  $-70$  mV, it may be necessary to hold the neuron at a more hyperpolarized potential. Similarly, the rationale for a test step to  $-15$  mV, is that this should enable clear visualization of both fast, TTX-sensitive and slow-TTX resistant currents so as to facilitate closely monitoring changes in the availability of both. If not enough slow current is active at this potential, a more depolarized test pulse should be used. Similarly, if so much slow current is activated that it is difficult to resolve the fast current, a more hyperpolarized test potential should be employed. Finally, if full current availability is not apparent with a prepulse to  $-120$  mV (i.e., current evoked with the test pulse to  $-15$  mV is not the same from  $-120$  and  $-110$  mV prepulse potentials) more hyperpolarized voltage-steps should be employed. A 10 mV voltage step can be used to get a rough idea of the process of inactivation, but small voltage steps should be employed if higher resolution is required.
17. It is often difficult to hold sensory neurons at the hyperpolarized potential needed to ensure full availability of the persistent current with these standard solutions. Including F<sup>-</sup> in the electrode solution as the major anion not only can be used to block voltage-gated Ca<sup>2+</sup> currents, but enables holding the neuron a very hyperpolarized potentials for long enough to ensure full availability of the persistent current.
18. It should become immediately obvious after studying K<sup>+</sup> currents in only a few sensory neurons, starting with an inactivation type of protocol, that there are both transient and sustained K<sup>+</sup> currents in sensory neurons that are subject to steady-state inactivation. The use of a longer test pulse (500 ms) may be necessary to determine whether a “delayed” rectifier type of current is really a slowly inactivating A-type current. If further isolation of currents is needed, pharmacological approaches should be employed. Readers should also be aware that there are high-threshold transient currents in sensory neurons as well. These are generally encoded by Kv3 family

members in contrast to the low threshold transient current encoded by Kv4 family members, both of which are present in sensory neurons (38).

19. Two additional considerations should be employed when studying the activation of voltage-gated K<sup>+</sup> currents in sensory neurons. First, because the inactivation rates of K<sup>+</sup> currents can vary dramatically with time constants well over an order of magnitude apart, it may be necessary to use two different protocols to adequately assess the currents present. That is, if only a long voltage step (~500 ms) is employed, it may not be possible to detect more rapidly inactivating currents present. Conversely, if only a short voltage step (~50 ms) is employed, it may not be possible to distinguish slowly inactivating from persistent currents. Second, it may be necessary to evoke currents from two different prepulse potentials if the steady-state inactivation curve reveals more than one phase of inactivation (i.e., see ref. 18).
20. Because the reversal potential for Ca<sup>2+</sup> currents is often difficult to determine, tail currents (the current associated with membrane repolarization to -60 mV or so after the test potential), can be used to generate a conductance-voltage curve where the instantaneous current determined by extrapolating the tail current back to the instant of the onset of the hyperpolarizing voltage-step, is plotted against the test potential. A relatively short activating voltage step is used to facilitate analysis of tail currents. However, if the reader is more interested in whether or not there is current decay during a sustained voltage-step, a longer voltage step should be employed. The reader should also note that one of the unique features of LVA current is that it deactivates relatively slowly and therefore is associated with large and long-lasting tail currents.
21. A time-locked protocol should be used to mitigate the impact of time-dependent changes in excitability.
22. If the current-voltage relationship is not linear over even three of the current pulses, a small depolarizing step can be used at the start of the series with decreasing current injection used on each subsequent step.
23. A slow (>2 s) AHP has been described in a small subpopulation of DRG neurons (24), so considerably longer sampling periods may be required. The reader should note that a brief current injection is used for this protocol so that the current injection does not influence impact of the ion channels in the neuron on membrane potential. We use this protocol before and after application of test agents as a screen to determine whether the test agent influences ion channels, which would be manifested by a change in the action potential waveform. The particular pattern of changes can be used to predict the ion channels that have been targeted (7).

24. A number of protocols have been employed. The question being addressed should be used to determine the most appropriate protocol. Some protocols are better for a “within cell design” where the acute impact of one manipulation or another is assessed in the same cell and a change in excitability is the critical end point. Other protocols are better for a “between cell design” where the excitability of one population of neurons will be compared to that of another.
25. We use this protocol to assess the impact of acute manipulations where it has the advantage of enabling us to monitor three parameters of excitability with a single protocol. In this context, we determine the magnitude of the current injection and then use that protocol to stimulate neurons once every 30 s. At least 90 s of baseline (three sweeps) data are collected prior to manipulating the neurons (i.e., applying test agents) to confirm stability and enable detection of changes. This stimulation interval is then maintained through the manipulation period so as to facilitate detection of changes. We define a change in any of the three parameters assessed with this protocol greater than two standard deviations from the mean baseline value as a change in excitability.
26. The main limitation to both the ramp and the ramp-and-hold protocols is that they cannot be used to generate action potentials in some neurons, particular large-diameter neurons. This is largely due to the fact that voltage-gated Na<sup>+</sup> channels underlying the action potential are inactivated by the “slow” membrane depolarization driven by the ramp current injection. We have used shorter ramps to address the problem (39), but a square pulse is the most commonly used alternative.
27. As a first pass, a large step 50–100 pA, can be used. Since both the rheobased and action potential threshold are determined with this protocol, higher resolution is generally desirable. We strive to obtain a resolution that is <10% of the rheobase for any given neuron (i.e., 5 pA for a neuron with a rheobase between 50 and 100 pA, 10 pA for a neuron with a rheobase between 100 and 500 pA, etc.). Because many sensory neurons will only fire a single action potential in response to current injection at rheobase, we assess the response to suprathreshold stimulation at 1.5, 2, 2.5, and 3 times rheobase.
28. A major limitation of perforated patch recording is that it takes significantly longer, often 15–20 min to obtain whole cell access. It is also often rarely possible to obtain access comparable to that achieved with the conventional whole cell patch configuration, although we routinely achieve access resistance well below 10 MΩ. Unfortunately, the extent to which this limitation is mitigated with the use of lower resistance electrodes can only be pushed so far as spontaneous whole cell access will

occur too easily if the patch electrode is too big. To balance all of the additional trouble associated with perforated patch recording, however, is the fact that it is a very stable recording configuration that enable the study of neurons for well over an hour.

---

## Acknowledgments

This work was supported by NIH grants DE018252 and NS063010. I would like to thank Nicole Scheff for valuable input on the preparation of this manuscript.

## References

1. McCarter, G. C., Reichling, D. B., and Levine, J. D. (1999) Mechanical transduction by rat dorsal root ganglion neurons in vitro, *Neurosci Lett* **273**, 179–182.
2. Caterina, M. J., Schumacher, M. A., Tominaga, M., Rosen, T. A., Levine, J. D., and Julius, D. (1997) The capsaicin receptor: a heat-activated ion channel in the pain pathway, *Nature* **389**, 816–824.
3. Thut, P. D., Wrigley, D., and Gold, M. S. (2003) Cold transduction in rat trigeminal ganglia neurons in vitro, *Neuroscience* **119**, 1071–1083.
4. Gold, M. S., and Caterina, M. J. (2008) Molecular Biology of Nociceptor Transduction, in *The Senses: A Comprehensive Reference* (Basbaum, A. I., and Bushnell, M. C., Eds.), pp 43–74, Academic Press, San Diego.
5. Flake, N. M., Lancaster, E., Weinreich, D., and Gold, M. S. (2004) Absence of an association between axotomy-induced changes in sodium currents and excitability in DRG neurons from the adult rat, *Pain* **109**, 471–480.
6. Flake, N. M., Bonebreak, D. B., and Gold, M. S. (2005) Estrogen and inflammation increase the excitability of rat temporomandibular joint afferent neurons, *J Neurophysiol* **93**, 1585–1597.
7. Harriott, A. M., Dessem, D., and Gold, M. S. (2006) Inflammation increases the excitability of masseter muscle afferents, *Neuroscience* **141**, 433–442.
8. Huang, L. Y., and Neher, E. (1996) Ca<sup>2+</sup>-dependent exocytosis in the somata of dorsal root ganglion neurons, *Neuron* **17**, 135–145.
9. Tomkins, C. E., Edwards, S. N., and Tolkovsky, A. M. (1994) Apoptosis is induced in post-mitotic rat sympathetic neurons by arabinosides and topoisomerase II inhibitors in the presence of NGF, *J Cell Sci* **107**, 1499–1507.
10. Hamill, O. P., Marty, A., Neher, E., Sakmann, B., and Sigworth, F. J. (1981) Improved patch-clamp techniques for high-resolution current recording from cells and cell-free membrane patches, *Pflugers Arch* **391**, 85–100.
11. Sakmann, B., and Neher, E., (Eds.) (1995) *Single-Channel Recording*, Second ed., Plenum, New York.
12. Ho, C., and O’Leary, M. E. (2011) Single-cell analysis of sodium channel expression in dorsal root ganglion neurons, *Mol Cell Neurosci* **46**(1), 159–166.
13. Waxman, S. G., Kocsis, J. D., and Black, J. A. (1994) Type III sodium channel mRNA is expressed in embryonic but not adult spinal sensory neurons, and is reexpressed following axotomy, *J Neurophysiol* **72**, 466–470.
14. Renganathan, M., Dib-Hajj, S., and Waxman, S. G. (2002) Na<sup>v</sup>1.5 underlies the ‘third TTX-R sodium current’ in rat small DRG neurons, *Brain Res Mol Brain Res* **106**, 70–82.
15. Xiao, Y., Blumenthal, K., Jackson, J. O., 2nd, Liang, S., and Cummins, T. R. The tarantula toxins ProTx-II and huwentoxin-IV differentially interact with human Nav1.7 voltage sensors to inhibit channel activation and inactivation, *Mol Pharmacol* **78**, 1124–1134.
16. Coste, B., Osorio, N., Padilla, F., Crest, M., and Delmas, P. (2004) Gating and modulation of presumptive Na<sup>v</sup>1.9 channels in enteric and spinal sensory neurons, *Mol Cell Neurosci* **26**, 123–134.
17. Cummins, T. R., Dib-Hajj, S. D., Black, J. A., Akopian, A. N., Wood, J. N., and Waxman, S. G. (1999) A novel persistent tetrodotoxin-resistant sodium current in SNS-null and wild-type small primary sensory neurons, *J Neurosci* **19**, RC43.

18. Gold, M. S., Shuster, M. J., and Levine, J. D. (1996) Characterization of six voltage-gated K<sup>+</sup> currents in adult rat sensory neurons, *J. Neurophysiol.* **75**, 2629–2646.
19. Zhang, X. L., Mok, L. P., Katz, E. J., and Gold, M. S. BKCa currents are enriched in a subpopulation of adult rat cutaneous nociceptive dorsal root ganglion neurons, *Eur J Neurosci* **31**, 450–462.
20. Lu, S. G., Zhang, X. L., Luo, Z. D., and Gold, M. S. Persistent inflammation alters the density and distribution of voltage-activated calcium channels in subpopulations of rat cutaneous DRG neurons, *Pain* **151**, 633–643.
21. Harriott, A. M., and Gold, M. S. (2009) Electrophysiological Properties of Dural Afferents in the Absence and Presence of Inflammatory Mediators, *J Neurophysiol.* **101**(6), 3126–3134.
22. Magistretti, J., Mantegazza, M., Guatteo, E., and Wanke, E. (1996) Action potentials recorded with patch-clamp amplifiers: are they genuine? *Trends Neurosci* **19**, 530–534.
23. Nicol, G. D., Vasko, M. R., and Evans, A. R. (1997) Prostaglandins suppress an outward potassium current in embryonic rat sensory neurons, *J Neurophysiol* **77**, 167–176.
24. Gold, M. S., Shuster, M. J., and Levine, J. D. (1996) Role of a Ca(2+)-dependent slow after-hyperpolarization in prostaglandin E<sub>2</sub>-induced sensitization of cultured rat sensory neurons, *Neurosci Lett* **205**, 161–164.
25. Scroggs, R. S., and Fox, A. P. (1992) Calcium current variation between acutely isolated adult rat dorsal root ganglion neurons of different size, *Journal of Physiology* **445**, 639–658.
26. Scroggs, R. S., Todorovic, S. M., Anderson, E. G., and Fox, A. P. (1994) Variation in IH, IIR, and ILEAK between acutely isolated adult rat dorsal root ganglion neurons of different size, *J Neurophysiol* **71**, 271–279.
27. Cardenas, C. G., Del Mar, L. P., and Scroggs, R. S. (1995) Variation in serotonergic inhibition of calcium channel currents in four types of rat sensory neurons differentiated by membrane properties, *J Neurophysiol* **74**, 1870–1879.
28. Eckert, S. P., Taddese, A., and McCleskey, E. W. (1998) Isolation and culture of rat sensory neurons having distinct sensory modalities, *J Neurosci Meth* **77**, 183–190.
29. White, G., Lovinger, D. M., and Weight, F. F. (1989) Transient low-threshold Ca<sup>2+</sup> current triggers burst firing through an afterdepolarizing potential in an adult mammalian neuron, *Proceedings of the National Academy of Sciences* **86**, 6802–6806.
30. Delree, P., Ribbens, C., Martin, D., Rogister, B., Lefebvre, P. P., Rigo, J. M., Leprince, P., Schoenen, J., and Moonen, G. (1993) Plasticity of developing and adult dorsal root ganglion neurons as revealed in vitro, *Brain Research Bulletin* **30**, 231–237.
31. Winter, J. (1998) Brain derived neurotrophic factor, but not nerve growth factor, regulates capsaicin sensitivity of rat vagal ganglion neurons, *Neurosci Lett* **241**, 21–24.
32. Akaike, N. (1996) Gramicidin perforated patch recording and intracellular chloride activity in excitable cells, *Prog Biophys Mol Biol* **65**, 251–264.
33. Vaughn, A. H., and Gold, M. S. Ionic mechanisms underlying inflammatory mediator-induced sensitization of dural afferents, *J Neurosci* **30**, 7878–7888.
34. Price, T. J., Cervero, F., Gold, M. S., Hammond, D. L., and Prescott, S. A. (2009) Chloride regulation in the pain pathway, *Brain Res Rev* **60**, 149–170.
35. Isom, L. L. (2001) Sodium channel beta subunits: anything but auxiliary, *Neuroscientist* **7**, 42–54.
36. Fitzgerald, E. M., Okuse, K., Wood, J. N., Dolphin, A. C., and Moss, S. J. (1999) Cyclic AMP-dependent phosphorylation of the tetrodotoxin-resistant voltage-dependent sodium channel, SNS, *J Physiol.* **516**(Pt 2), 433–446.
37. Reimann, F., Cox, J. J., Belfer, I., Diatchenko, L., Zaykin, D. V., McHale, D. P., Drenth, J. P., Dai, F., Wheeler, J., Sanders, F., Wood, L., Wu, T. X., Karppinen, J., Nikolajsen, L., Mannikko, M., Max, M. B., Kiselycznyk, C., Poddar, M., Te Morsche, R. H., Smith, S., Gibson, D., Kelempsioti, A., Maixner, W., Gribble, F. M., and Woods, C. G. Pain perception is altered by a nucleotide polymorphism in SCN9A, *Proc Natl Acad Sci U S A* **107**, 5148–5153.
38. Chien, L. Y., Cheng, J. K., Chu, D., Cheng, C. F., and Tsaur, M. L. (2007) Reduced expression of A-type potassium channels in primary sensory neurons induces mechanical hypersensitivity, *J Neurosci* **27**, 9855–9865.
39. Gold, M. S., Dastmalchi, S., and Levine, J. D. (1996) Co-expression of nociceptor properties in dorsal root ganglion neurons from the adult rat *in vitro*, *Neuroscience* **71**, 265–275.

## Indwelling Supradural Catheters for Induction of Facial Allodynia: Surgical Procedures, Application of Inflammatory Stimuli, and Behavioral Testing

Julie Wieseler, David Sprunger, Amanda Ellis, Steven F. Maier, and Linda R. Watkins

### Abstract

Migraine headaches are debilitatingly painful and poorly managed. Facial allodynia is often associated with migraine, and clinical evidence indicates that it is a critical point in migraine progression. That is, if the migraine can be treated prior to the onset of facial allodynia, the migraine can be halted using triptans, whereas if treatment is administered after facial allodynia has begun, the treatment is ineffective. The meninges and the immune cells therein have been implicated in migraine facial pain. Indeed, application of inflammatory mediators over the meninges has been used to study changes in pain responsive neurons in trigeminal complex, and changes in their receptive fields. Much of this research has been carried out in anesthetized rats, which limits the clinical application. Our indwelling supradural catheter model, in which inflammatory mediators can be administered to the meninges in awake and freely moving rats, allows for the assessment of behavioral changes shortly after injection. Following administration of inflammatory soup (histamine, serotonin, bradykinin, and prostaglandin E2) or the immunogenic HIV-1 coat protein gp120 results in reliable periorbital mechanical allodynia. This model provides an additional means to study the neurocircuitry and neuropharmacology of facial allodynia. Here, we describe detailed methods for the placement of the catheter, injection procedures, and assessment of facial allodynia.

**Key words:** Facial allodynia, Meninges, Migraine, Supradural catheter, Animal model

---

### 1. Introduction

Within the migraine population, facial allodynia (1, 2) and corpalgia (extracephalic allodynia) (3) are commonly experienced. Electrophysiological studies have shown that application of immune mediators over the meninges leads to enhanced responsivity to facial stimulation in the brain stem (4, 5). Much of what has been learned to date has been derived from studies performed in anesthetized

rats. These studies are limiting because (1) the anesthetics used are known to alter glial and neuronal activity as well as immune activity (6–12) and (2) the nature of the studies are such that the behavioral manifestations of immunogenic manipulation of the meninges cannot be measured, nor can they be manipulated.

The supradural catheter model was developed based on the findings from electrophysiological studies that application of inflammatory mediators over the transverse sagittal sinus activates neurons in the trigeminal nucleus caudalis (5). Thus, our model places the catheter tip such that it terminates at the superior sagittal sinus. Injection of proinflammatory mediators (histamine, serotonin, bradykinin, and prostaglandin E2) via the supradural catheters induces periorbital mechanical allodynia, validating this method as a model of facial allodynia (13). We further showed that application of the immunogenic HIV-1 coat protein gp120 via the supradural catheter also induces periorbital mechanical allodynia, supporting the hypothesis that the resident immune cells of the meninges can modulate facial allodynia.

Here, the procedure for supradural catheterization is thoroughly described, as is the procedure for supradural injections. The method for measuring facial allodynia is modified from Ren (14), and is also presented in detail. Determining the 50% threshold from the observed data will be described.

---

## 2. Materials

### **2.1. Indwelling Supradural Catheter Construction and Preparation**

1. Sterile polyethylene tubing (PE-10, Becton Dickinson, Franklin Lakes, NJ).
2. Scalpel handle with no. 11 scalpel blade.
3. Sterile 15-mL conical tube (Fisher Scientific, Houston, TX).
4. Sterile saline.
5. 75% Ethanol.
6. Black permanent marker.

### **2.2. Indwelling Supradural Catheter Surgery**

#### *2.2.1. Equipment*

1. Stereotaxic apparatus (Kopf Instruments, Tujunga, CA).
2. Ultra hot glass-bead sterilizer (World Precision Instruments, Sarasota, FL) to sterilize tools before and between uses.
3. Shaver.
4. Scalpel handle with no. 11 or no. 10 scalpel blades.
5. Sterile gauze (4×4 in.) to create a drape around the surgical site.
6. Sterile Q-tips to absorb blood and apply hydrogen peroxide.
7. Handheld drill used with a Dremel #107 engraving cutter bit.
8. #5 Fine-tipped forceps (Fine Science Tools, Foster City, CA; # 11254-20).

9. #7 Fine-tipped curved forceps (Fine Science Tools, #11274-20).
10. Two serrefine clamps (Fine Science Tools, #18050-35).
11. 50- $\mu$ L Hamilton syringe.
12. 9-mm Stainless steel wound clips (Stoelting, Wood Dale, IL).
13. Wound clip applicator (Fine Science Tools, #12031-09).
14. Supradural injectors.

#### 2.2.2. Reagents

1. Isoflurane (Halocarbon Laboratories, River Edge, NJ).
2. Oxygen.
3. Betadine.
4. 3% Hydrogen peroxide.
5. Superglue (cyanoacrylate).
6. Polysporin antibiotic (Pfizer, New York, NY).
7. Sterile saline.

#### 2.3. Supradural Catheters Injectors and Injection

1. 30-G, 1/2-in. hypodermic needles (Becton Dickinson, Franklin Lakes, NJ) with plastic hub removed.
2. PE-10 tubing (PE-10, Becton Dickinson, Franklin Lakes, NJ).
3. Autoclaved 100- $\mu$ L Hamilton glass syringes (Fisher Scientific).
4. Infusion pump (Razel Scientific Instruments, INC, Standford, CT; Model A-99, pump set at 36.9).

#### 2.4. Low-Threshold Mechanical Test

1. Leather glove.
2. Calibrated Semmes-Weinstein monofilaments (von Frey hairs; Stoelting, Wood Dale, IL). The hair stiffness ranges from 4.56 (4.00 g) through 5.88 (60.00 g) in a logarithmic series of seven monofilaments. Log stiffness of the hairs is defined as  $\text{Log}_{10}(\text{mg} \times 10)$  ~ nomenclature recognized by the intended reader. The seven stimuli have the following log stiffness values: 4.56 (4 g), 4.74 (6 g), 4.93 (8 g), 5.07 (10 g), 5.18 (15 g), 5.46 (26 g), and 5.88 (60 g).
3. PsychoFit is the computer program used to estimate 50% threshold values, and is available for both Macintosh and PC computers. The software can be downloaded from L.O. Harvey's website (<http://psych.colorado.edu/~lharvey>).

---

### 3. Methods

The methods and procedures delineated here are for: (1) construction and preparation of supradural catheters; (2) bilateral supradural catheter placement (see Note 1); (3) construction and preparation of supradural catheter injectors; (4) administration of immunogenic stimuli via supradural catheters; and (5) assessing facial allodynia

using von Frey filaments and submitting data to PsychoFit. The goal in the development of this model was to test immunogenic stimuli, and as such, all procedures are performed under sterile conditions. Procedures described for constructing catheters and injectors are carried out on sterile autoclave paper, and all instruments are sterilized using the hot-bead sterilizer.

### **3.1. Preparation of Supradural Catheter**

1. PE-10 tubing is cut in 6–8 cm lengths (see Note 2).
2. Prior to the day of surgery, catheters are filled with sterile saline and heat sealed at both ends such that no air bubbles are in the catheter.
3. Catheters are stored in 75% ethanol for 24 h prior to surgery.
4. Before implantation, catheters are removed from ethanol, dried, and marked with permanent marker at 4 mm from the end of the catheter that is to be threaded under the skull during surgery, and transferred to sterile saline.

### **3.2. Supradural Catheter Placement Surgery**

1. All surgical tools are sterilized in a glass-bead sterilizer before surgical procedures, and care is taken to keep the surgery environment as clean as possible.
2. Animal is placed in stereotaxic apparatus, and secured with ear bars maintaining the head in a level position.
3. Surgery is carried out under isoflurane anesthesia, 2.5% in oxygen, which is chosen because it has minimal effects on immune cell function compared to other commonly used anesthetics (6–12).
4. The surgical site is shaved and topical Betadine is liberally applied to the scalp.
5. A 3-cm incision is then made to expose bregma.
6. 3% Hydrogen peroxide is applied to the skull surface to minimize bleeding.
7. The surgical site remained exposed through the use of bilateral serrefine clamps directly attached to the scalp.
8. The handheld drill is used with Dremel #107 engraving cutter bit to bore an 8- 10-mm-long bilateral trough in the skull. The trough is approximately 2 mm wide and is made 3–4 mm lateral to bregma on either side (see Note 3). Caution is taken not to penetrate the dura. Troughs are drilled such that the thinnest points are 1 mm caudal to bregma (Fig. 1).
9. Catheters are inserted horizontally along the troughs at the 1 mm caudal point to the 4-mm mark on the catheter.
10. Once placed, catheters are secured with superglue, and allowed to dry for approximately 15 min.
11. Catheters are flushed with 5  $\mu$ L of sterile saline through using a 50- $\mu$ L Hamilton syringe, making sure to avoid any air bubbles

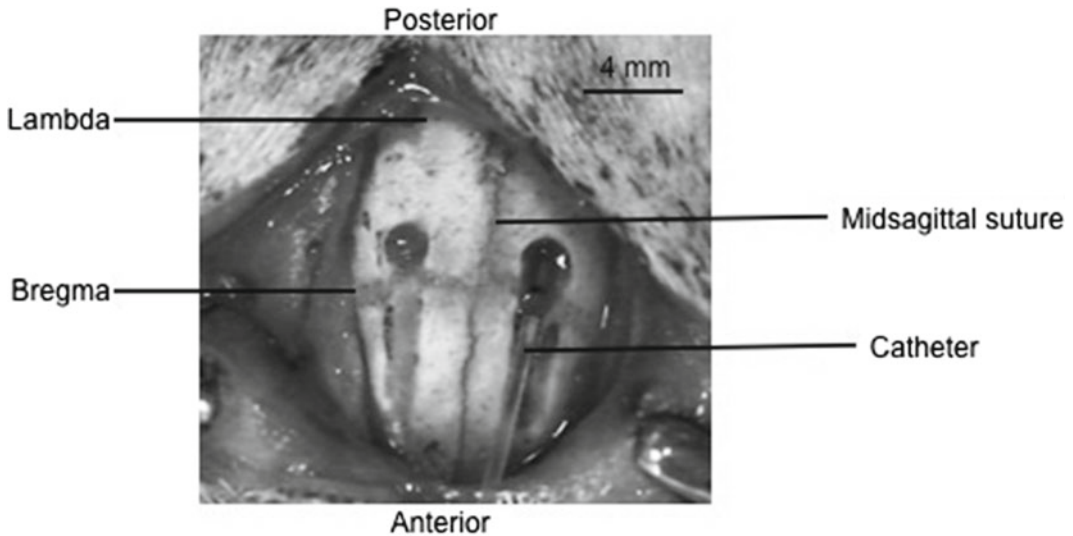


Fig. 1. This picture shows the drilled troughs, with a catheter, made from PE-10 tubing, guided into place via the trough. The troughs are drilled 2–3 mm lateral of midline, and stop 1 mm posterior of bregma. The troughs are approximately 4 mm in length, gradually becoming deeper at the most posterior point. The skull is pierced and caution is taken not to penetrate the dura. Modified with permission from ref. 13.

thereby to preventing clogging (see Note 4). The catheter is then resealed with heated forceps.

12. The wound is then sealed with 9-mm wound clips.
13. Powdered Polysporin antibiotic is liberally applied to the surgical site.
14. Rats are removed from stereotaxic apparatus and transferred to a heated recovery box to recover. Animals are returned to their home cage once ambulatory (see Note 5).

### **3.3. Supradural Catheter Injectors and Injection Procedures**

#### **3.3.1. Supradural Catheter Injectors**

1. Remove the plastic hub from a sterile 30-G, ½-in. hypodermic needle, and insert blunt end into a 30 cm length of PE-10 tubing.
2. Insert an intact 30-G, ½-in. hypodermic needle into the open end of the PE-10 tubing.
3. Store prepared injectors in a sterile and dry container until needed.

#### **3.3.2. Supradural Catheter Injections**

1. Tightly connect a PE-10 catheter injector to a 50- $\mu$ L autoclaved Hamilton glass syringe, both flushed with sterile, endotoxin-free water, and creating an airtight seal.
2. Create an air bubble by drawing up 1–2  $\mu$ L prior and then draw up immunogenic stimulus. We have found that the optimal volume of injection is 6  $\mu$ L. Sufficient volume is drawn up to

accommodate injection into the left and right catheter. The air bubble serves as a marker that can be followed during drug administration. Stable, consistent movement of the bubble indicates a good injection, whereas slow movement or compression of the air bubble and lack of movement indicate problems with drug delivery that may confound behavioral testing.

3. The Hamilton syringe is situated in the infusion pump, and integrity and flow of the injector are confirmed.
4. Animals are gently wrapped in a towel such that the hands of individual holding the animal is protected from the rat's paws.
5. The sealed catheter tips are clipped, and the injector connected to the catheter. The injection is slowly passed through the catheter via the infusion pump such that 6  $\mu$ L is infused over 2 min and 16 s. Following the infusion, the injector remains connected to the catheter for 1 min.
6. The injector is removed from the catheter, and the tip resealed using heated forceps, and the other catheter injected.
7. A second injection is then given 2 h after the first. We have shown that this paradigm testing inflammatory soup or gp120 is required to successfully induce facial allodynia (see Note 6) (13).

### **3.4. Low-Threshold Periorbital Mechanical Allodynia**

1. All animals are habituated to the testing environment as previously described (see Note 7). Briefly, rats are placed, and encouraged to stay, in a leather testing glove in a quiet room for 5 days, 5 min/day prior to surgery (Fig. 2).
2. Baseline measures are collected the day before surgery, and again just prior to administration of immunogenic stimuli (usually 4–5 days postsurgery).
3. On the day of testing, the rat is placed in the leather testing glove for 5 min. At the end of the 5 min period, baseline responses to monofilaments is assessed. The periorbital region is stimulated five times with each filament for 2 s on each side of the face, alternating sides, and separating stimulations by approximately 3 s.
4. A response is counted when the animals moves away from the von Frey stimulus, or moves the stimulus away by paw swipe.
5. Our testing paradigm begins with testing the behavior response to the lowest monofilament, 4.56 (4 g), and recording responses, until the animal responds to all five stimulations with a single monofilament.
6. All responses are recorded and submitted to “PsychoFit (fat)” to assess 50% threshold values (see Note 8).



Fig. 2. The rat is held in a leather glove for facial allodynia testing. Prior to experimental manipulation, rats are habituated to the glove, and encouraged to stay in the glove during daily habituations over a 5-day period.

7. When the experimental paradigm is such that both left and right sides receive the same manipulation, the data from both sides can be averaged prior to analysis.
8. All testing is performed blinded with respect to group assignment.

---

#### 4. Notes

1. We have had the most success performing surgeries on rats 250–350 g, and optimal results in rats 300 g or less. Surgical difficulties have been encountered when larger animals are used. The skulls of the larger animals are noticeably different from the smaller rats, and because of this, the method used for drilling has to be modified dependent on the animal.
2. Care should be taken in cutting the catheter to size. If the catheter is longer than described, the rats tend to pull them out. A shorter catheter limits the number of possible injections.
3. A significant challenge of these surgeries is placing the catheter without puncturing the dura. An additional challenge is to place the catheter 2–3 mm lateral to the midsagittal sinus, and 1–2 mm anterior to the transverse sagittal sinus. If the catheter falls beyond these boundaries, behavioral changes in response

to immune stimuli are not detectable. The gradually descending troughs were developed to deal with these two issues. When done correctly, the troughs guide between the skull and dura, aiding in not puncturing the dura, and guiding a straight catheter to 2–3 mm from midline.

4. Clogged catheters can be an issue in this model. Keeping the catheters free of air bubbles eliminates clogging, as does maintaining an extremely clean surgical environment. Here, all tools are sterilized between animals, and gloves are worn for all surgical procedures, during construction of catheters and injectors, and during injections. Using these precautions, it has been our experience that these catheters remain viable for up to 20 days postsurgery.
5. With practice, an expert surgeon can expect to complete the surgery placing bilateral supradural catheters within 25 min, with a success rate routinely of 100%. A novice to these surgical procedures can expect to complete the surgery within 45–50 min. With experience, the success rate is approximately 84%, with rats being excluded from analysis due to catheters that are misplaced or dislodged/missing (<1%) or to have pierced the dura (~16%).
6. Experimental verification of the methods can be tested by two injections of inflammatory soup (5, 13) consisting of 1 mM histamine, serotonin, and bradykinin, and 0.1 mM prostaglandin E2, separated by 2 h. Reliable periorbital mechanical allodynia is observable 2 h after the second injection.
7. We have found that accurate behavioral measurement is dependent on the amount of handling the rats experience. Rats are given 1 week to acclimate to the colony room, with handling beginning 4 days after the arrive, and continuing to the day of surgery, 10 days after they arrive.
8. Analysis of behavioral data is as previously described by Milligan et al. (15) with two exceptions. In the downloaded template from L.O. Harvey's website (1) the Alpha (starting value) is set to 4.56 instead of 3.61 and (2) the log force of the stimuli need to be changed to the values listed above (See Subheading 2.4, item 2).

---

## Acknowledgments

We would like to thank John Mahoney and Niloofar Rezvani for technical assistance. This work was supported by GlaxoSmithKline, and NIH grants DA015642, DA022042, and DE017782, and well as the University of Colorado Undergraduate Research Opportunities Program.

## References

1. Burstein, R., Levy, D., and Jakubowski, M. (2005) Effects of sensitization of trigeminovascular neurons to triptan therapy during migraine. *Rev. Neurol. (Paris)* **161**, 658–660.
2. Vickers, E. R., and Cousins, M. J. (2000) Neuropathic orofacial pain part 1 – prevalence and pathophysiology. *Aust. Endod. J.* **26**, 19–26.
3. Cuadrado, M. L., Young, W. B., Fernandez-de-las-Penas, C., Arias, J. A., and Pareja, J. A. (2008) Migrainous corpalgia: body pain and allodynia associated with migraine attacks. *Cephalalgia* **28**, 87–91.
4. Burstein, R., and Jakubowski, M. (2004) Analgesic triptan action in an animal model of intracranial pain: a race against the development of central sensitization. *Ann. Neurol.* **55**, 27–36.
5. Burstein, R., Yamamura, H., Malick, A., and Strassman, A. M. (1998) Chemical stimulation of the intracranial dura induces enhanced responses to facial stimulation in brain stem trigeminal neurons. *J. Neurophysiol.* **79**, 964–982.
6. Itoh, T., Hirota, K., Hisano, T., Namba, T., and Fukuda, K. (2004) The volatile anesthetics halothane and isoflurane differentially modulate proinflammatory cytokine-induced p38 mitogen-activated protein kinase activation. *J. Anesth.* **18**, 203–209.
7. Kudo, M., Aono, M., Lee, Y., Massey, G., Pearlstein, R. D., and Warner, D. S. (2001) Effects of volatile anesthetics on N-methyl-D-aspartate excitotoxicity in primary rat neuronal-glia cultures. *Anesthesiology* **95**, 756–765.
8. Martin, D. C., Plagenhoef, M., Abraham, J., Dennison, R. L., and Aronstam, R. S. (1995) Volatile anesthetics and glutamate activation of N-methyl-D-aspartate receptors. *Biochem. Pharmacol.* **49**, 809–817.
9. Roughan, J. V., and Laming, P. R. (1998) Large slow potential shifts occur during halothane anaesthesia in gerbils. *J. Comp. Physiol. [A]* **182**, 839–848.
10. Toda, N., Toda, H., and Hatano, Y. (2008) Anesthetic modulation of immune reactions mediated by nitric oxide. *J. Anesth.* **22**, 155–162.
11. Wentlandt, K., Samoilova, M., Carlen, P. L., and El Beheiry, H. (2006) General anesthetics inhibit gap junction communication in cultured organotypic hippocampal slices. *Anesth. Analg.* **102**, 1692–1698.
12. Wise-Faberowski, L., Pearlstein, R. D., and Warner, D. S. (2006) NMDA-induced apoptosis in mixed neuronal/glia cortical cell cultures: the effects of isoflurane and dizocilpine. *J. Neurosurg. Anesthesiol.* **18**, 240–246.
13. Wieseler, J., Ellis, A., Sprunger, D., Brown, K., McFadden, A., Mahoney, J., Rezvani, N., Maier, S. F., and Watkins, L. R. (2009) A novel method for modeling facial allodynia associated with migraine in awake and freely moving rats. *J. Neurosci. Methods* **185**, 236–245.
14. Ren, K. (1999) An improved method for assessing mechanical allodynia in the rat. *Physiol. Behav.* **67**, 711–716.
15. Milligan, E. D., Maier, S. F., and Watkins, L. R. (2004) Sciatic inflammatory neuropathy in the rat: surgical procedures, induction of inflammation, and behavioral testing. *Methods Mol. Med.* **99**, 67–89.

## An Experimental Model of Headache-Related Pain

Rebecca M. Edelmayer, Michael H. Ossipov, and Frank Porreca

### Abstract

Migraine patients often demonstrate cutaneous allodynia, defined as a hypersensitivity of the skin to touch or mechanical stimuli that are normally innocuous. The allodynia sometimes begins intracranially and spreads, via unknown mechanisms, to extracranial regions. The goal of the study was to develop and validate a model of cutaneous allodynia triggered by dural inflammation for this aspect of pain associated with headaches.

Inflammatory mediators (IM) were applied to the dura of non-anesthetized rats via previously implanted cannulas and sensory thresholds of the face and hindpaws were characterized. IM elicited robust and time-related facial and hindpaw allodynia which peaked after approximately 3 h. These effects were reminiscent of cutaneous allodynia seen in patients with migraine or other primary headache conditions, and were reversed by agents used clinically in the treatment of migraine. Facial and hindpaw allodynia associated with dural stimulation is a useful surrogate of allodynia associated with primary headache including migraine likely reflecting the development of central sensitization and may be exploited mechanistically for the development of novel therapeutic strategies for headache pain.

**Key words:** Migraine, Headache, Cutaneous allodynia, Dural inflammation, Inflammatory mediators, Central sensitization

---

### 1. Introduction

It is difficult to treat migraine and primary headache pain because the medications available are often used as a temporary abortive remedy for symptomatic relief, are not well tolerated or effective against pain in many patients, and do not resolve the underlying disorder. In order to advance migraine therapy, there needs to be a way to test new medications for the disorder as well as study the mechanism behind the neurophysiology of the disorder. One of the best ways to advance research is to develop an animal model with relevance to this clinical condition. Animal models are crucial for translational science; they provide the congruent intermediate

link between the basic science bench and the clinic. Therefore, the main goal of this work was to develop a working animal model of primary headache-related pain. The approach was one of reverse translation, attempting to model preclinically a symptom associated with migraine headache, specifically, cutaneous allodynia as a reflection of central sensitization that might be occurring clinically.

The frequency of migraine headaches and the symptoms experienced can vary greatly from patient to patient. However, some of the classic symptoms experienced by migraineurs include throbbing head pain, aura, phonophobia, photophobia, nausea, vomiting, muscle tenderness, weariness, and fatigue. One of the most intriguing yet lesser recognized symptoms is the spontaneous head pain that sometimes begins unilaterally on one side of the head and then spreads to other areas of the head, face, neck, and other extracranial locations (1–4). This symptom that migraineurs experience over their entire body is known as cutaneous allodynia; defined as a hypersensitivity of the skin to touch or mechanical stimuli that are non-noxious under normal circumstances. The development of allodynia within the referred pain area may reflect the sensitization of the trigeminal system and higher structures (5, 6).

Sensitization of the trigeminovascular system is thought to begin with the activation of primary afferent nerves innervating the dural meninges and dural vasculature (6, 7), with consequent activation and sensitization of second-order neurons within the brainstem trigeminal nuclei (i.e., central sensitization) (7, 8). Both human and animal studies appear to support this neurophysiological progression, with the primary throbbing head pain occurring early in the attack apparently the result of activation and sensitization of primary afferent trigeminal fibers, followed by the development of central sensitization and referred pain after a significant time delay (9, 10).

Our laboratory was particularly interested in this symptom of migraine headache. As the mechanisms by which extracranial allodynia occurs remain largely unknown, it was hypothesized that an animal model of migraine headache which produced reproducible and quantifiable cutaneous allodynia could be utilized to mechanistically study the development and maintenance of migraine-related pain. For these studies, we explored the time-related development of cutaneous allodynia following inflammatory mediator (IM) application to the dura using a procedure modified from the work of Burstein and colleagues (11) as a model for intracranial pain in non-anesthetized freely moving animals. The following text describes the surgical and behavioral testing procedures necessary for stimulation and measurement of IM-induced cutaneous allodynia. A single application of dural IM has been shown to elicit time-related allodynia of the periorbital facial region in the animals. Critically, expression of allodynia following IM is generalized to other regions of

the body including the hindpaws. The model was further validated as a model of headache-related pain through administration of clinically efficacious headache therapies, as well as, neuroanatomically assessed for activation and sensitization of the trigeminal nociceptive system (12).

---

## 2. Materials

### 2.1. Surgical Preparation

1. Male, Sprague–Dawley rats (250–300 g; Harlan, Indianapolis, IN, USA) maintained on a 12-h light/dark cycle (lights on 07:00 h/lights off 07:00 h) with food and water available ad libitum.
2. Anesthetic, ketamine/xylazine (80 and 12 mg/kg, pre-mixed solution administered i.p., Sigma, St. Louis, MO, USA).
3. Stereotaxic apparatus (model 51600, Stoelting, Wood Dale, IL, USA).
4. Gauze sponges and cotton-tipped applicators (for cleaning incision).
5. Scalpel with #10 blade and four hemostats (#13013-14 is suggested, Fine Science Tools, Inc., Foster City, CA, USA).
6. Hand drill (DH-0 Pin Vise, Plastics One Inc., Roanoke, VA, USA) with # 60 drill bit (Ace Hardware).
7. Guide cannula (22 GA, #C313G, special ordered 1 mm in length, Plastics One Inc.), cannula was shortened to 0.5 mm from the plastic pedestal using a Dremel (see Note 1).
8. Super-glue gel.
9. Stainless steel screws (#MPX-080-3F-1M, Small Parts Inc., Miami Lakes, FL, USA).
10. Small Phillips-head screw driver.
11. Forceps, for retracting skin and holding screws (#11027-12 is suggested, Fine Science Tools, Inc.).
12. Fine forceps, for cleaning bone out of craniotomy and fine drill bit (#11253-21 is suggested, Fine Science Tools, Inc.).
13. Dental resin/acrylic (HYG00367 Perm acrylic and HYG00384 Liquid for cold cure acrylic, Dental Design Supply, Tucson, AZ, USA).
14. Dummy cannula (#C313DC, Plastics One Inc.), cut to fit exact length of the guide cannula (see Note 1).
15. 3–0 Silk suture (may be necessary to close incision).
16. Antibiotic Amikacin C (5 mg/kg, i.m., Associated Medical Supply, Scottsdale, AZ, USA).

## **2.2. Injection Procedures and Reagents**

1. Injection cannula (28GA, #C313I, Plastics One Inc.) cut to fit the exact length of the dura guide cannula (see Note 2).
2. 25  $\mu$ l Hamilton Syringe (#1702SN-22 gauge, custom 0.375 in., beveled point, Hamilton Company, Reno, NV, USA).
3. Tygon tubing (95607-14, Cole-Parmer, Vernon Hills, IL, USA).
4. Synthetic interstitial fluid (SIF): 5 mM KCl, 1 mM MgCl<sub>2</sub>, 5 mM CaCl<sub>2</sub>, and 135 mM NaCl in 10 mM Hepes buffer, pH 7.3 (all reagents purchased separately from Sigma). Store  $-20^{\circ}\text{C}$ .
5. Inflammatory mediator (IM) cocktail: 2 mM histamine, 2 mM serotonin, 2 mM bradykinin, and 0.2 mM prostaglandin E<sub>2</sub> in 10 mM Hepes buffer, pH 5.0 (all reagents purchased separately from Sigma). Store  $-20^{\circ}\text{C}$ .
6. Saline or dH<sub>2</sub>O (to backfill the tubing and syringe).
7. Protective gloves (for animal restraint).

## **2.3. Behavioral Testing**

1. von Frey testing chambers (made in-house).
2. Calibrated von Frey filaments (Touch Test Sensory Evaluator Kit, model 58011, Stoelting).

---

## **3. Methods**

### **3.1. Dura Cannulation**

1. Anesthesia was induced with ketamine/xylazine. The top of the head was shaved using a hair clipper and cleaned with betadine and 70% ethanol. Rats were placed into the ear bars and incisor bar ( $-3.5$  mm) of the stereotaxic apparatus.
2. A 2-cm incision was made in the skin using a scalpel, and the underlying connective tissue and skin were retracted using hemostats to expose the skull.
3. The location of the bregma and midline bone sutures were identified, and a small hole (1 mm in diameter) was made 1 mm left of midline and 1 mm anterior to the coronal suture in the frontal bone of the skull (Fig. 1). The hole was drilled with a hand drill to carefully expose the dura (see Note 3).
4. Two additional 1-mm holes were made on either side of the midline, approximately 4–5 mm caudal to the cannula, to mount stainless steel screws.
5. A guide cannula, designed to extend 0.5 mm from the pedestal to avoid irritation of the dural tissue, was inserted into the hole and sealed in place with glue (see Note 4). The design of the cannula allowed delivery of solutions to the underlying dural membrane without penetration or damage to the membrane (Fig. 2).

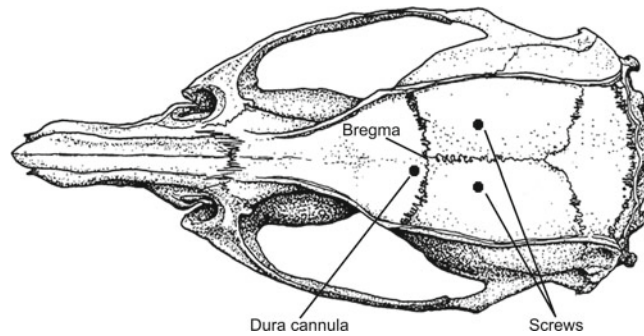


Fig. 1. Location of dura cannula. The location of the bregma and midline bone sutures was identified, and as indicated, a 1-mm hole was drilled for the dura cannula 1 mm left of midline and 1 mm anterior to the coronal suture in the frontal bone of the skull. Two additional 1-mm holes were made on either side of the midline approximately 4–5 mm caudal to the cannula to mount stainless steel screws. The screws were placed in the skull superficially to prevent damage to the underlying dural membrane. Skull diagram adapted with permission from Elsevier from ref. 14.

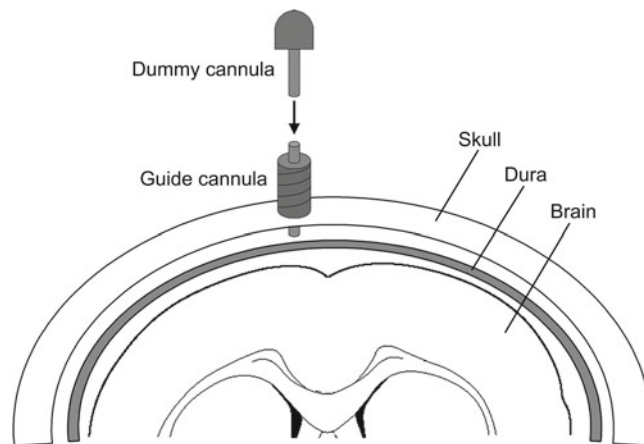


Fig. 2. Dura cannula design. A coronal section of the rodent brain displays the level of the dura cannula coordinates. A 1-mm hole was made in the frontal bone of the skull with a hand drill to carefully expose the dura. A guide cannula extending 0.5 mm from the pedestal to avoid irritation of the dural tissue was inserted into the hole and sealed in place with super-glue. Dental acrylic used to secure the cannula and screws to the skull. The design of the cannula allowed delivery of solutions to the underlying dural membrane without penetration of or damage to the membrane. A dummy cannula was inserted and secured to prevent contaminants from entering the guide cannula during the recovery period. Coronal brain section adapted with permission from Elsevier from ref. 14.

6. The screws were superficially placed in the skull to prevent damage to the underlying dural membrane (see Note 5).
7. The bone was cleaned dry of all blood and fluid before dental acrylic was applied to secure the cannula and screws to the skull (see Notes 6 and 7).

8. After the dental acrylic dried (5–10 min), a dummy cannula was inserted and secured to prevent contaminants from entering the guide cannula during the recovery period.
9. The skin was sutured closed around the dried acrylic and the antibiotic was administered (see Note 8).
10. Following recovery from anesthesia, animals were housed separately for a 6–8 day recovery period (see Note 9).

### **3.2. Injection Procedures and Reagents**

1. The animals, once removed from their testing chambers, were restrained by the hands of an experimenter during the entire length of the injection procedure (see Note 10). The dummy cannula was removed, but saved for reinsertion following the injection.
2. The 25- $\mu$ l Hamilton syringe joined to the injection cannula with a piece of Tygon tubing was backfilled with saline or dH<sub>2</sub>O before filling with experimental solutions (see Note 11).
3. The injection cannula was inserted into the guide cannula, the cannula snaps into place creating a closed seal around the guide cannula if inserted correctly.
4. A total volume of 10  $\mu$ l of the IM cocktail or vehicle (SIF) was then injected slowly (10–20 s) onto the dura. The IM and SIF compositions were adapted from solutions previously reported. The IM solution was formulated to yield a final concentration of 2 mM histamine, serotonin, and bradykinin, and 0.2 mM prostaglandin E2 in 10 mM Hepes buffer, pH 5.0, representing twice that used by Burstein and colleagues (8, 11). The SIF consisted of 10 mM Hepes, 5 mM KCl, 1 mM MgCl<sub>2</sub>, 5 mM CaCl<sub>2</sub>, and 135 mM NaCl, pH 7.3. Pilot studies were performed with varying IM concentrations, and the formulation providing a robust and consistent behavioral response was employed (see Notes 12 and 13).
5. Following the injection, the dummy cannula was replaced and the animals were returned to their corresponding testing chambers.

### **3.3. Behavioral Testing Protocols**

#### *3.3.1. Facial Sensory Testing of Non-noxious Tactile Stimuli in Rats*

1. Prior to surgery and on the day of testing, animals were acclimated to suspended plexiglass chambers (30 cm *L* × 15 cm *W* × 20 cm *H*) with a wire mesh bottom (1 cm<sup>2</sup>) for 30–60 min. The animals were allowed to freely move about their chambers during the entire testing protocol.
2. The baseline facial response thresholds to tactile stimuli were determined in response to probing with calibrated von Frey filaments. Each von Frey filament was applied for 3–6 s, perpendicular to the midline of the forehead, within a 3-mm diameter area at the level of the eyes, until buckling slightly.

A positive response was indicated by a sharp withdrawal of the head, which sometimes included an attempt to grasp and/or bite the filament.

3. Special care was taken when applying the filaments to the forehead to prevent a positive facial withdrawal response due to dynamic force and/or deflection of the facial hairs. The animals required some additional acclimatization to the experimenter's hand inside the cage before testing could begin. Animals were allowed to smell and explore the filament, and the gloved hand of the experimenter before the sequence of consecutive filaments was applied to the forehead.

### 3.3.2. Hindpaw Sensory Testing of Non-noxious Tactile Stimuli in Rats

1. Hindpaw measurements were always taken in the same animals that received the facial testing. The baseline hindpaw withdrawal thresholds to tactile stimuli were also determined in response to probing with calibrated von Frey filaments (see Note 14).
2. Each von Frey filament was applied perpendicularly to the plantar surface of both hindpaws until it buckled slightly, and was held for 3–6 s. A positive response was indicated by a sharp withdrawal of the hindpaw.

### 3.3.3. Experimental Testing Protocols

1. Baseline behavioral responses to probing of the face and hindpaws were obtained from all rats prior to drug administration.
2. Rats then received either SIF or IM via the dura cannula, and behavioral responses were determined at 1-h intervals, from time of injection, for 5–6 h (Fig. 3). Experimental drug administration can be performed either prior to dural cannula injection or at time points after dural injection to determine efficacy.

### 3.3.4. Calculation of Facial and Hindpaw Tactile Withdrawal Thresholds

1. The 50% facial/hindpaw withdrawal thresholds were determined using a non-parametric method (13). An initial probe equivalent to 1.0 g (facial) or 2.0 g (hindpaw) was applied. If the response was negative, the stimulus was increased one increment; otherwise, a positive response resulted in a decrease of one increment. The stimulus was incrementally increased until a positive response was obtained, then decreased until a negative result was observed. The following filament sequences were used for these studies: facial testing: 1.0, 2.0, 4.0, 6.0, and 8.0 g and hindpaw testing: 2.0, 4.0, 6.0, 8.0, and 15.0 g. This “up-down” method was repeated until three changes in behavior were determined.
2. The pattern of positive and negative responses was tabulated. The 50% facial/hindpaw withdrawal threshold is determined with the help of FlashDixon, a visual basic-based program developed in-house but available online at <http://www.u.arizona.edu/~michaelo/>. The thresholds can also be calculated using the equation  $(10^{[X_r + k\delta]}) / 10,000$ , where  $X_r$  = the value of the last

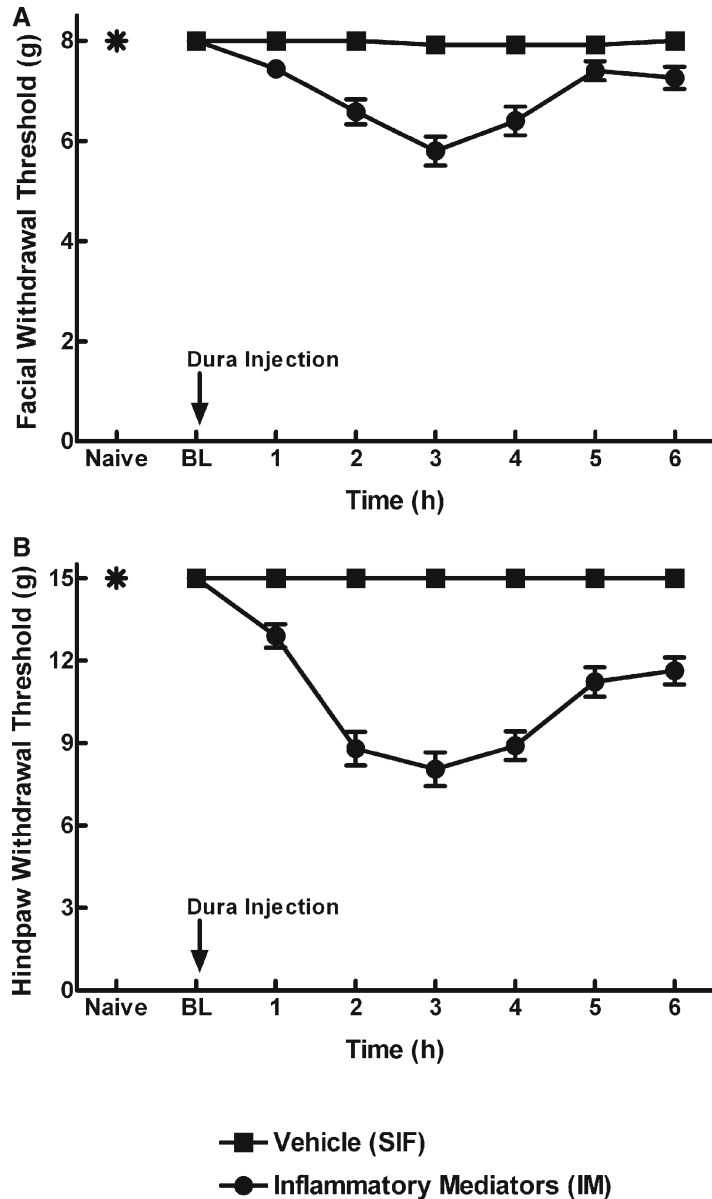


Fig. 3. Dural IM elicits cutaneous allodynia. Withdrawal thresholds to tactile stimuli applied to the face (a) and the hindpaw (b) were measured in rats before any surgical manipulations (naïve) and immediately before (BL, *baseline*) dural application of inflammatory mediators (IM, *circles*) or synthetic interstitial fluid (SIF, *squares*). No significant differences ( $P > 0.05$ ) between the responses of naïve rats and those receiving SIF indicated that surgery alone did not produce a sensitization of the face or hindpaws to tactile stimuli. Withdrawal responses to tactile stimuli applied to the face and hindpaws developed slowly over time and reached a maximal decrease in threshold 3 h after administration. Withdrawal responses to stimuli applied to the face and hindpaws approached baseline values 5 and 6 h, respectively, after IM administration. For both the face and hindpaw, two-factor analysis of variance indicated that response thresholds of IM-treated rats were significantly ( $P < 0.0001$ ) less than those of SIF-treated rats. Reproduced from *Medullary Pain Facilitating Neurons Mediate Allodynia in Headache-Related Pain*, 2009 with permission from John Wiley and Sons (12).

von Frey filament employed,  $k$ =Dixon value for the positive/negative pattern, and  $\delta$ =the mean (log) difference between stimuli.

3. Maximal filament strengths 8.0 and 15.0 g were used as the maximal cut-off values for non-noxious tactile stimulus of the face and hindpaw, respectively. Only animals with baselines of 8.0 g (facial) and 15.0 g (hindpaw) were used in the experiments.

### 3.3.5. Data Analysis

1. Withdrawal thresholds to probing the face and hindpaws were determined at 1-h intervals after administration of IM or SIF.
2. Comparisons among treatment groups were performed by 2-factor ANOVA for repeated measures.

---

## 4. Notes

1. Guide and dummy cannula preparation: tightly screw the dummy cannula into the guide cannula. Then use an electric Dremel with a fine sanding tool attachment to carefully sand down the metal column to 0.5 mm in length from the plastic white pedestal. It is important to hand sand any burrs that are present at the tip of the cannula. These burrs can irritate the dura once the cannula is cemented in place.
2. It is easiest to make injection cannulas at the same time that you prepare the guide cannulas. Insert the injection cannula into the guide cannula until it snaps into place, then sand down the injection cannula to equal the exact length of the guide. It is important to check the patency of the injector. If the cannula hole becomes sealed during sanding, it can be unblocked using the tip of a 30-gauge needle.
3. Drilling the hole for the cannula must be done very carefully. The length of the drill bit should extend  $\leq 0.5$  mm in length beyond the head of the drill. Using a hand drill instead of an electric Dremel is helpful because the hand drill will prevent accidental puncture of the dura and cortex. It is best to spin the drill carefully, cleaning the bit periodically to remove small pieces of bone. It may be necessary to remove any lingering skull bone from the hole with a fine pair of forceps.
4. Placing a very small amount of super glue on the white pedestal of the guide cannula not only helps to stabilize the cannula, but also helps to create a seal around the hole to prevent leakage during the injection.
5. It is best to drill the cannula and screw holes first. Glue the cannula into place and then insert the screws into their respective holes. This gives the glue some time to dry and set before applying the dental acrylic.

6. In some cases, it may be necessary to cauterize small blood vessels on the surface of the skull to make the bone as dry as possible. This will help the acrylic to adhere to the surface of the skull.
7. Mix a small amount of the dental resin and acrylic just before using. The consistency should be close to a wet paste. Pour or scoop the acrylic onto the skull around the cannula. Be sure that the screws are covered well and the acrylic covers only half of the white pedestal of the cannula; the dummy cannula needs to be able to tightly screw onto the guide cannula. The edges of the acrylic should be smooth to the touch; if there are sharp points the animal can easily grab hold of the corners and tear the headpiece off during recovery. The animal should look like it is wearing a small circular hat when the acrylic is completely dry.
8. It may not be necessary to suture the incision closed. If the skin incision is made small enough, it will easily heal around the cap. Only use sutures if there is larger than 0.5 cm of open incision still visible after the acrylic dries. There will be some inflammation around the incision site during the healing process and if the skin is sutured too tightly around the cap, it tends to cause the animal to scratch at the wound. If sutures are necessary, it is best to make them towards the back of the head, not close to the eyes. Behavioral testing of the head requires that the area above and between the eyes is free from debris and scarring.
9. In a separate group of practice animals or following an experiment, cannula placement and integrity of the dura can be confirmed with microinjection of 10  $\mu$ l of India ink, which in successful surgeries will spread 3–5 mm on the dorsal aspect of the dura without penetrating the brain.
10. Injections are easiest with two people; one person to perform the injection and the other to hold the animal. The animals dislike the injection, and they should be restrained on a flat surface where the experimenter can use two hands to immobilize the head and the body of the animal. There is a transient behavioral response related to the mechanical stimulus produced by the volume of the injection. The animals will vocalize and attempt to evade the handler during the injection. This behavior is normal and can be used as an indicator of successful drug delivery. If the animals do not vocalize or struggle, it is possible that leakage is occurring (between the skull and the acrylic or sometimes the cannula is clogged and leakage can be seen between the guide cannula and the injection cannula). Animals that do not receive a proper injection should be removed from the study.

11. Backfilling the syringe and tygon tubing with saline or dH<sub>2</sub>O can be helpful, because it is a pressurized injection. Leave a decent air bubble between the backfill solution and the IM or SIF solutions. The bubble is easy to follow and can be used to confirm a complete injection.
12. Aliquots of the IM and SIF cocktails should be stored at –20°C for no longer than 2 weeks. It is best to prepare new IM before an experiment because the stability of the compounds within the mixture cannot be verified. The IM cocktail is light sensitive and should be covered during storage and during preparation. It is the serotonin that is most sensitive to light.
13. When preparing IM, it is best to make a small stock solution of prostaglandin E<sub>2</sub> (PGE<sub>2</sub>) before adding it to the rest of the cocktail. PGE<sub>2</sub> can take some time to dissolve in the Hepes buffer. To speed up the process, the stock solution can be placed in a water bath sonicator for 15 min followed by vortexing. This solution can then be added to the IM cocktail.
14. Testing hindpaw behavioral responses should be conducted in both hindpaws because the dural injection is not necessarily lateralized. The injection is very close to midline and the spread of the IM and SIF will cross over the midline. If a positive response is recorded in one hindpaw, it is still important to continue to test both paws with the sequence of filaments using the “up-down” method. Data analysis from many animals indicates that the positive responses in the hindpaw are not lateralized following dural inflammation. The allodynia is generalized to both hindpaws.

## References

1. Burstein, R., Yarnitsky, D., Goor-Aryeh, I., Ransil, B. J., and Bajwa, Z. H. (2000) An association between migraine and cutaneous allodynia, *Ann. Neurol.* **47**, 614–624.
2. Cooke, L., Eliasziw, M., and Becker, W. J. (2007) Cutaneous allodynia in transformed migraine patients, *Headache* **47**, 531–539.
3. Dodick, D. and Silberstein, S. (2006) Central sensitization theory of migraine: clinical implications, *Headache* **46 Suppl 4**, S182–S191.
4. Guy, N., Marques, A. R., Orliaguet, T., Lanteri-Minet, M., Dallel, R., and Clavelou, P. (2010) Are there differences between cephalic and extracephalic cutaneous allodynia in migraine patients? *Cephalalgia* **30**, 881–886.
5. Ashkenazi, A., LoPinto, C., and Young, W. B. (2005) Referred cutaneous allodynia in a migraine patient without simultaneous headache, *Cephalalgia* **25**, 75–78.
6. Burstein, R., Cutrer, M. F., and Yarnitsky, D. (2000) The development of cutaneous allodynia during a migraine attack clinical evidence for the sequential recruitment of spinal and supraspinal nociceptive neurons in migraine, *Brain* **123 (Pt 8)**, 1703–1709.
7. Strassman, A. M., Raymond, S. A., and Burstein, R. (1996) Sensitization of meningeal sensory neurons and the origin of headaches, *Nature* **384**, 560–564.
8. Burstein, R., Yamamura, H., Malick, A., and Strassman, A. M. (1998) Chemical stimulation of the intracranial dura induces enhanced responses to facial stimulation in brain stem trigeminal neurons, *J. Neurophysiol.* **79**, 964–982.
9. Bigal, M. E., Ashina, S., Burstein, R., Reed, M. L., Buse, D., Serrano, D., and Lipton, R. B. (2008) Prevalence and characteristics of allodynia in headache sufferers: a population study, *Neurology* **70**, 1525–1533.
10. Landy, S., Rice, K., and Lobo, B. (2004) Central sensitisation and cutaneous allodynia in

- migraine: implications for treatment, *CNS. Drugs* **18**, 337–342.
11. Malick, A., Jakubowski, M., Elmquist, J. K., Saper, C. B., and Burstein, R. (2001) A neuro-histochemical blueprint for pain-induced loss of appetite, *Proc. Natl. Acad. Sci. USA*. **98**, 9930–9935.
  12. Edelmayer, R. M., Vanderah, T. W., Majuta, L., Zhang, E. T., Fioravanti, B., De, F. M., Chichorro, J. G., Ossipov, M. H., King, T., Lai, J., Kori, S. H., Nelsen, A. C., Cannon, K. E., Heinricher, M. M., and Porreca, F. (2009) Medullary pain facilitating neurons mediate allodynia in headache-related pain, *Ann. Neurol.* **65**, 184–193.
  13. Dixon, W. J. (1980) Efficient analysis of experimental observations, *Annu. Rev. Pharmacol. Toxicol.* **20**, 441–462.
  14. Paxinos, G. and Watson, C. (1998) The rat brain; In stereotaxic coordinates, 4th edition, Academic Press, San Diego, CA, USA.

## A Rodent Model of Trigeminal Neuralgia

David C. Yeomans and Mikhail Klukin

### Abstract

Trigeminal Neuralgia (Tic Douloureux) is a neuropathic pain syndrome caused by compression of the trigeminal nerve root and is characterized by severe paroxysms of pain in the face commonly triggered by light mechanical stimulation to the peri-oral area. Trigeminal neuralgia is very difficult to treat in part due to the lack of a suitable animal model for testing novel therapeutic approaches. This chapter describes a model of trigeminal neuralgia in which crystals of a superabsorbent polymer are placed next to the trigeminal nerve root of rats, producing ongoing mechanical compression of the nerve root. The chapter then describes means of behaviorally assessing the robust mechanical hypersensitivity consequent to the compression that can be used to determine the efficacy of potential therapies for this devastating condition.

**Key words:** Neuropathic pain, Orofacial, Trigeminal neuralgia, Tic Douloureux, Craniofacial, Rat behavior, Allodynia, Compression

---

### 1. Introduction

Considered one of the most painful of all medical conditions (1, 2), trigeminal neuralgia is a chronic neuropathic pain syndrome in which patients experience intense paroxysms of lancinating pain in the face along one or more branches of the trigeminal nerve (3–5). There is overwhelming evidence that trigeminal nerve root demyelination or dysmyelination is the underlying cause of trigeminal neuralgia, most frequently as a result of nerve root compression. Focal nerve root compression by an artery or vein as the cause of trigeminal neuralgia was first thoroughly described by Jannetta in 1967 (6), and it is now thought that 80–90% of all cases of trigeminal neuralgia result from vascular nerve root compression (7–14). Evidence for vascular compression is given by (a) recent imaging studies and intra-operative observations, consistently showing a blood vessel contacting the nerve root (10, 15, 16); (b) the fact that surgical microvascular decompression (MVD) provides at least

temporary pain relief in most patients (15, 17); (c) the finding that intra-operative recordings often show an immediate improvement of nerve conduction velocity slowing after MVD (15, 18); and (d) the observation that sensory deficits also recover after MVD, albeit more slowly (15, 19). Various other non-vascular compressive lesions have also been associated with trigeminal neuralgia, including posterior fossa tumors, cysts, and bony compression (14).

It has been shown convincingly that demyelination occurs at the site of nerve root compression in trigeminal neuralgia patients (14, 15, 20–22). In addition to demyelination associated with compression, there is a well-established association of multiple sclerosis (MS) and trigeminal neuralgia (15, 23–27). That the common pathological finding in trigeminal neuralgia patients with nerve root compression and those with MS is a demyelinated region of the nerve roots near the brainstem (28) provides strong evidence of demyelination, most commonly secondary to compression, as the underlying cause of trigeminal neuralgia. Furthermore, anatomical and physiological studies have demonstrated that peripheral nerve constriction results in substantial loss of large myelinated nerve fibers (25), with significant functional consequence (29–39). Demyelination leads to changes in sodium channel distribution along the axon, leading to enhanced excitability despite slowed conduction (40).

The extent to which new treatments can be developed based on mechanistic knowledge and empirical evidence has been limited by the lack of an adequate animal model that accurately reflects human pathology. This chapter describes a new rodent model for trigeminal neuralgia that simulates the natural cause and symptoms of the disease by introducing an artificial compression of the trigeminal nerve root. The model lends itself to behavioral, electrophysiological, molecular biological, anatomical, and pharmacological experiment assessments of the mechanisms and potential therapies for this devastating neuropathic disease.

---

## 2. Materials

### 2.1. Polymer Injection

1. Animal anesthesia machine (ours was custom built using a vaporizer from Ohio Medical Products, Airco, Madison, WI).
2. Isoflurane IsoThesia (Butler Animal Health Supply, Dublin, OH).
3. Single arm stereotaxic frame with 45° Ear Bars (WPI, Mod.502650).
4. Rat anesthesia mask adaptor (WPI, Mod.502054) can be used, but we prefer a custom built, prototype described in ref. 41.

5. Betadine Solution (Povidone-iodine 10%) (The Purdue Frederick Company, Stamford, CT).
6. Cotton-tipped applicators, 3 in. (Puritan Medical Products, Guilford, ME).
7. Electric shaver (Oster, Minnville, TN).
8. Fiber optic illuminator (WPI).
9. Germinator 500 Dry sterilizer (Roboz, Gaitherburg, MD).
10. Scalpel handle No. 3 (BRI Stainless, Germany).
11. Bard-Parker Rib-back scalpel blade (Becton Dickinson AcuteCare, Franklin Lakes, NJ).
12. 2 in. Bulldog clamps, curved (2) (BRI Stainless, Germany).
13. Hemostat Mixer 5½ in., curved (2) (Roboz, Gaitherburg, MD).
14. Cotton pellets No. 3 (Richmond, Charlotte, NC).
15. Forceps micro dissecting 4 in., straight serrated (Roboz, Gaitherburg, MD).
16. Wizard rotary tool (Black and Decker, New Britain, CT).
17. Micro Drill Steel Burr 1.4 mm (Meisinger, Germany).
18. Superabsorbent biocompatible polymer LiquiBlock 14G-50 (Emerging Technologies, Greensboro, NC).
19. Superabsorbent biocompatible polymer Norsocryl S-35 (Emerging Technologies, Greensboro, NC).
20. Polymer injection needle, custom built by tapering 3.5 in., Quincke point, 20 G, Spinal needle (Becton Dickinson AcuteCare, Franklin Lakes, NJ).
21. Bone Wax (Ethicon, Somerville, NJ).
22. Michel Clip Applying-Removing Forceps, 5 in. (Roboz, Gaitherburg, MD).
23. Michel wound clips, 7.5 mm (Perfect, France).
24. Antibiotic ointment (CVS Pharmacy, Woonsocket, RI).

**2.2. Feeding/Peri-oral  
Sensitivity  
Assessment**

1. Plexiglas observation cage (30 cm × 30 cm × 40 cm).
2. Rat chow biscuit (approx. 5 g each; LabDiet 5P00 Prolab RHM 3000; PMI, Gray Summit, MO).
3. Timer with alarm (Triple-Display Timer, VWR, Batavia, IL).
4. 10 × 10 Weigh paper (VWR, Batavia, IL).
5. Balance is (ZSA 80, Scientech Boulder, CO).

**2.3. Touch Allodynia  
Testing**

1. Rat cage.
2. Touch-test sensory evaluator (von Frey monofilaments) 1, 6, 10, 26, and 60 g (North Coast Medical, San Jose, CA).

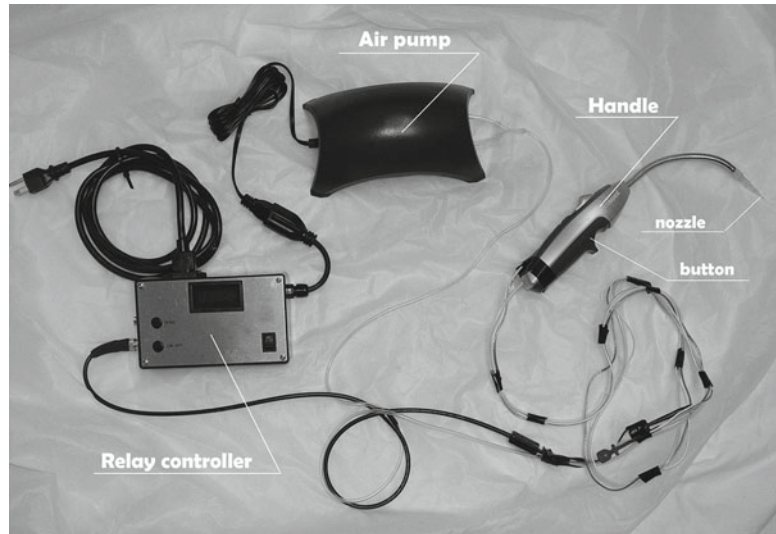


Fig. 1. Photographic illustration of air-puff stimulator. Individual components are indicated by *arrows and labels*.

#### 2.4. Air-Puff Testing

1. Rat cage.
2. Air-puff device is based on a Tetra Whisper 60 aquarium Air Pump with both outlets y-connected to a 4-mm elastic tubing. A Benzomatic flexible stem gas lighter was used to make a handle. After removing all lighter-related parts, 3.5-mm polyethylene tubing is run through the housing and connected it to a plastic nozzle glued to the tip of the stem. System produces force of 0.35 g—measured by fixing tip 7 mm from balance. For safety reasons, the pump is switched on and off with a relay controlled by a button installed in the handle (Fig. 1).

### 3. Methods

#### 3.1. Trigeminal Root Compression Model Using Stereotaxic Polymer Injection (See Note 1)

1. Adult, male Sprague–Dawley rats (250–300 g) are deeply anesthetized with isoflurane (2.5%) in a chamber, and then moved to a stereotaxic frame with ear bars coated with soft plastic to prevent tympanic membrane damage. The frame is equipped with a mask to deliver fresh isoflurane (2.5%) and remove expired isoflurane in a balance of oxygen-supplemented room air (30/70%).
2. The dorsal head and neck are shaved, and iodine solution applied to the area for asepsis.
3. Using a #10 scalpel blade, a midline skin incision is made from bregma to 10 mm caudal from the inter-aural line, spanning ~1.5 cm.

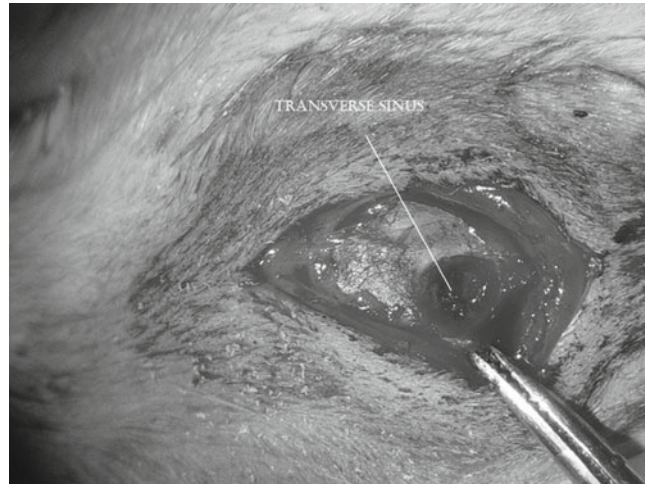


Fig. 2. Appearance and location of transverse sinus.

4. Connective tissue and periosteum are scraped clear on the entire left dorsal surface of interparietal bone.
5. Using a rotary tool with a round 1.4-mm burr bit a round trephination window (diameter 2.5–3 mm) is made in the left laterocaudal-most part of interparietal bone dorsal surface.
6. Bone hemostasis is then achieved with cotton pellets and bone wax (see Note 2).
7. The caudal edge of the left transverse sinus is, at this point, clearly visible through the intact meninges (Fig. 2). A tapered spinal injection needle with fitted steel stylet (20 gauge) preloaded with  $\sim 0.5 \text{ mm}^3$  of superabsorbent biocompatible polymer (SAP) granules is then installed in a micromanipulator at  $35^\circ$  caudally from perpendicular to the skull with the bevel side oriented laterocaudally, and zeroed to lambda (see Notes 3 and 4).
8. The manipulator is then used to position the needle 3.5 mm lateral and 3 mm caudal to lambda (Fig. 3).
9. Using a standard 23-G injection needle, meninges are carefully cut just caudally to the left transverse sinus, with attention paid to avoid damage to the sinus.
10. The injection needle is then advanced 8.5 mm into the trigeminal canal, its tip eventually sliding toward the *pars petrosa* of temporal bone and reaching the space between the trigeminal sensory root and the temporal bone.
11. The polymer crystals are then administered by manually pushing a metal stylet through the barrel of the injection needle such that it becomes flush with the tip.

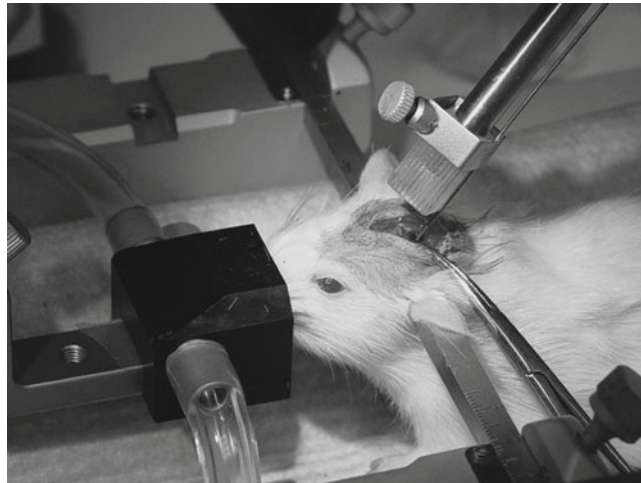


Fig. 3. Correct placement of injection needle.

12. The needle is then withdrawn, the hole in the dura and skull sealed with bone wax, and the incision closed using wound clips.
13. The rat is then placed in its home cage under a heat lamp until it has recovered from anesthesia.

### **3.2. Behavioral Testing**

Trigeminal neuralgia patients experience ectopic, spontaneous unilateral pain paroxysms as well as paroxysms evoked by light touch. Thus, natural behaviors, such as eating, as well as responses evoked by mechanical stimuli, such as von Frey monofilaments (39); and air puff (42–44) are used as an indication of the presence and extent of sensory disturbance in rats after trigeminal nerve root compression. These behavioral indices can be used to examine the potential efficacy of pharmacologic agents and other therapeutics in the treatment of trigeminal neuralgia.

#### *3.2.1. Feeding/Peri-oral Sensitivity Operant Assessment*

1. Before and at various time points after polymer injection, eating behaviors will be quantified as an indication of peri-oral hypersensitivity (see Note 5).
2. Rats are first habituated to the Plexiglas observation cage (30 cm × 30 cm × 40 cm) during three daily sessions and for at least 15 min on the first day of testing.
3. On the day before polymer application, rats are food deprived overnight for 12–14 h.
4. On the day of polymer application, rats are given a pre-weighed rat chow biscuit on a large piece of weigh paper and allowed 20 min to eat.
5. After 20 min, rats are removed from cage and remaining biscuit weighed.

6. At 7, 14, and 28 days after polymer injection, procedure is repeated to determine effects of trigeminal root compression on peri-oral sensitivity (see Notes 6 and 7).
7. At desired endpoints, some rats can be euthanized and trigeminal tissue removed for molecular biological or immunochemical analysis (see Note 8).

### 3.2.2. von Frey Allodynia Testing

1. Rats are tested in their own home cages after habituation to the investigator and the von Frey fibers until they appear indifferent to their presence.
2. Prior to polymer application, rats are subjected to five trials on each side of the face of stimulation, with each of the four different von Frey fibers used (0.4, 1.4, 6, and 15 g). The response to each stimulation trial is scored as: 0 = no response; 1 = non-aversive response (detection, weak withdrawal); 2 = mildly aversive response (moderate withdrawal and swipe towards the fiber with the forepaw); 3 = moderately aversive response (strong withdrawal and pushing the fiber away from the face with the forepaw); and 4 = strongly aversive response (attack or vocalization). This scoring method is similar to that described by Vos et al. (39).
3. The scores of the three trials are averaged for each side of the face in each rat and for each of the four fibers.
4. At 7, 14, and 28 days after polymer injection, rats are retested to determine effects of trigeminal root compression on tactile sensitivity.
5. At desired endpoints, some rats can be euthanized and trigeminal tissue removed for molecular biological or immunochemical analysis.

### 3.2.3. Air-Puff Allodynia Testing

1. A custom-designed, pressure-regulated air-puff stimulator is used to provide air stimulation to rats before and after trigeminal nerve root compression.
2. Rats are habituated to the investigator and the hand-held air-puff stimulator until they appear indifferent to their presence (at least 15 min).
3. Ten consecutive trials of constant-pressure air puffs, 4 s duration, 10 s interstimulus interval (42) is performed on each side of the face.
4. At 7, 14, and 28 days after polymer injection, rats are retested to determine effects of trigeminal root compression on tactile sensitivity.
5. At desired endpoints, some rats can be euthanized and trigeminal tissue removed for molecular biological or immunochemical analysis.

### 3.3. Other Measures

In addition to behavioral changes, anatomic changes (demyelination, nodal displacement, and ion channel rearrangement) and electrophysiologic changes (ectopic discharge, decreased thresholds, prolonged responses in trigeminal ganglia, and nucleus caudalis neurons) are useful in examining the mechanisms underlying the pain of trigeminal neuralgia.

---

## 4. Notes

1. The duration of the procedure is about ~35 min, including induction time.
2. Bleeding is usually easily controlled, and rats recover quickly.
3. Sham surgery is identical except that no polymer is loaded into the needle prior to insertion.
4. SAP is a biocompatible, non-toxic substance (sodium polyacrylate) that slowly expands over time by absorbing water or in this case, extracellular fluid. Within the closed volume of the skull, this increase takes place over several days, gradually producing an increasing degree of compression of the trigeminal nerve root (Fig. 4). This method allows for visual guidance of the needle, minimizing the risk of transverse sinus damage; it does not penetrate brain or skull structures; is at low risk of damaging the ventrally located motor trigeminal root. However, due to the precision necessary for this procedure, as well as individual anatomical variations, risks still exist of major bleeding or stroke from perforated sinus or other blood vessels, and from damage to the cerebellum or auditory nerve.



Fig. 4. Stereophotomicrograph of underside of brain 2 weeks after application of polymer to trigeminal root entry zone (*arrow*) demonstrating compression of the trigeminal nerve root.

5. Model provides a natural, operant assessment of peri-oral sensitivity—which is symptomatic of trigeminal neuralgia.
6. Additional time points can be added as needed.
7. Rats with trigeminal root compression typically “freeze” at certain points during biscuit eating. Freeze latencies and durations can also be measured by video analysis to provide assessment of paroxysmal sensations.
8. At any of the time points, experimental treatments can be used prior to testing in order to examine potential analgesic therapies.

---

## Acknowledgments

The authors would like to acknowledge the assistance of Dr. Yanli Qiao and Neil Manering. They would also like to acknowledge the support provided by PHS grant R01DE018531, “Chronic Compression of the Trigeminal Ganglia”.

## References

1. Fromm, G. H. (1991) *Trigeminal neuralgia: current concepts regarding pathogenesis and treatment*, Butterworth-Heinemann, Boston.
2. Turp, J. C., and Gobetti, J. P. (1996) Trigeminal neuralgia versus atypical facial pain. A review of the literature and case report, *Oral Surg Oral Med Oral Pathol Oral Radiol Endod* **81**, 424–432.
3. Bogduk, H. M. N. (1994) *Classification of chronic pain. Descriptions of Chronic Pain Syndromes and Definitions of Pain Terms*, IASP Press, Seattle.
4. Dubner, R., Sharav, Y., Gracely, R. H., and Price, D. D. (1987) Idiopathic trigeminal neuralgia: sensory features and pain mechanisms, *Pain* **31**, 23–33.
5. Kugelberg, E., and Lindblom, U. (1959) The mechanism of the pain in trigeminal neuralgia, *J Neurol Neurosurg Psychiatry* **22**, 36–43.
6. Jannetta, P. J. (1967) Arterial compression of the trigeminal nerve at the pons in patients with trigeminal neuralgia, *J Neurosurg* **26**, Suppl:159–162.
7. Haines, S. J., Jannetta, P. J., and Zorub, D. S. (1980) Microvascular relations of the trigeminal nerve. An anatomical study with clinical correlation, *J Neurosurg* **52**, 381–386.
8. Jannetta, P. J. (1980) Neurovascular compression in cranial nerve and systemic disease, *Ann Surg* **192**, 518–525.
9. Richards, P., Shawdon, H., and Illingworth, R. (1983) Operative findings on microsurgical exploration of the cerebello-pontine angle in trigeminal neuralgia, *J Neurol Neurosurg Psychiatry* **46**, 1098–1101.
10. Meaney, J. F., Eldridge, P. R., Dunn, L. T., Nixon, T. E., Whitehouse, G. H., and Miles, J. B. (1995) Demonstration of neurovascular compression in trigeminal neuralgia with magnetic resonance imaging. Comparison with surgical findings in 52 consecutive operative cases, *J Neurosurg* **83**, 799–805.
11. Bowsher, D. (1997) Trigeminal neuralgia: an anatomically oriented review, *Clin Anat* **10**, 409–415.
12. Hamlyn, P. J. (1997) Neurovascular relationships in the posterior cranial fossa, with special reference to trigeminal neuralgia. 2. Neurovascular compression of the trigeminal nerve in cadaveric controls and patients with trigeminal neuralgia: quantification and influence of method, *Clin Anat* **10**, 380–388.
13. McLaughlin, M. R., Jannetta, P. J., Clyde, B. L., Subach, B. R., Comey, C. H., and Resnick, D. K. (1999) Microvascular decompression of cranial nerves: lessons learned after 4400 operations, *J Neurosurg* **90**, 1–8.
14. Love, S., and Coakham, H. B. (2001) Trigeminal neuralgia: pathology and pathogenesis, *Brain* **124**, 2347–2360.

15. Nurmikko, T. J., and Eldridge, P. R. (2001) Trigeminal neuralgia – pathophysiology, diagnosis and current treatment, *Br J Anaesth* **87**, 117–132.
16. Boecher-Schwarz, H. G., Bruehl, K., Kessel, G., Guenther, M., Pernecky, A., and Stoeter, P. (1998) Sensitivity and specificity of MRA in the diagnosis of neurovascular compression in patients with trigeminal neuralgia. A correlation of MRA and surgical findings, *Neuroradiology* **40**, 88–95.
17. Jackson, E. M., Bussard, G. M., Hoard, M. A., and Edlich, R. F. (1999) Trigeminal neuralgia: a diagnostic challenge, *Am J Emerg Med* **17**, 597–600.
18. Leandri, M., Eldridge, P., and Miles, J. (1998) Recovery of nerve conduction following microvascular decompression for trigeminal neuralgia, *Neurology* **51**, 1641–1646.
19. Miles, J. B., Eldridge, P. R., Haggert, C. E., and Bowsher, D. (1997) Sensory effects of microvascular decompression in trigeminal neuralgia, *J Neurosurg* **86**, 193–196.
20. Hilton, D. A., Love, S., Gradidge, T., and Coakham, H. B. (1994) Pathological findings associated with trigeminal neuralgia caused by vascular compression, *Neurosurgery* **35**, 299–303; discussion 303.
21. Love, S., Hilton, D. A., and Coakham, H. B. (1998) Central demyelination of the Vth nerve root in trigeminal neuralgia associated with vascular compression, *Brain Pathol* **8**, 1–11; discussion 11–12.
22. Rappaport, Z. H., Govrin-Lippmann, R., and Devor, M. (1997) An electron-microscopic analysis of biopsy samples of the trigeminal root taken during microvascular decompressive surgery, *Stereotact Funct Neurosurg* **68**, 182–186.
23. Jensen, T. S., Rasmussen, P., and Reske-Nielsen, E. (1982) Association of trigeminal neuralgia with multiple sclerosis: clinical and pathological features, *Acta Neurol Scand* **65**, 182–189.
24. Moulin, D. E., Foley, K. M., and Ebers, G. C. (1988) Pain syndromes in multiple sclerosis, *Neurology* **38**, 1830–1834.
25. Hooge, J. P., and Redekop, W. K. (1995) Trigeminal neuralgia in multiple sclerosis, *Neurology* **45**, 1294–1296.
26. Love, S., Gradidge, T., and Coakham, H. B. (2001) Trigeminal neuralgia due to multiple sclerosis: ultrastructural findings in trigeminal rhizotomy specimens, *Neuropathol Appl Neurobiol* **27**, 238–244.
27. Osterberg, A., Boivie, J., and Thuomas, K. A. (2005) Central pain in multiple sclerosis – prevalence and clinical characteristics, *Eur J Pain* **9**, 531–542.
28. Fromm, G. H., Terrence, C. F., and Maroon, J. C. (1984) Trigeminal neuralgia. Current concepts regarding etiology and pathogenesis, *Arch Neurol* **41**, 1204–1207.
29. Bennett, G. J., and Xie, Y. K. (1988) A peripheral mononeuropathy in rat that produces disorders of pain sensation like those seen in man [see comments], *Pain* **33**, 87–107.
30. Weisl, H., and Osborne, G. V. (1964) The Pathological Changes in Rats' Nerves Subject to Moderate Compression, *J Bone Joint Surg Br* **46**, 297–306.
31. Laird, J. M., and Bennett, G. J. (1992) Dorsal root potentials and afferent input to the spinal cord in rats with an experimental peripheral neuropathy, *Brain Res* **584**, 181–190.
32. Laird, J. M., and Bennett, G. J. (1993) An electrophysiological study of dorsal horn neurons in the spinal cord of rats with an experimental peripheral neuropathy, *J Neurophysiol* **69**, 2072–2085.
33. Cragg, B. G., and Thomas, P. K. (1961) Changes in conduction velocity and fibre size proximal to peripheral nerve lesions, *J Physiol* **157**, 315–327.
34. Ebeling, P., Gilliat, R. W., and Thomas, P. K. (1960) A clinical and electrical study of ulnar nerve lesions in the hand, *J Neurol Neurosurg Psychiatry* **23**, 1–9.
35. Thomas, P. K. (1960) Motor nerve conduction in the carpal tunnel syndrome, *Neurology* **10**, 1045–1050.
36. Kitagawa, J., Takeda, M., Suzuki, I., Kadoi, J., Tsuboi, Y., Honda, K., Matsumoto, S., Nakagawa, H., Tanabe, A., and Iwata, K. (2006) Mechanisms involved in modulation of trigeminal primary afferent activity in rats with peripheral mononeuropathy, *Eur J Neurosci* **24**, 1976–1986.
37. Burchiel, K. J. (1980) Abnormal impulse generation in focally demyelinated trigeminal roots, *J Neurosurg* **53**, 674–683.
38. Vos, B. P., and Strassman, A. M. (1995) Fos expression in the medullary dorsal horn of the rat after chronic constriction injury to the infraorbital nerve, *J Comp Neurol* **357**, 362–375.
39. Vos, B. P., Strassman, A. M., and Maciewicz, R. J. (1994) Behavioral evidence of trigeminal neuropathic pain following chronic constriction injury to the rat's infraorbital nerve, *J Neurosci* **14**, 2708–2723.
40. England, J. D., Levinson, S. R., and Shrager, P. (1996) Immunocytochemical investigations of sodium channels along nodal and internodal portions of demyelinated axons, *Microsc Res Tech* **34**, 445–451.

41. Davis, J. A. (2008) Mouse and rat anesthesia and analgesia, *Curr Protoc Neurosci Appendix 4*, Appendix 4B.
42. Ahn, D. K., Jung, C. Y., Lee, H. J., Choi, H. S., Ju, J. S., and Bae, Y. C. (2004) Peripheral glutamate receptors participate in interleukin-1beta-induced mechanical allodynia in the orofacial area of rats, *Neurosci Lett* **357**, 203–206.
43. Ahn, D. K., Kim, K. H., Jung, C. Y., Choi, H. S., Lim, E. J., Youn, D. H., and Bae, Y. C. (2005) Role of peripheral group I and II metabotropic glutamate receptors in IL-1beta-induced mechanical allodynia in the orofacial area of conscious rats, *Pain* **118**, 53–60.
44. Jung, C. Y., Lee, S. Y., Choi, H. S., Lim, E. J., Lee, M. K., Yang, G. Y., Han, S. R., Youn, D. H., and Ahn, D. K. (2006) Participation of peripheral group I and II metabotropic glutamate receptors in the development or maintenance of IL-1beta-induced mechanical allodynia in the orofacial area of conscious rats, *Neurosci Lett* **409**, 173–178.

## New Models of Experimental Parotitis and Parotid Gland Distension in Rats

Akiko Okada-Ogawa, Masamichi Shinoda, Kuniya Honda,  
and Koichi Iwata

### Abstract

A significant reduction of the escape threshold to mechanical stimulation of the lateral facial skin was observed bilaterally at days 2 and 3 after unilateral complete Freund's adjuvant (CFA) administration into parotid gland. A slight reduction of mechanical escape threshold was also observed in rats with saline administration. The parotid gland inflammation was verified and quantified by measuring the tissue Evans' blue dye extravasation. The Evans' blue concentration in the parotid gland tissues was significantly greater in the CFA-injected rats than that of the saline-injected rats at 72 h after treatment. On day 10 after CFA administration into the parotid gland, the Evans' blue concentration was recovered to the control level. The administration of capsaicin into the parotid gland did not alter neuronal activities in the transition zone between the trigeminal spinal subnucleus interpolaris and caudalis (Vi/Vc). In contrast, capsaicin administration induced significant increases in the receptive field size and mechanical and cold responses of neurons located in superficial laminae of the C1/C2. The subgroup of C1/C2 neurons responded to mechanical distension of the parotid gland, whereas no Vi/Vc neurons responded to parotid distension.

**Key words:** Parotitis, Deep pain, Chronic inflammation, Parotid distention, Trigeminal nerve

---

### 1. Introduction

Saliva is secreted from many minute glands, and three major salivary glands: the parotid, submandibular and sublingual glands. The three major salivary glands have unique structures. These salivary glands are independent organs embedded deeply in oral and craniofacial regions, and the duct-ends of these salivary glands open in the mouth. The parotid gland is the largest in these three glands and is involved in inflammatory diseases with chronic pain such as mumps, parotitis, and sialadenitis (1). Similar to visceral and

temporomandibular joint pain (2–4), parotid pain is characterized by its referral to the surrounding skin, ear, or neck (5–8). The major symptoms of parotitis are tenderness, diffuse swelling, altered salivary discharge, a hard mass in the parotid gland, and spontaneous pain (9–12). Parotitis sometimes affects the jaw and orofacial motor functions, resulting in a functional deficit in mastication. The chronic pain following parotitis is severe with distinctive features (13, 14).

The rat with a parotid gland inflammation is a good model for deep pain experienced in the orofacial regions, which does not require any special surgical treatment. An inflammatory agent can simply be injected into the parotid gland through the duct. Further, the inflammation can be restricted to the body of the salivary gland without spreading to the surrounding structures.

It is also well known that obstructive sialadenitis is due to calculi choked in the parotid duct resulting in an expansion of the gland body with a large amount of saliva in the parotid body. The expansion of the parotid gland causes severe pain in the orofacial regions.

We have therefore developed an experimental parotitis model in rats and assessed parotid gland pain induced by parotid gland distension for studying orofacial deep pain.

### **1.1. Parotitis Model**

The parotid gland, located in the lateral face with the parotid bed, is composed of specialized structures including a thin duct opening to the oral cavity through which saliva is released. We have developed a rat model with parotid gland inflammation by administering the inflammatory agent, complete Freund's adjuvant (CFA), directly into the parotid gland through the parotid duct without skin incision, and the inflammation is restricted in the gland. Therefore, our approach has distinct advantages in studying the effect of inflammatory injury restricted within the parotid body.

### **1.2. Rat Model with Parotid Gland Distension**

Obstructive sialadenitis is due to calculi, fibromucinous plugs, duct stenosis, foreign bodies, anatomical variations, or malformations of the duct leading to a mechanical obstruction associated with stasis (1). The sialolithiasis pain is caused due to large amount of saliva accumulation in the parotid gland following blockage of the salivary ducts by calculi. It has been reported that the parotid gland is innervated by small diameter nerve fibers which express substance P or calcitonin gene-related peptide, indicating that the parotid gland is innervated by nociceptive fibers (15). We have developed an acute parotid pain model in rats using balloon distention and capsaicin exposure of the parotid gland.

---

## 2. Materials

### 2.1. Parotitis Model

1. Sodium pentobarbital (50 mg/kg, i.p.).
2. 27-Gauge needle (Terumo, Tokyo, Japan).
3. CFA (Sigma-Aldrich, Saint Louis, MO) is suspended in an oil/saline (1:1) emulsion.
4. Surgical glue (Super Glue, Konishi, Tokyo, Japan).
5. Evans' blue dye (Sigma-Aldrich).
6. Formamide (3 ml/g).
7. Touch test Sensory Evaluator kit (Stoelting, Wood Dale, IL).
8. Rabbit anti-c-Fos (1:20,000: c-Fos ab-5, Oncogene, Cambridge, MA).
9. Peroxidase-conjugated avidin–biotin complex (1:100; ABC, Vector Labs, Burlingame, CA).
10. 3,3'-Diaminobenzidine-tetra HCl (DAB, Sigma-Aldrich).

### 2.2. Rat Model with Parotid Gland Distension

1. Double-barreled balloon catheter (2-WAY foley form 8Fr.).
2. Capsaicin (8-methyl-*N*-vanillyl-6-noneamide; Sigma-Aldrich).
3. 10% (*v/v*) Tween 80 (MP Biomedical, Morgan Irvine, CA).
4. Polyethylene tube (PE-10, Natsume, Tokyo, Japan).
5. Enamel-coated tungsten microelectrode (impedance = 10–12; FHC, Bowdoin, ME).
6. Pancuronium bromide (Merck, Whitehouse Station, NJ).
7. Stereotaxic frame (Narishige, Tokyo, Japan).

---

## 3. Methods

### 3.1. Parotitis Model

#### 3.1.1. CFA Administration into the Parotid Gland

Rats are anesthetized with sodium pentobarbital (50 mg/kg, i.p.). An end-rounded tip of 27-gauge needle is inserted into the opening of the parotid duct toward the back ear area under an optical microscope (Fig. 1a) (see Note 1). The opening site is located about 3 mm inside from the corner of the mouth. One can find the opening site easily after removing the saliva over the opening site with a cotton swab (Fig. 1b). CFA is suspended in an oil/saline (1:1) emulsion. Three-hundred microliters of CFA is injected into the left parotid gland through the 27-gauge needle (see Note 2). Following administration, the area behind the ear over the parotid body becomes swollen (Fig. 2a, b) (see Note 3). One should be able to determine if the CFA is leaking in the opening site or duct

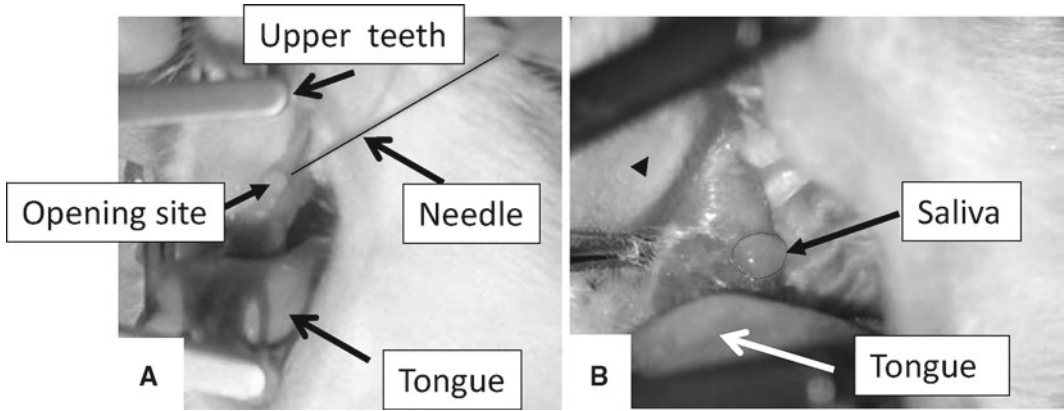


Fig. 1. (A) Insertion of a needle into the opening site of the parotid duct. (B) Landmark of the opening site of the parotid duct. Oozing saliva from the opening site is indicated by the arrow in (B).

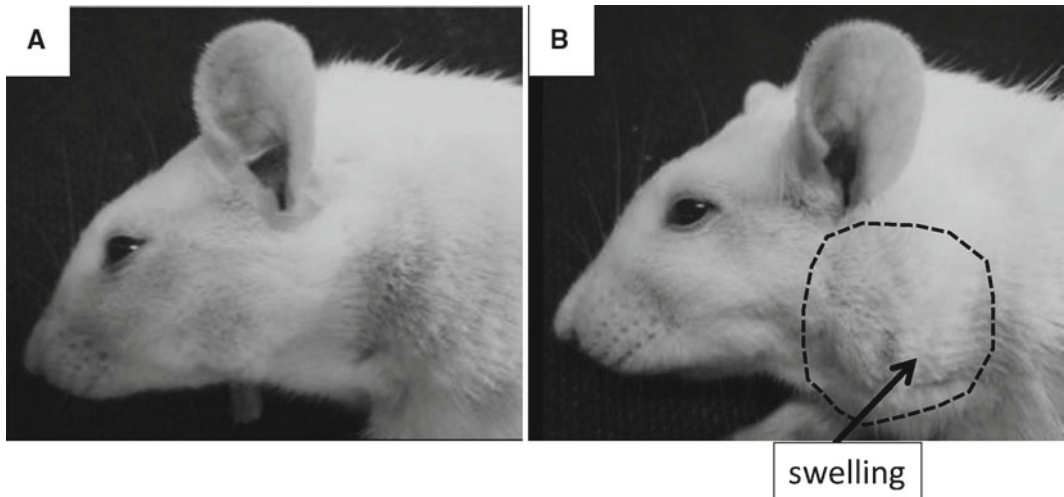


Fig. 2. Lateral view of rat face before (A) and after (B) complete Freund's adjuvant (CFA) administration into the parotid gland. Swollen parotid gland following the CFA administration is indicated by the dotted line in (B).

by checking if the rat's cheek becomes slightly swollen after injection (see Note 4). After administration, a small volume (0.01 ml) of surgical glue is placed on the opening of the parotid duct to prevent CFA leakage.

### 3.1.2. Behavioral Testing

It is necessary to determine if the CFA administration into the parotid gland causes pain in the parotid gland. Rats are trained to keep drinking 10% sucrose solution during noxious mechanical stimulation of the lateral face (see Note 6). Mechanical stimuli are applied to the lateral facial skin with von Frey filaments through a small hole (1 cm in diameter) in the lateral wall of the plastic cage.

The mechanical stimuli are applied to the lateral portion of the face, 5 mm below and 5 mm caudal to the lower edge of the external ear in an ascending manner (0.5–36 g). Rats are trained to continually drink sucrose solution for 10 min without escape from mechanical stimuli with the intensity up to 36 g in advance. Normally, the rats should gain body weight across the training session (mean weight gain, 9.6 g/day). Once this level of training is reached, CFA is administered into the parotid gland. Prior to and 1 day after the CFA administration, all rats are tested with von Frey filaments. Each filament is applied twice at an interval of 5 s. The bending force of the first filament to evoke an escape response is designated as the escape threshold intensity, which is determined prior to and daily after CFA administration for 20 days. The escape threshold value before administration is considered “100%” that is used to calculate the relative escape threshold for each post-CFA injection day.

### *3.1.3. Verification of Parotid Inflammation*

One can evaluate CFA-induced parotid inflammation by examining plasma extravasation (see Note 5). Evans' blue dye is injected through the femoral vein of the rats at 2 h to 20 days after CFA administration to verify the extent of inflammation. Thirty minutes after Evans' blue injection, rats are perfused with warm saline. The parotid region is first exposed and the site is carefully examined under a dissecting microscope for the appearance of extravasated dye in the tissues surrounding the parotid gland. The bilateral parotid glands are then removed. The dissected tissues are weighed and immersed in formamide (3 ml/g). The sample is incubated overnight at room temperature with agitation, and the supernatant is separated. The absorbency of this supernatant at 620 nm is determined by a spectrophotometer. To calculate the extravasated dye per gram weight of tissue ( $\mu\text{g/g}$ ), the absorbency of the supernatant is compared with a standard curve which is generated from a series of the same extractions mixed with known amounts of Evans' blue dye.

### *3.1.4. Fos Protein Immunohistochemistry*

Rats are anesthetized with sodium pentobarbital (80 mg/kg, i.p.) and perfused through the aorta with 500 ml of 0.02 M phosphate-buffered saline (PBS, pH 7.4) followed by 500 ml of 4% paraformaldehyde in 0.1 M phosphate buffer (pH 7.4). Fifty-micron-thick sections are cut from caudal brainstem and upper cervical spinal cord with a freezing microtome and every fourth section is collected in PBS. Free-floating tissue sections are rinsed in PBS, and processed for Fos immunohistochemistry. In transverse sections, the trigeminal spinal subnucleus interpolaris ( $V_i$ ) is at about 1.0–3.0 mm rostral to the obex. The transition zone between  $V_i$  and trigeminal spinal subnucleus caudalis ( $V_c$ ) is about 0.2–0.8 mm rostral to the obex. The  $V_c$  extends caudally to the C2–C3 spinal cord. The C2 spinal cord is a 3-mm segment centered at about 6.0 mm

caudal to the obex. The number of Fos-like immunoreactive (LI) cells in the Vi/Vc transition zone, paratrigeminal nucleus (Pa5), and the upper cervical cord (C1/C2) are analyzed.

### **3.2. Rat Model with Parotid Gland Distension**

#### **3.2.1. Insertion of a Balloon Catheter into the Parotid Gland**

Rats are anesthetized with sodium pentobarbital (50 mg/kg, i.p.). A small incision is made in the skin 5 mm below the ear to expose the rat's parotid gland, which consists of three lobes. The middle one is the largest and is a flat sac about 2 cm in length and 1 cm in width (1). A small incision is made in the middle of the parotid body. A double-barreled balloon catheter (2-WAY foley form 8Fr.) is inserted into the middle lobe of the parotid gland (see Note 8). The balloon is ball shaped with 1.5 ml volume. The catheter consists of two thin tubes on one side, and a balloon on the other side. The balloon is expanded by air through a thin catheter to achieve parotid gland distension.

Capsaicin is also administrated into the parotid gland through the catheter connected with the balloon catheter to test if neurons respond to local administration of irritants. Capsaicin (2.0%) is dissolved in a solution containing 10% (v/v) ethanol and 10% (v/v) Tween 80 in sterile normal saline. Capsaicin or vehicle is injected from the tip of the balloon through another thin catheter attached to the balloon catheter. One distal end of the catheter is connected to a 2.5-ml syringe for inflating the balloon with air (0.5, 1.0, and 1.5 ml). The other end is connected to a 1-cm<sup>3</sup> syringe through polyethylene (PE-10) tubing for capsaicin administration. The balloon catheter is sutured to the parotid gland and the incision is then closed.

#### **3.2.2. Single-Neuron Recording**

The parotid acute pain model is also used for electrophysiology experiments. Extracellular neuronal activity of nociceptive neurons is recorded from the Vc, C1/C2, and Vi/Vc (see Note 9). The Vi/Vc is located approximately 0–1 mm caudal to obex, and the C1/C2 is located approximately 3–4 mm caudal to obex. Detailed receptive field properties of each nociceptive neuron are precisely analyzed, and then evoked responses to mechanical and thermal stimuli applied to the cutaneous receptive field and evoked responses to balloon distension applied to the parotid gland are examined. Nociceptive neurons in Vc, Vi/Vc, and C1/C2 are classified as wide dynamic range (WDR) and nociceptive specific (NS) neurons according to their response to mechanical stimulation of the receptive fields. WDR neurons respond to non-noxious and noxious stimuli, whereas NS neurons respond to noxious stimulation of the receptive field. Graded distension of the parotid gland is applied by filling the balloon with 0.5, 1.0, and 1.5 cm<sup>3</sup> of air. Following two baseline trials for mechanical and thermal stimuli, 50 µl of 2% capsaicin is administrated into the parotid gland, and stimulus trials are repeated at 20 and 60 min after administration (see Note 10).

## 4. Results

### 4.1. Parotitis Model

#### 4.1.1. Nocifensive Behavior

A significant reduction of the escape threshold to mechanical stimulation of the lateral face in the ipsilateral side to the CFA administration has been observed at days 1–6 after CFA administration as compared to that of pre-CFA controls (Fig. 3a). A significant reduction of the escape threshold on the contralateral side has also been observed at days 2 and 3 after CFA administration. A slight reduction of relative escape threshold in rats with saline administration has also been observed at days 1 and 2 after administration, but the differences do not reach significance (data not shown).

#### 4.1.2. Quantification of CFA-Induced Inflammation

The parotid gland inflammation is verified and quantified by measuring Evans' blue dye extravasation in the tissue (see ref. 16) (see Note 6). The level of Evans' blue is significantly greater in the CFA administration group than that of the saline administration group at day 3 after treatment (Fig. 3b). Ten days after CFA administration into the parotid gland, the level of Evans' blue is recovered to

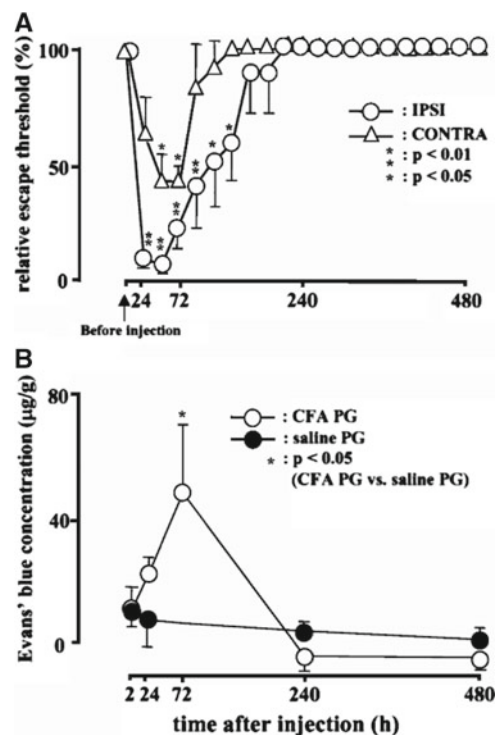


Fig. 3. (A) Time-course of escape threshold to mechanical stimulation of the lateral face in the ipsilateral side (IPSI) or contralateral side (CONTRA) to the complete Freund's adjuvant (CFA) administration into the parotid gland. CFA administration produces a significant reduction of the response threshold on both sides compared to pre-administration values. (B) Time-course of Evans' blues extravasation after CFA (CFA PG) or saline (saline PG) administration into the parotid gland. Reproduced with kind permission from Springer Science + Business Media (16).

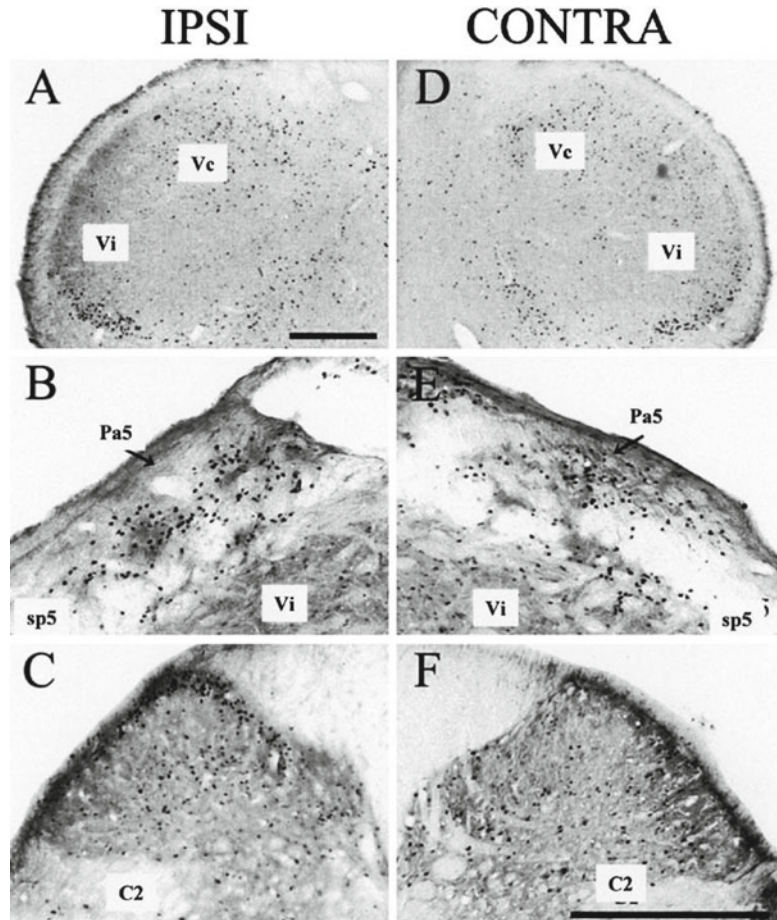


Fig. 4. Photomicrographs of Fos protein-LI cells in the ipsilateral (A–C) and contralateral (D–F) Vi/Vc transition zone (A, D), Pa5 (B, E), and C2 region (C, F) at day 3 after complete Freund's adjuvant administration into the parotid gland. *Scale bars* indicate 0.5 mm. Reproduced with kind permission from Springer Science + Business Media (16).

the control levels. After the rats are perfused with warm saline, the Evans' blue dye can be observed in the parotid gland and duct, but not in any surrounding tissue. The administration of saline into the parotid gland does not produce any visible sign of distension and swelling of the gland. The parotid gland inflammation is verified and quantified by measuring the tissue Evans' blue dye extravasation.

#### 4.1.3. Fos Protein Expression After CFA Administration

Many Fos positive neurons are observed in Vi/Vc on the side ipsilateral to CFA administration (Fig. 4a). The number of Fos-LI cells is significantly increased at 2–72 h after CFA or saline administration. On the ipsilateral side, CFA administration leads to a greater Fos expression at day 3 compared with that at 2 h and day 2 after CFA injection (Fig. 5). On the contralateral side, the Fos expression is significantly greater in the CFA group at day 3

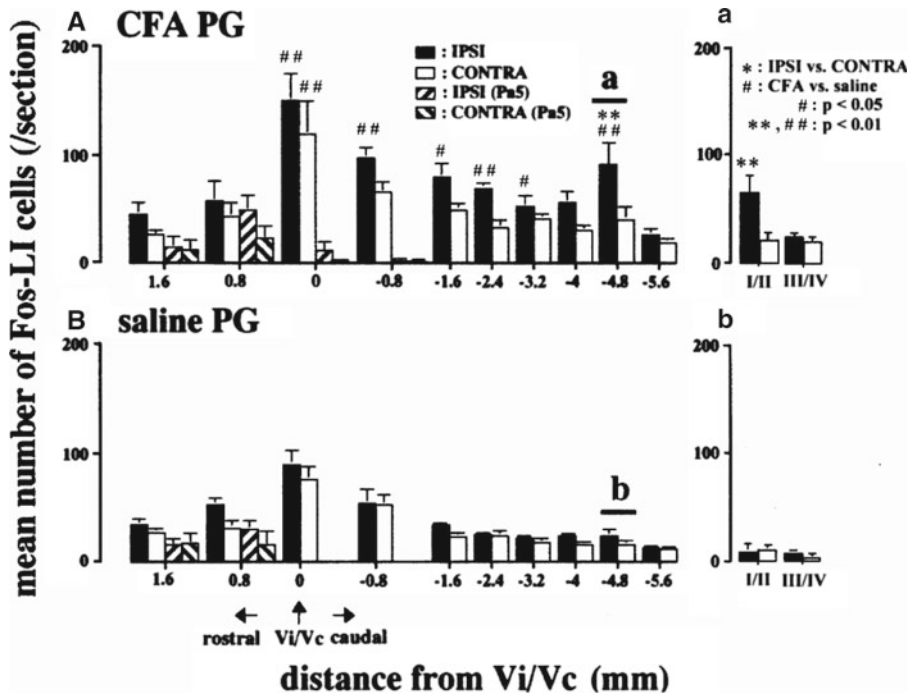


Fig. 5. Rostro-caudal distribution of Fos protein-LI cells in the caudal medulla and upper cervical spinal cord from rats at day 3 after complete Freund's adjuvant (CFA) PG (A) and saline PG (B) administration. The mean number of Fos protein-LI cells in the superficial laminae (laminae I/II) and intermediate laminae (laminae III/IV) of the C2 spinal cord with CFA PG (a) and saline PG (b) is illustrated at the *right*. A significant IPSI versus CONTRA difference was observed only in the CFA PG rats in the superficial laminae of the C2 cord. IPSI and CONTRA: ipsilateral and contralateral Vc and upper cervical spinal cord, respectively, IPSI (Pa5) and CONTRA (Pa5): ipsilateral Pa5 and contralateral Pa5, respectively. Reproduced with kind permission from Springer Science + Business Media (16).

compared with that in the saline-injected group (Fig. 5). In C1/C2, few Fos positive cells are observed in the saline-injected rats over 20 days after CFA administration. A significant increase in Fos protein-LI cells is observed in the ipsilateral, but not contralateral side (Fig. 5). CFA administration into the parotid gland only induces a significant increase in Fos protein-LI cells in the ipsilateral Pa5 at day 3 after administration compared to the corresponding saline group (Figs. 4b, c, and 5Aa, Bb).

## 4.2. Rat Model with Parotid Gland Distension

### 4.2.1. Results

One can analyze WDR neurons received inputs from the facial skin. The C1/C2 neurons responded to distension of the parotid gland grade their firing frequencies following increased intensity of parotid distension (Fig. 6). The administration of capsaicin into the parotid gland does not affect spike frequencies in Vi/Vc neurons. In contrast, capsaicin induces significant increases in the peripheral receptive field size, and enhances mechanical and cold-evoked responses in superficial laminae neurons of C1/C2 (Fig. 7: receptive field; Fig. 8: mechanical responses; Fig. 9: heat responses; and Fig. 10: cold responses). These results are surprising given that

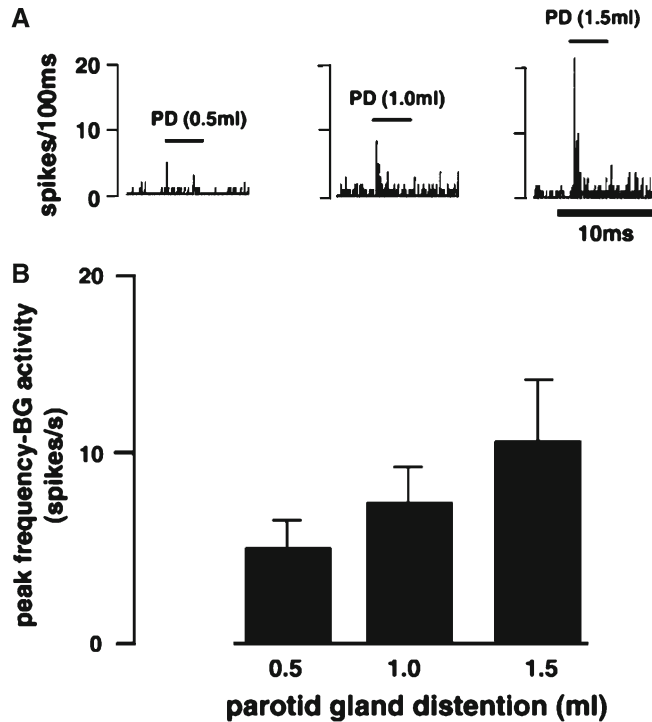


Fig. 6. A typical example of a Vi/Vc neuron responsive to balloon distension of the parotid gland. (A) The administration of 0.5, 1.0, and 1.5 ml of air into the balloon causes graded neuronal spikes in response to parotid distension. PD parotid distension with balloon. (B) Peak frequency of neuronal responses to distension stimulation applied to the parotid gland (Reproduced with kind permission from Elsevier Japan: Ogawa et al., *Brain Res.*, 2006, 1106:123–133).

Vi/Vc neurons do not respond to mechanical distension of the parotid gland, whereas many C1/C2 neurons do after capsaicin administration. The present results suggest that Vi/Vc and C1/C2 are involved in functionally distinct responses to inflammation of the parotid gland and parotid distension.

## 5. Notes

1. The rat mucous membrane is very soft and vulnerable to damage. A blunt and small needle should be used for CFA administration.
2. After subtracting the dead space of the duct (0.03–0.04 ml), the amount of CFA entering the parotid gland should be less than 0.3 ml. An overdose administration of CFA into the parotid gland induces inflammation of the surrounding tissue. The amount of CFA we used is suitable to fill all three parotid bodies.

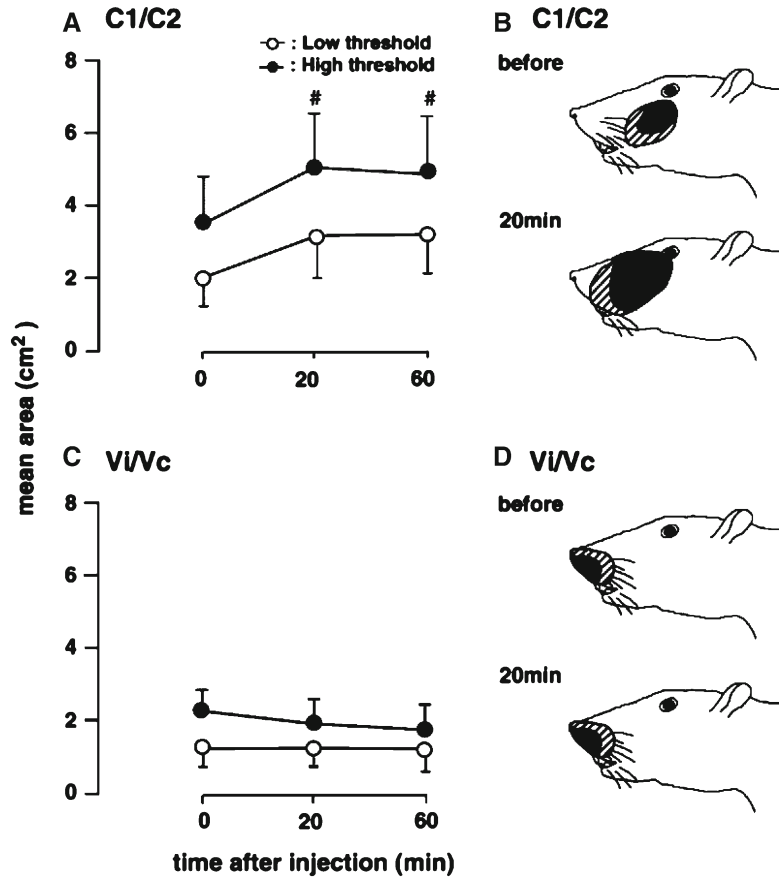


Fig. 7. Receptive fields of neurons in the C1/C2 and Vi/Vc regions following capsaicin administration into the parotid gland. The area of both low (*open circle*) and high (*filled circle*) threshold responses increases in C1/C2 neurons following capsaicin treatment (A), whereas no expansion of the receptive field occurs in Vi/Vc neurons (C). Representative examples of the capsaicin effects on receptive field sizes in a C1/C2 neuron (B) and Vi/Vc neuron (D) before and after capsaicin treatment. Low threshold areas responded to gentle touching with camel hair and noxious mechanical stimulation by small arterial clip (*solid areas*), and high threshold areas responded to only noxious mechanical stimulation (*shaded areas*) are indicated (Reproduced with kind permission from Elsevier Japan: Ogawa et al., Brain Res., 2006, 1106:123–133).

3. The parotid gland filled with CFA can be checked by touching the parotid gland. If CFA is successfully administered into the parotid gland, the gland can be felt as a little hard round tissue under the skin.
4. Because the lacrimal gland locates close to the parotid gland, care is needed not to administrate CFA into the lacrimal gland. The lacrimal gland looks like a cyst and the color is ochre. The parotid gland is irregular, wedge shaped, and unilobular.
5. Evans' blue dye dissolved in sterile water (50 mg/ml) is injected (1 mg/kg) though the femoral vein under sodium pentobarbital

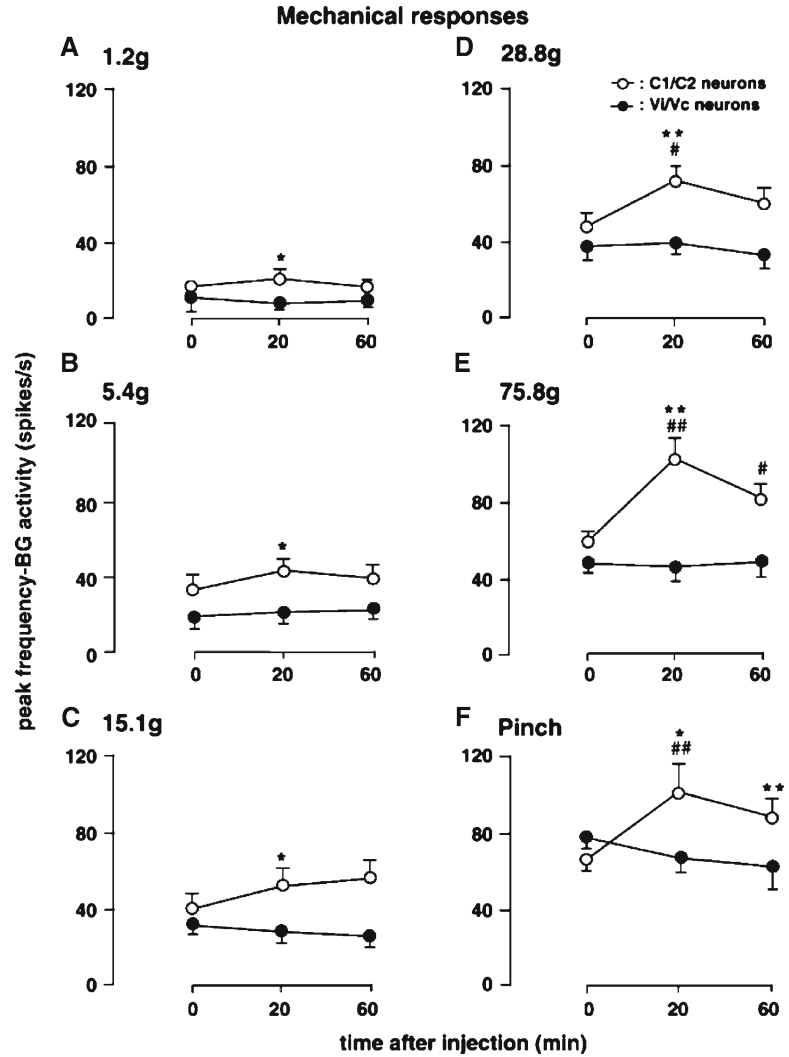


Fig. 8. Peak firing frequency following graded mechanical stimulation of the cutaneous receptive field. Capsaicin administration into the parotid gland significantly increases mechanically evoked responses of C1/C2 (*open circle*), but not Vi/Vc (*filled circle*) neurons. Peak firing frequency in control stimulation trials is not different between Vi/Vc and C1/C2 neurons. Stimulus intensities to the receptive field are indicated at the *top left corner* of each panel (A-F). # $P < 0.05$ , ## $P < 0.01$  versus pre-capsaicin controls. \* $P < 0.05$ , \*\* $P < 0.01$  versus Vi/Vc neurons (Reproduced with kind permission from Elsevier Japan: Ogawa et al., *Brain Res.*, 2006, 1106:123–133).

anesthesia (50 mg/kg, i.p.). Half hour after Evans' blue injections, rats are perfused with warm hypertonic saline. Even after perfusion with saline, buccal skin looks blue. The parotid gland is also removed after perfusion to see whether the inflammation is restricted in the parotid gland.

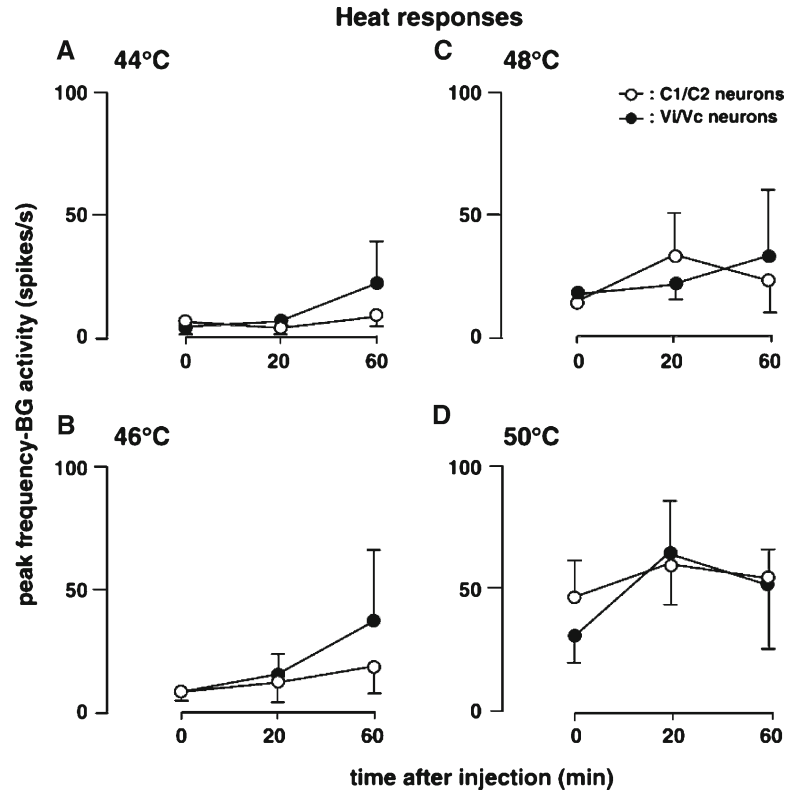


Fig. 9. Peak firing frequency of Vi/Vc neurons (*filled circle*) and C1/C2 neurons (*open circle*) following graded heat stimulation of the receptive field after capsaicin administration into the parotid gland. Unlike mechanically evoked responses, heat-evoked responses are not affected by capsaicin administrations. Stimulus intensities are indicated at the *top left corner* of each panel (A-D) (Reproduced with kind permission from Elsevier Japan: Ogawa et al., *Brain Res.*, 2006, 1106:123–133).

6. The behavioral testing is sometimes unstable, because the rats can realize the instruments for mechanical stimulation before application of the stimuli, and they move their face in various directions to avoid the stimulation. Therefore, we train rats to stay in the cage quietly for 10–20 min during testing before CFA or vehicle administration. Training and handling of rats are very important to obtain stable behavior data.
7. The rats are perfused with warm saline under deep anesthesia, and the parotid gland is removed half hour after intravenous administration of Evans' blue. The amount of Evans' blue in the parotid gland is measured according to the method described in our previous paper (see ref. 16).
8. A small incision is made in the facial skin and parotid gland to insert the balloon. The incisions should be tightly sutured.
9. Enamel-coated tungsten microelectrodes are used for single-neuron recording experiments. Spikes are sometimes easy to

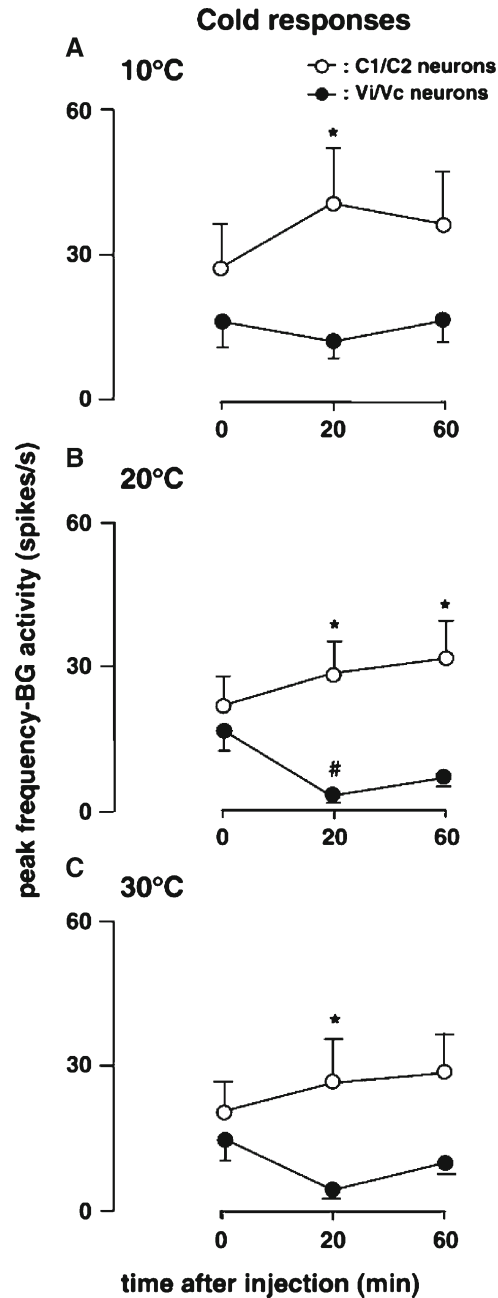


Fig. 10. Changes in peak firing frequency of Vi/Vc neurons (*filled circle*) and C1/C2 neurons (*open circle*) following graded cold stimulation of the receptive fields after capsaicin administration into the parotid gland. Stimulus intensities are indicated at the *top left corner* of each panel (A-C). The reduction in cold stimulation evoked activity in Vi/Vc neurons reaches a statistical significance at 20°C following capsaicin administration. The evoked responses of C1/C2 neurons are significantly larger than those of Vi/Vc neurons following capsaicin administration. # $P < 0.05$  versus pre-capsaicin controls. \* $P < 0.05$  versus Vi/Vc neurons (Reproduced with kind permission from Elsevier Japan: Ogawa et al., Brain Res., 2006, 1106:123–133).

loose, so care is necessary to keep recording stable. If spike height becomes smaller, the electrodes should be moved deeper or shallower. The spike shape should be monitored during recordings.

10. The primary afferent fibers innervating the receptive field and parotid gland are sensitized following frequent noxious mechanical or thermal stimulation. The noxious stimulation should be applied to the receptive field less than two times. Since capsaicin also sensitizes the C-fibers, frequent administration of capsaicin should be avoided.

---

## Acknowledgments

This study was supported in part by Sato and Uemura Funds from Nihon University School of Dentistry, and a grant from the Dental Research Center, Nihon University School of Dentistry; Nihon University multidisciplinary research grant for KI; grants from the Ministry of Education, Culture, Sports, Science, and Technology to promote multidisciplinary research project “Translational Research Network on Orofacial Neurological Disorders” at Nihon University School of Dentistry and “Kakenhi #18890204” to AO, and Nihon University School of Dentistry. We also thank Dr. DA Thomas for correcting English usage.

## References

1. Hall H.D. and Schneyer C.A. (1973) Role of autonomic pathways in disuse atrophy of rat parotid *Proc Soc Exp Biol Med* **143**, 19–23.
2. Hathaway C.B., Hu J.W. and Bereiter D.A. (1995) Distribution of Fos-like immunoreactivity in the caudal brainstem of the rat following noxious chemical stimulation of the temporomandibular joint *J Comp Neurol* **356**, 444–56.
3. Imbe H., Dubner R. and Ren K. (1999) Masseteric inflammation-induced Fos protein expression in the trigeminal interpolaris/caudalis transition zone: contribution of somatosensory–vagal–adrenal integration *Brain Res* **845**, 165–75.
4. Korzeniewska-Rybicka I. and Plaznik A. (2001) Role of serotonergic and noradrenergic systems in a model of visceral pain *Pol J Pharmacol* **53**, 475–80.
5. Marchettini P., Simone D.A., Caputi G. and Ochoa J.L. (1996) Pain from excitation of identified muscle nociceptors in humans *Brain Res* **740**, 109–16.
6. Ochoa J. and Torebjork E. (1989) Sensations evoked by intraneural microstimulation of C nociceptor fibres in human skin nerves *J Physiol* **415**, 583–99.
7. Simone D.A., Marchettini P., Caputi G. and Ochoa J.L. (1994) Identification of muscle afferents subserving sensation of deep pain in humans *J Neurophysiol* **72**, 883–9.
8. Sluka K.A. (2002) Stimulation of deep somatic tissue with capsaicin produces long-lasting mechanical allodynia and heat hypoalgesia that depends on early activation of the cAMP pathway *J Neurosci* **22**, 5687–93.
9. Leipzig B. and Obert P. (1979) Parotid gland swelling *J Fam Pract* **9**, 1085–93.
10. Orser B. (1990) Facial pain in the recovery room secondary to acute parotitis *Anesthesiology* **72**, 1090–1.
11. Vasama J.P. (2000) Tympanic neurectomy and chronic parotitis *Acta Otolaryngol* **120**, 995–8.
12. Watkin G.T., Hobsley M. (1986) Natural history of patients with recurrent parotitis and punctate sialectasis *Br J Surg* **73**, 745–8.

13. Nozaki H., Harasawa A., Hara H., Kohno A., Shigeta A. (1994) Ultrasonographic features of recurrent parotitis in childhood *Pediatr Radiol* **24**, 98–100.
14. Stanley R.B., Fernandez J.A., Peppard S.B. (1983) Cervicofacial mycobacterial infections presenting as major salivary gland disease *Laryngoscope* **93**, 1271–5.
15. Ekstrom J., Asztely A. and Tobin G. (1996) Non-adrenergic, non-cholinergic influences on parotid acinar degranulation in response to stimulation of the parasympathetic innervation in the anaesthetized rat *Exp Physiol* **81**, 935–42.
16. Ogawa A., Ren K., Tsuboi Y., Morimoto T., Sato T. and Iwata K. (2003) A new model of experimental parotitis in rats and its implication for trigeminal nociception *Exp Brain Res* **152**, 307–6.

## A Rat Pain Model of Facial Cancer

Kentaro Ono, Nozomu Harano, Kiyotoshi Inenaga,  
and Osamu Nakanishi

### Abstract

Cancer pain is a very severe problem for patients with advanced or terminal cancer. However, the induction mechanism remains unknown. Orofacial cancer patients often report difficulties in eating and swallowing, different from patients with cancer in other regions. Although several cancer pain animal models have been reported, these models have focused on the sciatic nerve areas. To understand the mechanisms of pain associated with orofacial cancer, we recently created a rat facial cancer model by inoculation of cancer cells into the vibrissal pad. This model provides mechanical allodynia, thermal hyperalgesia, and feeding disorder characteristics, similar to orofacial cancer patients. Hence, this model is useful for the evaluation of cancer pain of the trigeminal nerve area. In this chapter, we describe in detail the generation of a facial cancer pain model of rats by inoculation of Walker carcinosarcoma 256B cells.

**Key words:** Rats, Facial cancer pain, Mechanical allodynia, Thermal hyperalgesia, Walker carcinosarcoma 256B

---

### 1. Introduction

Cancer-induced pain is a very severe problem in patients with advanced and terminal cancer. In patients with orofacial cancer, the pain causes difficulties in feeding and swallowing (1), so the symptoms may be more severe than those of patients with cancers in other regions. Over the last decade, several experimental models of cancer have been developed to study the induction and the mechanism of the cancer-induced pain, and behavioral and neurochemical changes with tumor progression have been investigated (2–5). However, since these studies have almost always concentrated on the sciatic nerve areas, it is necessary to develop an orofacial cancer pain model to understand the mechanisms of orofacial cancer-induced pain (6). Therefore, we recently developed a model that

involves inoculating cancer cells into the vibrissal pad of Wistar rats (7, 8). The facial cancer model showed the development of allodynia and hyperalgesia, followed by difficulties of ingestive behavior (8), similar to symptoms in orofacial cancer patients. As far as we know, there are to date only two models for orofacial cancer pain: our model (7, 8) and another gingival cancer model (9).

In this chapter, we describe in detail the generation of the facial cancer pain model of rats through inoculation of Walker carcinoma 256B cells into one side of the vibrissal pad. This cancer cell line originates from a mammary gland carcinoma of Wistar rats and is commonly used in cancer research, and thus has already been used for some sciatic nerve-targeted cancer pain rat models (10, 11). The development of mechanical allodynia, thermal hyperalgesia, and feeding disorder in the facial cancer model will be also described.

---

## 2. Materials

### 2.1. Cancer Cell Culture

1. Walker carcinosarcoma 256B cells (kindly provided by Shionogi Pharm., Osaka, Japan; Fig. 1). Stored at  $-80^{\circ}\text{C}$ .
2. Minimum Essential Medium Alpha (MEM Alpha; Gibco). Stored at  $4^{\circ}\text{C}$ .
3. Fetal bovine serum (FBS; Gibco; see Note 1). Stored at  $-20^{\circ}\text{C}$ .
4. Penicillin G (10 mg/mL) (ICN).
5. Trypsin (Gibco).
6. 70% Ethanol (v/v).

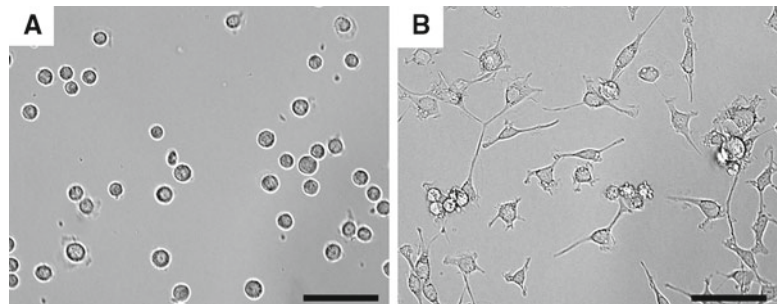


Fig. 1. Microphotographs of Walker 256B cells originating from a mammary gland carcinoma of Wistar rats. Horizontal bars, 100  $\mu\text{m}$ . (a) Cell appearance just after passage. (b) Cell appearance after 1 day in culture. The cancer cells change from round- to spindle-shaped with some long processes.

7. Sterile 100-mm tissue culture dishes (IWAKI).
8. Sterile 50- and 15-mL centrifuge tubes (IWAKI).
9. Sterile 1.5-mL plastic sample tubes.
10. Cellbanker 1 (Mitsubishi Chemical Medience). Stored at 4°C.
11. Cryogenic Vials Inner Cap Type (Sumitomo Bakelite).
12. Hemocytometer (Troma deep 0.1 mm, N28513, Erma).

### **2.2. Pretreatment of Solutions**

1. Pretreatment of FBS: FBS is divided into 10-mL aliquots in sterile 15-mL plastic tubes after heat-inactivation (57°C for 30 min). After writing the date and descriptive numbers on the tube-labeling area (see Note 4), the tubes are frozen at -20°C until use.
2. Culture medium: After completely melting the stock FBS (10 mL), it is mixed with 45 mL MEM Alpha, 5 mL FBS and 50 µL Penicillin (10 mg/mL) and aliquoted into two sterile 50-mL tubes. The tubes are maintained at 4°C and used within 1 month.
3. Phosphate-buffered saline (PBS): For a 10× stock solution, 80 g NaCl, 29 g Na<sub>2</sub>PO<sub>4</sub>·12H<sub>2</sub>O, 2 g KCl, and 2 g KH<sub>2</sub>PO<sub>4</sub> are mixed in Milli-Q water up to 1 L. The stock solution is diluted to a final 1× solution (137 mM NaCl, 8.1 mM Na<sub>2</sub>PO<sub>4</sub>, 2.68 mM KCl, and 1.47 mM KH<sub>2</sub>PO<sub>4</sub>) and autoclaved prior to use.
4. Trypsin solution: 0.05% trypsin solution diluted in MEM Alpha is divided into 50-mL aliquots in sterile 50-mL plastic tubes and frozen at -20°C. Once the solution is melted for use, the remaining solution is maintained at 4°C and used within 1 week.

### **2.3. Generation of Facial Cancer Model and Pain Tests**

1. 1-mL syringes (TERUMO).
2. 26-G needles (TERUMO).
3. Male young Wistar rats (50–70 g; Kyudo Co., LTD., see Note 2).
4. Thiopental (Mitsubishi Tanabe Pharma Corporation).

### **2.4. Pain Tests for the Facial Cancer Model**

1. Stopwatch.
2. von Frey hair filaments (Semmes-Weinstein monofilament set, Muromachi; pressures 0.16, 0.4, 0.6, 1.0, 1.4, and 2.0 g).
3. Thermo-stimulator (DPS-705, Dia Medical System Co.) with a hand-made black-corn to focus 7 mm×7 mm beam of light (see Note 3) with the aperture 10 cm from the stimulation site.

### 3. Methods

The methods described below include treatments of cancer cells (Subheading 3.1), inoculation of cancer cells into the rat facial region (Subheading 3.2) and observations of pain-related behaviors (Subheading 3.3).

#### 3.1. Treatments of Cancer Cells

All procedures described in this section are conducted on a clean bench using sterile techniques (including spraying of 70% ethanol on hands and bottles).

##### 3.1.1. Cell Culture

1. Prior to seeding the supplied cancer cells, 10 mL culture medium is plated in a sterile 100-mm culture dish and warmed to 37°C in the 95%-CO<sub>2</sub> incubator for at least 5 min.
2. The frozen cancer cell suspension is melted in a 37°C water bath.
3. After disinfection around the cap of the bottle with 70% ethanol, the melted cell contents are plated in a pre-warmed culture dish.
4. The culture dish is rocked gently and then placed in the 95%-CO<sub>2</sub> incubator at 37°C for a few days.
5. It is necessary to check the cell proliferation, shape, and presence of contamination daily during the beginning stages of cell culture.

##### 3.1.2. Passing Cells

1. When the cell confluence of the culture dish is greater than 90%, the cells have to be divided into multiple plates (split). After aspiration of the culture medium, the cells are rinsed once with 1× PBS to remove the FBS, which inhibits trypsin enzyme activity, and then incubated in 5 mL trypsin solution for 5 min at 37°C.
2. During the incubation period in step 1, new culture dishes with 10 mL culture medium are pre-warmed in the 95%-CO<sub>2</sub> incubator at 37°C.
3. After step 1, all cells are completely stripped from the dish bottom by gentle spraying of the solution using a 1-mL micropipette with a blue tip.
4. The cell suspension is dispensed into sterile 1.5-mL sample tubes and pelleted in a minicentrifuge at 2,000 × *g* for 5 min.
5. After aspiration of the supernatant, each cell pellet is resuspended in 1 mL culture medium containing FBS to inactivate the trypsin, and the cells are then plated uniformly into a whole dish (from step 2).
6. The culture dish is incubated in 95% CO<sub>2</sub> at 37°C again for 3–4 days (see Note 5).
7. All used instruments and aspirated solutions are autoclaved and disposed of appropriately.

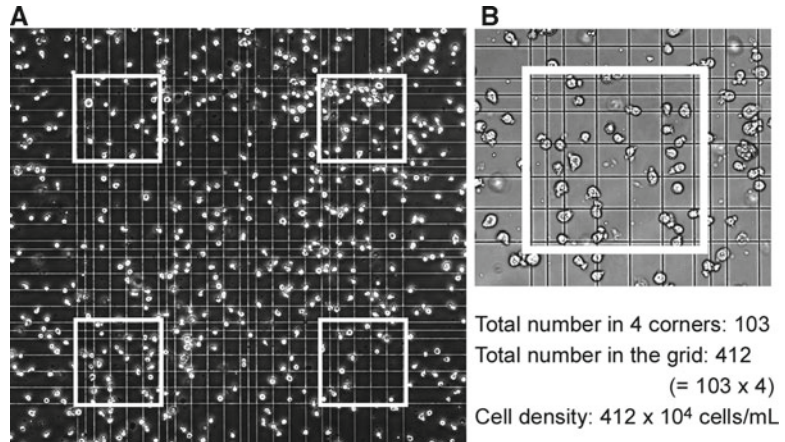


Fig. 2. Cell counting with a hemocytometer. (a) Low-magnification microphotograph of Walker 256B cells on the hemocytometer grid. *Wide* and *narrow* separations between lines indicate 50 and 25  $\mu\text{m}$ , respectively, and the total area of the large (*outside*) square is 1  $\text{mm}^2$ . (b) High-magnification microphotograph of one corner of the grid (the *left-bottom corner* from (a)).

### 3.1.3. Freezing Cells for Preservation

The cancer cells must be preserved if they are not to be used for an extended time.

1. Culture medium is aspirated, and the cells are washed with PBS and incubated in 3 mL trypsin solution in the 95%- $\text{CO}_2$  incubator at 37°C for a short period of time.
2. After the cells are stripped from the plate, the cell suspension is collected into two 1.5-mL plastic tubes, and these tubes are then centrifuged as described above.
3. After discarding the supernatant, the cell pellets are resuspended by Cellbanker 1. The cancer cell suspensions are aliquoted into serum tubes (cryogenic vials) and frozen at  $-80^\circ\text{C}$  until use.

### 3.1.4. Counting of Cancer Cells

1. A portion of the cell suspension (10–30  $\mu\text{L}$ ) is pipetted onto a hemocytometer grid.
2. A cover glass is placed onto the hemocytometer until the appearance of Newton's rings.
3. The total number of cells in the four corners of the grid (Fig. 2) is counted and multiplied by 4. The cell density is this number  $\times 10^4$  cells/mL.
4. After counting, the hemocytometer and cover glass are washed with water.

### 3.2. Inoculation of Cancer Cells into the Rat Facial Region

1. A culture dish containing cells that are 100% confluent (see Note 6) is rinsed once with PBS, and the culture medium is then changed to 3 mL trypsin solution followed by incubation in 95%  $\text{CO}_2$  at 37°C for 5 min.

2. After cell stripping, the cell suspension is transferred into two 1.5-mL plastic tubes and centrifuged at  $2,000 \times g$  for 5 min.
3. The two cell pellets are resuspended in culture medium containing FBS to inactivate the trypsin activity and centrifuged again.
4. After washing twice with PBS to remove the culture medium, the cell pellet is resuspended in 1 mL PBS, and then a cell count is performed using the hemocytometer.
5. To create the facial cancer model, it is necessary to collect  $4 \times 10^6$  cancer cells in 0.1 mL PBS (see Note 7). Therefore, the cell density has to be adjusted to  $4 \times 10^7$  cells/mL in a volume equal to the dead-space volume of the injection syringe (0.15–0.2 mL). For example, if the total cell number in the whole hemocytometer grid is 800 (thus,  $8 \times 10^6$  cells/mL, see Subheading 3.1.4), the cell pellet in the tube after centrifugation should be resuspended in 0.2 mL PBS.
6. A 1-mL plastic syringe is filled with the cell suspension using a 26-G needle. Another syringe filled with PBS only is prepared for the sham animals (control).
7. Prior to injection of the cancer cells or PBS, pain tests are performed on all rats to establish the baseline level for the pain parameters (see Subheading 3.3).
8. After anesthesia by i.p. injection of thiopental (50 mg/kg), a 26-G needle with cancer cells or PBS is inserted into the center of the right vibrissal pad (Fig. 3a). After touching the bone, the tip of the needle is drawn back approximately 1 mm, and the cancer cells are slowly injected (see Note 8).
9. The used syringes are autoclaved and disposed appropriately.

### **3.3. Observation of Pain-Related Behaviors**

1. Facial grooming is measured for 10 min during a certain period of time (18:00–20:00, see Note 9). The durations of rubbing and/or scratching of the inoculated facial region by forepaw are measured, while the grooming of regions other than the inoculated facial region is not evaluated.
2. Head withdrawal thresholds to von Frey hair stimulation and head withdrawal latencies after radiant heat are measured against the inoculated and contralateral skin surfaces of the vibrissal pads (see Note 10). Each measurement is repeated five times and data are averaged after the exclusion of maximal and minimal values.
3. According to the ethical guidelines of the International Association for the Study of Pain (12), all model animals are euthanized on day 14 at the latest post-inoculation. After the experiments, we found that it is best to stain the facial region of the models with hematoxylin and eosin (Fig. 3c) to confirm the development of tumor tissue.

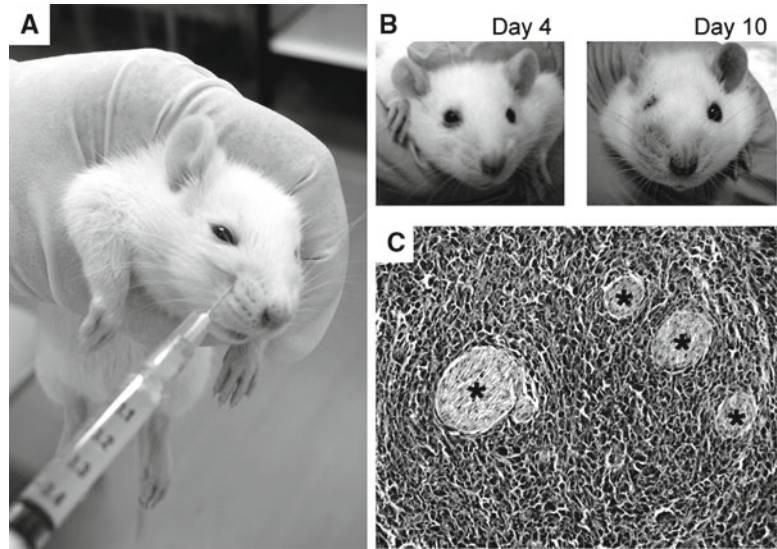


Fig. 3. Facial cancer model and its characteristics. (a) Photograph illustrating the method used to inoculate Walker 256 B cells into rats. (b) Morphological changes in the right face after inoculation of Walker 256 B cells. (c) Microphotograph of the vibrissal pad stained with hematoxylin and eosin 7 days after inoculation. The *asterisks* indicate nerve bundles surrounded by tumor tissue.

#### 4. Notes

1. Serum quality is uncertain and variable even in different lots from the same supplier. Therefore, FBS should be preselected by checking a few samples of different lot numbers in the cell culture protocol.
2. In our previous study (7), rats of various ages are examined to create a facial cancer model, and the highest cancer incident (32/37 animals, 86%) was found in 3-week-old Wistar rats. Furthermore, injection of Walker 256B cells into the facial region failed to produce tumor tissue in other strains of rats, for example, SD rats.
3. After the beginning of the heat stimulation, the skin temperature reaches 37°C in approximately 2.5 s and above 43°C in 3.3 s (13).
4. If there are ten tubes, for example, numbers must be labeled as 1/10, 2/10, 3/10...10/10 rather than as 1, 2, 3...10. The use of such a notation allows one to easily know how many stock tubes are present.

5. In our culture conditions, cell proliferation of Walker 256B cells proceeds by approximately one division per day. Therefore, since 3–4 days of culturing increases the cell number by  $2^3$ – $2^4$  times (i.e., 8–16 times), the timing of cell passage is set to be sufficient for the cells to reach 90% confluence.
6. In order to create the facial cancer model, it is necessary to inject all cancer cells from one culture dish into one rat. Since cancer cells in stock tubes experience some damage due to freezing, the cells should be passed at least five times before being inoculated.
7. A confluence level of 80% is not enough to collect the  $4 \times 10^7$  cells needed to inject into one rat. Therefore, the cell numbers present at the last passage must be controlled to provide 90–100% confluence on the day of inoculation.
8. If the needle tip becomes attached to the bone, it is sometime hard to inject the cell suspension, and thus the cell suspension cannot fully disseminate throughout the tissue. Therefore, the needle should be pulled back after touching the bone to provide an inoculation space, and the injection speed should be slow (0.1 mL/10 s). Note that gradual swelling of the vibrissal pad should be confirmed during injection of the cancer cell suspension.
9. Facial grooming time must be measured during the conscious period. Since the beginning of the light/dark cycle in our animal house is set to 8:00/20:00, the observation is performed during 18:00–20:00. Minimally, this observation must be performed at a consistent time.
10. Since the facial region in the facial cancer model is gradually inflated (Fig. 3b), the two pain tests are performed in rats held by hands. However, since rats spontaneously shake their heads, data for head withdrawal sometimes vary widely. Therefore, it is necessary to acclimate the rats to this holding position in advance.

---

## Acknowledgments

The authors thank Dr. H. Fukushima and Dr. S. Xu for their comments on the manuscript. The work was supported by a grant from the academic association of the alumni association of Kyushu Dental College to K. Ono and N. Harano and a Grant-in-Aid from the Ministry of Education, Culture, Sports, Science and Technology, Japan, to O. Nakanishi (20592377).

## References

1. Connelly, S. T. and Schmidt, B. L. (2004) Evaluation of pain in patients with oral squamous cell carcinoma. *J. Pain* **5**, 505–510.
2. Asai, H., Ozaki, N., Shinoda, M., et al. (2005) Heat and mechanical hyperalgesia in mice model of cancer pain. *Pain* **117**, 19–29.
3. Shimoyama, M., Tanaka, K., Hasue, F. and Shimoyama, N. (2002) A mouse model of neuropathic cancer pain. *Pain* **99**, 167–174.
4. Schwei, M. J., Honore, P., Rogers, S. D., et al. (1999) Neurochemical and cellular reorganization of the spinal cord in a murine model of bone cancer pain. *J. Neurosci.* **19**, 10886–10897.
5. Urch, C. E., Donovan-Rodriguez, T. and Dickenson, A. H. (2003) Alterations in dorsal horn neurones in a rat model of cancer-induced bone pain. *Pain* **106**, 347–356.
6. Benoliel, R., Epstein, J., Eliav, E., et al. (2007) Orofacial pain in cancer: part I – Mechanisms. *J. Dent. Res.* **86**, 491–505.
7. Nagahata, S., Harano, N., Shiiba, S. and Nakanishi, O. (2007) A rat model for cancer pain in the trigeminal nerve area. *J. Jpn. Dent. Soc. Anesthesiol.* **35**, 21–28.
8. Ono, K., Harano, N., Nagahata, S., et al. (2009) Behavioral characteristics and c-Fos expression in the medullary dorsal horn in a rat model for orofacial cancer pain. *Eur. J. Pain* **13**, 373–379.
9. Nagamine, K., Ozaki, N., Shinoda, M., et al. (2006) Mechanical allodynia and thermal hyperalgesia induced by experimental squamous cell carcinoma of the lower gingiva in rats. *J. Pain* **7**, 659–670.
10. Brigatte, P., Sampaio, S. C., Gutierrez, V. P., et al. (2007) Walker 256 tumor-bearing rats as a model to study cancer pain. *J. Pain* **8**, 412–421.
11. Mao-Ying, Q. L., Zhao, J., Dong, Z. Q., et al. (2006) A rat model of bone cancer pain induced by intra-tibia inoculation of Walker 256 mammary gland carcinoma cells. *Biochem. Biophys. Res. Commun.* **345**, 1292–1298.
12. Zimmermann, M. (1983) Ethical guidelines for investigations of experimental pain in conscious animals. *Pain* **16**, 109–110.
13. Imamura, Y., Kawamoto, H., Nakanishi, O. (1997) Characterization of heat-hyperalgesia in an experimental trigeminal neuropathy in rats. *Exp. Brain Res.* **116**, 97–103.

# Chapter 11

## Orofacial Pain Models and Behavior Assessment

Timothy K.Y. Kaan, Peter T. Ohara, and Luc Jasmin

### Abstract

Orofacial pain remains an understudied area in pain research given that most attention has been focused on the spinal system. In this chapter, animal models of neuropathic and inflammatory orofacial pain are presented. Four different types of pain behavior tests are then described for assessing evoked and spontaneous pain behavior in addition to conditional reward behavior. The use of a combination of different pain models and behavior assessments is needed to aid in understanding the mechanisms contributing to orofacial pain in humans for developing effective therapy.

**Key words:** Orofacial pain, Neuropathic pain, Inflammatory pain, Behavior, Formalin, Infraorbital nerve, Allodynia, Conditional rewarding, Spontaneous pain behavior, Trigeminal

---

### 1. Introduction

Orofacial pain may arise following trigeminal nerve injury, dental disease, temporomandibular joint disorder, and sinus disease. Given the majority of pain research has been carried out on spinal cutaneous afferents and some of the pathophysiology of this system may differ from that of the trigeminal system, there is a need to further understand the etiology underlying orofacial pain (1, 2). There are also experimental advantages to studying nociception using the trigeminal system. The trigeminal nerve is made up of three major branches, the ophthalmic, maxillary, and mandibular nerves (1), and the first two of these branches are different from the spinal nerve in being purely sensory. This allows a more straightforward interpretation of nociceptive behavioral observations based on nerve injury without the confounding issues of motor axon involvement. The anatomy of the trigeminal ganglion is also

well-established; neurons of each of the three branches have been mapped to different regions of the ganglion, and each ganglion innervates the same side of the face and cranium only.

Commonly, pain is classified into neuropathic and inflammatory pain, and models of each type will first be discussed. The neuropathic pain model presented here is the chronic constriction injury (CCI) of the infraorbital nerve (ION; the main branch of the maxillary nerve). The CCI of ION model was first developed over a decade ago and proven to demonstrate behavioral changes similar to clinical conditions (3). Key elements are the spontaneous and evoked nociceptive behavior seen in this model in addition to ectopic electrical activity and changes in gene expression in the trigeminal ganglion and brainstem (1, 3–7). The inflammatory pain model we will discuss is the orofacial formalin injection, which is similar to the forepaw/hindpaw formalin test (8). Following subcutaneous injection of formalin, animals exhibit spontaneous nociceptive behavior in two phases. An early and short-lasting first phase, proposed to be due to the direct stimulation on peripheral nociceptors, is followed by a second prolonged phase, thought to be dependent upon central plastic changes in the central nervous system, with a short quiescent period between the two (9). The formalin model allows the animal to be observed for ongoing persistent nocifensive behavior following one single stimulus injection without any restraints (10).

It is preferable to use multiple types of animal behavior assay to more accurately reflect the pain conditions experienced in humans. Therefore, in the second section of this chapter, we discuss in detail the methods for carrying out four different orofacial pain behavior assessments that include evoked mechanical withdrawal reflexes with von Frey filaments, spontaneous behaviors of eye closures and face rubbing, and an operant measure based on conditional reward behavior. The latter assays of spontaneous behaviors and operant measure are suggested to more closely resemble clinical conditions. Thus, they may perhaps provide more reliable indicators for investigating novel effective analgesics than the more commonly used evoked response assays (11).

We provide here the detailed procedures required to assess pain behavior based on the two orofacial pain models described. We will not discuss other orofacial pain models, such as cancer pain (12, 13), and other trigeminal neuropathic pain models (14) or behavioral assays, such as orofacial heat and cold hyperalgesia (15–17), and thermal operant facial behavioral assay (18, 19).

## 2. Materials

### 2.1. Models of Orofacial Pain

#### 2.1.1. Chronic Constriction Injury of the Infraorbital Nerve

We have described this procedure in detail (20) so we will only provide a brief description here:

1. Anesthetics: xylazine and ketamine; enflurane as supplemental anesthetic if necessary.
2. Stereotaxic head holder; if this is unavailable, any other arrangement to immobilize the head would be sufficient.
3. Sterile surgical tools: fine and coarse forceps, hemostats, no. 11 and 20 scalpel blades, retractors, and fine scissors.
4. A modified dental needle is used to aid placing the ligature in order to gain easier access to the ION with minimal disturbance of the eye. Eight centimeters of 5-0 chromic gut suture is threaded into a hypodermic needle (<http://www.henry-schein.com>, Monoject needles: 25 g long, item code: 1949460) while leaving 5 mm to protrude from the needle tip. The tip of the needle is bent to a smooth curve of approximately 90° using a hemostat with the opening of the needle on the inside of the bend. It is optimal to have the needle bend no longer than 3 mm and at an angle no more acute than 90° since otherwise, it would be harder to insert the needle around the orbit and thus increase the likelihood of damaging the eye bulb.

#### 2.1.2. Formalin Test

1. Formalin preparation: dilute 10% neutral buffered formalin stock (Sigma) with sterile saline to achieve a final concentration of 2.5%.
2. A 100 µl Hamilton glass syringe connected to a 30-g beveled needle for formalin injection.
3. Timer.

### 2.2. Behavior Assessment

#### 2.2.1. Mechanically Evoked Withdrawal Reflex (von Frey Filaments)

1. A transparent plastic cage with thin layer of bedding.
2. von Frey filaments (2, 10, and 50 g, corresponding to log units of 4.31, 5.07, and 5.88, respectively).

#### 2.2.2. Spontaneous Eye Closures and Face Rubbing

1. A Plexiglass testing chamber with mirrors placed behind the side and back walls of the chamber to allow videotaping and observation of both of the rat's eyes for the spontaneous eye closures test. (Mirrors may not be necessary for the face-rubbing pain behavior assessment.)
2. Video camcorder with tripod to record spontaneous eye closures and face rubbing for post-test analysis (see Note 1).
3. Timer.

### 2.2.3. Conditional Reward Testing

1. Sugar-sweetened water (20% v/w sucrose) prepared fresh daily.
2. A testing chamber (20×20×20 cm) with a 5×5×3 cm alcove in one wall that has a stainless steel drinking spout located at its back (Med Associates) for delivering sweetened water. Brushes, used as innocuous stimuli, are positioned on the side of the drinking alcove that is ipsilateral to the injury/noxious stimulation and/or treatment so that the rats have to press their snouts against the stiff-bristled brushes while drinking. The number and position of the brushes are such that they stimulate the rat's vibrissal pad and the perinasal and perioral areas (see Fig. 2a, b).
3. The measured parameters are the number of attempts to drink from the spout (successful and unsuccessful), the number of licks on successful attempts, the amount of time spent licking, and the amount of liquid consumed. All the parameters except the number of licks can be manually recorded by an experimenter. The number of licks can be measured with a conductance-measuring device (Lickometer; Med Associates) attached to the drinking spout. The most efficient way to record these parameters is by using an experimental setup that incorporates sensors to detect when the rat places its head in the drinking alcove, the number of licks and the elapsed time during licking. In this case, the data can be recorded automatically.
4. Scale for weighing the rats to normalize data.
5. Timer.

---

## 3. Methods

### 3.1. Models of Orofacial Pain

#### 3.1.1. Chronic Constriction Injury of the Infraorbital Nerve (Details in Ref. 20)

1. Rats are anesthetized with a mixture of ketamine and xylazine (90 and 5 mg/kg, respectively, i.p.) and supplemented with an inhalant anesthetic (1–2% enflurane with 40% oxygen and room air).
2. After the rat is anesthetized, the skin above the eye is shaved and the rat is placed in a stereotaxic head holder to immobilize the head.
3. An anterior–posterior skin incision approximately 7 mm long is made 2 mm above the left eye along the curvature of the frontal bone to expose the skull and nasal bone.
4. The eye is then retracted after gently teasing away the fascia and muscle laterally from the bone. The ION can then be seen approximately 8 mm deep within the orbit and lying on the maxillary bone.

5. At least 5 mm of the ION should be freed to ensure enough space for placing two ligatures (see Note 2).
6. Now, the suture-loaded needle can be inserted into the orbit cavity and slid under the nerve in order to place the bent needle tip medial to the ION (see Note 3). Gently retract the ION to reveal the needle tip and the protruding end of the chromic gut, then use a pair of forceps to grip and pull about 5 cm of the gut further medial to the ION. Reposition the forceps to grasp the gut nearer to the needle tip before withdrawing the needle laterally. Now, both ends of the gut become freely accessible for tying the ligatures (see Note 4).
7. Similar to the CCI model of the sciatic nerve (21), the two ligatures are placed 3–4 mm apart and each ligature is tightened until the ION is barely constricted followed by a second knot to prevent slippage. Excess gut is cut from the ligatures and 5–0 silk is used to suture the incision above the eye.
8. Surgery for sham animal controls should be similarly followed except no needle is inserted for tying ligatures (steps 6 and 7).

### 3.1.2. Orofacial Formalin Test

1. One day prior to the formalin test, the rats are acclimatized for at least 1 h in testing chambers.
2. On the testing day, 50  $\mu$ l of 2.5% formalin solution is injected subcutaneously with a 30 g hypodermic needle into the left upper lip, just lateral to the midline and the nose of the rat (Fig. 1) (see Note 5). The spread of the formalin solution is



Fig. 1. Location for orofacial formalin injection. (An insulin syringe needle is used for injecting 50  $\mu$ l of 0.25% formalin. *Arrow* indicates the tip of the needle).

restricted to the upper lip and the rostral half of the vibrissal pad (10). The rat may react to the formalin injection by head withdrawal.

3. Following the injection, the rat is immediately placed into the testing chamber and continuously observed for 44 min, during which its nociceptive behavior (see Subheading 3.2.3) is quantified.
4. One hour after formalin injection, the rats are euthanized by intracardiac perfusion of fixatives and tissues are collected for analysis.
5. Despite being the only nociceptive behavior outcome, face rubbing has been demonstrated to be a reliable measure and is positively correlated to formalin concentration (up to 2.5%), not evoked by saline injection, and reduced following systemic and local administration of analgesic drugs, including morphine and cyclooxygenase inhibitors (10, 22–25). A control group that receives saline injection only may be used to quantify normal face washing as the baseline for non-nociceptive face-rubbing behavior.

### 3.2. Behavior Assessment (see Note 6)

#### 3.2.1. Mechanical Allodynia Testing (von Frey)

1. Rats may be tested in their home cage or placed individually in a transparent plastic cage (Fig. 2a). In the latter case before testing, rats are acclimatized for a minimum of 15 min during which the experimenter reaches into the cage periodically to allow the animals to adapt to the reaching movements.
2. Mechanical stimulation is first applied contralateral the experimental side. Be careful not to deflect the von Frey filament on

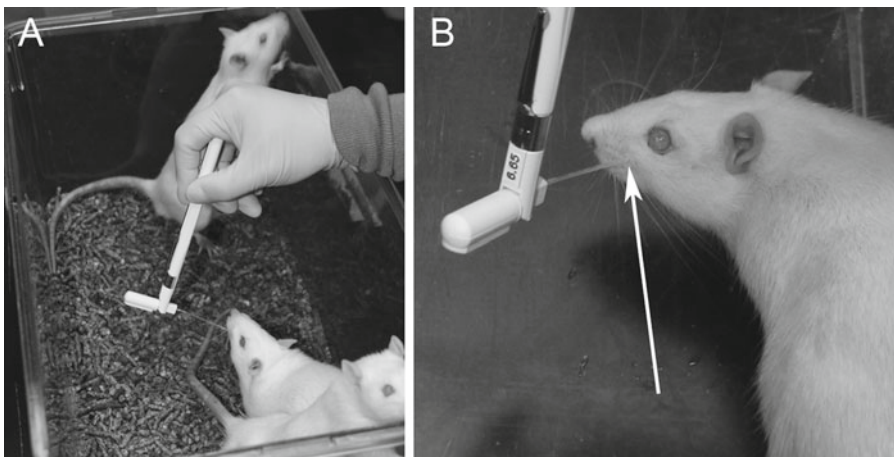


Fig. 2. Orofacial mechanical allodynia testing using von Frey filament. (a) Testing may be done in the rat's home cage singly or with cage mates. (b) Location of von Frey filament stimulation is indicated by the arrow.

the vibrissae when testing for mechanical responsiveness. Three von Frey filaments of increasing force (2, 10, and 50 g) are applied 5–6 times consecutively at 5 s intervals in different areas at the center and around the vibrissal pad and in the perioral and perinasal territory (Fig. 2b). Behavioral responses are scored according to refs. 3, 6, 7 as follows:

- (0) No detection.
- (1) Detection and exploration of the von Frey filament (head movement toward the direction of applied stimulus, sniffing, and licking).
- (2) Withdrawal and/or single grabbing/face wiping movement (head movement away slowly/briskly away from applied stimulus and single forepaw movement).
- (3) Attack and/or escape (attack: active movement toward the von Frey stimulus and/or biting and/or vocalization and/or multiple grabbing movements, escape: entire body movement away from stimulus which may result in a crouching position).
- (4) Active asymmetrical face grooming (prolonged series of more than one face stroking toward stimulated area).

The highest score for each hair is then recorded. Data can be presented separately for each hair or as the average of the highest scores obtained from the three different hairs (6, 7).

### 3.2.2. Spontaneous Eye Closures

1. Rats are placed individually in the testing chamber with mirrors placed behind the side and back walls of the chamber to ensure the head and eyes of the rat can be observed at all times. The rats are habituated to the testing chamber for a minimum of 3 days before testing. On the day of testing, they are acclimatized for at least 15 min.
2. The number of unilateral eye closures ipsilateral and contralateral to the side receiving the lesion or treatment and bilateral eye closures are counted during testing. Spontaneous eye closures are counted and videorecorded for post-test analysis in three sessions of 2 min each at 5 min intervals. Results are expressed as the mean number of eye closures per minute (see Note 7).

### 3.2.3. Face Rubbing

1. Rats are placed inside the testing chamber and assessment may begin immediately following noxious stimulation, such as formalin injection. The rat is videotaped for the entire period in the testing chamber.
2. The recorded behavior is face stroking directed to the upper lip and whisker pad with the ipsilateral forepaw. Depending on the model used, varying lengths of assessment can be carried out.

For the formalin test, usually bins of 3–4 min are used for an observation period of 44 min (26, 27) while shorter periods of 7–10 min have been reported to be sufficient in demonstrating nociceptive behavior in orofacial neuropathic and cancer pain models (3, 13). Data are expressed as face-rubbing time in seconds per bin (see Note 8).

#### 3.2.4. Conditional Reward Testing (Operant Behavior Assay)

1. Rats are acclimatized to the testing chamber for 1 h or until they find and drink from the spout that delivers sugar-sweetened water (20% sucrose) (Fig. 3a). The rats are placed in the testing chamber each day for training until they begin drinking within minutes of being placed in the cage. They are then left alone for 10 min, which is the standard testing period. The rats have a strong preference for sweetened water and no water or food deprivation is required to induce them to drink (28).
2. Once trained, the rats are tested for avoidance of an innocuous stimulus (i.e. brushes) when attempting to obtain the reward of sweetened water. Rats are placed individually inside the testing chamber. The number of licks when the rats drink from the spout while having their face in contact against the side brushes is counted (Fig. 3b, c).
3. The testing period lasts for a minimum of 5 min or after ten attempts to drink from the spout before returning the rats to the home cage. The experimenter (or computer if an automated system is used) records the number of both successful and unsuccessful licking attempts. A licking episode, referred to as a successful attempt, is when the rat has a minimum of six licks before withdrawing its head from the drinking alcove. The licking episode can either be one continuous series or several periods of licks as long as the head is not removed from the alcove. If the rat licks five times or fewer before removing its head from the opening, an unsuccessful attempt is recorded. The limit of five licks is based on preliminary testing that shows five or fewer licks are part of exploratory behavior whereas drinking episodes always consist of more than five licks. The number of licks is corrected for the weight of the rat. Data are presented as the number of licks per licking episode per kilogram weight of the rat for successful attempts and the amount of water consumed is also recorded per rat (see Note 9).

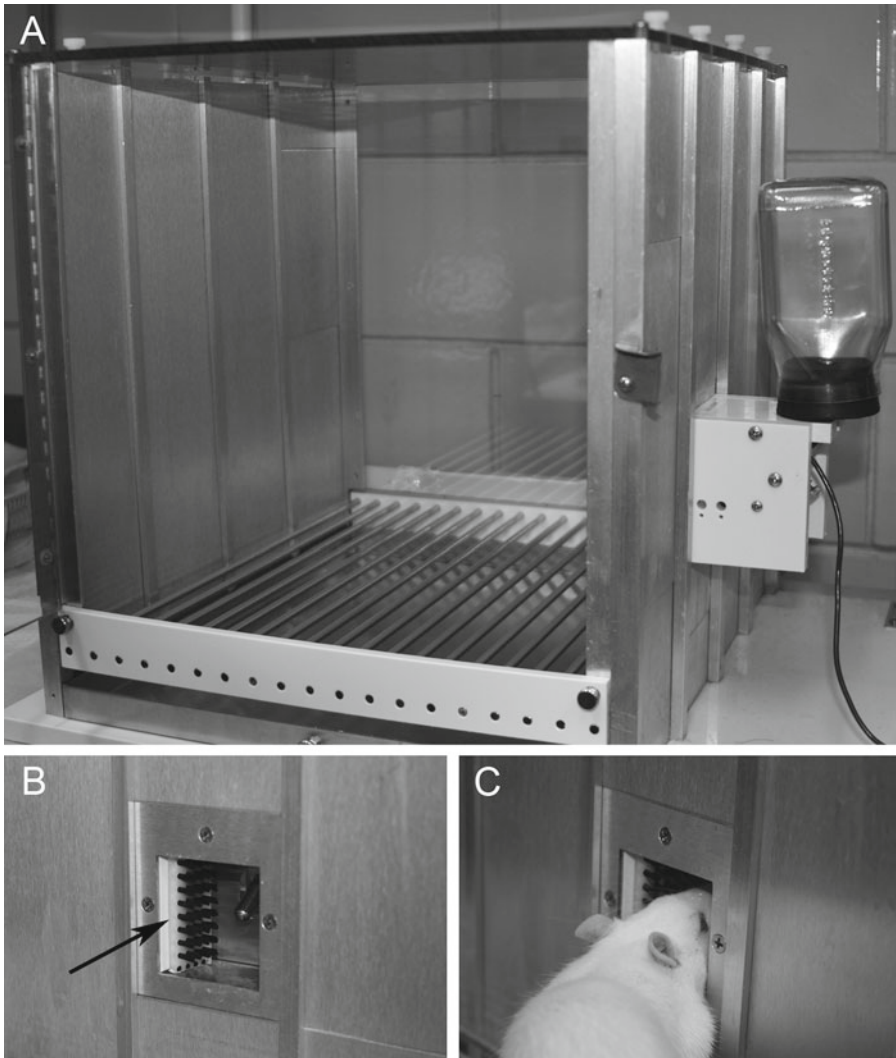


Fig. 3. (a) Conditional reward testing apparatus with the drinking spout located to the right. (b) Close-up from inside, the cage showing the drinking spout with brushes mounted on the side (indicated by the *arrow*) as innocuous stimuli. (c) Rat drinking from the spout with face pressed against the brushes.

---

#### 4. Notes

1. Pocket video cameras, such as the Flip or Kodak Zi8, are found to be excellent low-cost options for recording.
2. During exposure of the ION, be careful not to damage any surrounding nerve, particularly the anterior ethmoidal nerve that crosses perpendicularly above the ION.

3. The bone acts as a natural barrier, and it can be used as a guide to determine when the needle has been inserted far enough.
4. Keep all parts of the chromic gut moist during procedures with sterile saline. Otherwise, dried gut can be difficult to position around the ION and harder to remove from the needle.
5. A formalin concentration of 0.5–2.5% was determined to be the most optimal range used for orofacial pain behavior testing (23). Although concentrations outside this range resulted in similar intensity of nociceptive responses in the first phase, a minimum concentration of 1.5% is required to elicit second phase responses. On the other hand, concentrations above 2.5% may cause a paradoxical decrease in responses due to other behavioral responses, such as freezing, and reduce the ability to observe antinociceptive or pronociceptive drug effects.
6. It is essential for all behavior tests to be done by an experimenter blinded to treatment and surgery to avoid experimental bias. Randomization may be done following taking the averaged baseline values taken on multiple days prior to the study.
7. Eye closures are not counted during periods of face grooming since we are interested in the blinking reflexes independent of facial sensations. Animals with CCI of the ION show a significantly increased number of spontaneous ipsilateral eye closures compared with baseline and the contralateral side (7, 29).
8. Face rubbing may also be referred to as face grooming and has been validated to be a reliable normal rodent behavior (for thermoregulation, social signaling, and body cleaning) (30). In contrast to models of orofacial pain (including CCI of the ION, injection of carcinosarcoma cells and noxious stimuli that include formalin and capsaicin into the vibrissal pad area), injection of non-noxious substances, such as mineral oil and saline in addition to bupivacaine as an anesthetic blockade, does not induce more face-rubbing behavior than in unstimulated control animals (3, 13, 27, 30, 31). Therefore, face rubbing can be quantified as a specific nocifensive behavior that is not due to non-nociceptive sensory disturbances.
9. Previously, we have also characterized the volume of lick, number of unsuccessful drinking attempts, and time to make ten attempts and found that they do not vary significantly between control and rats with orofacial pain behavior, at least in the CCI of ION model (7). We found that the number of licks per successful licking episode is the most reliable assay for facial nociceptive behavior.

## Acknowledgments

This work is supported by NIH grants NS051336 and NS061241.

## References

1. Fried, K., Bongenhielm, U., Boissonade, F. M., and Robinson, P. P. (2001) Nerve injury-induced pain in the trigeminal system, *Neuroscientist* **7**, 155–165.
2. Kitt, C. A., Gruber, K., Davis, M., Woolf, C. J., and Levine, J. D. (2000) Trigeminal neuralgia: opportunities for research and treatment, *Pain* **85**, 3–7.
3. Vos, B. P., Strassman, A. M., and Maciewicz, R. J. (1994) Behavioral evidence of trigeminal neuropathic pain following chronic constriction injury to the rat's infraorbital nerve, *J Neurosci* **14**, 2708–2723.
4. Vos, B. P., and Strassman, A. M. (1995) Fos expression in the medullary dorsal horn of the rat after chronic constriction injury to the infraorbital nerve, *J Comp Neurol* **357**, 362–375.
5. Imamura, Y., Kawamoto, H., and Nakanishi, O. (1997) Characterization of heat-hyperalgesia in an experimental trigeminal neuropathy in rats, *Exp Brain Res* **116**, 97–103.
6. Ohara, P. T., Vit, J. P., Bhargava, A., and Jasmin, L. (2008) Evidence for a role of connexin 43 in trigeminal pain using RNA interference in vivo, *J Neurophysiol* **100**, 3064–3073.
7. Vit, J. P., Ohara, P. T., Bhargava, A., Kelley, K., and Jasmin, L. (2008) Silencing the Kir4.1 potassium channel subunit in satellite glial cells of the rat trigeminal ganglion results in pain-like behavior in the absence of nerve injury, *J Neurosci* **28**, 4161–4171.
8. Dubuisson, D., and Dennis, S. G. (1977) The formalin test: a quantitative study of the analgesic effects of morphine, meperidine, and brain stem stimulation in rats and cats, *Pain* **4**, 161–174.
9. Dallel, R., Raboisson, P., Clavelou, P., Saade, M., and Woda, A. (1995) Evidence for a peripheral origin of the tonic nociceptive response to subcutaneous formalin, *Pain* **61**, 11–16.
10. Raboisson, P., and Dallel, R. (2004) The orofacial formalin test, *Neurosci Biobehav Rev* **28**, 219–226.
11. Mogil, J. S. (2009) Animal models of pain: progress and challenges, *Nat Rev Neurosci* **10**, 283–294.
12. Nagamine, K., Ozaki, N., Shinoda, M., Asai, H., Nishiguchi, H., Mitsudo, K., Tohnai, I., Ueda, M., and Sugiura, Y. (2006) Mechanical allodynia and thermal hyperalgesia induced by experimental squamous cell carcinoma of the lower gingiva in rats, *J Pain* **7**, 659–670.
13. Ono, K., Harano, N., Nagahata, S., Seta, Y., Tsujisawa, T., Inenaga, K., and Nakanishi, O. (2009) Behavioral characteristics and c-Fos expression in the medullary dorsal horn in a rat model for orofacial cancer pain, *Eur J Pain* **13**, 373–379.
14. Holland, G. R. (1996) Experimental trigeminal nerve injury, *Crit Rev Oral Biol Med* **7**, 237–258.
15. Chichorro, J. G., Zampronio, A. R., Souza, G. E., and Rae, G. A. (2006) Orofacial cold hyperalgesia due to infraorbital nerve constriction injury in rats: reversal by endothelin receptor antagonists but not non-steroidal anti-inflammatory drugs, *Pain* **123**, 64–74.
16. Morgan, J. R., and Gebhart, G. F. (2008) Characterization of a model of chronic orofacial hyperalgesia in the rat: contribution of NA(V) 1.8, *J Pain* **9**, 522–531.
17. Okada-Ogawa, A., Suzuki, I., Sessle, B. J., Chiang, C. Y., Salter, M. W., Dostrovsky, J. O., Tsuboi, Y., Kondo, M., Kitagawa, J., Kobayashi, A., Noma, N., Imamura, Y., and Iwata, K. (2009) Astroglia in medullary dorsal horn (trigeminal spinal subnucleus caudalis) are involved in trigeminal neuropathic pain mechanisms, *J Neurosci* **29**, 11161–11171.
18. Neubert, J. K., Widmer, C. G., Malphurs, W., Rossi, H. L., Vierck, C. J., Jr., and Caudle, R. M. (2005) Use of a novel thermal operant behavioral assay for characterization of orofacial pain sensitivity, *Pain* **116**, 386–395.
19. Rossi, H. L., Vierck, C. J., Jr., Caudle, R. M., and Neubert, J. K. (2006) Characterization of cold sensitivity and thermal preference using an operant orofacial assay, *Mol Pain* **2**, 37.
20. Kernisant, M., Gear, R. W., Jasmin, L., Vit, J. P., and Ohara, P. T. (2008) Chronic constriction injury of the infraorbital nerve in the rat using modified syringe needle, *J Neurosci Methods* **172**, 43–47.
21. Bennett, G. J., and Xie, Y. K. (1988) A peripheral mononeuropathy in rat that produces disorders

- of pain sensation like those seen in man, *Pain* **33**, 87–107.
22. Clavelou, P., Pajot, J., Dallel, R., and Raboisson, P. (1989) Application of the formalin test to the study of orofacial pain in the rat, *Neurosci Lett* **103**, 349–353.
  23. Clavelou, P., Dallel, R., Orliaguet, T., Woda, A., and Raboisson, P. (1995) The orofacial formalin test in rats: effects of different formalin concentrations, *Pain* **62**, 295–301.
  24. Eisenberg, E., Vos, B. P., and Strassman, A. M. (1996) The peripheral antinociceptive effect of morphine in a rat model of facial pain, *Neuroscience* **72**, 519–525.
  25. Chichorro, J. G., Lorenzetti, B. B., and Zampronio, A. R. (2004) Involvement of bradykinin, cytokines, sympathetic amines and prostaglandins in formalin-induced orofacial nociception in rats, *Br J Pharmacol* **141**, 1175–1184.
  26. Jasmin, L., Vit, J. P., Bhargava, A., and Ohara, P. T. (2010) Can satellite glial cells be therapeutic targets for pain control?, *Neuron Glia Biol* **6**, 63–71.
  27. Vit, J. P., Ohara, P. T., Sundberg, C., Rubi, B., Maechler, P., Liu, C., Puntel, M., Lowenstein, P., Castro, M., and Jasmin, L. (2009) Adenovector GAD65 gene delivery into the rat trigeminal ganglion produces orofacial analgesia, *Mol Pain* **5**, 42.
  28. Davis, J. D., and Campbell, C. S. (1973) Peripheral control of meal size in the rat. Effect of sham feeding on meal size and drinking rate, *J Comp Physiol Psychol* **83**, 379–387.
  29. Vit, J. P., Jasmin, L., Bhargava, A., and Ohara, P. T. (2006) Satellite glial cells in the trigeminal ganglion as a determinant of orofacial neuropathic pain, *Neuron Glia Biol* **2**, 247–257.
  30. Vos, B. P., Hans, G., and Adriaensen, H. (1998) Behavioral assessment of facial pain in rats: face grooming patterns after painful and non-painful sensory disturbances in the territory of the rat's infraorbital nerve, *Pain* **76**, 173–178.
  31. Pelissier, T., Pajot, J., and Dallel, R. (2002) The orofacial capsaicin test in rats: effects of different capsaicin concentrations and morphine, *Pain* **96**, 81–87.

# Chapter 12

## Unilateral T13 and L1 Dorsal Root Avulsion: Methods for a Novel Model of Central Neuropathic Pain

Julie Wieseler, Amanda Ellis, Steven F. Maier, Linda R. Watkins, and Scott Falci

### Abstract

Central neuropathic pain is associated with many disease states including multiple sclerosis, stroke, and spinal cord injury, and is poorly managed. One type of central neuropathic pain that is particularly debilitating and challenging to treat is pain that occurs below the level of injury (below-level pain). The study of central neuropathic pain is commonly performed using animal models of stroke and spinal cord injury. Most of the spinal cord injury models currently being used were originally developed to model the gross physiological impact of clinical spinal cord injury. In contrast, the T13/L1 dorsal root avulsion model of spinal cord injury described here was developed specifically for the study of central pain, and as such, was developed to minimize confounding complications, such as paralysis, urinary tract infections, and autotomy. As such, this model induces robust and reliable hindpaw mechanical allodynia. Two versions of the model are described. The first is optimal for testing systemically administered pharmacological manipulations. The second was developed to accommodate intrathecal application of pharmacological manipulations. This model provides an additional means by which to investigate central pain states associated with spinal cord injury, including below-level pain. Finally, a brief discussion of at-level pain measurement is described as it has been suggested in the literature that the mechanisms underlying below- and at-level pain are different.

**Key words:** Spinal cord injury, Hindpaw allodynia, Grid walk, Central neuropathic pain

---

### 1. Introduction

Central neuropathic pain is commonly associated with various disease states including stroke, multiple sclerosis, traumatic brain injury, tumors, epilepsy, and spinal cord injury. Chronic pain is common following spinal cord injury, affecting 65% of the patients. Of the patients experiencing chronic pain, 34% described the pain as severe and intolerable (1–3). Extreme pain adversely impacts psychological

and social functioning (4, 5), and inhibits rehabilitative efforts (6). While animal models of spinal cord injury are used to study central pain, they were originally developed to mirror the clinical gross pathology associated with traumatic spinal cord injury (7–11). As such, the degree of damage and loss of voluntary motor control associated with these models are not ideal for exploring mechanisms underlying central neuropathic pain.

The avulsion model described here was developed with the expressed purpose of studying central neuropathic pain. Neuronal activity measured in spinal cord injured patients experiencing neuropathic pain and having avulsed roots shows spontaneous neuro-electrical hyperactivity at the avulsion site (12). Our goal was to cause an avulsion spinal cord injury that induced pain 4–6 dermatomes below the injury site. This was the explicit goal because such a model would allow discrete spinal cord dorsal horn injury (T13/L1) to be located sufficiently rostral to the hindpaw dermatomes (L5/L6) so to avoid any confounding damage to sensory/motor function of the hindlimbs. Consistent with this, avulsion of T13 and L1 induces hindpaw allodynia (Fig. 1). Unilateral avulsion of either T13 or L1 dorsal roots alone does not result in robust and reliable below-level pain, whereas combined unilateral avulsion of T13 and L1 dorsal roots induces robust and reliable hind paw allodynia (Wieseler et al., under review). Hindpaw allodynia develops over time, with reliable allodynia developing

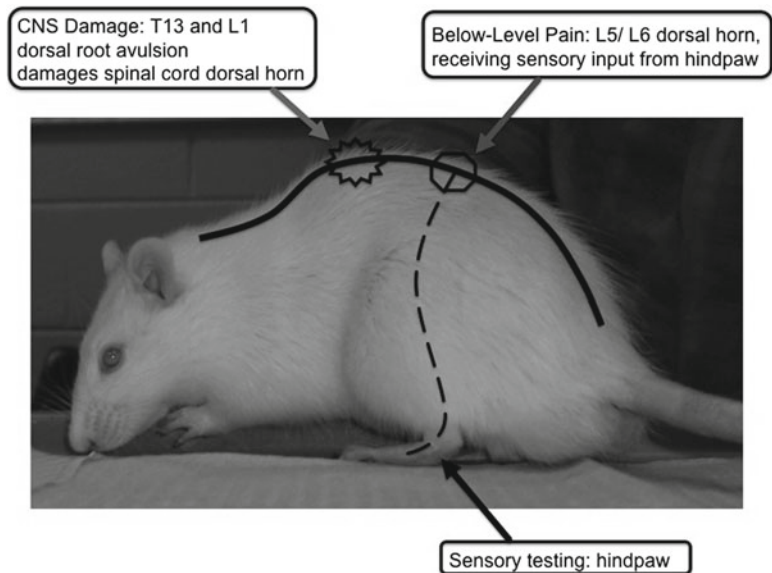


Fig. 1. Photograph generally illustrating the location of injury relative to the level the pain is experienced. Avulsion of both thoracic (T)13 and lumbar (L)1 dorsal roots induces mechanical allodynia four dermatomal levels (L5/L6) below the site of injury, measured in the hindpaw.

(compared to sham-operated controls) by 3 weeks postsurgery and lasting approximately 9 weeks postsurgery. The avulsion causes discrete tissue damage limited to the dorsal horn.

Here, the detailed method for unilateral T13/L1 dorsal root avulsion model is presented. Two versions of the model are presented. The first is a surgical procedure that is shorter in duration and suitable for the study of systemically administered pharmacological agents. The second requires a longer surgical period due to inclusion of suturing the dura. This second method was developed to allow for intrathecal application of pharmacological manipulations to the injury site after re-establishment of the CSF space upon healing of the incised dura. Finally, in order to test motor effects, the method for assessing behavior on the grid walk is described.

---

## 2. Materials

### 2.1. Avulsion Surgery

1. Scalpel handle and No. 10 scalpel blades.
2. Two #5 stainless steel straight fine tip forceps (Fine Science Tools, #11254-20), one pair with the tips bent to form a slight hook.
3. #7 Stainless steel curved fine tip forceps (Fine Science Tools, #11274-20).
4. Fine-tipped Rongeurs (Fine Science Tools, #16021-14).
5. Hemostats (Fine Science Tools, #13004-14).
6. Toothed forceps (Fine Science Tools, #11023-14).
7. Suture hemostats with scissors (Fine Science Tools, #12502-14).
8. 4-mm spring scissors (Fine Science Tools, #15018-10).
9. Small scissors (Fine Science Tools, #14058-11).
10. 23-G  $\frac{3}{4}$  in. hypodermic needle.
11. 22-G  $\frac{1}{2}$  in. hypodermic needle.
12. 1 cc Syringe.
13. Sterile Q-tips to absorb blood.
14. Sterile gauze (5.08 cm  $\times$  5.08 cm).
15. Magnifying glasses (Cabela's Inc., Sidney, NE; #IJ-711125, 3 $\times$ ).
16. Gelfoam sponge sheets (Upjohn, Kalamazoo, MI).
17. Oxycel (cut into 1 mm  $\times$  1 mm pieces stored in a sterile vial until needed; for absorption of blood).
18. 500- $\mu$ L Centrifuge tubes.
19. Sterile silk suture (3-0) with attached needle (cutting FS-1; Ethicon, Somerville, NJ).

20. 16 mm Stainless steel Michel clips (Alimed, Dedham, MA).
21. Wound clip applicator (Fine Science Tools, #12028-12).
22. Shaver.
23. Ultra hot glass-bead sterilizer to autoclave surgical tools.
24. Foam padding (~4.31 cm thick, purchased from fabric store).
25. Cardboard boxes (sized to fit within home cage).
26. Draping material (e.g. paper towel with a hole cut in the center to allow access to the surgery site).
27. Sterile silk suture (6-0) with attached needle (cutting P-1; Ethicon, Somerville, NJ).
28. Isoflurane (Halocarbon Laboratories, River Edge, NJ).
29. Oxygen.
30. Sterile physiological saline.
31. 70% Ethanol.
32. Betadine.
33. Polysporin powder.
34. Antibiotics (e.g., Twin-Pen, Combi-Pen 48).

### **2.2. Motor Assessment via Grid Walk**

1. Horizontal ladder elevated on a table (a set of 20 round, smooth, stainless steel bars, secured between two 2 in. × 4 in. pieces of wood in holes drilled such that the bars fit snugly. Each metal bar is 1.77 cm in diameter and the bars are spaced evenly every 3.43 cm on center).
2. 30.5 cm × 30.25 cm Black plastic box.
3. Stopwatch.

---

## **3. Methods**

### **3.1. Avulsion Surgery**

Two versions of the avulsion surgery are described, the first surgery is of shorter duration and used for the study of systemically administered pharmacological agents. The second surgery includes suturing the dura, reinstating an intact cerebrospinal fluid space. This second surgery was developed for intrathecal administration of pharmacological agents after the incised dura heals. In both cases, sham surgeries are carried out as described below with the exception that the roots are not avulsed. The first few steps are identical for both approaches and are noted below followed by the individual approaches. Following both surgeries, rats are transferred to their home cages fitted with cardboard boxes and foam padding to confine movement and protect it while recovering from anesthesia.

### 3.1.1. Common Surgical Steps for Both Models

1. Surgery is conducted under isoflurane anesthesia, 2.5% in oxygen. Isoflurane is chosen due to its minimal effects on immune cells compared to other anesthetics (13–19).
2. The anesthetized rat is placed, dorsal side up, with the body lying parallel to the table's edge. The back is shaved, starting from mid rib cage and extending 7.5 cm caudally.
3. The exposed skin is cleaned with 70% ethanol.
4. The appropriate spinal level is identified using vertebral landmarks relative to T13, the rostral aspect of which is level with the 13th rib (the floating rib). A midline incision is made through the skin, extending 3.5 cm rostral and 3.5 cm caudal of this point. After opening the skin, the muscle is bilaterally separated as close to the vertebral dorsal processes as possible, by first slitting the fascia and underlying muscle down to the vertebral bone on each side of the dorsal processes and then scraping the dorsal processes and lamina with a #10 scalpel blade to clean remaining tissue from the bones. The midline tissue that “caps” the tops of the dorsal processes is removed, revealing the dorsal aspects of spinous processes of T11, T12, and T13.
5. The floating rib is used to identify the T13 dorsal process, and it is removed to improve access to the caudal aspect of T12 vertebral bone for laminectomy. Using toothed forceps to elevate and stabilize the vertebral column, rongeurs are used to remove the dorsal aspect of the T12 vertebra as well as the ipsilateral subarticular process of T13 and ipsilateral caudal end of T11, thereby exposing the dura-encased spinal cord. Care is taken to ensure that the laminectomy leaves no loose bone shards and no points of intact bone protruding toward the spinal cord as these could damage the spinal cord if swelling occurs in response to surgery. Dorsal roots T13 and L1 enter the spinal cord under the T12 vertebra.
6. Gelfoam sponge is teased apart into tiny pieces (~1.5 mm × 2 mm), and placed in a 500- $\mu$ L centrifuge tubes containing sterile physiological saline (see Note 1).

### 3.1.2. Avulsion Surgery Alone

1. The exposed dura is gently nicked using a 23-G  $\frac{3}{4}$  in. hypodermic needle as a knife, by repeated gentle rostrocaudal strokes upon the dura parallel to midline of the spinal cord, but avoiding the dorsal midline blood vessel. The repeated exposure to the needle weakens the dura (see Note 2). When an opening appears, the hooked #5 forceps are used to very gently pick up the dura, and then open it using spring scissors such that an opening spans the opened vertebral space, and exposes T13 and L1 roots.
2. The dorsal roots are identified and individually isolated. L1 dorsal root enters the spinal cord at the caudal end of T12

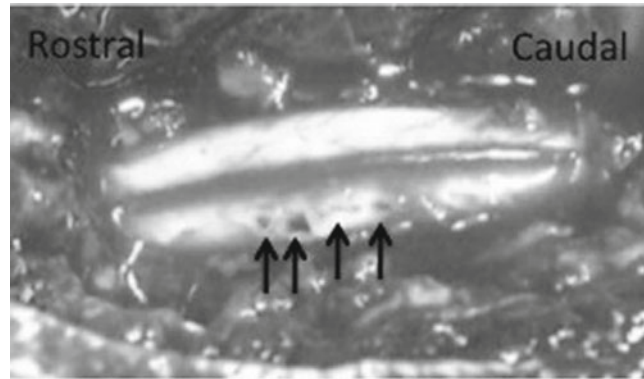


Fig. 2. Photograph of spinal cord immediately following dorsal root avulsion. Rats undergo laminectomy and retraction of the dura, exposing the dorsal roots entering the spinal cord. The dorsal roots are individually identified, isolated, and rapidly avulsed from the spinal cord. This avulsion disrupts the dorsal horn, leaving holes in the spinal cord at the point the roots entered the spinal cord. Modified from Wieseler, et al. (20) with permission from Mary Ann Liebert, Inc.

vertebra, and T13 enters the spinal cord at the rostral end of T12 vertebra. These nerves are identified and traced to the dorsal root entry zone. The root, as it enters the spinal cord, is firmly grasped with fine-tipped curved forceps at the dorsal root entry zone and rapidly torn away from the dorsal horn. Successful avulsion disrupts the dorsal horn, and red dots of blood appear where the nerve previously had entered the spinal cord (Fig. 2).

3. After avulsion, saline-moistened gel foam is placed over the exposed spinal cord.
4. After draping the rat to avoid suture dragging through the rat's fur, the two sides of the muscle incision are gently pulled together and sutured using 3-0 silk suture, and the skin closed using 16-mm Michel clips.
5. Following surgery, rats are returned to their home cages to recover from anesthesia. The rat is placed in a foam-padded cardboard box, such as the box from a case of 1-cc syringes, cut down to allow the cage top to close. Foam padding is also placed in the cage, against the vertical walls for few hours to protect the rats from unintended spinal cord injury during the brief ataxic period associated with recovery from anesthesia (see Note 3).
6. Antibiotics (0.3 mL per rat) are administered at the time of surgery and then daily (0.2 mL per rat) for 4 days following surgery.
7. Avulsion surgery without dura suturing produces robust and reliable hindpaw mechanical allodynia compared to sham surgery 13–15 days postsurgery (see Notes 4, 6–9).

### 3.1.3. Avulsion Surgery with Dura Suturing

1. Upon completion of laminectomy, saline-moistened gelfoam is placed on the dura to keep it soft. The rat is then draped so to avoid suture from contacting rat fur. The drape extends beyond the rat's body so to provide a clean surface upon which the needed surgical tools are placed:
  - (a) 6-0 silk, moistened by pulling it through a wet gauze pad to ensure that the suture is clean, flexible, and kink free. The tail end of the suture is grasped with a pair of hemostats, placed between the rat's body and the surgeon on the drape. This anchoring of the suture is to protect against unintended tugs on the suture that can cause the surgeon to lose the suture placement in the dura.
  - (b) Curved microforceps (#7 forceps), straight microforceps (#5 forceps) with a hooked tip, straight microforceps with no hooked tip, microscissors, 23-G Hypodermic needle.
2. The exposure of dorsal roots is accomplished as two separate incisions: one caudally and the other one rostrally (see Note 2). This is necessary because the extreme challenge for dura suturing lies in the accessibility of the lateral dural edge for inserting the suture. As the incision gets longer, and as spinal cord swelling occurs (beginning as soon as the dura is first incised), access to the lateral dura edge rapidly degrades to impossible.
3. After pushing the moistened gelfoam aside to expose the caudal dura, the 23-G hypodermic needle is used as a knife to gently cut a slit opening in the dura. Immediately grasp the needle of the 6-0 silk suture with the curved microforceps and, with the other hand, isolate and elevate the lateral cut edge of the dura with the hooked straight microforceps. Immediately insert the 6-0 silk through the lateral edge of the dura to gain a secure hold on the lateral dura. Note that it is extremely easy to tear the suture out of the lateral dura. All manipulation of the needle and suture must be with great gentleness. Hold a well-moistened (with either blood or saline) Q-tip gently atop the dura while pulling the suture through the dura to help prevent tearing. As blood makes it stick to the microforceps (used to pull the suture through), be very aware of this so that the stickiness does not result in unintentional pulling on the dura. Pull the suture through until restrained by the far end of the suture being held by the hemostats. Remove the moistened Q-tip and lay the needle end of the suture next to the hemostat, thus moving the suture out of the surgical field during the avulsion.
4. The dorsal roots are identified and individually isolated, as described above (Subheading 3.1.2, step 2). Using #5 forceps, the nerves are traced to the dorsal root entry zone, grasped

tightly with the forceps, and rapidly torn away from the spinal cord.

5. Upon completion of the avulsion, the medial edge of the dura is elevated with the hooked straight microforceps, the needle of the 6-0 silk inserted through, a moistened Q-tip used to help prevent tearing of the dura by the suture as it is pulled through. Unclasp the tail end of the suture from the hemostat and complete the pulling of the suture so that a short tail of suture remains beyond the lateral dura. Gently tie the suture using flat (not hooked) microforceps, and trim with microscissors. Clean the 6-0 suture with a saline-moistened gauze pad to remove the sticky blood and insure there is not tissue stuck to the suture that would tear the dura when again used to suture dura.
6. Gently move the rostral gelfoam caudally over the just-sutured caudal site, thereby exposing the rostral section of dura-encased spinal cord. Repeat steps 3-5.
7. Following dura suturing, moistened gel foam is gently placed to cover the entire exposed spinal cord, and the muscle wall and skin are sutured in layers as described above (Subheading 3.1.2, step 4).
8. Rats are returned to their home cage with foam padding, as described (Subheading 3.1.2, step 5).
9. Antibiotics (0.5 mL per rat) are administered at the time of surgery then daily (0.4 mL per rat) for 4 days following surgery.
10. Avulsion surgery with dura suturing produces robust and reliable hindpaw mechanical allodynia compared to sham surgery 15-20 days postsurgery (see Notes 4, 5, 7-9).

### **3.2. Motor Assessment via Grid Walk**

1. The ladder is placed on a well-lit, stable table and a black plastic box were placed at one end to encourage animals to travel in one direction across the ladder (towards the box, Fig. 3).
2. Rats undergo three habituation periods during which they are trained to walk across a horizontal ladder, to the black box.
3. For all baseline and postoperative testing, animals are required to walk across the ladder three consecutive times without stopping. If they stop on the ladder, they are gently prodded to continue.
4. Baseline measures are collected the day before surgery. Following surgery, rats are tested weekly.
5. Dependent measures used for analysis are the time needed to cross the ladder and the total number of hind-limb footfalls (missteps) for each trial. The time or number of missteps is averaged and used for analysis. Ipsilateral and contralateral hindpaw data are analyzed separately.

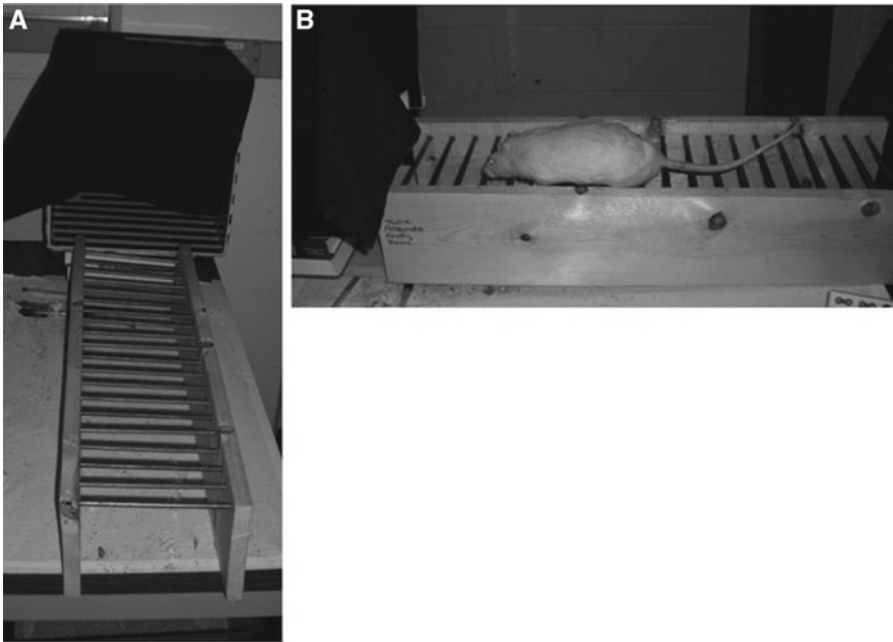


Fig. 3. Photograph of horizontal ladder used to assess motor ability in the grid walk. (a) The horizontal ladder has metal rungs spaced 2.54 cm apart. The ladder consists of 20 rungs, with only the middle 10 being used to test behavior, that way the behavioral measurement is not affected by the first uncertain steps, or the last rushed steps. (b) With habituation, a naive rat rapidly and effortlessly moves across the horizontal ladder.

---

#### 4. Notes

1. These surgeries can be initially time intensive, and resulting animal behavior is extremely sensitive to the amount of time the spinal cord is exposed. If there are environmental distractions that need to be dealt with, moistened gel foam can be placed on exposed cord with dura intact for a short amount of time, and the surgery continued with the expected results. If the dura has been cut, for a successful surgery, the remaining steps should be completed as seamlessly as possible. Once the dura has been cut, the spinal cord begins to swell, and continues to change for the duration of exposure.
2. A significant challenge with this surgery is completing it without otherwise damaging the spinal cord or local blood vessels. The key to successfully avulsing the dorsal roots and not nicking a blood vessel or otherwise injuring the spinal cord is that many of surgical actions are carried out in synchrony with the animal's breathing. Laying on a hard surface, the spinal cord moves up vertically as the animal breathes, and thus facilitates forcep tips or needles unintentionally penetrating the parenchyma.

When slitting the dura, it is optimal to make each cutting motion on the rat's exhale as at this point there is a pause in the movement of the spinal cord with respiration.

3. Following surgery, the rats are extremely vulnerable to further injury to the spinal cord, and as such care is taken when handling them and in housing them following surgery. Immediately following surgery, the rat is returned to its home cage containing a box with foam padding along the vertical walls and floor to confine movement during anesthetic recovery. The padding is removed once the animal completely recovers. Food is placed directly in the cage and the water bottle has an extended spout, all done to prevent the rat from further injury to the spinal cord. Additionally, the rats are handled with extreme care, always using two hands to fully support the rat and minimize struggling.
4. Following a successful avulsion surgery, sham- and avulsion-operated rats show hindpaw allodynia over the first 2 weeks, at which point the behavior of the sham operated animal approaches baseline levels, with sham-operated rats completely returned to baseline by 3 weeks. During the first 2 weeks, avulsion-operated rats, with or without dura suturing, show some paresis in the left hindpaw. Recovery from surgery is marked by loss of paresis and when there is no difference between naïve, sham-operated and avulsion-operated rats with respect to movement across the horizontal ladder. Hindpaw mechanical allodynia is induced 100% of the time with successful avulsion of both T13 and L1 dorsal roots. Approximately 4% of the rats show autotomy (evidenced by the development of sore on or near the ipsilateral knee) during the first 3–4 weeks, and resolves in about a week. We have treated the autotomy with antibiotics and have not found that it interferes with hindpaw allodynia. When the spinal cord and/or surrounding blood vessels are injured or if the forceps slip into the cord during surgery, usually one or both hindpaws are paralyzed, and the animal does not completely recover from surgery.
5. Successful dura suturing can be tested after the animal has recovered from the surgery by co-administering Evan's blue and lidocaine intrathecally to the injury site. Lidocaine paralyzes the animal at the dermatomal level it is administered, and as such serves as a functional measure to the viability of an intrathecal injection. The paralysis is evident as soon as the animals recover from anesthesia. Thirty minutes after the intrathecal injection and behavioral verification, the animal is deeply anesthetized and transcardially perfused with saline to facilitate visualization of the dye. If the surgery with dura suturing is successful, the Evan's blue dye will remain within the cerebrospinal fluid space around spinal cord, will not be found outside

of the dura indicative of a leak. In our experience, intrathecal injections were successful 5 days postsurgery for avulsion with dura suturing.

6. Histological confirmation of successful dorsal root avulsion can be obtained by cresyl violet staining, and by taking advantage of the interaction between 3,3-diaminobenzidine (DAB; Sigma-Aldrich) and endogenous peroxidases expressed by red blood cells. Spinal cord slices are reacted using DAB for 15 min, and glucose oxidase (Sigma-Aldrich; type V-s; 0.02%) and  $\beta$ -D-glucose (0.1%) are used to generate hydrogen peroxide. Nickelous ammonium sulfate is added to the DAB solution (0.025%, w/v) to intensify the reaction product. Slides are then dried overnight, cleared, and coverslipped with Permount. Successful avulsion readily shows influx of red blood cells 24 h after surgery. With cresyl violet staining, one can visualize the tissue disruption caused by the avulsion.
7. When first learning this surgery, a surgeon can expect to complete the avulsion alone surgery within 75 min. Once one becomes expert at the avulsion alone surgery (which now takes about 20–25 min), first learning the avulsion with dura suture surgery extends the surgical time to about 60 min. This decreases to about 40–45 min with expertise. As already discussed, the challenge is not injuring the spinal cord other than that caused by avulsing the dorsal roots. A high-percentage loss when learning the dura suturing surgery stems from a combination of factors including inability to secure the suture through the lateral dural edge, tearing of the dura while avulsing the roots, etc. With practice, the surgery can be done in about 40 min with rare loss of rats. There will, however, be rats whose blood vessel patterns make it impossible to do an avulsion without having a blood-obscured surgical field. These rats can be assigned as sham-operated controls or discarded, whichever is preferred.
8. Hindpaw mechanical allodynia is induced 100% of the time with successful avulsion of both T13 and L1 dorsal roots. The time a novice surgeon requires to complete the surgery potentiates the pain, which is observed in sham-operated rats such that the sham rats are indiscernible from avulsion rats for at least 2–4 weeks. The time to complete surgery is significantly shortened with experience, and the behavioral profile of sham- and avulsion-operated rats differs significantly within the first 2 weeks following surgery.
9. As this chapter is being written, we are optimizing methods for the measurement of at-level pain. We have been successful at detecting trunk allodynia in 1 and 2 ipsilateral dermatome levels above and below T13 and L1, and these same dermatomes on the contralateral side, as well as at T13 and L1.

The animal is transferred in its home cage to a dimly lit, quiet behavioral testing room. All testing takes place in the animal's home cage, and is measured by the number of times out of 10 that the animal responds to the 4.56 (3.363 g) von Frey filament per side, each stimulation lasting up to 3 s. Baseline measures are collected the day before surgery, and weekly testing begins 2 weeks after surgery. A behavior is determined to be avoidant if the animal either bit at the filament, jumped away, escaped to another area of the cage, or vocalized.

---

## Acknowledgments

Sources of financial and material support: Craig Hospital and DA024044.

## References

1. Baastrup, C., and Finnerup, N. B. (2008) Pharmacological management of neuropathic pain following spinal cord injury. *CNS Drugs* **22**, 455–475.
2. Siddall, P. J. (2009) Management of neuropathic pain following spinal cord injury: now and in the future. *Spinal Cord* **47**, 352–359.
3. Siddall, P. J., McClelland, J. M., Rutkowski, S. B., and Cousins, M. J. (2003) A longitudinal study of the prevalence and characteristics of pain in the first 5 years following spinal cord injury. *Pain* **103**, 249–257.
4. Jensen, M. P., Kuehn, C. M., Amtmann, D., and Cardenas, D. D. (2007) Symptom burden in persons with spinal cord injury. *Arch. Phys. Med. Rehabil.* **88**, 638–645.
5. Summers, J. D., Rapoff, M. A., Varghese, G., Porter, K., and Palmer, R. E. (1991) Psychosocial factors in chronic spinal cord injury pain. *Pain* **47**, 183–189.
6. Westgren, N., and Levi, R. (1998) Quality of life and traumatic spinal cord injury. *Arch. Phys. Med. Rehabil.* **79**, 1433–1439.
7. Christensen, M. D., Everhart, A. W., Pickelman, J. T., and Hulsebosch, C. E. (1996) Mechanical and thermal allodynia in chronic central pain following spinal cord injury. *Pain* **68**, 97–107.
8. Christensen, M. D., and Hulsebosch, C. E. (1997) Chronic central pain after spinal cord injury. *J. Neurotrauma* **14**, 517–537.
9. Hulsebosch, C. E., Xu, G. Y., Perez-Polo, J. R., Westlund, K. N., Taylor, C. P., and McAdoo, D. J. (2000) Rodent model of chronic central pain after spinal cord contusion injury and effects of gabapentin. *J. Neurotrauma* **17**, 1205–1217.
10. Lampert, A., Hains, B. C., and Waxman, S. G. (2006) Upregulation of persistent and ramp sodium current in dorsal horn neurons after spinal cord injury. *Exp. Brain Res.* **174**, 660–666.
11. Tan, A. M., Stamboulian, S., Chang, Y. W., Zhao, P., Hains, A. B., Waxman, S. G., and Hains, B. C. (2008) Neuropathic pain memory is maintained by Rac1-regulated dendritic spine remodeling after spinal cord injury. *J. Neurosci.* **28**, 13173–13183.
12. Edgar, R. E., Best, L. G., Quail, P. A., and Obert, A. D. (1993) Computer-assisted DREZ microcoagulation: posttraumatic spinal deafferentation pain. *J. Spinal Disord* **6**, 48–56.
13. Itoh, T., Hirota, K., Hisano, T., Namba, T., and Fukuda, K. (2004) The volatile anesthetics halothane and isoflurane differentially modulate proinflammatory cytokine-induced p38 mitogen-activated protein kinase activation. *J. Anesth.* **18**, 203–209.
14. Kudo, M., Aono, M., Lee, Y., Massey, G., Pearlstein, R. D., and Warner, D. S. (2001) Effects of volatile anesthetics on N-methyl-D-aspartate excitotoxicity in primary rat neuronal-glia cultures. *Anesthesiology* **95**, 756–765.
15. Martin, D. C., Plagenhoef, M., Abraham, J., Dennison, R. L., and Aronstam, R. S. (1995) Volatile anesthetics and glutamate activation of N-methyl-D-aspartate receptors. *Biochem. Pharmacol.* **49**, 809–817.
16. Roughan, J. V., and Laming, P. R. (1998) Large slow potential shifts occur during halothane

- anaesthesia in gerbils. *J. Comp. Physiol.* **182**, 839–848.
17. Toda, N., Toda, H., and Hatano, Y. (2008) Anesthetic modulation of immune reactions mediated by nitric oxide. *J. Anesth.* **22**, 155–162.
  18. Wentlandt, K., Samoilova, M., Carlen, P. L., and El Beheiry, H. (2006) General anesthetics inhibit gap junction communication in cultured organotypic hippocampal slices. *Anesth. Analg.* **102**, 1692–1698.
  19. Wise-Faberowski, L., Pearlstein, R. D., and Warner, D. S. (2006) NMDA-induced apoptosis in mixed neuronal/glia cortical cell cultures: the effects of isoflurane and dizocilpine. *J. Neurosurg. Anesthesiol.* **18**, 240–246.
  20. Wieseler, J., Ellis, A. L., McFadden, A., Brown, K., Starnes, C., Maier, S. F., Watkins, L. R., and Falci, S. (2010) Below level central pain induced by discrete dorsal spinal cord injury. *J Neurotrauma* **27**, 1697–1707.

## A Lumbosacral Ventral Root Avulsion Injury and Repair Model for Studies of Neuropathic Pain in Rats

Leif A. Havton

### Abstract

Neuropathic pain may develop after a variety of injuries to peripheral nerves and roots. Most injury models have included a direct injury to primary afferent fibers or neurons. Recently, it has been demonstrated that injury to motor fibers in ventral roots may also result in neuropathic pain. A lumbosacral ventral root avulsion injury results in acute and persistent mechanical allodynia, but not thermal hyperesthesia. Interestingly, an acute replantation of the avulsed ventral roots into the spinal cord results in amelioration of the neuropathic pain. A detailed description of this injury and repair model is provided.

**Key words:** Cauda equina, Spinal cord, Axotomy, Sensory testing, Allodynia

---

### 1. Introduction

In animal pain models, a spinal segmental nerve ligation (1), dorsal root ganglionectomy (2), or a peripheral nerve injury (3) is commonly performed to induce allodynia or hyperesthesia. All of these models include a direct injury to axons of primary afferents. In recent years, it has been shown that also a ventral root transection injury, which lesions efferent axons, but spares the majority of primary afferent axons, may induce hyperalgesia and allodynia within the same segmental dermatome (4, 5). Although the studies on the effects of ventral root injuries suggest that an efferent injury may also induce neuropathic pain, it is possible that the pain may be in response to the transection of a sub-population of afferent fibers making U-turn loops within the ventral root (6). However, we have recently demonstrated that an avulsion injury to the L6 and S1 ventral roots results in an early onset and persistent mechanical allodynia affecting the adjacent L5 dermatome (7) (Figs. 1 and 2).

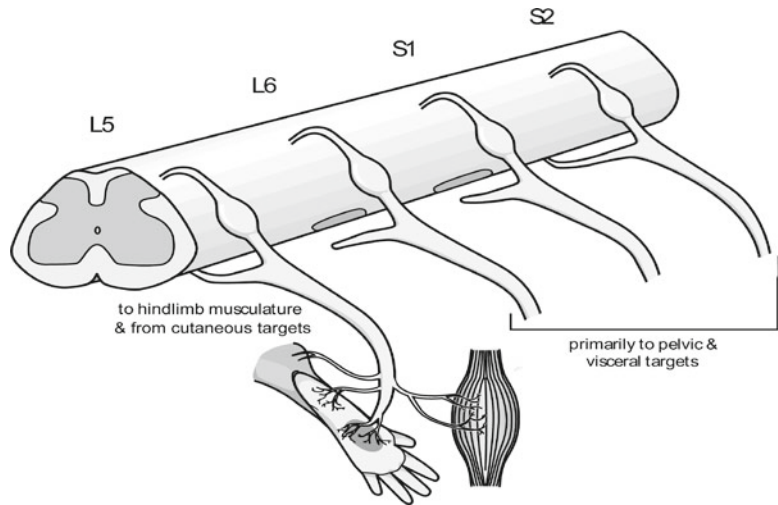


Fig. 1. Lumbosacral ventral root avulsion (VRA) injury model. Note unilateral injury of the L6 and S1 ventral roots. Sensory testing for mechanical allodynia and thermal hyperesthesia is performed on the adjacent L5 dermatome. (Reprinted from ref. 7 with permission from Elsevier).

Interestingly, an acute replantation of the avulsed ventral roots into the spinal cord results in amelioration of pain. This chapter will provide a detailed description of the methodological considerations related to this primary afferent-sparing new model for the study of neuropathic pain after ventral root injury and repair.

---

## 2. Materials

The surgical procedures require a general rodent surgery set-up, including a surgical microscope and a gas anesthesia system. In addition, procedure specific items are detailed below for the surgical ventral root injury and repair procedures and behavioral testing.

### **2.1. Animals, Surgical, and Post-surgical Supplies**

1. Adult female rats (Sprague–Dawley; Charles River Laboratories, Wilmington, MA).
2. Isoflurane.
3. Betadine® surgical scrub solution (povidone–iodine, 7.5%).
4. Sterile wipes saturated with 70% isopropyl alcohol.
5. Dumont #5 and #55 microsurgery forceps (Fine Science Tools, Foster City, CA). These fine forceps are needed to avulse individual lumbar-sacral ventral roots.
6. Friedman Pearson Micro Rongeurs with extra fine and curved tips (Fine Science Tools). A fine set of Rongeurs is needed to perform a lumbar laminectomy in rats.

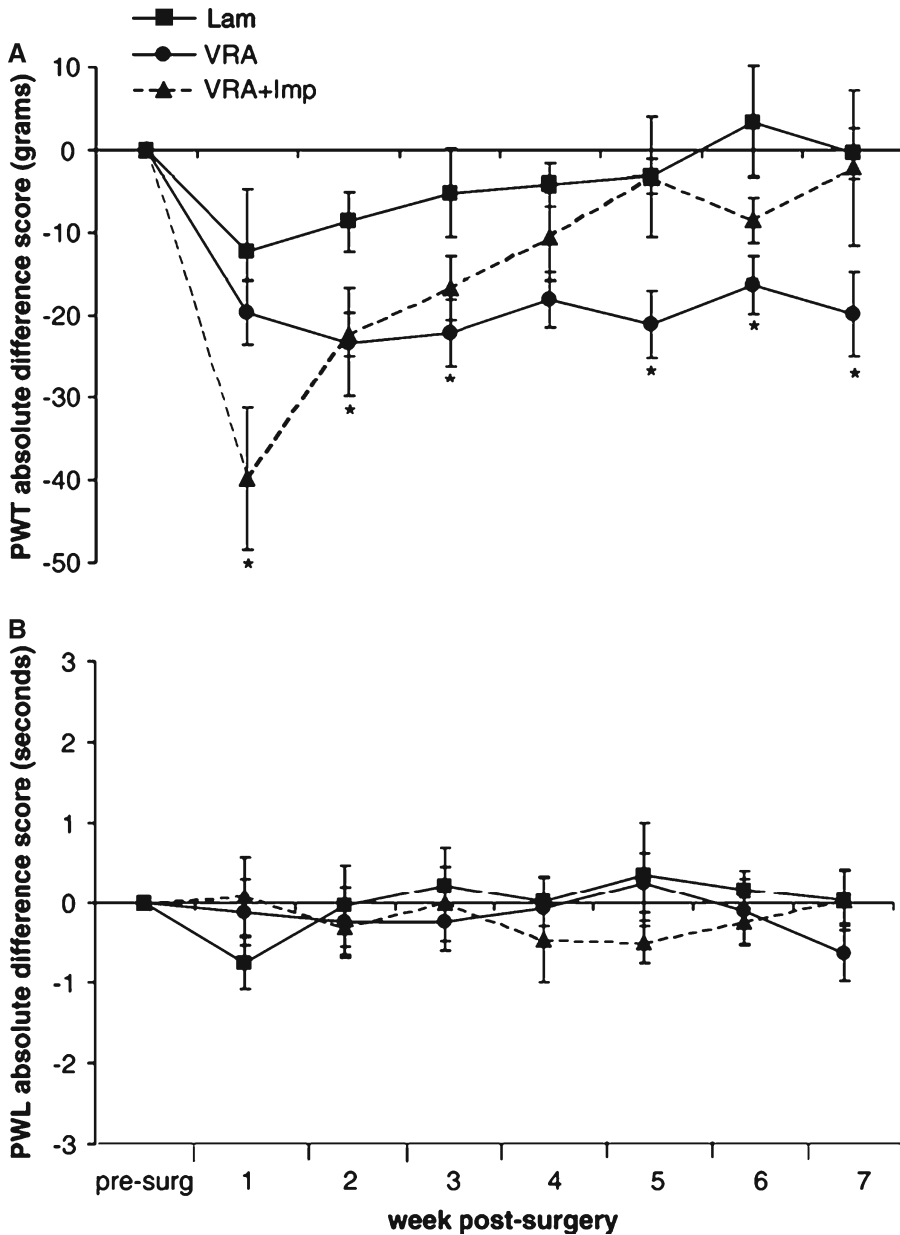


Fig. 2. Behavioral testing demonstrates acute and persistent mechanical allodynia (a), but not thermal hyperesthesia (b) after a unilateral L6 and S1 ventral root avulsion (VRA) injury. Note amelioration of the neuropathic pain when the injury is followed by acute replantation of the avulsed ventral roots into the spinal cord. Three groups of rats were included: (1) laminectomy controls (Lam); (2) rats undergoing unilateral L6 + S1 VRA injury (VRA); (3) rats undergoing unilateral VRA injury followed by acute implantation of avulsed roots into the spinal cord (VRA + Imp). The paw withdrawal threshold (PWT) in grams of force to a mechanical stimulus and the paw withdrawal latency in seconds to a radiant heat source were used to assess for mechanical allodynia and thermal hyperesthesia, respectively. (Reprinted from ref. 7 with permission from Elsevier).

7. Microdissecting spring scissors.
8. Glass probes.
9. Gelfoam® (Pharmacia and Upjohn, Kalamazoo, MI). Gelfoam® is used to provide a layer of protection between the exposed spinal cord and over lying titanium mesh (see below).
10. Standard scalpel blade holder (#3).
11. Scalpel blades #10 and #11. The #10 blade has a rounded cutting edge and is used for the initial skin incision as well as for scraping the lumbar vertebrae clean from paraspinous muscles, tendons, and connective tissue prior to the laminectomy. The #11 blade has an angle at the tip and is suitable for making the small incision into the spinal cord for replantation of avulsed ventral roots.
12. Titanium micro mesh (120×60 mm, 0.1 mm thick) (Ace Surgical Supply Co, Brockton, MA). The titanium mesh is used to make a customized cage to provide stabilization of the spine and to protect the spinal cord and nerve roots from compression injury.
13. Surgical sutures.
14. Buprenorphine.
15. Hypodermic needles.
16. Syringes.

### **2.2. Pain Behavioral Studies**

1. Electronic Von Frey Anesthesiometer (IITC Inc., Woodland Hills, CA). This handheld instrument includes a rigid probe attached to a force transducer. It is used to determine the grams of force needed to induce a limb withdrawal response in rats.
2. Plantar Analgesia System (IITC Inc, Woodland Hills, CA). This system includes a plexiglass box on a glass surface and a radiant heat source. It is used to evaluate to determine the latency for a limb withdrawal response to applied heat.

---

## **3. Methods**

Experimental models that rely on correct surgical identification of individual lumbosacral nerve roots in mammals are challenged by the anatomical separation of vertebral and spinal cord levels. Specifically, the lumbosacral segments of the spinal cord are located more rostrally than their corresponding vertebrae. For instance, the tip of the conus medullaris is typically located at the level of the L1/L2 vertebrae in rats. As a result, intro-operative identification of lumbosacral spinal cord segments may be difficult, and the

surgeons often depend on a variety of anatomical landmarks and features to correctly identify the individual roots of the cauda equina.

In the present rat model, the correct identification of individual lumbosacral ventral roots is critical for the successful completion of each experiment and interpretation of corresponding pain behavioral studies.

Marked differences exist between the functional properties of efferent fibers exiting the spinal cord in different lumbosacral ventral roots and the relationships of individual lumbosacral roots and specific peripheral targets. In the rat, the motor axons contributing to the sciatic nerve are primarily located in the L4 and L5 ventral roots and to a lesser degree also in the L6 ventral root. Motor axons contributing to the external urethral and anal sphincters are primarily located in the L6 and S1 ventral roots. In addition, the efferent axons of preganglionic parasympathetic neurons exit the spinal cord via the L6 and S1 ventral roots.

**3.1. Surgical  
Procedures for Ventral  
Root Avulsion Injury  
and Surgical  
Replantation  
of Lesioned Roots**

1. Adult female rats are anesthetized using general inhalation anesthesia (2–2.5% isoflurane). The back is shaved and prepped for surgery using three alternating applications of Betadine® surgical scrub solution and sterile wipes saturated with 70% isopropyl alcohol.
2. A midline incision is made over the lumbar vertebrae. Paraspinal muscles and tendons are removed over the dorsal surface of the L1–L4 vertebrae using a standard #3 scalpel equipped with a #10 scalpel blade. A set of Friedman Pearson Micro Rongeurs with extra fine and curved tips are used for a unilateral L1–L3 hemi laminectomy. The spinous processes are left intact (see Note 1).
3. A pair of microdissecting spring scissors is used to open the dura and expose the underlying spinal cord and lumbosacral nerve roots (see Note 2).
4. The ipsilateral lumbosacral roots are gently manipulated using a glass probe to identify the L5–S2 ventral roots (see Notes 3 and 4).
5. The L6 and S1 ventral roots are avulsed from the surface of the spinal cord using a jeweler's forceps by applying a constant traction along the normal course of each individual root (see Note 5).
6. For rats in the root repair series, the tip of a #11 scalpel blade is used to make small stab incisions, each approximately 1 mm deep, into the ipsilateral lateral funiculus of the L6 and S1 segments (see Note 6). The avulsed L6 and S1 ventral roots are next individually replanted into the scalpel incision sites of the lateral funiculus using a fine jeweler's forceps (see Notes 7 and 8).

7. In all rats, a thin layer of Gelfoam® is placed over the dorsal surface of the L6 and S1 segments. A titanium mesh cage is next positioned over the laminectomy site and sutured to the soft tissues attached to the adjacent spinous processes (see Note 9). The overlying muscle and skin are closed in layers.
8. All rats are allowed to recover and are expected to maintain independent locomotion as well as bladder and bowel functions (see Notes 10 and 11). Post-operatively, subcutaneous injections of buprenorphine (0.2–0.5 mg/kg) are provided every 12 h for 48 h post-operatively.

### **3.2. Behavioral Testing for Sensory Changes and Pain**

1. Behavioral testing is performed both pre- and post-operatively. The testing is performed under stable and consistent conditions. Pre-operative testing is performed at two time points prior to the surgery (see Note 12).
2. Post-operatively, sensory testing is performed for testing for allodynia and hyperalgesia. For testing of mechanical allodynia, a rigid probe attached to a handheld force transducer of an Electronic Von Frey Anesthesiometer is applied to the L5 dermatome of both hindlimbs (see Note 13). The force required to induce a withdrawal of the paw is recorded automatically by the force transducer and is also typically associated with a pain behavioral response (see Note 14). The mean of three responses for each limb is recorded at each testing time. For testing of thermal hyperesthesia, the Plantar Analgesia System is used. For this purpose, rats are placed in a plexiglass box, allowed to acclimate, and a radiant heat source is applied to the plantar surface of each hindlimb. The latency to paw withdrawal is recorded automatically. The limb withdrawal is also here typically associated with head turning as well as limb licking or biting to suggest that the withdrawal did not reflect a random movement. Each hindlimb is tested three times at each time point, and the average of the collected measurements is recorded.

### **3.3. Tissue Collection and Lesion Verification**

1. At the end of the study period, the rats are sacrificed for either fresh tissue collection or by intravascular perfusion with fixative solution for subsequent anatomical studies. The termination of the experiment also allows for anatomical verification of the originally lesioned root levels (see Note 15).

---

## **4. Notes**

1. A minimally invasive surgical approach, which leaves the spinous processes intact, is suggested, as it preserves spine stability. A bilateral laminectomy would create an unstable spine

and risk for post-operative complications, including secondary injury to the spinal cord and roots from moving segments of the vertebral column. If an unstable spine is created as a result of an extensive multilevel laminectomy, a spine stabilization procedure is needed. Spine stabilization using a titanium mesh approach in rats can successfully provide the protection for the exposed spinal cord and lumbosacral nerve roots (8).

2. The conus medullaris of the rat spinal cord is typically located at the L1/L2 vertebral level of the spine. Lumbosacral dorsal and ventral roots extend caudally to the tip of the conus medullaris as the cauda equina.
3. Glass probes do not conduct electricity and can be used to manipulate nerve roots without risk of inducing an electrical stimulation of roots with subsequent sudden muscular movements.
4. The L5 ventral root is markedly larger in caliber than the L6 and sacral ventral roots in rats. Qualitatively, the L5 ventral root typically appears white in coloration, whereas the L6 and the S1 ventral roots, which contain more unmyelinated fibers, may exhibit a slight yellow appearance.
5. The ventral root will typically separate from the surface of the spinal cord. Motor axons are myelinated by oligodendrocytes in the spinal cord and Schwann cells in the periphery. The transition between the CNS myelin and PNS myelin at the ventral root exit zone represents the “weak link”. As a result, traction applied to nerve roots results in avulsion injuries with separation of ventral roots from the anterior surface of the spinal cord.
6. The #11 scalpel blade has a pointed tip, which is well suited for making a small lesion in the lateral funiculus. We also make the lesion in the longitudinal plane, so that the injury follows the direction of the long ascending and descending white matter tracts in an attempt to minimize any axonal transection injury of the intramedullary pathways.
7. The ventral roots are separated from the anterior surface of the spinal cord. However, surgical replantation at the site of anatomical separation is very challenging when using a dorsal surgical approach. Instead, implantation of the avulsed ventral roots into the lateral funiculus of the spinal cord offers an attractive alternative, which is surgically accessible and practical.
8. No tissue glue or sutures are normally needed to secure the avulsed ventral roots in the replanted position. Typically, the surrounding white matter of the spinal cord incision site is able to hold the roots in place. Note that ventral roots have a very thin epineurium and are poor candidates for suture repairs.
9. A piece of a titanium micro mesh (0.1 mm thick) is cut to cover the laminectomy site. The titanium mesh is secured both

rostrally and caudally to the laminectomy site and will serve to stabilize the spine and prevent injury of the exposed nerve roots and spinal cord from overlying paraspinal muscles and soft tissues (8).

10. An unilateral L6 and S1 ventral root avulsion (VRA) injury primarily denervates pelvic targets. However, the L6 ventral root also contributes some motor axons to the sciatic nerve. Thus, a slight weakness in ipsilateral ankle movements may be detected while ambulating post-operatively. However, rats are ambulatory with and capable of limb withdrawal to sensory stimulation.
11. An unilateral L6 and S1 VRA injury results in significant ipsilateral denervation of pelvic targets, including the external urethral and anal sphincters as well as the major pelvic ganglion, which contains post-ganglionic parasympathetic neurons. However, the bladder is a midline organ receiving bilateral innervation and a unilateral injury does not result in any detectable urinary retention. However, monitoring of bladder function is recommended post-operatively, but long-term bladder expressions are not normally required.
12. Extensive variations may exist for sensory thresholds between animals. Each subject provides its own baseline responses, thereby controlling for inter-individual variations in sensory thresholds. Daily acclimation to the test environment for about 10 min/day for 3 days prior to baseline testing also acts to reduce variability between testing occasions.
13. In this experimental model, sensory testing of both hindlimbs allows for detailed comparisons of sensory thresholds between the injured ipsilateral side and the intact contralateral side at each testing occasion.
14. The hindlimb withdrawal response is usually accompanied by head turning as well as licking or biting of the tested paw.
15. By dissecting out the lumbosacral roots to each intervertebral foramen, a firm anatomical verification of the completeness of injury and segmental level of injury is obtained.

---

## Acknowledgments

The author wishes to thank the NIH (NS042719) and the Dr. Miriam and Sheldon G. Adelson Medical Research Foundation for support.

## References

1. Kim, S.H., Chung, J.M. (1992) An experimental model for peripheral neuropathy produced by segmental spinal nerve ligation in the rat. *Pain* **50**, 355–363.
2. Li, Y., Dorsi, M.J., Meyer, R.A., Belzberg, A.J. (2000) Mechanical hyperalgesia after an L5 spinal nerve lesion in the rat is not dependent on input from injured nerve fibers. *Pain* **85**, 493–502.
3. Dorsi, M.J., Chen, L., Murinson, B.B., Pogatzki-Zahn, E.M., Meyer, R.A., Belzberg, A.J. (2008) The tibial neuroma transposition (TNT) model of neuroma pain and hyperalgesia. *Pain* **134**, 320–334.
4. Li, L., Xian, C.J., Zhong, J.H., Zhou, X.F. (2002) Effect of lumbar 5 ventral root transection on pain behaviors: a novel model for neuropathic pain without axotomy of primary sensory neurons. *Exp. Neurol.* **175**, 23–34.
5. Sheth, R.N., Dorsi, M.J., Li, Y., Murinson, B.B., Belzberg, A.J., Griffin, J.W., Meyer, R.A. (2002) Mechanical hyperalgesia after an L5 ventral rhizotomy or an L5 ganglionectomy in the rat. *Pain* **96**, 63–72.
6. Coggeshall, R.E. (1980) Law of separation of function of the spinal roots. *Physiol. Rev.* **60**, 716–755.
7. Bigbee, A.J., Hoang, T.X., Havton, L.A. (2007) At-level neuropathic pain is induced by lumbosacral ventral root avulsion injury and ameliorated by root implantation into the spinal cord. *Exp. Neurol.* **204**, 273–282.
8. Nieto, J.H., Hoang, T.X., Warner, E.A., Franchini, B.T., Westerlund, U., Havton, L.A. (2005) Titanium mesh implantation – A method to stabilize the spine and protect the spinal cord following a multilevel laminectomy in the adult rat. *J. Neurosci. Methods* **147**, 1–7.

# Chapter 14

## A Rat Chronic Pain Model of Spinal Cord Contusion Injury

Kelli Sharp, Amin Boroujerdi, Oswald Steward, and Z. David Luo

### Abstract

Spinal cord injury-induced pain is a common clinical problem affecting adversely the quality of daily lives of spinal cord injured patients. Management with current pain medications can only lead to partial pain relief in some spinal cord injured patients, which is usually associated with unfavorable side effects. Development of specific medications for spinal cord injury-induced pain states relies on identification of new targets and/or pathways that contribute to chronic pain development post injury. We describe here the generation of a spinal cord contusion injury model that mimics the etiology and phenotypes of chronic pain states in spinal cord injured patients. Therefore, this model can be a useful tool for studying spinal cord injury mechanisms, functional recovery, research, and development of new medications for better functional and symptomatic improvements, including pain management.

**Key words:** Neuropathic pain, Spinal cord injury, Contusion device, Injury model, Sensory testing

---

### 1. Introduction

It is estimated that over 500,000 people in the United States alone suffer from spinal cord injuries (SCI), and this number is increasing at a rate of 11,000 new cases per year (1). In addition to loss of sensory and motor functions, more than half of the SCI patients develop chronic pain syndromes that include reduced thresholds to normally non-noxious mechanical stimuli (tactile allodynia) or exaggerated painful sensations to mildly painful stimuli (hyperalgesia) (2). More than half of these patients use pain medications for improving the quality of their daily lives (3, 4). Unfortunately, few of the current pain medications for SCI-pain management are target specific due to the fact that mechanisms underlying SCI-induced chronic pain are poorly understood. As a consequence, the long-term use of current pain medications can only cause partial

pain relief in a subpopulation of SCI patients, which is usually associated with severe side effects. Therefore, there is an urging demand for better pain medications for SCI-pain management. Accordingly, we need to have a validated SCI-induced chronic pain model for studying mechanisms underlying SCI-induced pain processing and for development/validation of the next generation of medications for SCI-pain control. In this chapter, we describe the generation of a rat chronic pain model derived from T9 spinal cord contusion injury, which shows chronic pain states in approximately half of the SCI rats, similar to that seen in SCI patients.

---

## 2. Materials

### **2.1. Animal Preparation and Surgical Procedures**

1. Animal clippers with 40 blade (Fisher Scientific, Pittsburgh, PA).
2. Hot bead sterilizer (Kent Scientific, Torrington, CT).
3. Betadine (Fisher Scientific, Pittsburgh, PA).
4. Scalpel blades # 10 and #11 (Electron Microscopy Sciences, Hatfield, PA).
5. Chromic Gut 5–0 (Henry Schein, Melville, NY).
6. Wound Clips (Fisher Scientific, Pittsburgh, PA).
7. Gauze 4 × 4 (Fisher Scientific, Pittsburgh, PA).
8. Cotton Swabs (Fisher Scientific, Pittsburgh, PA).
9. Infinite Horizon Impactor (Precision Systems and Instrumentation, Fairfax, VA).
10. Friedman-Pearson Rongeur, micro curette (1 mm diameter), Addison forceps (Fine science Tools, Foster City, CA).
11. Lactated Ringer Solution (Fisher Scientific, Pittsburgh, PA).
12. Ketamine (Western Medical Supply, Inc, Arcadia, CA).
13. Xylazine (Western Medical Supply, Inc).
14. Puralube eye ointment (Henry Schein, Melville, NY).
15. Warm water recirculator heating jackets (Kent Scientific, Torrington, CT).
16. ALPHA-dri® (Shepherd, Hubbard, OR).
17. Adult female Harlan Sprague Dawley rats (180–200 g, Harlan Laboratories) (see Notes 1 and 2).

### **2.2. Behavioral Test**

1. Von Frey filaments (Stoelting, Wood Dale, IL. No. 58011).
2. Von Frey test apparatus: [40(*D*) × 76(*W*) × 69(*H*) cm] (see Fig. 1).



Fig. 1. An example of von Frey filament testing apparatus. Plexiglass chambers are shown on top of the mesh floor.

3. Plexiglass chamber [ $22 (D) \times 10 (W) \times 30 (H)$  cm].
4. Hot Box (Hargreaves test): please see Chapter 2 in the First Edition of this book for more detail information (5).

---

### 3. Methods

#### **3.1. Preparing the Surgical Area and Animal for Surgery**

1. All surgeries are conducted using aseptic procedures (see Note 3).
2. Animal is anesthetized with approved and recommended anesthetics: intraperitoneal injection of ketamine/xylazine (100:10 mg/kg).

3. The hair overlying the incision site is removed using animal clippers with a close surgical blade (#40).
4. The skin is cleaned and disinfected using BETADINE® Solution and a sterile gauze sponge to scrub the surgical site, scrubbing along the incision line, then proceeding outward to cover the entire surgical area.
5. Eye ointment should be applied to the eyes to prevent burning or dehydration during the surgical procedure.
6. Surgical instruments are sterilized using a hot bead sterilizer prior to any surgical procedures. Tools are cleaned with 70% alcohol and re-sterilized with the hot bead sterilizer between animals.
7. Animals are placed on a circulating water jacket in order to maintain body temperature during surgery.

**3.2. Performing  
the Laminectomy  
and Contusion  
of the Animal**

1. Prior to any surgical procedures, ensure the animal is properly anesthetized by testing with toe or a tail pinch. Only when you do not elicit a reflex response then begin the surgical procedures. Every 5 min, check the animals' anesthesia level to ensure the animal is properly anesthetized.
2. Using aseptic surgical procedures, a midline incision is made with a scalpel with a #11 blade over the spinous processes of T2–T10.
3. Paravertebral muscles are separated from the vertebrae bilaterally by cutting parallel with the spinous processes of T6–T10. If bleeding occurs, cotton swabs and gauze will be used to remove the blood from the surgical site.
4. The spinous process and laminae of T9 are removed with rongeurs, while holding onto T8 transverse processes with Adson forceps. The spinous process of T8 and T10 are to remain intact.
5. The remaining paravertebral muscles are removed gently with micro curette. Clearing the paravertebral muscles is needed in order to clamp rostral and caudal to the laminectomy site of T9.
6. The animal is placed in a spinal stereotax platform to immobilize the spinal column with forceps attached to the rostral transverse processes of T8 and caudal processes of T10 being extremely careful not place the forceps in the space between the vertebrae.
7. The platform is placed into the Infinite Horizon Impactor and then secured with spring clamps.
8. The exposed spinal cord needs to be level, and the probe on the device should be centered over the spinal cord prior to using the device (6) (see Notes 4 and 5).

9. Once the spinal cord is level, a defined force (measured in kilodynes) is applied using an impact probe with an integrated, computer-controlled real-time force transducer to control and monitor impact. The force range can vary to produce a mild, moderate, or severe injury model. A 200 kD is used to produce a moderate injury in rats, so that SCI rats are not permanently paralyzed and some, but not all, of them develop below level behavioral hypersensitivities (7).
10. Make sure to note the actual hit received by the animal and evaluate the force curves on the computer read out to ensure the animal received a proper contusion.

### **3.3. Closing Procedures**

1. After the contusion, the animal's vertebral muscles are sutured with 5–0 chromic gut, so the stitches will dissolve and not produce irritations. Stitches are placed above and below the injury site, to prevent the stitches interfering with the lesion site.
2. Connective tissues and skin are closed with wound clips. Then the surgical area on the animal is cleaned with BETADINE® Solution.
3. The animal is then placed in a housing cage that is placed on water circulating heating jacket until it regains consciousness.
4. All instruments including the stereotaxic platform and probe are sterilized between each animal.

### **3.4. Postsurgical Care**

The postoperative care is extremely important for the survival of the SCI animals; thus, the following steps should be carefully performed.

1. Immediately postsurgery, animals are given subcutaneous injections of warm saline (5 mL/100 g), Buprenex (3 mg/kg) and prophylactic Baytril (2.5 mg/kg/day) to prevent dehydration and urinary tract infection, and placed on heating pads until they recovered from anesthesia.
2. After anesthesia recovery, SCI animals are placed in cage with soft bedding (ALPHA-dri®).
3. Daily injections of saline (5 mL/100 g), Buprenex (3 mg/kg) are for 3 days, and daily injections of prophylactic Baytril (2.5 mg/kg/day) are for 7 days.
4. Bladder functions are usually impaired in SCI animals, so they should receive manual bladder expression twice daily for 10–14 days until their bladder functions are fully recovered (see Note 6).

### **3.5. Behavioral Testing for Tactile Allodynia in SCI Rats**

1. When SCI animals regain their hindpaw movements and are able to support their bodyweights post injury, the development of tactile allodynia then can be assessed (see Note 7).

2. Each animal is placed in a bottomless plexiglass chamber on top of a wire mesh surface and allowed to acclimate for at least 30 min prior to testing (see Note 8).
3. A series of calibrated von Frey filaments (see Note 9) are used to determine their 50% paw withdrawal thresholds using the up and down method described by Dixon (8). Initially, the filament with a 2.0 g force is applied in a perpendicular manner onto the glabrous plantar surface of the hindpaws. Enough pressure must be applied to cause the filament to buckle. This pressure is maintained for 5 s or until a paw withdrawal response occurs, indicating a positive response and prompting the use of the next stronger filament. The absence of a paw withdrawal response after 5 s prompts the use of the next weaker filament. This paradigm is continued until six measurements are obtained, starting with the one before the first change in response, or until four consecutive positive (assign a minimum score of 0.25 g) or five negative (assign a maximum score of 15 g) measurements occur. Please see Chapter 8 in the First Edition of this book for more detail information (9).
4. The 50% paw withdrawal threshold is obtained from the resulting scores for each paw using the formula described by Chaplan et al. (10) (see Note 10). An averaged value is calculated from data obtained from both sides. Due to daily fluctuation in their sensitivity to mechanical stimuli, it is important to test for tactile allodynia as often as possible and at a consistent time to best determine if SCI animals developed tactile allodynia. Our behavioral testing results from female adult SCI rats have shown that their paw withdrawal thresholds to von Frey filament stimulation start to drop at post injury day 10, and peak tactile allodynia is evident by approximately 30–40 days post injury in approximately 50% of SCI rats (7), a percentage similar to that observed in SCI patients (11). The hindpaw behavioral sensitivities of non-allodynic SCI rats to von Frey filament stimulation are similar to that of sham SCI control rats (7). The injury-induced tactile allodynia can recover beyond post injury day 60 (Fig. 2) in this model (see Notes 11 and 12).

### **3.6. Behavioral Testing for Thermal Hyperalgesia in SCI Rats**

1. Since different sensory fibers are linked to different modalities, and SCI patients also show hyperalgesia (2, 11), we also tested if this SCI model has thermal hyperalgesia, when the SCI animals regain their hindpaw movements and are able to support their bodyweights post injury (see Note 7).
2. The procedure for testing thermal hyperalgesia (Hargreaves test) is described in Chapter 2, the First Edition of this book (5) (see Note 13).

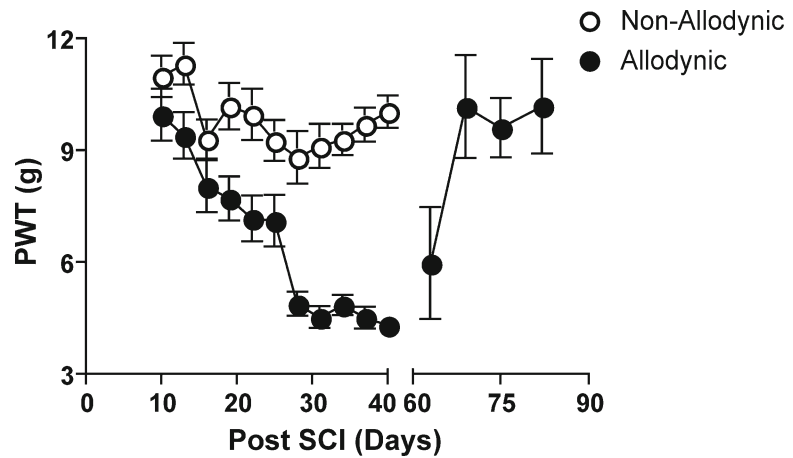


Fig. 2. Spinal cord injuries (SCI) induce tactile allodynia in some SCI rats. The 50% hindpaw withdrawal thresholds (PWT) to von Frey filament stimulation were tested at the hindpaw glabrous plantar surface of SCI rats at designated time points post injury as described. Tactile allodynia is shown as reduced PWT to a level below 5 g. The PWT of non-allodynic SCI rats are similar to that observed in sham SCI control rats (7). Data presented are the means  $\pm$  SEM from at least 25–28 rats in the allodynic or non-allodynic groups, respectively, up to 40 days post injury, and five allodynic rats after 60 days post injury.

---

#### 4. Notes

1. Female rats should be used for easy post-SCI bladder function management as discussed in Note 5.
2. Different rat (and mouse) strains are shown to have different susceptibilities to injury-induced pain states (12–18). Therefore, it is important to use animal strains known to be susceptible to the development of SCI-induced pain states for your studies.
3. It is important to have a separate area for prepping the animal for surgery and the actual surgical area to reduce the contamination of the surgical area.
4. Important to note, proper training is required prior to using the device in order to ensure successful and reliable contusion injuries.
5. Proper clamping of the animal onto the platform prior to the contusion is critical for a successful contusion. It is key to make sure the animal's spinal cord is level and centered prior to hitting the animal. You can adjust the location of the clamps rostral and caudal to ensure proper placement on the transverse processes. Adjusting the arms on the platform can aid in leveling the animal.

6. Animals usually exhibit impaired motor and bladder functions post-SCI. Urinary retention and subsequent urinary infection are major complications for the death of SCI animals. Therefore, manual bladder expression is critical in post-SCI care.
7. SCI rodents usually regain movement in their hindpaws within 10 days post injury. For testing locomotor function recovery post-SCI, Basso, Beattie, and Bresnahan (BBB) locomotor rating scales can be examined (19).
8. The plexiglass enclosure is typically about  $22 \times 10 \times 30$  cm for an adult rat. This chamber sizes is approximate and should be suitable for animals with a body weight of approximately 250 g. Smaller chamber size may be used for smaller animals. The chamber size should be large enough to provide just enough room for the animal to assume a normal crouching posture and sufficient height to prevent the animal to escape readily by climbing or jumping.
9. The series of filaments used to assess the presence of tactile allodynia range from 0.4 to 15.0 g of force for rats (0.04–2.0 g of force for mice).
10. The formula used to calculate 50% response threshold =  $10^{(X_f + \kappa\delta)}/10,000$ , where  $X_f$  = the value (in log units) of the final von Frey filament used,  $\kappa$  = the value (from Table in Chaplan et al. (10)) for the positive and/or negative response patterns, and  $\delta$  = the mean difference (in log units) between stimulus strengths.
11. The percentage of SCI rats with tactile allodynia, and their severity and duration of pain states vary among different surgical groups. So it is advised to increase the estimated animal numbers in your experimental plan.
12. Similar testing can be performed for at-level and above-level mechanical hypersensitivities.
13. We have observed that thermal hyperalgesia is evident in all tested SCI rats, independent of the presence or absence of tactile allodynia when some, but not all, of the SCI rats have developed tactile allodynia at 30–40 days post injury (as shown in Fig. 2). This supports that different sensory fibers and pathways mediate tactile allodynia and thermal hyperalgesia. While it is difficult to test in SCI animals spontaneous pain sensations, which are apparent in SCI patients (11), our data suggest that this model is suitable for studying the mechanisms of evoked pain sensations that may derive from malfunctions of different sensory pathways, and for drug development related to better management of SCI-induced pain states.

## Acknowledgments

This study is supported in part by grants from the National Institutes of Health (NS064341), the Christopher & Dana Reeve Foundation, and the Roman Reed Spinal Cord Injury Research Fund of California (Z.D. Luo). A. Boroujerdi was the recipient of a Roman Reed Pre-doctoral Fellowship.

## References

1. Yeziarski, R. P. (2005) Spinal cord injury: a model of central neuropathic pain, *Neurosignals* **14**, 182–193.
2. Yeziarski, R. P. (1996) Pain following spinal cord injury: the clinical problem and experimental studies, *Pain* **68**, 185–194.
3. de Miguel, M., and Krachete, D. C. (2009) Pain in patients with spinal cord injury: a review, *Rev Bras Anestesiol* **59**, 350–357.
4. Miladinovic, K. (2009) [Spinal cord injury and chronic pain], *Med Arb* **63**, 106–107.
5. Allen, J. W., and Yaksh, T. L. (2004) Assessment of acute thermal nociception in laboratory animals, in *Pain Research: Methods and Protocols* (Luo, Z. D., Ed.), pp 11–23, Humana Press Inc., Totowa.
6. Scheff, S. W., Rabchevsky, A. G., Fugaccia, I., Main, J. A., and Lump, J. E., Jr. (2003) Experimental modeling of spinal cord injury: characterization of a force-defined injury device, *J Neurotrauma* **20**, 179–193.
7. Boroujerdi, A., Zeng, J., Sharp, K., Kim, D., Steward, O., and Luo, Z. D. (2011) Calcium channel alpha-2-delta-1 protein upregulation in dorsal spinal cord mediates spinal cord injury induced neuropathic pain states, *Pain* **152**, 649–655.
8. Dixon, W. J. (1980) Efficient analysis of experimental observations, *Annual Review of Pharmacology and Toxicology* **20**, 441–462.
9. Higuera, E. S., and Luo, Z. D. (2004) A rat pain model of vincristine-induced neuropathy, *Methods Mol Med* **99**, 91–98.
10. Chaplan, S. R., Bach, F. W., Pogrel, J. W., Chung, J. M., and Yaksh, T. L. (1994) Quantitative assessment of tactile allodynia in the rat paw, *Journal of Neuroscience Methods* **53**, 55–63.
11. Tasker, R. R., DeCarvalho, G. T., and Dolan, E. J. (1992) Intractable pain of spinal cord origin: clinical features and implications for surgery, *J Neurosurg* **77**, 373–378.
12. LaCroix-Fralish, M. L., Rutkowski, M. D., Weinstein, J. N., Mogil, J. S., and DeLeo, J. A. (2005) The magnitude of mechanical allodynia in a rodent model of lumbar radiculopathy is dependent on strain and sex, *Spine* **30**, 1821–1827.
13. Valder, C. R., Liu, J. J., Song, Y. H., and Luo, Z. D. (2003) Coupling gene chip analyses and rat genetic variances in identifying potential target genes that may contribute to neuropathic allodynia development, *J Neurochem* **87**, 560–573.
14. Yoon, Y. W., Lee, D. H., Lee, B. H., Chung, K., and Chung, J. M. (1999) Different strains and substrains of rats show different levels of neuropathic pain behaviors, *Exp Brain Res* **129**, 167–171.
15. Mills, C. D., Hains, B. C., Johnson, K. M., and Hulsebosch, C. E. (2001) Strain and model differences in behavioral outcomes after spinal cord injury in rat, *J Neurotrauma* **18**, 743–756.
16. Mogil, J. S., Wilson, S. G., Bon, K., Lee, S. E., Chung, K., Raber, P., Pieper, J. O., Hain, H. S., Belknap, J. K., Hubert, L., Elmer, G. I., Chung, J. M., and Devor, M. (1999) Heritability of nociception II. ‘Types’ of nociception revealed by genetic correlation analysis, *Pain* **80**, 83–93.
17. Mogil, J. S., Wilson, S. G., Bon, K., Lee, S. E., Chung, K., Raber, P., Pieper, J. O., Hain, H. S., Belknap, J. K., Hubert, L., Elmer, G. I., Chung, J. M., and Devor, M. (1999) Heritability of nociception I: responses of 11 inbred mouse strains on 12 measures of nociception, *Pain* **80**, 67–82.
18. Kerr, B. J., and David, S. (2007) Pain behaviors after spinal cord contusion injury in two commonly used mouse strains, *Exp Neurol* **206**, 240–247.
19. Basso, D. M., Beattie, M. S., and Bresnahan, J. C. (1995) A sensitive and reliable locomotor rating scale for open field testing in rats, *J Neurotrauma* **12**, 1–21.

# Chapter 15

## The Spared Nerve Injury Model of Neuropathic Pain

Marie Pertin, Romain-Daniel Gosselin, and Isabelle Decosterd

### Abstract

The spared nerve injury (SNI) model mimics human neuropathic pain related to peripheral nerve injury and is based upon an invasive but simple surgical procedure. Since its first description in 2000, it has displayed a remarkable development. It produces a robust, reliable and long-lasting neuropathic pain-like behaviour (allodynia and hyperalgesia) as well as the possibility of studying both injured and non-injured neuronal populations in the same spinal ganglion. Besides, variants of the SNI model have been developed in rats, mice and neonatal/young rodents, resulting in several possible angles of analysis. Therefore, the purpose of this chapter is to provide a detailed guidance regarding the SNI model and its variants, highlighting its surgical and behavioural testing specificities.

**Key words:** Neuropathic pain, Nerve injury, Rodent models, Surgery, Sciatic

---

### 1. Introduction

Researches undertook to understand neuropathic pain arising from traumatic nerve damages take advantage of the supposedly easy animal-to-human translation of the experimental outcomes, based upon assumed similarities in the cell responses from comparable injuries. In other words, virtually any strategy injuring a nerve will relevantly mirror some subsets of human painful nerve injury. Therefore, a wide range of experimental setups has been used, differing in both the site of intervention (distal or proximal nerve and spinal roots) and the nature of the injury (nerve tight or loose ligation, cut, crush and inflammation). Although each might pertinently offer opportunities to understand subgroups of clinical cases, the generated results appear to be puzzling to unify, due to considerable discrepancies in cell and behavioural response in such a variety of protocols.

Over the years, it has appeared that the pillars for the most relevant protocols are as follows: (1) the pain behaviours must be testable, therefore a significant degree of integrity should be preserved in the nociceptive pathway (this should exclude approaches with complete nerve transection); (2) a maximum reproducibility must be sought, combining a majority of animals displaying neuropathic changes and a low level of individual variation in such changes (the trauma must be important and irreversible, but affecting an easily identifiable nerve portion in order to confidently reproduce the lesion); (3) when working on the mechanisms linking the trauma and the sensory abnormalities, the cellular basis of the nerve damage should be kept at the “most neuropathic” level, with limited multisystem (inflammatory, immune, hormonal, etc.) contributions.

Thus, has the SNI model been developed (1), where two of the three branches of the sciatic nerve (namely, the tibial and common peroneal nerves) are cut distal from the sciatic trifurcation, leaving the third one (sural) intact. This model allows testing sensory modalities in the paw due to the presence of an uninjured sural innervation, it is associated with a reproducible, long-lasting and sound hypersensitivity (both allodynia and hyperalgesia), and finally it does not involve any excessive inflammation due to foreign material left in situ. Beyond sensory testing, the SNI model allows biochemical as well as cellular investigations in injured and non-injured territories separately at either peripheral (nerve tissue, dorsal root ganglion) or central (spinal dorsal horn) levels. Initially developed in adult rats, the SNI model has been successfully extended to juvenile rats and mice since then (2–4).

---

## 2. Materials

### 2.1. Animals

We usually recommend using young (see Note 1) adult male (see Note 2) Sprague–Dawley rats (200–250 g) or C57BL/6 (6 weeks old) mice from a single vendor (see Note 3). The animals are housed in groups (see Note 4) of 3–4 animals in plastic cages with wood-shaving bedding (see Note 5), under a 12/12 h light/dark cycle, and are given free access to food and water. They are kept at least 3 days under these conditions before surgery.

### 2.2. Equipments, Materials and Surgical Tools

1. Anaesthesia: A vaporizer for volatile anaesthesia.
2. Isoflurane.
3. Oxygen tank with tubing connected to a vaporizer.
4. Induction box.
5. Surgical silk thread 5/0 and 6/0.
6. Surgical tools: For operations on either rats or mice, the size of surgical tools must be adjusted.

- (a) A scalpel with a surgical blade (N°15).
- (b) A pair of micro-scissors (12 cm for rats and 8.5 cm for mice).
- (c) Two curved micro-surgical forceps.
- (d) A small animal retraction system (FST, Heidelberg, Germany, see Note 6).
- (e) A needle holder.
- (f) Wound clips (see Note 7).
- (g) A binocular microscope (especially for mice surgery).

---

### 3. Methods

1. Prior to anaesthesia, a presurgical evaluation including a measurement of body weight is performed.
2. Anaesthetize the animals. Induction (in a well-sealed plexiglas box, see Note 8) and maintenance (with a snout connector) of anaesthesia are achieved using isoflurane delivered in a 100% O<sub>2</sub> flow. This technique allows rapid induction and recovery (within 1–5 min) and a quick and easy control of anaesthesia level. In our hands, rats are induced and maintained with 2% isoflurane and mice with 1–1.5%, but these conditions must be adjusted depending on individual sensitivity to anaesthesia: animals must continue to breathe with a normal rate and their plantar paw skin colour must remain pink. Depth of anaesthesia is evaluated by a loss of responsiveness after a pinch on the tail or paw. Animals must be regularly monitored all the time during the procedure (10–15 min or less per animal in our hands). All usual precautions during anesthesia and surgery are applied in accordance with our regulatory authorities.
3. Surgical preparation: under sedation, the fur of the left thigh is shaved. Animals are then placed in lateral position on their right side, with the snout placed in the anaesthetic mask. The left-hind paw is slightly elevated by placing a tissue roller (rats, Fig. 1a) or a small piece of cork (mouse, Fig. 1d) under the leg, and the hind paw is then taped to the operating table, stretched perpendicularly to the animal's body. Surgical tools must be clean, but not necessarily autoclaved.
4. Surgical procedure for rats: the skin on the lateral surface of the thigh is incised with a scalpel blade as follows. By palpation, identify the *trochanter major* of the pelvis and the *iliaca cresta*. Draw an imaginary line between these two points and incise the skin for about 1 cm from the middle point of this line toward the toes, with an angle of 60° (Fig. 1a). On the surface

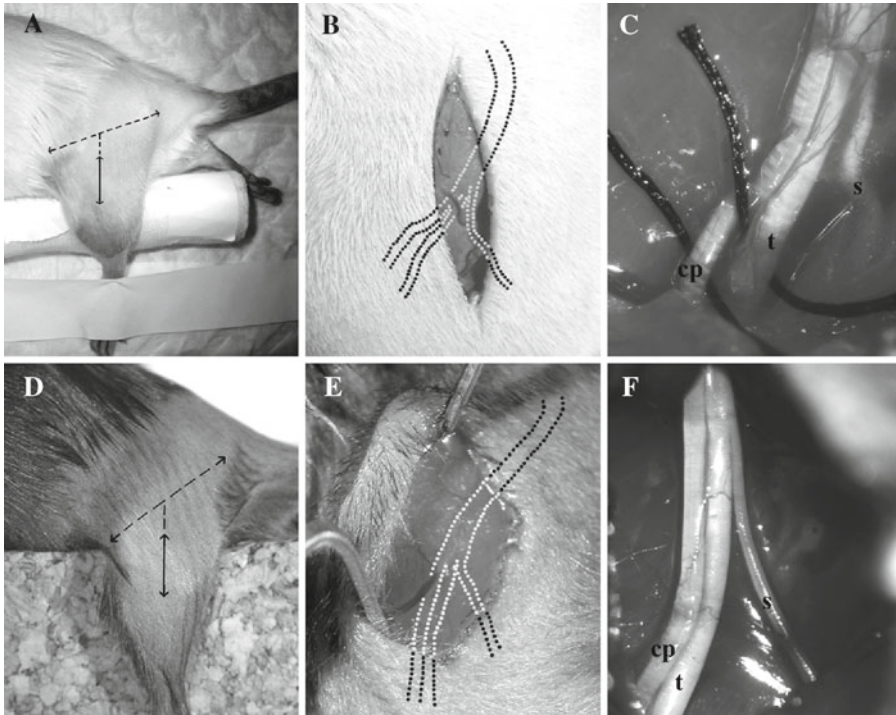


Fig. 1. SNI surgery in rats (a–c) and in mice (d–f). The incision (filled double arrow) is made at the middle position of the thigh at a 60° angle from a fictive axe (dashed double arrow) between trochanter major and iliaca cresta (a, d). Dotted lines in (b) and (e) show the position of the sciatic trifurcation underneath the artery *genus descendes* and biceps femoris. In (c) and (f), the three bared branches of the sciatic nerve are shown (cp common peroneal, t tibial, s sural). The threads aiming at suturing the common peroneal and tibial nerves are shown in (c) before ligation.

of the *biceps femoris* muscle, a small vessel (artery *genus descendes*) is visible. This vascular structure is a good landmark, as the trifurcation of sciatic nerve should be right below (Fig. 1b). An incision is directly made through the *biceps femoris* from the fictive line in the direction of point of origin of the vascular structure, exposing the sciatic nerve and its three terminal branches.

Install the retractor to help maintaining the incision open. Do not stretch too much with the retractor as any stretch of the sural nerve could damage it. Identify the three branches (Fig. 1c), normally from left to right: common peroneal, tibial and sural nerves (see Note 9). The tip of a curved micro-surgical forceps is delicately placed below the common peroneal nerve (see Note 10) to slide the thread (silk 5/0) under the nerve. The nerve is tightly ligated (see Note 11) using two curved micro-surgical forceps and sectioned approximately 5 mm distal to the ligation with micro-scissors. A nerve piece of 2–4 mm is removed from the distal stump (see Note 12). Proceed the same way with the tibial nerve. Great care should be taken to avoid any contact with or stretching of the intact sural nerve (see Note 9). The

muscle is sutured with a 5/0 silk thread using the needle holder and the skin is closed with wound clips. Anaesthesia is then disrupted and the animal is placed in a new cage with a warm plastic blanket (to maintain body temperature) used as a mattress until complete recovery.

As control, we perform a sham procedure that consist of the same surgery (skin and muscle incisions) without ligation and transection of the nerves; instead a 3-mm long 5/0 silk thread is placed longitudinally to the sciatic nerve at the level of the trifurcation (see Note 13).

5. Surgical procedure for mice: the surgical procedure for mice is globally similar to rat procedure, except for the following details. As soon as the muscle is open, we recommend using a binocular lens to perform the surgery (Fig. 1d–f). One major difference from rat surgery is that tibial and common peroneal nerves are tight-ligated and transected together with a 6/0 silk thread, and a piece of only 1–2 mm of nerve is removed. However, we still use a 5/0 to suture the muscle. Possibly, some anatomical variations between mice can occur, such as sural nerve separation into two smaller branches. In this case, the two branches should be spared. If mice are scheduled to undergo sensory testing, we recommend closing the skin with thread-suture instead of wound clip (see Note 7).
6. SNI variants: In the standard SNI model, the spared nerve is the sural one. Some variants have been developed (2, 3) where the spared nerves are different: SNIv(t), sparing the tibial nerve; SNIv(s, cp), sparing both sural and common peroneal nerves. In our hands, only the SNIv(s, cp) demonstrates a mechanical hypersensitivity in the sural nerve territory comparable to the SNI model. A detailed discussion regarding these variants is available elsewhere (3).
7. Sensory testing: The purpose of this paragraph is not to describe in details the methods of the different neuropathic pain behavioural assessments, but to point out the specificities and difficulties encountered with SNI model in particular.

One advantage of the SNI model is the distinct anatomical distribution with an absence of co-mingling of injured and non-injured nerve fibres distally to the lesion. Thus, peripherally, injured and non-injured nerves and skin territories can be easily identified and manipulated for further analysis, such as retrograde tracing, specific nerve treatment or recording and behavioural assessment.

SNI rats develop behavioural signs of neuropathic pain, such as secondary heat hyperalgesia (radiant heat), mechanical hyperalgesia (pin-prick test), mechanical allodynia (Von Frey monofilaments test) and cold allodynia (acetone drop). This hypersensitivity develops strongly in the very lateral surface of the plantar side of the paw, in the skin territory innervated by

the intact sural nerve, as well as in the dorsal sural territory albeit less important in this latter. Moreover, stimulating other plantar nerve territories (i.e. saphenous) will result in less-pronounced albeit significant allodynic behaviours. Consequently, the sensory testing should be carefully conducted by accurately stimulating the skin area of the plantar sural nerve territory (see Note 14). SNI mice develop substantial and reproducible mechanical allodynia-like behaviour. When testing cold-induced responses, we observed a repulsive and uncontrollable effect of acetone on the global behaviour of the mouse that definitively impairs an accurate recording.

The time course for the development of pain hypersensitivity has been well described. Three days after surgery, the animals develop strong pain behavioural hallmarks. Although neuropathic pain-related behaviour is already detectable 3 days post-surgery, its peak should occur 5–7 days post-surgery (see Note 15).

Moreover, due to ligation and transection of common peroneal and tibial nerves that contain not only sensory fibres but also motor fibres, the animals present a neuromuscular defect that leads to a pronation of the lesioned paw, which can also complicate the testing especially in mice due to the small size of the paw. To facilitate this testing in mice, we use small Plexiglas boxes that are only 7 cm × 7 cm × 5 cm ( $L \times W \times H$ ) in order to hamper vertical activity and straightening up of the animals, and we regularly use a frontal light to facilitate both accuracy of stimulation and visual analysis of fine movements. The typical withdrawal response is described extensively in the study of Bourquin et al. (3) with additional videos.

---

## 4. Notes

1. We generally use young adult animals, as they are easier to operate. Moreover, the sensory testing post-surgery can last for many weeks, and young animals are easier to monitor for a longer period of time. For younger animals, we recommend ref. (4).
2. To reduce the variability due to the oestrus cycle on both the neuropathy and nociceptive behaviours, we usually work with male animals. Nevertheless, in mice, this might be overcome or at least minimally important (3).
3. The strain of animals is an important variable. It is now well established that different strains or even same strains, but from different suppliers, might be dissimilar in the development of the neuropathy. Pilot studies and appropriate controls are suggested if using different strains or gender. In our case, we use Sprague–Dawley rats (CrI:CD(SD)) and C57/BL6J mice from Charles River (Charles River, L'Arbresle, France).

4. As much as possible, it is recommended to house rodents in groups as they are profoundly perturbed and stressed when left alone in their cages, especially when working with rats. After surgery, rats rarely try to remove their sutures, a behaviour that can conversely be seen with mice. In contrast, mice must be monitored on a regular basis after surgery (two or three times a day) and re-sutured the incision if necessary. After 1 day of good healing, the risk is minimal.
5. Depending on the type of bedding used following SNI, animals may occasionally (<1%) develop autoblaby behaviour (5), i.e. self-mutilation behaviour by eating their toes.
6. For mouse surgeries, the small animal retraction system from Fine Science Tool is a very satisfactory alternative. It includes interchangeable retractor tips (from 1 to 7.5 mm width) fixed with magnetic fixators on a magnetic stainless plate.
7. Wound-clip system is an easy, rapid and efficient way to close the skin of animals after surgery. However, it should be avoided in mice when performing sensory testing as the size and weight of the clips might impair animal mobility and ability to withdraw their paw upon stimulation.
8. The Plexiglas chamber must be hermetically sealed in order to both secure a proper anaesthesia and prevent the experimenter from anaesthetic intoxication.
9. If the three branches are not very well identifiable, try to reposition the hind paw of the animal by switching it a little bit. The sural nerve is easily identifiable: it is the thinnest one and very individualized at a posterior position; the tibial nerve is the thickest one and goes deeper in the structure, under a blood vessel, whereas the common peroneal branch has an intermediate size and stays more superficially above the blood vessel. If your nerve exposure is not perfectly completed, we recommend stopping the surgical procedure, or to use this animal for a sham procedure. The key point is to avoid injury to the sural nerve by touching, stretching or damaging it. Therefore, great care must be given to avoid disturbing the sural nerve during the surgery. We recommend discarding any animal that underwent acknowledged sural damage. The sural nerve must be visualized in the surgical field during all the procedure. If any damage occurs to the sural, a late development of pain hypersensitivity has been noticed (usually, a delay of 1 week or more).
10. Start the procedure with the common peroneal nerve as it is the most lateral. Additionally, it will free the tibial nerve for further processing.
11. As a control, a tight ligation of common peroneal nerve should provoke a brief flick of the toes, whereas the tight ligation of tibial nerve provokes normally twitches in the surrounding muscles.

12. Silk suture and removal of the piece of nerve cut are made to prevent nerve fibre regrowth and self repair. This is a key point as the sole crushing of the nerve is insufficient to produce a long-lasting pain hypersensitivity, as in this case the mechanical allodynia resolves after 60 days to reach values undistinguishable from baseline thresholds (1).
13. We recommend using sham and not naive animals for control, as the sham procedure mimics all the inflammatory events that are linked to the surgery itself and that can impact on the basal sensitivity.
14. When stimulating the sural nerve territory with Von Frey monofilaments, a great care must be taken not to touch the hairs located between the hairy and glabrous part of the paw, as this could provoke a brisk false withdrawal response.
15. In our hands, 100% of animals subjected to the SNI surgery develop increases in pain sensitivities after 5 days. An absence of allodynia-like behaviour at this stage likely indicates damage to the sural nerve (this may happen to an experimenter not yet fully comfortable with SNI surgery), we therefore recommend to discard the corresponding animal.

## References

1. Decosterd, I., and Woolf, C. J. (2000) Spared nerve injury: an animal model of persistent peripheral neuropathic pain. *Pain* 87, 149–158.
2. Shields, S. D., Eckert, W. A., 3rd, and Basbaum, A. I. (2003) Spared nerve injury model of neuropathic pain in the mouse: a behavioral and anatomic analysis. *J Pain* 4, 465–470.
3. Bourquin, A. F., Suveges, M., Pertin, M., Gilliard, N., Sardy, S., Davison, A. C., Spahn, D. R., and Decosterd, I. (2006) Assessment and analysis of mechanical allodynia-like behavior induced by spared nerve injury (SNI) in the mouse. *Pain* 122, 14 e11–14.
4. Howard, R. F., Walker, S. M., Mota, P. M., and Fitzgerald, M. (2005) The ontogeny of neuropathic pain: postnatal onset of mechanical allodynia in rat spared nerve injury (SNI) and chronic constriction injury (CCI) models. *Pain* 115, 382–389.
5. Wilkie, I. C., Dolan, S., Lewis, J., and Blake, D. R. (2007) ‘Autotomy’: A terminological inexactitude. *Pain* 128, 286–287.

## A New Rat Pain Model of Thrombus-Induced Ischemia

Jang-Hern Lee

### Abstract

Pathophysiology of peripheral ischemic pain has not been fully demonstrated since the proper animal model has not been established. We designed this study to develop a new thrombus-induced ischemic pain (TIIP) animal model mimicking human peripheral ischemic pain by using ferrous chloride ( $\text{FeCl}_2$ ) in rats. Histological examination and Evans blue experiment revealed that the application of  $\text{FeCl}_2$  onto the femoral artery produced an excessive thrombosis and ischemic condition in ipsilateral hind paw. Furthermore, ischemia-sensitive markers, such as hypoxia inducible factor-1 alpha ( $\text{HIF-1}\alpha$ ) and vascular endothelial growth factor (VEGF) were upregulated in the ipsilateral plantar muscles of  $\text{FeCl}_2$ -applied rats. The mechanical allodynia was induced in bilateral hind paws from 1 day after  $\text{FeCl}_2$  application and sustained for 30 days. However, thermal threshold of bilateral hind paws did not change in this animal model. In conclusion, we have developed a novel animal model of TIIP, which is characterized by the development of bilateral mechanical allodynia, but not thermal hyperalgesia. Thus, we suggest that this TIIP model can be useful in investigating the pathophysiological mechanisms that underlie human peripheral ischemic pain.

**Key words:** Thrombus, Ferrous chloride, Ischemic pain, Animal model

---

### 1. Introduction

Peripheral limb ischemia is commonly accompanied by ischemic pain. However, its pathophysiology is still unclear since proper animal model mimicking human peripheral ischemic pain has not been established. Although several animal models have been developed by restriction of blood flow (1, 2), none of these models mimics the mechanisms of peripheral ischemia observed in human clinic.

In order to develop a new animal model for ischemic pain, we used  $\text{FeCl}_2$  to induce injury of arterial wall and subsequently produce a severe thrombosis (3). Peripheral ischemic condition was confirmed by Evans blue experiment, histological examination and upregulated ischemia-sensitive markers, such as hypoxia-inducible factor-1 alpha ( $\text{HIF-1}\alpha$ ) and vascular endothelial growth factor (VEGF). Mechanical

allodynia and thermal hyperalgesia of bilateral hind paws were assessed until 30 days after FeCl<sub>2</sub> application. In this chapter, we describe the detail method for the generation of this model.

---

## 2. Materials

### 2.1. Animals and Surgical Preparation

1. Male Sprague–Dawley rats (300–500 g body weight) (see Note 1). Animals are housed in a standard environment consisting of a 12 h light/dark cycle, a constant room temperature (maintained between 20 and 25°C), and 40–60% humidity. Food and water are given ad libitum during the entire experiment period.
2. General anesthesia: combination of 2 ml of Zoletil 50® (tiletamine HCl 25 mg + zolazepam HCl 25 mg in 1 ml, Virbac laboratories, Carros Cedex, France) and 1 ml of Rompun® (xylazine HCl 23.32 mg/1 ml, Bayer Korea, Ansan, Korea) in 2 ml of saline.
3. Microscope for microsurgery (World Precision Instruments, Surgioscope PSMB, Sarasota, FL) connected to an illuminator (Chiu technical Corp., FO-150, NY) is used for accurate surgery.
4. Heating pad: tubing system with a hot water circulator (Fisher scientific, 9005 US/160A, Pittsburgh, PA) is used to maintain the body temperature of animals during surgery.
5. Disinfectants: 5% povidone-iodine solution and 70% ethyl alcohol.
6. Animal hair clipper.
7. Two Iris forceps (serrated, curved, 11 cm, F.S.T., North Vancouver, Canada).
8. Kelly hemostatic forceps (serrated, curved, 14 cm, FST).
9. Strabismus scissors (Straight, 11.5 cm, FST).
10. Halsey needle holder (13 cm, FST).
11. Dressing forceps (14 cm, Jeungdo B&P, Seoul, Korea).
12. Kalt suture needle (3/8 circle cutting needle, FST).
13. Suture silk (5/0, Won, Shihung, Korea).
14. Heat-controlled animal recovery chamber: maintain ambient temperature at 28°C until rats recover from the anesthesia (51 × 51 × 70 cm size).

### 2.2. Thrombus Formation

1. Ferrous chloride (FeCl<sub>2</sub>, Sigma, St. Louis, MO): 20% (v/v) ferrous chloride is dissolved in sterile saline solution (see Note 2).
2. Moisture-resistant film (Parafilm®, Pechiney Plastic Packaging, Chicago, IL): 1 × 2.5 cm size.
3. Filter paper (No. 2, Toyo Roshi Kaisha, Ltd., Japan): 0.5 × 0.5 cm size.

### **2.3. Measurement of Evans Blue Concentration in Plantar Muscle**

1. Evans blue (Sigma): 1 ml (40 mg/ml).
2. Formamide (Sigma).
3. Needle (24 gauge) and syringe (1 ml volume) for insertion of Evans blue.
4. Micro High Speed Centrifuge (Micro 17R, Hanil, Incheon, Korea).
5. Microplate absorbance reader (model 680, Biorad, Hercules, CA).

### **2.4. Western Blot Assay**

1. Homogenizer; TissueRuptor® (Qiagen, Darmstadt, Germany).
2. Homogenizing buffer; 1 M Tris-HCl (pH 7.5), 1% NP-40, 0.5 M EDTA (pH 7.5), 50 mM EGTA, 1 M dithiothreitol, 1 M benzanidine, 0.1 M PMSF (phenylmethylsulfonyl fluoride).
3. Bradford dye assay (Bio-Rad Laboratories, Hercules, CA).
4. Electrophoresis (Bio-Rad Laboratories); 10% SDS-polyacrylamide gel electrophoresis.
5. Tris-buffered saline with Tween-20 (TBST); 10 mM Tris-HCl (pH 7.6), 150 mM NaCl, 0.05% Tween-20.
6. Antibody for HIF-1 $\alpha$  and VEGF (Santa Cruz Biotechnology, Delaware, CA).
7. Antibody for  $\beta$ -actin (Sigma).
8. Second antibody; Peroxidase-conjugated goat anti-rabbit IgG (Calbiochem, EMD Chemicals, Inc.).
9. Buffer for antibodies; 5% skim milk in TBST.
10. Enhanced chemiluminescence (Amersham Pharmacia Biotech, England, UK).
11. Image analysis system (Metamorph®, version 6.3r2, Molecular Devices Corporation, PA, USA).

### **2.5. Behavioral Measurement**

1. Mechanical allodynia: von Frey filament of 4.0 g (North Coast Medical, Morgan Hill, CA) and metal mesh grid box.
2. Thermal hyperalgesia: plantar analgesia meter apparatus (Series 8, Model 390, IITC Life Science Inc., Woodland Hills, CA).

---

## **3. Methods**

### **3.1. Surgical Procedure**

1. Rats are deeply anesthetized using combination of Zoletil 50®, Rompun® and saline (a ratio of 2:1:2, respectively). The proper volume of combined anesthetic solution (0.1 ml/100 g body weight) is intraperitoneally injected (see Note 3).
2. After clear cutting of hair in surgery region, heating pad is placed underneath the anesthetized animal (see Note 4).

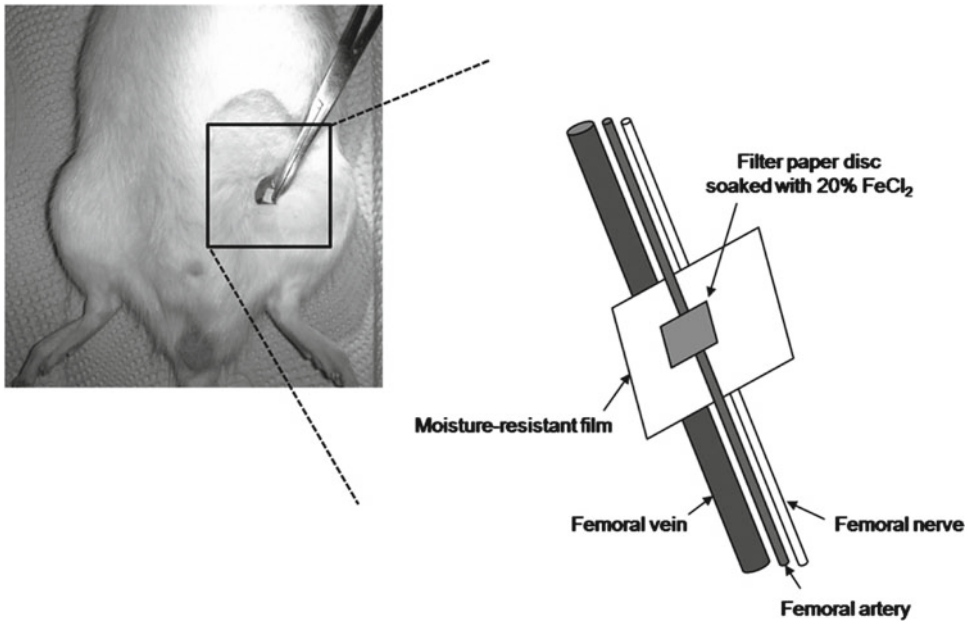


Fig. 1. Schematic diagram shows the method of thrombus generation. After blunt dissociation of femoral artery, vein, and nerve, moisture-resistant film is placed underneath femoral artery to prevent possible damage to femoral vein and nerve by  $\text{FeCl}_2$ . Subsequently, filter paper disc soaked with 20%  $\text{FeCl}_2$  is placed onto the femoral artery for 20 min.

3. A small incision (1 cm, approximately) is performed in the femoral triangle of the left hind limb. The femoral artery is then carefully separated from the femoral vein and nerve (see Note 5).
4. During the application of  $\text{FeCl}_2$  solution, a piece of moisture-resistant film is placed underneath the femoral artery to prevent possible damage of the femoral vein and nerve by  $\text{FeCl}_2$  (4) (see Note 6).
5. A filter paper disc ( $0.5 \times 0.5$  cm) soaked with 20%  $\text{FeCl}_2$  solution is placed on the femoral artery for 20 min as shown in Fig. 1.
6. After the incision is surgically closed and covered by surgical dressing, animals are kept in a heat-controlled chamber ( $28^\circ\text{C}$ ) until they completely recover from the anesthetic (see Note 7).

### **3.2. Confirmation of Thrombosis and Ischemic Condition**

#### *3.2.1. Measurement of Evans Blue Concentration in Plantar Muscle*

1. Rats are anesthetized using same anesthetic (combination of Zoletil 50<sup>®</sup>, Rompun<sup>®</sup> and saline) before Evans blue experiment.
2. Evans blue solution (1 ml, 40 mg/ml in saline) is injected into the external jugular vein following the modified method of a previous report (5) (see Note 8).
3. Plantar muscles from both hind paws are collected 1 min after Evans blue injection.
4. Collected samples (about 70 mg) were immersed in 1 ml of formamide at  $60^\circ\text{C}$  for 24 h.

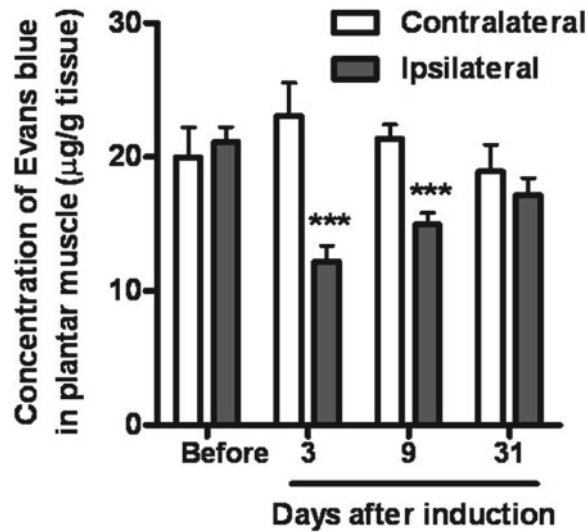


Fig. 2. The development of ipsilateral peripheral ischemia using Evans blue in anesthetized rats. The concentration of Evans blue ( $\mu\text{g/g}$  tissue) in the ipsilateral hindpaw is significantly reduced in peripheral ischemia-induced rats at 3 and 9 days post- $\text{FeCl}_2$  application as compared with the concentration in the contralateral hind paw ( $N=5$  before and  $N=6$  after  $\text{FeCl}_2$  treatment.  $***P<0.001$ ). (This figure has been reproduced from ref. 8 with permission of the International Association for the Study of Pain (IASP)).

5. After the muscle samples are centrifuged ( $8,010\times g$ , 30 s at room temperature), absorbance of supernatant (200  $\mu\text{l}$ ) is measured at 620 nm by a microplate reader.
6. The concentration of Evans blue in the plantar muscles is then calculated as  $\mu\text{g/g}$  tissue based on a preliminary standard curve experiment. Ipsilateral Evans blue concentration was compared with that of contralateral side at each time point. The result is shown in Fig. 2.

### 3.2.2. Histological Examination in Femoral Artery

1. The femoral artery is isolated from normal animals and from animals at days 3, 7, and 31 after  $\text{FeCl}_2$  application, respectively.
2. The ipsilateral femoral artery is removed from rats in each group, fixed with 10% neutral-buffered formaldehyde and embedded in paraffin by classical method. Histological sections through the artery are cut and the sections are subsequently stained with hematoxylin and eosin (see Note 9).

### 3.2.3. Western Blot Analysis for HIF-1 $\alpha$ and VEGF

1. Three days after saline (sham surgery) or  $\text{FeCl}_2$  application, plantar muscles from the ipsilateral hindlimb are collected from anesthetized rats.
2. The muscle samples are homogenized in homogenizing buffer. The total amount of protein in each sample is determined using

the Bradford dye assay prior to loading on polyacrylamide gels.

3. The muscle tissue homogenates (20  $\mu$ g protein) are separated by 10% SDS-polyacrylamide gel electrophoresis and transferred to nitrocellulose. After the blots are washed with TBST, the membranes are blocked with 5% skim milk for 1 h and incubated with primary antibodies against HIF-1 $\alpha$  (1:1,000) or VEGF (1:1,000) or  $\beta$ -actin (1:1,000).
4. After the secondary antibody reaction, the bands are visualized with enhanced chemiluminescence (see Note 10).

### **3.3. Behavioral Measurement**

#### *3.3.1. Assessment of Mechanical Allodynia*

1. After FeCl<sub>2</sub> application, the number of paw withdrawal responses to normally innocuous mechanical stimuli is measured in ipsilateral and contralateral hind paws by using a von Frey filament of 4.0 g (6).
2. Rats are placed on a metal mesh grid under a plastic chamber, and allowed to acclimate for 10 min before testing (see Note 11).
3. The von Frey filaments are applied from underneath the metal mesh flooring to each hind paw for ten trials at approximately 10-s intervals.
4. The number of paw withdrawal responses to each set of ten stimuli is then counted.
5. The results of mechanical allodynic behavior in each experimental animal are presented as the percentage of withdrawal response frequency (WRF, %).
6. Mechanical allodynia test is performed at 1, 2, 3, 5, 7, 9, 12, 15, 18, 21, 24, and 31 days after FeCl<sub>2</sub> application. The examples of results in ipsilateral and contralateral hind paws are shown in panel a and b of Fig. 3.

#### *3.3.2. Assessment of Thermal Hyperalgesia*

1. To assess nociceptive responses to heat stimuli, the paw withdrawal response latency (WRL) was measured using plantar analgesia meter apparatus (7).
2. Rats are placed in a plastic chamber with a glass floor and allowed to acclimate for 10 min before testing.
3. A radiant heat source is positioned under the glass floor beneath the hind paw to be tested and withdrawal latency is measured by using a photoelectric cell connected to a digital clock (see Note 12).
4. The test is duplicated (about 5 min intervals) in each hind paw at each time point and the mean withdrawal latency is calculated (see Note 13).
5. Thermal hyperalgesia was also measured at 1, 2, 3, 5, 7, 9, 12, 15, 18, 21, 24, and 31 days after FeCl<sub>2</sub> application (see Note 14). An example of results is shown in panel c of Fig. 3.

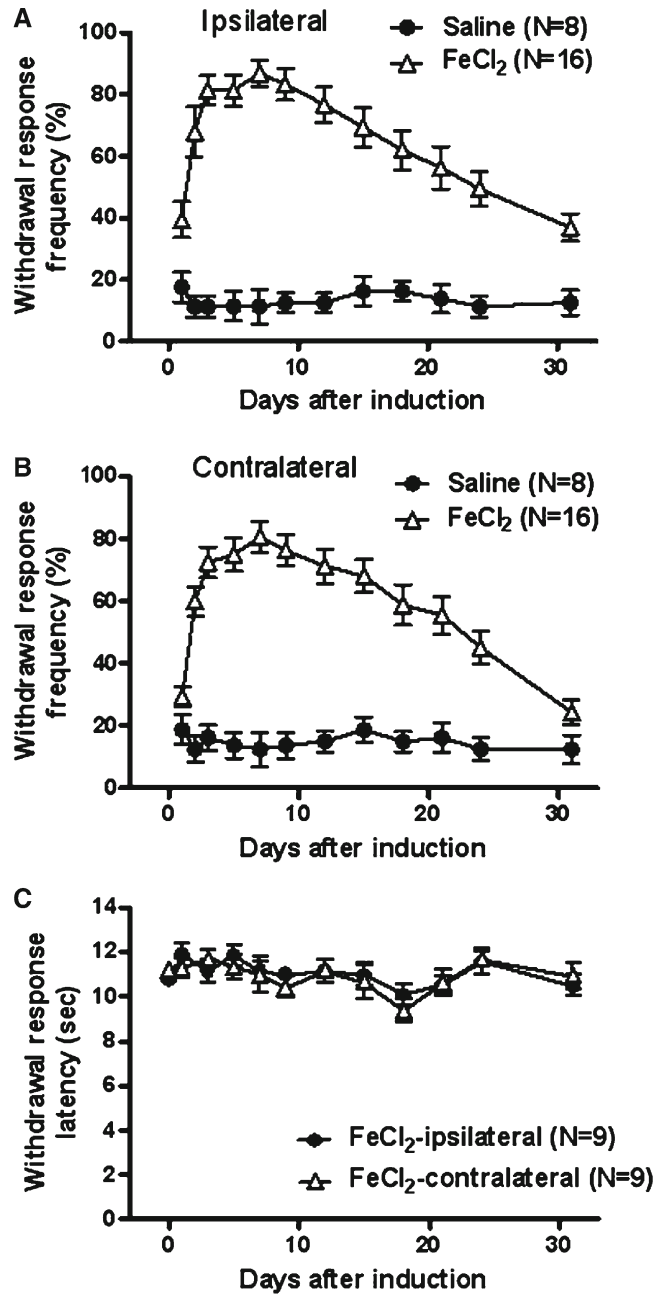


Fig. 3. Graphs illustrating the development of thrombus-induced ischemic pain (TIIP) in FeCl<sub>2</sub>-treated rats. FeCl<sub>2</sub> application results in the development of mechanical allodynia in both the ipsilateral (a) and contralateral (b) hind paws. TIIP peaks at 9 days post-FeCl<sub>2</sub> application and gradually decreases through day 31, the last day of the experiment. As illustrated in (c), the withdrawal latency to heat stimuli does not change in both ipsilateral and contralateral hind paw, indicating that thermal hyperalgesia is not induced by FeCl<sub>2</sub> application. (This figure has been reproduced from ref. 8 with permission of the International Association for the Study of Pain (IASP)).

---

## 4. Notes

1. The body weight of male Sprague–Dawley rats used in this experiment ranged from 300 to 500 g. The preferred body weight is about 400 g because the surgical manipulation can be achieved more easily than younger rats.
2. Ferrous chloride should be stored in desiccator box and freshly prepared on the day of experiment because it is highly hygroscopic and the amounts of thrombus produced by ferrous chloride may be reduced with the degree of hygroscopicity.
3. The volume of anesthetics may be different according to species of animals. The induction time for full anesthesia is about 5–10 min in male Sprague–Dawley rats.
4. The body temperature of anesthetized animal is controlled on a heating pad, and ambient temperature is also kept between 25 and 28°C. Too low ambient temperature may interfere with thrombus formation by ferrous chloride.
5. When femoral artery, vein and nerve are exposed using blunt dissection, and only femoral artery is separated, one should be careful to prevent a damage induced by using sharp forceps because artery, vein, and nerve are closely adjacent. In addition, the presence of a neuronal damage can also induce peripheral neuropathic pain.
6. A piece of moisture-resistant film placed underneath femoral artery should be much larger than a filter paper disc soaked with 20% FeCl<sub>2</sub> solution as described in the next step.
7. After the animals recover from surgery, one needs to observe whether motor impairment is present in operated animals as compared to sham surgery animals or naïve animals. This can be the indication of whether the animals are affected by surgery due to femoral nerve injury. If some animals are showing motor impairment, they should be excluded from the experiment.
8. We have performed the calculation of Evans blue concentration at 3, 9 and 31 days after FeCl<sub>2</sub> treatment as shown in Fig. 2 (from ref. 8 with permission) (3).
9. Histological examination indicates that the FeCl<sub>2</sub> application time-dependently induced excessive thrombosis in ipsilateral hind limb as shown in Fig. 4 (from ref. 8 with permission).
10. Western blot analysis suggests that the FeCl<sub>2</sub> application-induced thrombosis evokes ischemic condition in ipsilateral hind limb as shown in Fig. 5 (from ref. 8 with permission).
11. The acclimation time should be over 10 min, and it may vary according to species of animals. We recommend the duration of 30 min for animal acclimation before testing.

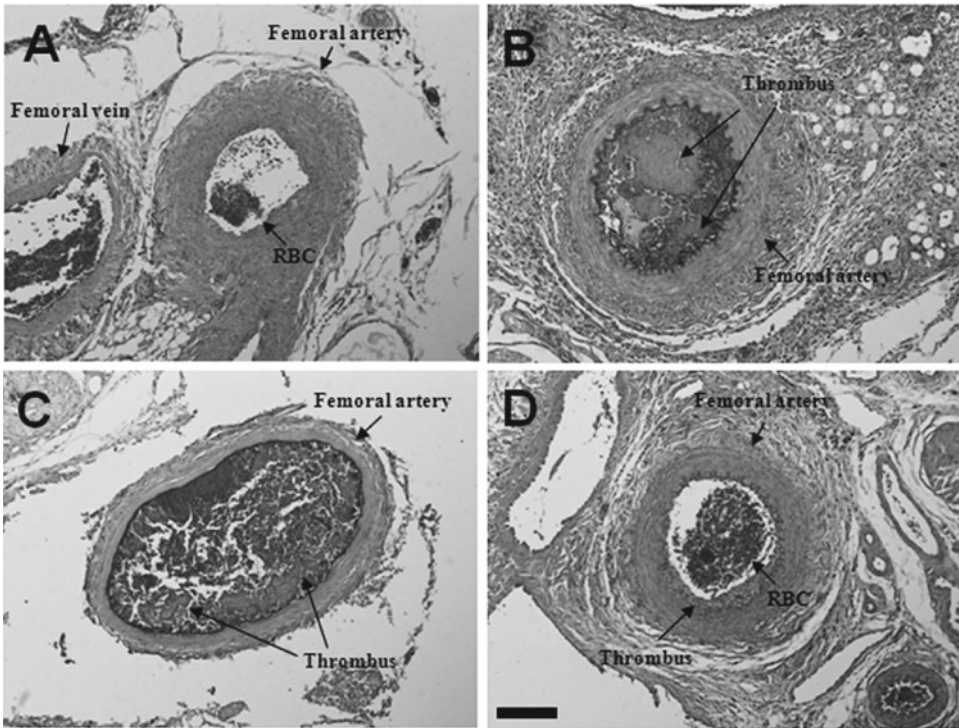


Fig. 4. Representative photomicrographs illustrating the presence of  $\text{FeCl}_2$ -induced thrombus formation and arterial obstruction in the femoral artery. There is no evidence of thrombus formation or occlusion in femoral arteries taken from animals with no  $\text{FeCl}_2$ -treatment (a). A large  $\text{FeCl}_2$ -induced occlusive thrombus is present in the lumen of all femoral arteries examined at day 3 (b) and at day 7 (c) post- $\text{FeCl}_2$  treatment. By day 31 post-treatment, the majority of the thrombus disappears from the lumen, with only a small amount remaining along the tunica intima of the vessel wall (d). Scale bar indicates 200  $\mu\text{m}$ . (This figure has been reproduced from ref. 8 with permission of the International Association for the Study of Pain (IASP)).

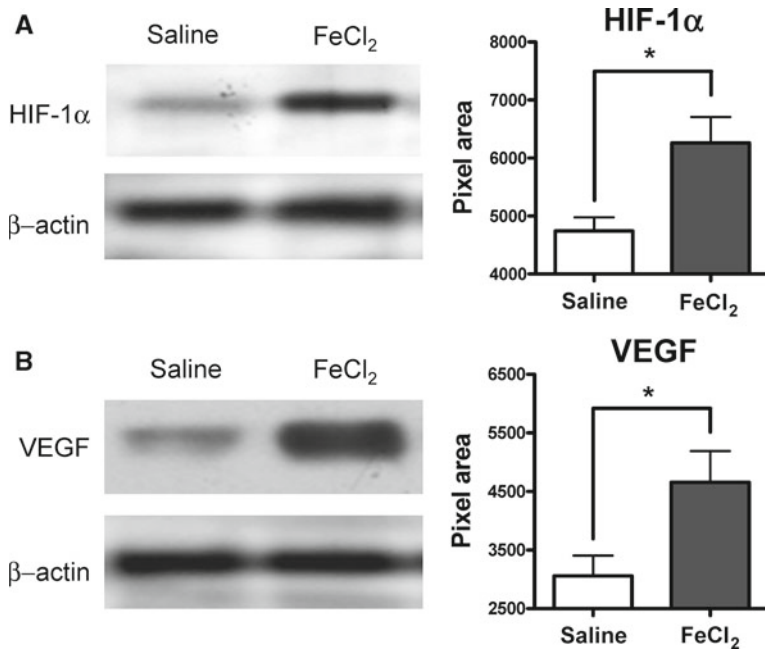


Fig. 5. Documentation of ipsilateral peripheral ischemia using western blot analysis. Immunoblots of ipsilateral plantar muscle tissue taken 3 days after  $\text{FeCl}_2$  application or saline application indicating significant increases in the ischemia specific markers HIF-1 $\alpha$  (a) and VEGF (b) ( $N=4$  in each group. \* $P<0.05$ ). (This figure has been reproduced from ref. 8 with permission of the International Association for the Study of Pain (IASP)).

12. The intensity of the light source is calibrated to produce a withdrawal response within 10–12 s in normal animals.
13. A cutoff time of 20 s is used to protect the animal from excessive tissue damage.
14. All behavioral tests, including pharmacological study, should be performed blindly.

---

## Acknowledgments

This research was supported by a grant (2009 K001256) from Brain Research Center of the 21st Century Frontier Research Program funded by the Ministry of Education, Science and Technology, the Republic of Korea.

## References

- 1.Coderre, T.J., Xanthos, D.N., Francis, L., and Bennett, G.J. (2004) Chronic post-ischemia pain (CPIP): a novel animal model of complex regional pain syndrome-type I (CRPS-I; reflex sympathetic dystrophy) produced by prolonged hindpaw ischemia and reperfusion in the rat. *Pain* **112**, 94–105.
- 2.Nicholson, C.D. (1996) Experimental models of chronic lower extremity arterial occlusive disease: lessons for drug development. *Vasc. Med.* **1**, 43–49.
- 3.Cho, J., Seo, H., Yun, C., Koo, B., Yoshida, S., Koga, T., Dan, T., and Kim, H. (2000) In vitro and in vivo studies of AT-1362, a newly synthesized and orally active inhibitor of thrombin. *Thrombosis research* **100**, 97–107.
- 4.Kurz, K.D., Main, B.W., and Sandusky, G.E. (1990) Rat model of arterial thrombosis induced by ferric chloride. *Thrombosis research* **60**, 269–280.
- 5.St-Pierre, P., Bouffard, L., Papirakis, M.E., and Maheux, P. (2006) Increased extravasation of macromolecules in skeletal muscles of the Zucker rat model. *Obesity* **14**, 787–793.
- 6.Roh, D.H., Kwon, Y.B., Kim, H.W., Ham, T.W., Yoon, S.Y., Kang, S.Y., Han, H.J., Lee, H.J., Beitz, A.J., and Lee, J.H. (2004) Acupoint stimulation with diluted bee venom (apipuncture) alleviates thermal hyperalgesia in a rodent neuropathic pain model: involvement of spinal alpha 2-adrenoceptors. *J. Pain* **5**, 297–303.
- 7.Hargreaves, K., Dubner, R., Brown, F., Flores, C., and Joris, J. (1988) A new and sensitive method for measuring thermal nociception in cutaneous hyperalgesia. *Pain* **32**, 77–88.
- 8.Seo, H.S., Kim, H.W., Roh, D.H., Yoon, S.Y., Kwon, Y.B., Han, H.J., Chung, J.M., Beitz, A.J., and Lee, J.H. (2008) A new rat model for thrombus-induced ischemic pain (TIIP); development of bilateral mechanical allodynia. *Pain* **139**, 520–532.

## Rat Models of Pancreatitis Pain

Karin N. Westlund and Louis Vera-Portocarrero

### Abstract

Pancreatic pain is often severe and difficult to treat clinically. Many animal models that mimic pancreatic pain are typically short term and invasive in nature. The present chapter describes the development and characterization of two non-invasive rat models of pancreatitis, one acute and one chronic. The two models described here are simple to replicate, giving them advantage over other animal models of pancreatic inflammation. A goal of this chapter is also to detail their usefulness as visceral pain models.

**Key words:** Acute pancreatitis, Chronic pancreatitis, Visceral pain, Model development, Alcohol

---

### 1. Introduction

Visceral pain is of great clinical concern, constituting a majority of pain treated by the medical community. With cancerous or inflamed pancreas, severe intractable pain is often a major complaint. Severe pain was reported in over 70% of the 32,000 cancer patients expected to die in 2004 from pancreatic cancer, the fourth leading cause of cancer death overall. Abdominal pain is the major presenting complaint of nearly all patients seeking medical attention with acute or chronic pancreatitis and those later discovered to have pancreatic cancer. The annual incidence of new cases of acute pancreatitis reported in the US is 20 per 100,000 acute and 8 per 100,000 chronic pancreatitis cases. Chronic alcohol consumption is the primary factor attributed to development of pancreatitis. Over 50% of patients with idiopathic and alcoholic pancreatitis report chronic pain.

Most present knowledge about pancreatic pain relief has come from clinical work. While the majority of cases are induced after prolonged alcohol consumption, in many cases the cause of pancreatitis is

unknown and can even occur in children. Pancreatitis is characterized by severe histopathological changes, such as the presence of inflammatory mediators, acinar atrophy, fat necrosis, intraductal hemorrhage, periductal fibrosis, and stromal proliferation (1–3). Elevated serum lipase and amylase levels serve as biochemical markers of acute pancreatitis. Pancreatitis begins as a mild edematous condition that can heal without intervention, but the condition may progress to more severe inflammation with constant simmering pain progressing to intolerable pain. The level of pain experienced by these patients is directly linked to decreased pancreatic functioning and increased length of stay during hospitalizations. In patient surveys, 32% of patients in chronic pain report being willing to try any new therapy for relief, and some may resort to suicide for this intractable pain state. Thus, the need to pursue novel pain relief strategies for pancreatitis and pancreatic cancer remains high.

It is well known that somatic and visceral pain differ substantially in perception (4). Explanations for this phenomenon and other differential features, such as pharmacology, have been reviewed by Giamberardino et al. and McMahon et al. (5, 6). In particular, a classic feature of visceral pain is its referral to another part of the body, e.g., appendicitis and heart pain, often following a dermatomal pattern. This pattern of referred pain is also evident in animal models (Fig. 1) (5). There has thus far been very little information forthcoming concerning nociceptive neurotransmitter

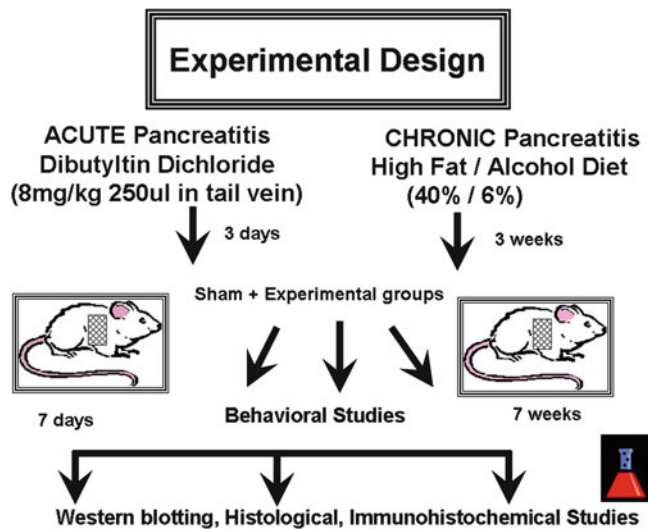


Fig. 1. Experimental design used for the induction of acute and chronic pancreatitis models in rats. The acute model is induced with a tail vein injection of DBTC and nociceptive hypersensitivity peaks at 1 week. Hypersensitivity develops within 3 weeks in Fisher rats fed a high fat and alcohol diet and persists for 7 weeks. In both models, referred pain is present on the rat's abdomen and in a cutaneous band extending dorsally to the shoulder and neck (hatched region).

mechanisms mediating pancreatitis pain. Since there is very little information available concerning pancreatitis pain mechanisms, animal models of pancreatic pain relevant to acute bouts of pancreatitis have been developed in the last decade. Both acute (1 week) and chronic (4 week) pancreatitis models have been developed by us for translational study of visceral pain (7–10). This chapter will more explicitly detail two animal models of pancreatitis induced in rats under study by the authors and biochemical changes assessed in these models. These visceral pain models are induced (1) by a chemical plasticizer dibutyltin dichloride (DBTC) to mimic clinical characteristics of acute pancreatitis bouts or (2) with a high fat and alcohol diet. The animal models allow study of relevant nociceptive mechanisms (Fig. 1).

---

## 2. Materials

### 2.1. Acute Pancreatitis Model

1. Male Sprague–Dawley or Lewis inbred rats (Harlan, Indianapolis) weighting between 150 and 200 g at the start of the experiments.
2. DBTC (Sigma Aldrich, St Louis, USA).
3. 100% Ethanol.
4. Glycerol.
5. Teklab diet 8626.
6. Isoflurane anesthesia.
7. 4% Paraformaldehyde in Phosphate Buffered Saline (PBS, pH 7.4).
8. Hematoxylin and Eosin (Sigma Aldrich, St Louis, USA).
9. A 4 g (39.23 mN) von Frey filament.
10. Plexiglas boxes (Plastics Plus, Tucson, AZ).
11. Hargreaves, hotplate and von Frey behavioral systems (Ugo Basile, Collegeville, PA).
12. Analgesiometer apparatus (Columbus Instruments).

All animals used for pain studies should be fed a rice-based, low soy diet (except the chronic diet-induced pancreatitis) since the phytoestrogens found in conventional soy-based lab chow will reduce sensitization. Feeding animals a chow with low soy content, such as mouse breeder food (Teklad 8626) will increase experimental group differences.

### 2.2. Chronic Pancreatitis Model

1. Male Fisher rats (Harlan, Indianapolis) weighing 80–90 g.
2. High fat commercial diet with 28% fat (LD101A with LD104, TestDiet, Richmond, IN).
3. 95% Alcohol (methanol free).

4. Apple juice.
5. Corn oil.
6. Lard.
7. Alfalfa (local pet store).

The control animals for the chronic pancreatitis studies are fed the typical soy-based rodent diet, such as Teklad 2018 (Purina), to increase experimental group differences.

---

## 3. Methods

### **3.1. Acute Pancreatitis Model**

The acute pancreatitis model is induced chemically with a tail vein injection of the organic compound, DBTC in rats. The nociceptive sensitivity persists for at least 1 week with this model and is maintained by providing alcohol in their drinking water. In this model, young Lewis in-bred rats (150–200 g) are tail vein injected under isoflurane anesthesia with DBTC or vehicle. Injections must be made very carefully by skilled laboratory personnel familiar with the tail vein injection procedure because any leakage of the caustic DBTC outside the vein will require sacrifice of the animal due to severe tail tissue breakdown and ulceration.

#### *3.1.1. Pre-injection Procedure*

1. Rats are anesthetized with an isoflurane/oxygen/nitrogen mixture (2–3 L/min, 4.0%/vol until anesthetized, then 2.5%/vol throughout the procedure).
2. The abdominal area of the rats is shaved with rat clippers.
3. Rats are allowed to recover from anesthesia (30 min) before baseline behavioral testing (see Subheading 3.1.3).

#### *3.1.2. Injection Procedures*

1. The DBTC is dissolved first in 100% ethanol and then glycerol. The ratio of ethanol-to-glycerol is 2:3. The DBTC solution is adjusted according to the individual weight of the rat with the injected dose of 8 mg/kg of body weight in 200  $\mu$ l.
2. The DBTC solution is injected into the tail vein of the rat. The injection should be made slowly (1 min) to avoid leakage into the tissue (see Notes 1–3).
3. After injection, rats are returned to their homecages and allowed to recover from the isoflurane anesthesia.
4. For control animals, 0.2 ml of the vehicle solution (two parts ethanol and three parts glycerol) is injected under the same conditions as the DBTC injection.
5. In Lewis rats, 95% alcohol (without trace methanol) can be substituted.

### 3.1.3. Behavioral Procedures

1. Prior to behavioral testing, all animals are environmentally acclimated to the clear Plexiglas cubicle (4 × 4 × 10 in.) testing apparatus with fiberglass mesh on three prior days.
2. Mechanical hypersensitivity in the abdominal area is quantified by measuring the number of withdrawal events, either abdominal withdrawal from the von Frey filament and/or consequent licking of the abdominal area, or whole body withdrawal.
3. To perform this test, rats are placed inside Plexiglas cubicles on an elevated, fine fiberglass screen mesh and acclimated for 60 min prior to testing. The von Frey filaments are applied from underneath the mesh floor, to the foot at different, random points (or shaved abdominal area limited to the epigastric/upper abdomen) (see Note 4).
4. A single trial consists of ten applications of the von Frey filament applied once every 10 s to allow the animal to cease any previous response and return to a relatively inactive position. The up-down method can also be used.
5. The mean occurrence of withdrawal events in each trial is expressed as the frequency of responses out of ten applications, where 0 indicates no withdrawals and 10 indicates the maximum number of withdrawals. Three trials are performed in each animal. Withdrawal events are averaged to obtain a single value per rat.

### 3.1.4. Histological Procedures

1. Pancreatic tissues are removed from anesthetized animals and the tissue is placed in several 0.1 M PBS (pH 7.4) washes until blood elements are removed (see Note 5).
2. After the washes, pancreatic tissue is placed in 4% paraformaldehyde for 3 h, subsequently diced into smaller pieces and kept in the fixative solution for 2 days (see Note 6).
3. The tissue is dehydrated through graded ethanol solutions (80, 95, and 100% twice each). Pancreatic tissue is then transferred to xylene washes (2×) and placed in crucibles with a solution of xylene and melted paraffin (50:50 ×2). Tissue is placed in cassettes and embedded in paraffin.
4. Paraffin blocks are cut in 8- $\mu$ m sections and stained with hematoxylin and eosin (H&E, see Notes 7 and 8).

## 3.2. Chronic Pancreatitis Model

A chronic model of pancreatitis for study of visceral pain is produced by feeding young Fisher rats with a liquid high fat and alcohol diet.

### 3.2.1. Induction of Pancreatitis Procedures

Fisher rats are ordered weighing 80–100 g (see Note 9). After 1 week acclimatization, animals are tested for baseline behaviors. They are switched to the liquid diet with no EtOH with some regular chow pellets on the cage floor for 1 week. When animals

reach 125 g, the young rats are fed a high fat commercial diet with 28% fat (LD101A with LD104) prepared in a food blender by mixing the powdered food (LD101A), the maltodextran supplement (LD104), apple juice, and additional water to make 1 L. Increasing percentages of alcohol are mixed into the food over the subsequent 3 weeks (4, 5, and 6%). The diet is maintained at 6% alcohol after week 3 and an additional 4% corn oil is added. The animals also receive 8 g of lard each (Days 1–4) to increase their weight gain. In the second week, 4% alcohol is added to the diet. The alcohol content is incrementally increased weekly from 4 to 5% and then 6%. The alcohol diet is supplemented with lard on Days 1–4 to maintain weight and with alfalfa on Days 10–14 (see Note 10). Behavioral testing is performed weekly. Pharmacological testing can begin 1 week after the addition of the 6% alcohol. Histological evidence of pancreatitis is present at this time.

*Pancreatitis liquid diet food preparation* (see Note 11)

Baseline–No EtOH Diet.

1,000 g Diet–140 g LD101A Food Mix.  
 90 g Maltodextrin.  
 100 g (100 ml) Apple Juice.  
 770 g (770 ml) Water.

Week 1–4% EtOH Diet.

1,000 g Diet–140 g LD101A Food Mix.  
 90 g Maltodextrin.  
 100 g (100 ml) Apple Juice.  
 40 g (52 ml) EtOH.  
 630 g (630 ml) Water.

Week 2–5% EtOH Diet.

1,000 g Diet–140 g LD101A Food Mix.  
 90 g Maltodextrin.  
 100 g (100 ml) Apple Juice.  
 50 g (65 ml) EtOH.  
 605 g (605 ml) Water.

Week 3–6% EtOH Diet.

1,000 g Diet–140 g LD101A Food Mix.  
 90 g Maltodextrin.  
 100 g (100 ml) Apple Juice.  
 60 g (79 ml) EtOH.  
 591 g (591 ml) Water.

Week 4–experiment end–6% EtOH, 30% Fat Diet.

1,000 g Diet–140 g LD101A Food Mix.  
 90 g Maltodextrin.  
 100 g (100 ml) Apple Juice.  
 60 g (79 ml) EtOH.  
 591 g (591 ml) Water.  
 33 g (36 ml) Corn Oil.

### 3.2.2. Behavioral Procedures

Behavioral procedures for mechanical sensitivity in the chronic pancreatitis model are identical to those described above for the acute pancreatitis model. However, in the chronic model hypersensitivity is noted upon testing the footpad as well as the shaved abdomen in Fisher rats (see Note 13). The development of thermal hypersensitivity on the footpads is also evident with the hot plate test in an Analgesiometer apparatus. The procedure is as follows:

1. Rats are gently placed on the hot-plate surface set to 50°C by an observer blinded to the treatment group.
2. The response latency to nociceptive behaviors of shaking or licking paws, or jumping from the hot plate is recorded and animals removed immediately from the hot plate.
3. A cut-off time point of 20 s is used to diminish the potential of thermal injury.
4. Three trials separated by over 10 min are averaged for each data point (see Notes 14 and 15)

### 3.3. Discussion of the Pancreatitis Models

#### 3.3.1. Acute Pancreatitis Model in Rats

Animals with both the DBTC and the high fat and alcohol-induced pancreatitis have disrupted histological inflammatory characteristics evident only in their pancreas, but not in liver, lung, bladder, or colon (Fig. 2) (7–11). Most notably, morphologic changes include tissue edema, exuberant inflammatory cell infiltration, acinar cell atrophy and loss, with corresponding widened inter- and intra-lobular ducts, and extensive periductal fibrosis with disruption of tissue integrity or cytoarchitecture (Fig. 2b). We have reported reversal of these morphological changes after direct pancreatic injections of a replication defective human Herpes simplex overexpression vector producing excess amounts of met-enkephalin (10). Also increased in the DBTC-inflamed pancreas is the chemokine CCL5 formerly named “regulated on activation, normal T cells expressed and secreted” (RANTES). CCL5 is an 8 kDa protein classified as a chemotactic cytokine or chemoattractant protein that is active in bringing inflammatory cells into the region. Measureable increases in neurokinin (NK1) (Fig. 3) (8), and mu opioid receptors were also reported in pancreas for this DBTC-induced pancreatitis model at 1 week (10).

This model of pancreatitis continues to develop over a week’s time and is best tested for alterations in normal open-field behavior at its peak on days 6–7 (10). The behavioral indications of the presence of a pronociceptive state are accompanied by a staining increase in the endothelin receptor type A in thoracic DRGs (Fig. 4, Vera-Portocarrero and Westlund, unpublished). The type A endothelin receptor is a transmembrane G-coupled receptor protein that is known to increase intracellular calcium upon activation.

Potential problems with use of this model include the necessity of placing the caustic chemical squarely and solely into the tail vein

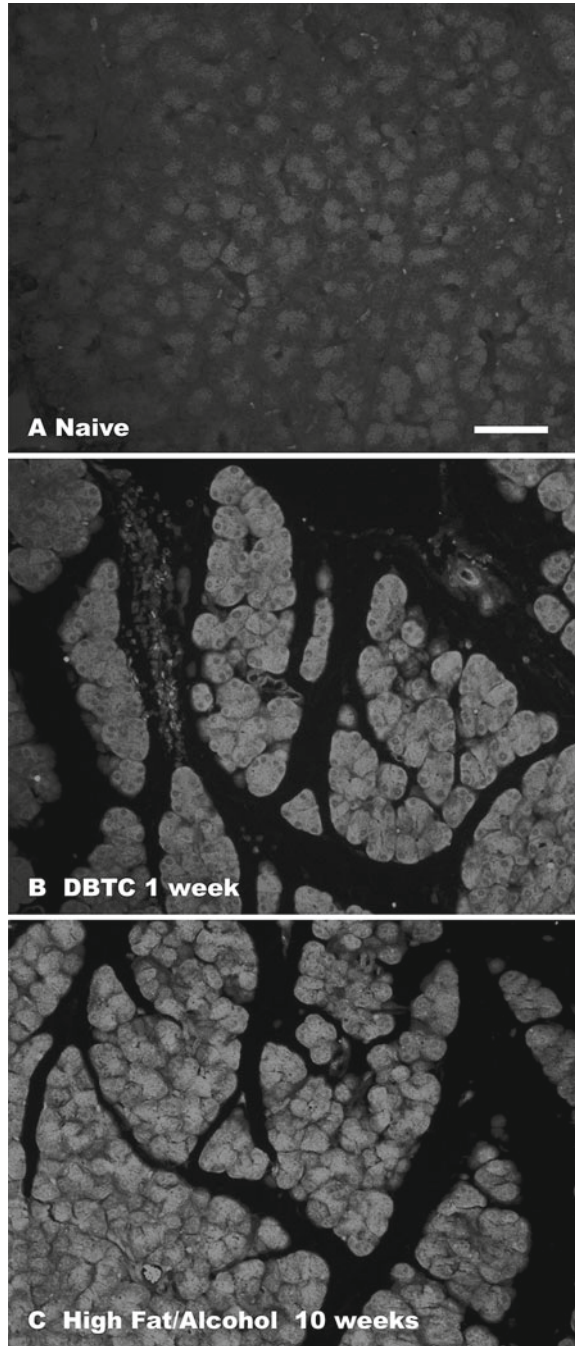


Fig. 2. Photomicrographs of immunohistochemical staining of regulated on activation, normal T cells expressed and secreted (RANTES) in the pancreas (a) from a naive rat, (b) from a rat 1 week after dibutyltin dichloride (DBTC)-induced pancreatitis and (c) from an animal 10 weeks after induction of pancreatitis with a diet of high fat and alcohol (6%). RANTES is a chemokine attracting inflammatory cells to the inflamed pancreas. The small particles evident in the widened ducts (*spaces*) surrounding the pancreatic exocrine cells are the invading inflammatory cells (leukocytes) Scale Bar: 50  $\mu$ m.

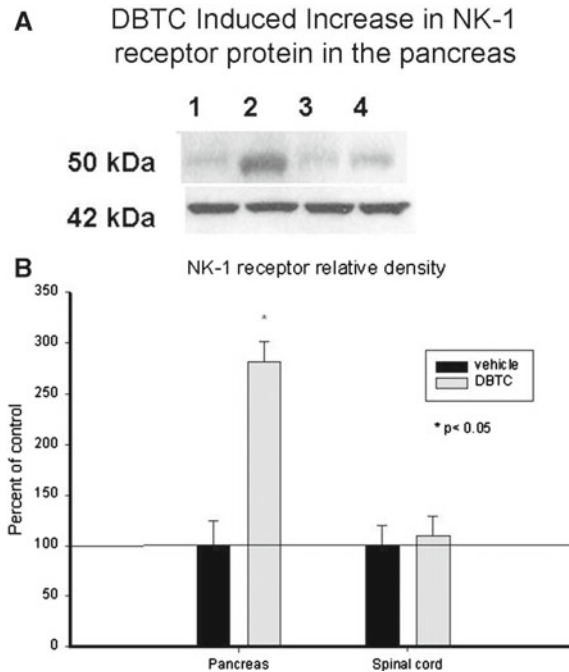


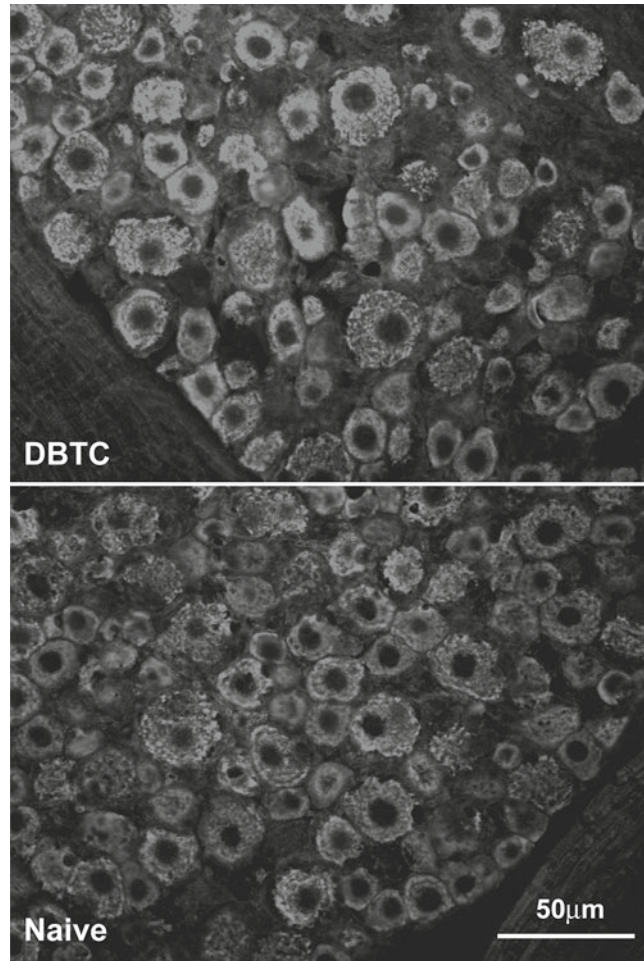
Fig. 3. (a) Representative Western blots of NK-1 protein and  $\beta$ -actin showing control levels in lanes 1 and 3 from vehicle-treated animals. Increased levels of NK-1 protein expressed in DBTC-treated animals with pancreatitis are shown in lanes 2 and 4. (b) The bar graph depicts quantification of the density of the bands. NK-1 receptor protein in the pancreas and spinal cord is expressed as a percent of the  $\beta$ -actin control density value. Reprinted with permission from ref. 8.

to avoid tissue ulceration and deterioration. Some animals will succumb (2%) to multi-organ failure with use of the caustic DBTC method (see Note 1).

### 3.3.2. Chronic Pancreatitis Model in Rats

The combined high fat and alcoholic diet ingested greatly accelerates the induction of pancreatitis. Pancreatitis and the accompanying abdominal and bilateral footpad hypersensitivity develop within 3 weeks. This makes the study economically feasible with commercially available rats. The chronic model in Fisher rats is a significant improvement over our previous model in Lewis rats. It is also a significant improvement over other methods that use alcohol that may take up to 6 months to develop and require higher levels of alcohol with inconsistent results (see Note 12).

Histological signs of chronic pancreatitis, specifically intraductal fibrosis and inflammatory infiltrates, are evident by 3 weeks with the model described here (Fig. 2c). RANTES was still elevated 10 weeks after initiation of the high fat and alcohol diet. Behavioral testing with the hotplate confirmed sensitized responses are fully developed by 3–4 weeks (Fig. 5) (9). However, the hypersensitivity persists significantly longer than with other models tested, i.e., through the 10 weeks tested with no mortality (see Note 9).



**Endothelin receptor A (ETR-A) stain in the thoracic DRG of control rat and DBTC induced pancreatitis rat**

Fig. 4. Endothelin A receptor is shown localized in rat thoracic dorsal root ganglia (DRG) on day 7 after induction of pancreatitis with DBTC. ET-A staining in DRG of naïve animals appeared to be significantly less.

The chronic pancreatitis model has also been used to determine the time course of reduced hypersensitivity provided by herpes viral vector preproenkephalin overexpression products (9). The overexpression of met-enkephalin significantly reduces the hypersensitivity for over 4 weeks.

### *3.3.3. Comparison of the Acute and Chronic Pancreatitis Models for Rats*

Interestingly, mechanical or thermal stimulation evokes sensitized responses testable on the abdomen in the acute DBTC model and on the paws in the chronic diet-induced pancreatitis model. The pancreas of rat is innervated by axons sending central projections primarily to T8–T12. Thus, the cutaneous stimulation on the abdomen is a referred pain region, and the regional sensitivity is not dissimilar to that reported in humans in a band across the

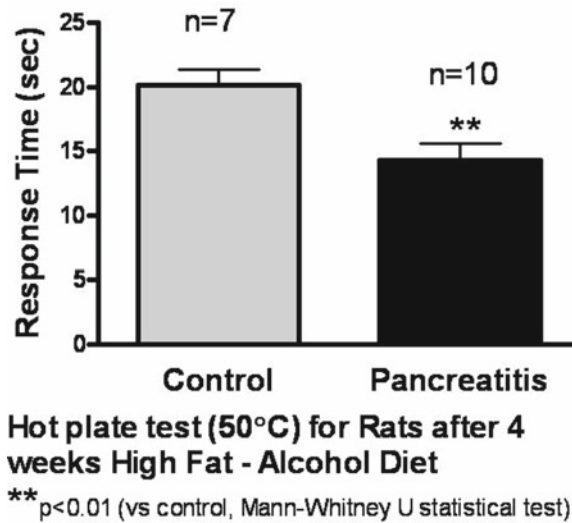


Fig. 5. The response times to hotplate are shown for control rats and rats fed the high fat and alcohol diet for 4 weeks. Responses times that are significantly less for the animals with pancreatitis for 3–6 weeks indicate hypersensitivity of the animals fed the high fat and alcohol diet.

abdomen and onto the back and shoulder. Hypersensitivity evident on both footpads in the chronic diet-induced pancreatitis model in Fisher rats is evidence of central sensitization. Footpad sensitivity is not present in the acute DBTC model nor was it found in the chronic alcohol and high fat diet model when induced in Lewis strain rats as previously reported (9).

Abundant cFos is evident in laminae X around the central canal in both of the pancreatitis models (9, 10), implying that this rarely discussed region is involved in pain processing and/or autonomic responses to the visceral insults.

## 4. Notes

### *Notes about the acute pancreatitis model*

1. The injection of DBTC into the tail vein of rats must be done carefully. Leakage of DBTC into the subcutaneous tissue may lead to tissue ulceration and necrosis. This point must be emphasized. While some animals may recover after 1 week, others may succumb to multi-organ failure, thus euthanasia immediately after the study is recommended.
2. It is recommended to use an IV catheter (BD Insyte-N auto-guard winged, 24GA 0.56 in.) for the tail vein injection, as this catheter fits very well into the thin tail vein of the rat. It is also

recommended to immerse the tail of the rat into warm water (35–40°C) to produce vasodilation and make it easier to inject the tail vein.

3. Another method for tail vein injection is to use a microdialysis pump. When the rat is anesthetized, put the IV catheter into the freshly cleaned (with alcohol pad) tail vein. Once the catheter is installed, pull the needle out (to collect at least 0.5 cc of blood in a tube by milking its tail for serum verification of altered amylase levels) and replace it with the connector/interlink that is attached to the pump. Turn the pump on and tape the tubing to the gauze roll, placed underneath the tail (to keep it elevated and in one place). Let the pump run until the allotted amount of either vehicle or DBTC has gone through to the rat (about 200–250 µl), usually about 10 min. Watch closely toward the end. Press stop and disconnect the rat. With a sterile gauze pad, put gentle pressure on the rat's tail to stop the bleeding or apply a styptic powder.
4. It is important not to test the same spot on the foot or abdominal area, as this might lead to sensitization of the responses. Testing can be repeated after 10 min in the same animal. Shaving the abdomen decreases the standard error, assuming the procedure does not sensitize the abdomen.
5. To make PBS: Add 13.4 g of sodium phosphate dibasic and 8 g of sodium chloride to 900 ml of distilled water. Stir until dissolved. Obtain a pH of 7.4 by slowly adding 2 N hydrochloric acid to the mixture. Bring to a final volume of 1 L with distilled water. Store at 4°C.
6. To make 4% paraformaldehyde: Heat 500 ml distilled water to 55°C and then add 40 g of paraformaldehyde. Stir until dissolved. Carefully add 2 N sodium hydroxide until the solution clears. Cool to room temperature and filter (filter paper #2). Add 500 ml of PBS and stir. Store at 4°C up to 1 week. It is best to use freshly prepared (unpolymerized).
7. For the histological procedures, a basic protocol that can be followed for the H&E staining appears below for paraffin-embedded pancreas sections, which provide the best histological preservation and can typically be immunostained first as well. For frozen sections, begin the staining at step 4.

Hematoxylin and Eosin tissue staining:

1.	Xylene	2 × 3 min
2.	100% Alcohol	2 × 1 min
3.	95% Alcohol	2 × 1 min
4.	Running water	5 min
5.	Hematoxylin	6 min

6.	Running water	5 min
7.	Acid alcohol	20 dips
8.	Running water	5 min
9.	Bluing (Scott's water or ammonia water)	20 dips
10.	Running water	5 min
11.	95% Alcohol	20 dips
12.	Eosin	12 min
13.	80% Alcohol	20 dips
14.	95% Alcohol	2 × 20 dips
15.	100% Alcohol	2 × 20 dips
16.	Xylene	2 × 20 dips
17.	Xylene	Coverslip

8. The protocols for the chemicals to be used for the H&E staining are as follows:

1. Harris' hematoxylin (always filter before use).
2. 1% Stock alcoholic eosin

Eosin Y, water soluble	1 g
ddH <sub>2</sub> O	20 ml
Dissolve and then add: 95% Alcohol	80 ml (64 ml 100% Alcohol + 16 ml ddH <sub>2</sub> O)

#### Eosin working solution

1 part of Eosin stock solution	60 ml
3 parts of 80% Alcohol	180 ml (144 ml 100% Alcohol + 36 ml ddH <sub>2</sub> O)
Just before use add: Glacial acetic acid	0.5–100 ml Eosin working solution; stir 1.2–240 ml

3. Acid alcohol

70% Alcohol	100 ml (70 ml 100% Alcohol + 30 ml ddH <sub>2</sub> O)
Hydrochloric acid	1–2.5 ml

## 4. Ammonia water (we used)

Tap water	100 ml
Ammonia hydroxide	0.2–0.3 ml

## 5. Scott solution

Sodium bicarbonate	2 g
Magnesium sulfate	20 g
ddH <sub>2</sub> O	1,000 ml
Add a pinch of thymol to retard mold.	

*Notes about the chronic pancreatitis model*

9. A body weight of 80–90 g for a rat will be the ideal weight after the prescribed 1 week IACUC acclimatization period and subsequent diet transition week without alcohol. If the diet is begun in rats weighing less than 125 g, the risk of mortality is increased due to alcohol dehydration and nutritional deprivation of rapidly growing juvenile rats (slack neck skin and ruffled fur). In all cases, animals are supplemented with lard to prevent severe weight loss and alfalfa to provide vitamin K during the critical second week of the alcohol diet.
10. While the diet as commercially sold is nutritionally complete, animals should nonetheless be monitored carefully for weight loss or dehydration. While water is supplied ad libitum, the addition of alfalfa on Days 10–14 to supplement vitamin K and the lard supplement on Days 1–14 will provide adequate weight gain and general health for the rats.
11. The diet must be administered from normal stoppered feeding bottles, but the tube must be kept clear with a toothpick to guard against being stopped up. Other delivery means are subject to alcohol evaporation, as well as failure to produce pancreatitis and accompanying hypersensitivity. The liquid food which is more expensive should be supplied in minimally adequate and increasing amounts supplied fresh every other day in clean bottles as the animals grow in this chronic model. Any extra diet must be stored at 4°C in a tightly covered container (such as the apple juice jug), but not kept longer than 1 week.
12. A similar model has been described previously with home-made high fat chow in an in-bred rat strain by a group in Japan (11). Alternatively, the commercially available Lieber-DiCarli diet which has 36% of its calories from ethanol may be used to produce the pancreatitis. We suggest the lard supplements and 6% alcohol diet we describe.

13. The chronic model was originally described (9, 10) for Lewis rats bred at the Harlan Houston facility prior to hurricane Ike in 2007. These animals were responsive only on the abdomen, but are no longer available. Fisher rats from Harlan (Indianapolis) are now used in the chronic pancreatitis study since the pancreatitis model with hypersensitivity is also consistently produced when these rats are given the high fat and alcohol diet. Fortuitously, the high fat and alcohol diet produces hypersensitive nociceptive responses to stimuli on the shaved abdomen *and* on both footpads. Thus, conventional pain testing with von Frey fibers applied onto the footpad can be utilized. Responses are sensitized on both feet in this visceral pain model.
14. Alcohol diet models in adult rats take longer period to produce (~8 months), provide inconsistent results, are time consuming and expensive. While ingestion or gavage of high percentages of alcohol (>10%) is used by others studying alcohol effects on brain function, these methods cannot be used to induce prolonged animal models of pancreatitis for pain study since the animals are stuporous and the alcohol is toxic.
15. Data produced in alcoholic rats may be complicated by somnolence or withdrawal effects depending on the experimental paradigm employed, however the alcohol diet model described here is reasonably resistant to these complications since the final alcohol percentage is 6% and the alcohol diet is removed for 4–6 h prior to behavioral testing. Withdrawal effects are most severe prior to this time (30 min to 3 h).

## References

1. Merkord, J., Jonas, L., Weber H., Kroning, G., Nizze, H., Hennighausen, G. (1997) Acute interstitial pancreatitis in rats induced by dibutyltin dichloride (DBTC): Pathogenesis and natural course of lesions. *Pancreas* **15**, 392–401.
2. Sparmann, G., Merkord, J., Jaschke, A., Nizze, H., Jonas, L., Lohr, M., Liebe, S., Emmrich, J. (1997) Pancreatic fibrosis in experimental pancreatitis induced by dibutyl dichloride. *Gastroenterology* **112**, 1664–1672.
3. Schmidt, J., Compton, C.C., Rattner, D.W., Lewandrowski, K., Warsaw, A.L. (1995) Late histopathological changes and healing in an improved rodent model of acute necrotizing pancreatitis. *Digestion* **56**, 246–252.
4. Head, H. (1896) On disturbances of sensation with especial reference to the pain of visceral disease. *Brain* **19**, 11–276.
5. Giamberardino M.A., Affaitati, G., and Constantini, R. (2006) Referred pain from internal organs. In: **Ch. 24, Handbook of Clinical Neurology**, F. Cervero and T.S. Jensen, eds. Elsevier B.V., pp. 343–361.
6. McMahon, S.B., Dmitrieva N., Koltzenburg M. (1995) Visceral pain. *Br. J. Anaesth* **75**(2), 132–144.
7. Vera-Portocarrero, L.P., Lu, Y., Westlund, K.N. (2003) Nociception in Persistent Pancreatitis in Rats: The Effects of Morphine and Neuropeptide Alterations. *Anesthesiology* **98**(2), 474–484.
8. Vera-Portocarrero, L.P., Westlund, K.N. (2004) Attenuation of nociception in a model of acute pancreatitis by an NK-1 antagonist. *Pharmacol. Biochem. Behav.* **77**, 631–610.
9. Yang H., McNearney T.A., Chu R., Lu Y., Ren Y., Yeomans D.C., Wilson S.P., Westlund K.N. (2008) Enkephalin-encoding herpes simplex

- virus-1 decreases hyperalgesia and inflammation in a chronic pancreatitis model induced by a high-fat and alcohol diet. *Molecular Pain* **4**(1), 8(1–21).
10. Lu, Y., McNearney, T.A., Lin, W., Wilson, S.P., Yeomans, D.C., Westlund, K.N. (2007) Treatment of inflamed pancreas with enkephalin encoding HSV-1 recombinant vector reduces inflammatory damage and behavioral sequelae. *Mol. Therapy* **15**, 1812–1819.
  11. Tsukamoto, H., Towner, S.J., Yu, G.S., French, S.W. (1988) Potentiation of ethanol-induced pancreatic injury by dietary fat. Induction of chronic pancreatitis by alcohol in rats. *Am. J. Pathol.* **131**, 246–257.

## The Monosodium Iodoacetate Model of Osteoarthritis Pain in the Rat

Cheryl L. Marker and James D. Pomonis

### Abstract

Osteoarthritis (OA) is one form of degenerative joint disease characterized by progressive loss of articular cartilage, decreased function and is frequently accompanied by chronic pain. Given the success of arthroplasty as a treatment for late-stage OA, there is considerable interest in developing therapies pertaining to the management of pain associated with OA as well as therapies designed to slow or reverse the progression of the disease. To this end, establishment of relevant animal models that are amenable to testing novel therapies is of considerable value to the scientific community. Here, we describe a model of OA-related pain in which progressive joint destruction is induced by injection of monosodium iodoacetate into the articular space of the knee of the rat. Further, we describe three different methods to measure pain-related behaviors in this model: hind limb weight bearing, primary mechanical hyperalgesia, and hind limb grip strength.

**Key words:** Osteoarthritis, Degenerative joint disease, Weight bearing, Hyperalgesia, Grip strength

---

### 1. Introduction

Osteoarthritis (OA) is one member of the family of degenerative joint diseases, which together are commonly referred to as arthritis. OA is characterized by progressive destruction of articular cartilage and is frequently accompanied by chronic pain. OA has a high prevalence, with an estimated 27 million Americans suffering from the disease in 2005 according to the Centers for Disease Control (1). This high prevalence, combined with the fact that age is the greatest risk factor for OA (2), have kept a significant level of interest in developing new therapies for the management of OA-related pain.

Although several animal models of OA have been in use for quite some time, such models had primarily been used to investigate the potential etiology of the disease, and had not focused on their utility as models of the pain associated with OA. One potential

reason for the paucity of behavioral studies pertaining to OA-related pain may have been due in part to the fact that the vast majority of assays used for the assessment of pain-related behaviors focused on altered nociceptive thresholds (allodynia or hyperalgesia) in the hind paw. Given that experimentally induced OA typically employs the knee joint, investigation of sensitivity to mechanical or thermal stimuli in the hind paw appears to lack face validity. Further, in patients presenting with OA of the knee, sensitivity in the foot ipsilateral to the affected joint is rarely, if ever, reported.

As such, behavioral assays that are more sensitive to musculoskeletal (rather than cutaneous) nociceptive input are considered by many to be critical for developing predictive animal models of human OA-related pain. Here, we describe three approaches for the assessment of pain-related behaviors that can be used in a variety of models of OA in the rat.

---

## 2. Materials

### **2.1. Animals and Induction of OA**

1. Male, Sprague–Dawley rats weighing approximately 150–175 g at the time of OA induction.
2. Monosodium iodoacetate (MIA) dissolved in isotonic saline to a final concentration of 40 mg/mL. Note: MIA is highly toxic and all appropriate personal protective equipment should be worn while handling the powder or solution. Also, store MIA powder in a dessicator and prepare solution for injection fresh as needed.
3. 1-cc or smaller syringes fitted with 27 gauge, ½-in. needles.
4. Isoflurane and induction system or other method of rodent anesthesia.

### **2.2. Behavioral Assessment**

1. Hind limb weight bearing device (Linton Incapacitance Tester or similar)—and/or—
2. Digital paw pressure Randall-Selitto instrument and accompanying sling suit (IITC Life Science)—and/or—
3. Grip strength meter with modification for the measurement of hind limb grip strength (IITC Life Science or similar).

---

## 3. Methods

There are several methods (either chemical or surgical) that can be used to induce joint degeneration in rats that mimic what is seen in human OA. For the purposes of this chapter, we focus exclusively

on intra-articular injection of MIA as a chemical means of inducing an OA-like pathology in rats. However, even if other chemical or surgical methods are employed, the methods described for behavioral assessment are still applicable to these models as well. MIA is a selective inhibitor of glyceraldehydes-3-phosphate dehydrogenase, a critical enzyme in the Krebs Cycle. As such, injection of MIA into the synovial space of the joint results in profound chondrocyte toxicity—not due to any affinity of MIA to this cell type, but rather due to the abundance of these cells in the articular space. The death of the chondrocytes leads to thinning of and lack of cellularity in articular cartilage, appearance of subchondral bone spicules (osteophytes) and occasional separation of the articular cartilage from the subchondral bone.

When initially establishing these models in a laboratory, it is important to characterize the time course of each behavioral endpoint (weight bearing, primary mechanical hyperalgesia, and grip strength) in order to understand when pain-related behaviors are most stable and when investigational therapies can be applied. In the case of MIA-induced OA, there is an immediate period of hypersensitivity that resolves within approximately 7 days after MIA injection, which likely is due to acute inflammation and/or irritation of the knee joint and does not reflect any pathology relating to OA per se. Importantly, this early phase is followed by a chronic and progressive period of pain-related behaviors beginning approximately 10 days after MIA injection (3–6, Fig. 1a).

The success of using the MIA model (or any other model of OA) in subsequent studies is, of course, verification of the development of joint degeneration if possible, dependent upon or at the very least, the presence of pain-related behaviors. While the injections of MIA into the joint are not technically difficult, the joint capsule can be pierced during injection, resulting in leakage of the MIA outside of the capsule, and the subsequent failure to induce toxicity of the chondrocytes. Confirmation of MIA-induced joint destruction can be achieved using either standard histological techniques, such as H&E staining, or by gross observation of the patella, femoral groove, femoral chondyles, and tibial plateaus as described by Guingamp et al. (3). Initial studies should compare MIA-injected joints to saline-injected joints, but the addition of a saline-treated (sham) group should not be necessary for most studies once the model has been validated in your laboratory.

### **3.1. Animals and Induction of OA**

1. Prior to injection of MIA, pre-injury baseline values for the behavioral endpoint(s) to be assessed may be measured.
2. The total volume of solution that will be injected into the synovial space of the joint is 50  $\mu$ L. The recommended amount of MIA injected in this volume is 2 mg, but can be adjusted anywhere in the range of 1–3 mg.

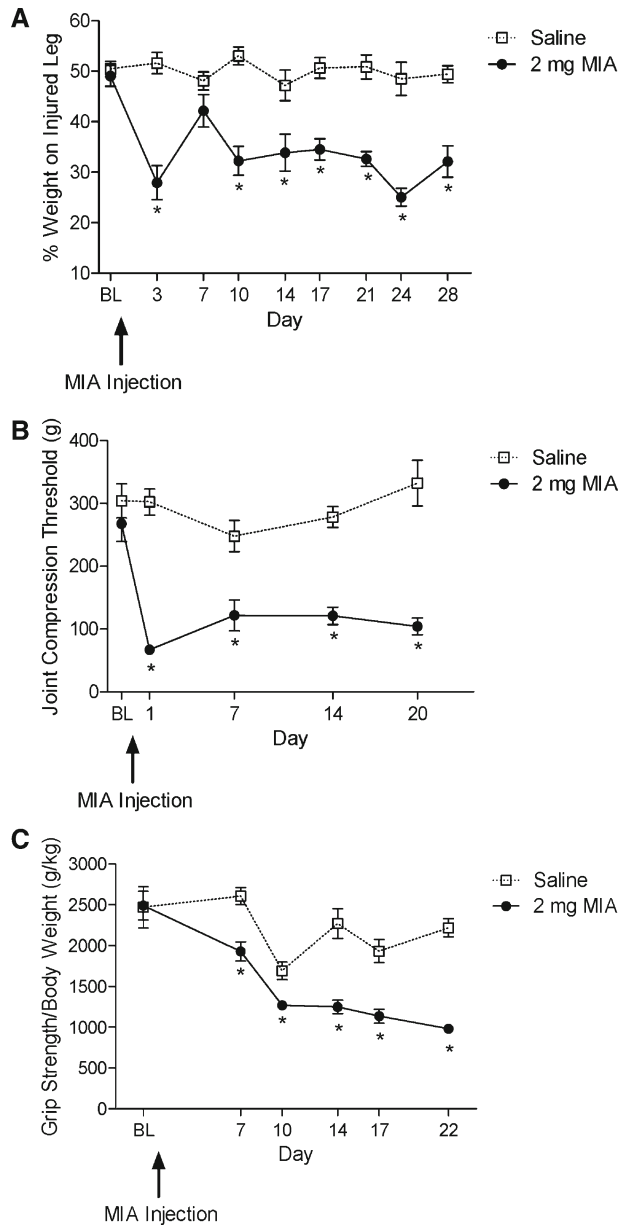


Fig. 1. Time course of the development of OA-related pain behaviors in the MIA model of OA in the rat. Intra-articular injection of 2 mg MIA produces significant and prolonged behavioral changes indicative of OA-related pain including alterations in hind limb weight bearing (a), primary mechanical hyperalgesia at the affected knee (b) and decreased hind limb grip strength (c).

3. Under isoflurane anesthesia, place the rat on its back and hold one hind limb at approximately a 90° angle.
4. Inject the MIA into the synovium of the knee by inserting the needle through the patellar tendon. Inject the entire volume

(50  $\mu$ L) slowly, over a period of approximately 10 s. Slowly remove the needle and briefly hold a piece of gauze over the injection site to minimize backflow and leakage (see Note 1).

5. Place the rat on a warming pad or under a heat lamp until recovery from anesthesia.

### **3.2. Assessment of Hind Limb Weight Bearing**

1. These instructions assume that a Linton Incapacitance Tester (Linton Instruments, UK) will be used for measuring hind limb weight bearing. Similar equipment can be purchased from other manufacturers or vendors, and the steps should be similar regardless of what model is used.
2. Tare and calibrate the unit at the beginning of each day as per manufacturer's instructions. If the unit does not tare or calibrate properly, the balance pads may need to be removed and cleaned with a mild soap and alcohol to remove any residue causing the pads to stick to the sides of the apparatus.
3. Following the manufacturer's instructions, set the duration of time for each recording session to 3 s.
4. Leave the animals in the testing room for at least 30 min prior to beginning any testing.
5. Insert the rat into the restraint chamber and allow the animal to acclimate to the environment prior to taking the first reading. This may take several minutes. In order for the animal's posture (and hence, the subsequent reading) to be considered valid, each hind paw must be placed solely on the respective balance pad, both front limbs either resting on the front, slanted portion of the chamber, or not resting on any portion of the chamber at all. Further, the animal must be facing forward without any noticeable lateral curvature of the spine (Fig. 2 and see Note 2).
6. For each time point tested, record a total of three measurements, ensuring that the animal is calm and displaying correct posture as stated in step 3 above.
7. For each reading, record the weight borne for each hind limb.
8. When analyzing data, the percent weight bearing score (%WBS) is calculated for each reading using the following formula:  $\%WBS = [\text{weight on injured leg} / (\text{weight on uninjured leg} + \text{weight on injured leg})] \times 100$ . Apply this formula for each trial, and determine the mean %WBS for each rat at each time point using all three readings (Fig. 1a and see Note 5).

### **3.3. Assessment of Primary Mechanical Hyperalgesia**

1. These instructions assume that a digital paw pressure Randall-Selitto instrument (IITC Life Science) with a blunted (0.5 cm) tip is used, but may be adapted to work with other, similar devices.
2. Leave the animals in the testing room for at least 30 min prior to beginning any testing.

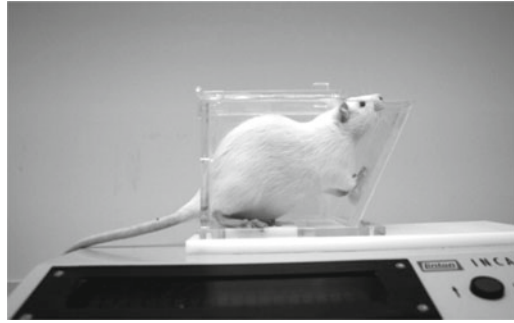


Fig. 2. Evaluation of hind limb weight bearing in the rat. When assessing hind limb weight bearing, the positioning of the animal in the chamber is critical to obtaining accurate and reliable readings. Ensure that, as in this photograph, the rat is facing forward with the fore paws either resting on the sloped, front aspect of the chamber (or are not touching any other surface). Each hind paw should be placed entirely on each balance pad, the animal is not resting against one side of the chamber, and if possible, the tail should extend through the opening in the back of the chamber. Three readings per time point should be taken for each animal.

3. Place the animal in the sling suit with the hind limbs through the holes and secure the back closure. If necessary, gently pull the hind limbs through the holes so that the joint to be measured is exposed and readily accessible (Fig. 3a and see Note 3).
4. Gently grasp the paw of the limb to be tested in one hand and gently place the caliper heads on the medial and lateral aspects of the joint, being careful to ensure that the caliper does not slip off the joint (Fig. 3b).
5. Slowly increase the pressure on the joint until a nocifensive response is observed and record the maximum force applied. Nocifensive responses include an attempt to withdraw the joint from the caliper, vocalization, or other struggle.
6. The maximum pressure to be applied is 500 g, at which point the testing session is terminated and a value of 500 is recorded (see Note 5).
7. Repeat steps 4–6 above for the other (contralateral) joint.

### **3.4. Assessment of Hind Limb Grip Strength**

1. These instructions assume the use of a grip strength meter (IITC Life Science) that has been adapted with a piece of plexiglass to prevent the animal from grabbing the mesh with its forepaws (Fig. 4).
2. Leave the animals in the testing room for at least 30 min prior to beginning any testing.
3. Weigh each animal prior to the first testing session on a given day.
4. Allow the animal to enter the enclosure head first while maintaining a grasp on the base of the tail.

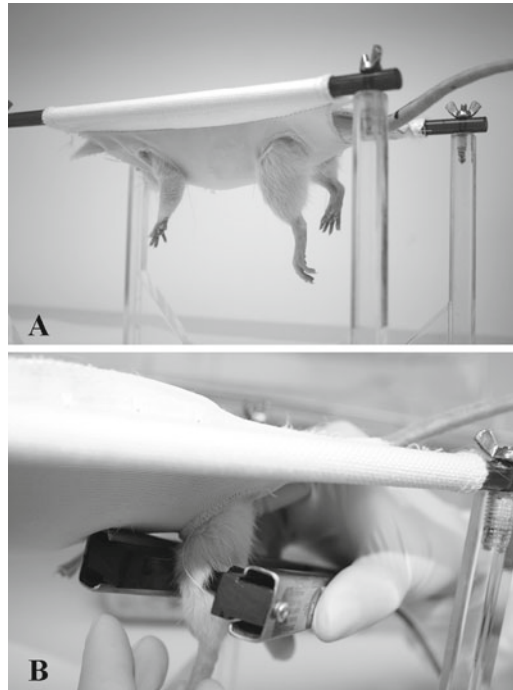


Fig. 3. Evaluation of primary mechanical hyperalgesia of the knee in the rat. In order to assess primary mechanical hyperalgesia in the knee, the rat must first be restrained in a sling suit to both immobilize the animal and allow access to the joint. When placing the animal in the sling suit, ensure that each hind limb extends completely through the holes in the suit (a). To assess mechanical hyperalgesia, gently grasp the paw with your free hand and place the calipers on the medial and lateral aspects of the joint (b) while gradually increasing the applied pressure until a nocifensive behavior is observed.

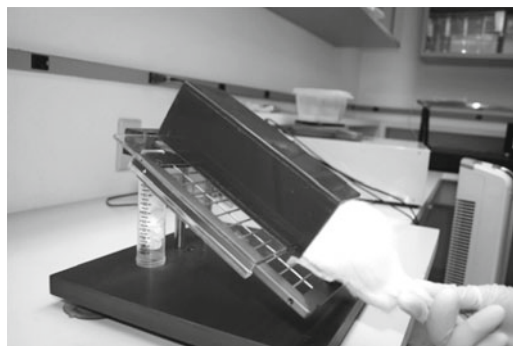


Fig. 4. Evaluation of hind limb grip strength in the rat. The commercially available device has been modified by creating a plexiglass cover and enclosure to prevent the animal from grasping the mesh with its fore limbs. When the animal is in the enclosure, gently pull the tail until the animal begins to grip the mesh with both hind paws. At this point, gently but firmly pull on the tail, parallel to the mesh until the animal releases its grip on the mesh.

5. Gently pull the animal by the base of the tail until both hind paws are gripping the mesh (Fig. 4 and see Note 4).
6. Stop pulling on the tail and zero the instrument.
7. Gently pull the animal by the tail parallel to the mesh until both hind paws are no longer gripping the mesh.
8. If the affected paw (ipsilateral to MIA injection) releases well before the nonaffected paw, the reading is considered invalid and should be repeated.
9. Record the grip strength from the device display.
10. When analyzing data, express data as grip strength per kilogram of body weight (Fig. 1c). This is especially important when testing animals over multiple days during the rapid growth phase as absolute grip strength values will increase as the animal grows (see Note 5).

---

## 4. Notes

### 1. Intra-articular injections

- (a) For training purposes, inject dye (e.g., Evans blue) into the joint and do an immediate postmortem dissection to verify the presence and confinement of the injectate in the intracapsular space.
- (b) Hair can be plucked from knee to make the injection site easier to see.
- (c) For intra-articular injections, the needle should go in about 1/8th in. before hitting bone. If you feel the needle hit bone after piercing the patellar tendon, pull the needle back slightly and inject as described.
- (d) For intra-articular injections, hold the leg bent with the index finger behind the joint and the thumb on the anterior surface of the ankle pulling gently upward to open up the joint.
- (e) MIA is most often injected into the knee, it can also be injected into other weight bearing joints. In particular, we have found the ankle to be a suitable alternative to the knee. The protocols for using the ankle in place of the knee are identical with the exception of the injection itself. To inject into the ankle, hold the leg with the paw flexed and inject on the lateral side behind the tendon and slightly above the ankle.

### 2. Hind limb weight bearing

- (a) Upon first exposure to the weight bearing device, animals typically show significantly elevated levels of exploratory

behavior. It is therefore recommended that the first behavioral assessment time point be done prior to MIA injection.

- (b) It is preferable that the animal's tail extend out through the hole in the back of the restraining chamber. However, this is not critical, especially with animals weighing less than 200 g. If the tail does not extend out through the restraining chamber, be sure that the animal is not standing on the tail or using it in any way for support.
- (c) When possible, allow the animals to readjust their posture between each of the three readings, but do not remove them from the chamber.

### 3. Joint compression with the digital Randall-Selitto device

- (a) Situate the animal in the sling suit with as little stress as possible and keep them in the suit for as short a time as possible.
- (b) Do not put the front legs through the holes as this only increases stress and the amount of time the animal is in the suit.
- (c) If the animal struggles while in the suit, cover the front of the suit with your free hand to calm the animal.
- (d) Place the flat side of the dRS device against the medial side of the joint and slowly close the device onto the lateral surface.
- (e) The knee is more difficult to test than the ankle because of the increased muscle mass. The device must be placed on the joint, not the muscle. Therefore, early training and validation approaches may best be performed applying the above procedures to the ankle before moving to the knee.
- (f) Make sure the entire leg (to the hip) is through the hole when measuring at the knee (this is not necessary for measuring at the ankle).
- (g) To help keep the device from sliding off the knee, you can place the index finger of the hand holding the paw very gently on the patella (be sure not to close the device on your finger).

### 4. Hind limb grip strength

- (a) Use your free hand to catch the animal after it releases from the grid.
- (b) Preinjury readings are important for this model to assess pain state.
- (c) Make sure you are watching the output, as sometimes after the animal releases the grid with its hind paws, it will grab with the front paws and increase the score.

- (d) Make sure you are pulling at the same angle as the grid. Pulling down or up will alter the score.
  - (e) Inspect paws after each reading, the animals can lose toenails.
  - (f) Be sure the animal is actually gripping the grid with the ipsilateral side throughout the whole reading.
5. All data collected using the methods described above can be analyzed using standard parametric statistical tests.

## References

1. Center for Disease control [http://www.cdc.gov/arthritis/data\\_statistics/arthritis\\_related\\_stats.htm](http://www.cdc.gov/arthritis/data_statistics/arthritis_related_stats.htm)
2. Elders, M. J. (2000) The increasing impact of arthritis on public health *J Rheumatol* **60**, 6–8.
3. Guingamp, C., Gefout-Pottie, P., Phillipe, L., Terlain, B., Netter, P., and Gillet, P. (1997) Mono-iodoacetate-induced experimental osteoarthritis: a dose-response study of loss of mobility, morphology, and biochemistry *Arthritis Rheum* **209**, 1670–9.
4. Fernihough, J., Gentry, C., Malcangio, M., Fox, A., Rediske, J., Pellas, T., Kidd, B., Bevan, S., and Winter, J. (2004) Pain related behavior in two models of osteoarthritis in the rat knee *Pain* **112**, 83–93.
5. Pomonis, J. D., Boulet, J. M., Gottshall, S. L., Phillips, S., Sellers, R., Bunton, T., and Walker, K. (2005) Development and pharmacological characterization of a rat model of osteoarthritis pain *Pain* **114**, 339–46.
6. Chandran, P., Pai, M., Biomme, E. A., Hsieh, G. C., Decker, M. W., Honore, P. (2009) Pharmacological modulation of movement evoked pain in a rat model of osteoarthritis *Eur J Pharmacol* **613**, 39–45.

## K/BxN Serum Transfer Arthritis as a Model of Inflammatory Joint Pain

Christina A. Christianson, Maripat Corr, Tony L. Yaksh, and Camilla I. Svensson

### Abstract

In this chapter, we describe the usage of this rheumatoid arthritis model to investigate pain-like behavior in mice, including the assessment of clinical changes and the time-dependent changes in nociceptive behavior during disease progresses.

**Key words:** Rheumatoid arthritis, Persistent pain, Mice, Allodynia

---

### 1. Introduction

Chronic pain is a major health problem affecting approximately 20% of the population, resulting in markedly reduced quality of life for the individual as well as extensive costs for society. Approximately 1% of the population is diagnosed with rheumatoid arthritis (RA), a systemic autoimmune-mediated disease comprising synovial inflammation and matrix destruction. Swelling is particularly prominent in the small joints of the hands and feet. Pain is frequently the most egregious symptom reported and can persist after resolution of joint swelling with anti-inflammatory treatment. The inflammatory processes that result in rheumatoid arthritis are complex, with interactions among the cytokine network, autoantibodies, and the complement cascade. While the peripheral inflammation is an important component in generating pain in RA, the peripheral pathology cannot fully explain the amount of pain the arthritis patient experiences and facilitation of pain processing at the level of the spinal cord has been implicated (1). Despite the efficacy of new

therapeutics (e.g., TNF and interleukin blockers) and treatment strategies (e.g., combination therapies), pain is still a significant problem. In a recent survey, more than 85% of RA patients described their RA as somewhat completely controlled, yet greater than 75% of them reported moderate to severe pain within the previous 2 months (2). Drug development in the area of chronic inflammatory pain has hitherto been insufficient. Thus, it is critical to increase our understanding for how chronic pain emerges during and subsequent to joint inflammation and how it is regulated in order to identify new targets and treatment strategies for pain relief. Here, we describe protocols for the usage of the K/BxN serum transfer arthritis (K/BxN) model, a well-described mouse model of inflammatory arthritis with similarities to rheumatoid arthritis, which has been characterized for studies of pain mechanisms and evaluation of analgesics (3). We believe that this model will add significantly to the repertoire of experimental “inflammatory pain” models. There is great interest in preclinical surrogate models for human inflammatory pain states. Models based on intraplantar injection irritants, such as carrageenan and formalin, have great popularity for the study of pain mechanisms and pharmacology. However, many of these models have a limited time frame (hours to days). Thus, changes in pain-related processes during chronic diseases, such as RA, may not be revealed and therefore there is a need for more chronic and disease-relevant models.

The KRN mice are transgenic for a T-cell receptor that is cognate for a peptide derived from bovine pancreatic RNase (4). A request for a material transfer agreement for the use of these mice can be made through the Institut de Génétique et de Biologie Moléculaire et Cellulaire (Strasbourg, France) and Drs. D. Mathis and C. Benoist (currently, Harvard Medical School, Boston, Massachusetts, USA). Crossing KRN mice on the C57Bl/6 background with nonobese diabetic (NOD) mice generates K/BxN mice. These mice develop severe destructive arthritis that resembles human rheumatoid arthritis in many respects. Serum transfer from the K/BxN mice reliably induces transient inflammatory arthritis in the joints of a wide range of mouse strains (4) utilizing autoantibodies against glucose-6-phosphate isomerase (5). This broad susceptibility distinguishes the K/BxN serum transfer model from other common models of RA, e.g., the collagen-induced arthritis model. As recipient mice receive the same quantity of autoantibodies at the time of injection, the K/BxN serum transfer model has a predictable onset of clinical signs of arthritis. The clinical profile has a severe inflammatory phase that reliably resolves as the antibodies are cleared and not replaced by B cells. While well-established for disease-mechanistic studies in the RA field, the K/BxN serum transfer arthritis model is new as an experimental model of inflammatory joint pain. Mice injected with K/BxN serum display robust and highly reproducible mechanical allodynia with an onset that correlates

with joint and paw inflammation. Of importance, the mechanical hypersensitivity does not return to baseline concurrent with resolution of the joint swelling, but outlasts the inflammation by at least 2–3 weeks. Thus, this model provides an opportunity to study nociception not only during the ongoing joint inflammation, but also in the postinflammatory state.

---

## 2. Materials

### 2.1. Arthritis Induction and Scoring

1. Animals: Adult mice 25–30 g. This protocol is referring to male C57Bl/6 mice. K/BxN serum transfer is highly dependent upon the alternative complement pathway for arthritis development. Background strains have been screened for indications of clinical indices with Balb/c, C57Bl/10, PL, DBA/1, CBA, MRL/Mp, NZW, C3H/He, SJL, 120/Sv showing susceptibility to K/BxN serum transfer-induced arthritis, and DBA/2, FvB/N, NZB, and NOD showing no induction of arthritis (6). If strains other than C57BL/6 are preferred, pilot studies and appropriate controls are suggested as different strains may show different susceptibility to K/BxN serum-mediated induction of hypersensitivity (and arthritis) (see Notes 1 and 2).
2. K/BxN serum: Typically, 200  $\mu$ L per mouse total. See extensive protocols in refs. 7, 8 for the breeding and maintenance of the colony. Blood is collected either by complete exsanguination or by serial bleeding according to protocols as approved by local animal use committees. Blood is collected, briefly allowed to clot (10–20 min at room temperature), and then placed on ice. Samples are centrifuged for 5 min at  $5,000 \times g$  at 4°C and serum is pooled to produce maximal homogeneity of autoantibodies. Serum can be stored indefinitely at –70°C.
3. Control serum: Use serum from syngeneic mice and collect according to item 2. In this protocol, control serum is referring to serum collected from naïve C57Bl/6.
4. 1-cc plastic syringe with 23-G needle for intraperitoneal (i.p) injection of serum.
5. Calipers.

### 2.2. Behavioral Testing

#### 2.2.1. Von Frey

1. Von Frey stand with an elevated wire mesh surface with approximately  $\frac{1}{4}'' \times \frac{1}{4}''$ -square openings.
2. A clear plexiglass container placed on top of the wire mesh surface, in which to acclimate and test the mice. It must be large enough to allow the animals to turn around and tall enough that they cannot escape from it. A 3''  $\times$  3''-square box is sufficient.

3. Von Frey filaments (Stoelting. 0.04 g, 0.07 g, 0.16 g, 0.4 g, 0.6 g, 1.0 g, 2.0 g which correspond to 2.44 N, 2.83 N, 3.22 N, 3.61 N, 3.84 N, 4.08 N, 4.31 N).
4. Timer.

### 2.2.2. Thermal

1. Modified Hargreaves-type device: This includes a temperature-variable glass surface upon which the mice are placed and a triggerable, movable, focused heat source. Frequently, this heat source is attached to a mirror to allow for easy visualization of the heat source on the appropriate portion of the footpad. Here, we use a device from UARDG, Department of Anesthesiology, University of California, San Diego.
2. Clear plexiglass containers that can be placed on top of the thermal testing device. These must be large enough to allow the animals to turn around and tall enough that they cannot escape from it. A 3" × 3"-square box is sufficient.
3. Timer.

### 2.2.3. Activity

1. Individual cages modified to allow insertion in the shorter end of an infrared motion detector which is shielded by a wire screen to supplement cage integrity.
2. Infrared motion detector (here, we use model SL-5407A) to establish positional changes caused by changes in mouse heat signatures.
3. Multichannel switching box to power detectors and interface via USB with computer running DigSigMon software. This software measures triggers (input) and data collection (output). The current configuration records an activity score of 0 (minimum) to 15 (maximum) per minute, tallied every minute continuously 24 h a day for multiple days. The room dedicated for activity testing is on timed 12-h light and 12-h dark cycle.
4. Mice are housed one per cage, up to 15 cages monitored in a dedicated room.

---

## 3. Methods

### 3.1. Arthritis Induction and Scoring

#### 3.1.1. Prior to Serum Transfer, Determine the Ankle Thickness of Both Hind Limbs

1. Lightly scruff the mouse.
2. Place calipers over the thickest part of the ankle joint (malleoli) and lightly tighten until resistance. Read and record values. *Following arthritis induction, it is important to only tighten the calipers until they just touch the skin. The volume of edema present at the ankle from the arthritis can cause confound readings if it is compressed.*
3. Repeat every 1–3 days as desired.

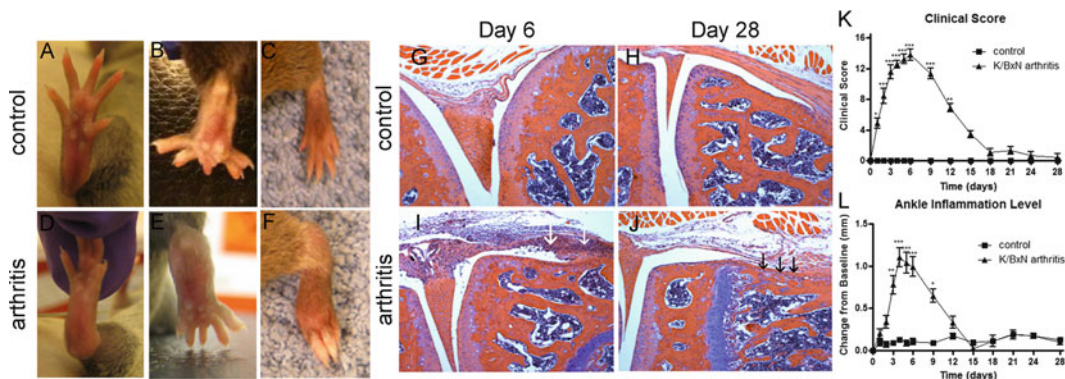


Fig. 1. Clinical and pathological signs following induction of K/BxN serum transfer arthritis. Images of footpads (a, b) and joints (c) from control serum-treated mice are readily differentiable from images of footpads (d, e) and joints (f) from K/BxN serum transfer arthritis. The swelling in arthritic mice is sufficient to make the ankle wider than the midfoot region and to produce distinct redness and swelling of individual knuckles. Histopathology of the knee joints from arthritic and control mice on days 6 and 28 was sectioned and stained with hematoxylin and eosin. There is a prominent inflammatory infiltration on day 6 in the mice that received K/BxN sera (i; white arrow) and residual bony erosions on day 28 (j; black arrow), which are absent in control sections (g, h). Representative images are shown (original  $\times 50$  magnification). Graphs display (k) arthritis clinical scores assessed for 28 days, demonstrating an increase in clinical signs of arthritis day 1–12 and (l) ankle thickness measured with calipers showing a significant ankle swelling in arthritic animals day 3–9. Each time point represents mean  $\pm$  SEM ( $n=9$  mice/group),  $*p<0.05$ ,  $**p<0.01$ , and  $***p<0.001$  by Bonferroni post-test. Panels g–l have been reproduced from ref. 3 with permission from the International Association for the Study of Pain (IASP).

4. Data can be reported as an increase (in mm) from baseline or as a percentage change from the baseline.

Ankle thickness and clinical scoring are usually maximal 4–8 days following induction of serum transfer. Panels a–c in Fig. 1 display three views of a control hind paw for comparison to panels d–f, which display views of a hind paw from a K/BxN serum transfer mouse on day 6 during maximal inflammation. These external indications of inflammation correspond to changes in the joint. In Fig. 1, panels g (day 6) and h (day 28), histology of ankle joints from control mice are contrasted to joints from K/BxN serum transfer arthritis mice, where the white arrows indicate inflammatory infiltrate in panel i (day 6) and black arrows indicate bone erosion in panel j (day 28). While clinical signs resolve, the ankle thickness frequently remains slightly elevated from baseline due to a combination of aging and the remodeling of the joints induced by K/BxN serum transfer arthritis (Fig. 1j, k).

### 3.1.2. Prior to Serum Transfer, Determine Clinical Scores

There are multiple methods of scoring the clinical signs of arthritis in this model. Here, we describe two methods with the most important facet of scoring being consistency in the observer. From day 2 to 3 after K/BxN serum injection, the inflammation is quite obvious and with practice the scoring is highly reproducible. It is recommended though, that for more subtle investigations concerning alterations in clinical scoring from drug or genotype, deviations are conducted by an experienced, blinded investigator.

1. Lightly scruff the mouse.
2. Carefully examine and record clinical signs according to method 1 or method 2 (described below).
3. Repeat scoring every 1–3 days at the same interval as ankle thickness and other parameters are recorded.
4. Data are presented as a total score per time point.

#### *Method 1*

Data presented in this protocol are recorded using method 1. For each of the four limbs (maximum four points per limb, up to a combined total of 16), score points (1–4) according to the presence of the feature with the greatest point value.

- 1 point if there is only redness of the bottom of the footpad
- 2 points if there is visible thickening of the paw
- 3 points if the swelling of the ankle is sufficient to make the ankle equal to or greater in width than the mid footpad
- 4 points if there is swelling of at least one digit

#### *Method 2*

This is an extended scoring protocol that is commonly used in the research laboratory. The clinical score ranges from 1 to 15 for each paw, with a maximum score of 60 per mouse, based on the number of inflamed joints in each paw and inflammation being defined by swelling.

- 1 point per swollen digit, with a maximum of 5 per paw
- 5 points if swelling is observed on the dorsal side of the mid-paw
- 5 points if swelling of the ankle is observed

#### *3.1.3. Arthritis Is Induced with Two 100 $\mu$ L i.p. Injections of K/BxN Serum*

1. Serum is stored frozen at  $-70^{\circ}\text{C}$ . Thaw and lightly spin down serum prior to injection. Debris may still be present and should be avoided during injections.
2. On day 0, lightly scruff the mouse so that the ventrum is exposed and the head is pointing downward; this causes the freely moveable abdominal organs to move toward the diaphragm, reducing the risk of accidentally puncturing internal organs.
3. Inject 100  $\mu$ L K/BxN serum or control serum i.p. Insert the 23-gauge needle into the abdominal cavity in the lower right quadrant of the mouse to avoid the cecum and urinary bladder. The needle should be directed toward the animal's head at an angle of  $15\text{--}20^{\circ}$  and inserted approximately 5 mm.
4. On day 2, inject 100  $\mu$ L K/BxN serum or control serum as described in Subheading 3.1.3.

Figure 1k shows a representative experiment in which the clinical score has been assessed with method 1. K/BxN serum-treated

arthritic mice display maximal inflammation on day 6 and resolution of clinical signs by day 18. Figure 1 shows that the increase in clinical score correlates with an increased ankle thickness in K/BxN serum transfer arthritic mice. Due to swelling of the limbs, mice with K/BxN serum transfer arthritis have reduced gripping ability as compared to control mice. Food should, therefore, be placed on the bottom of the cage to ensure adequate nutrition and to prevent body weight loss. Long sipper tubes in the water bottles may be needed. Serum from naïve mice of the same strain as used in the study is the most appropriate control serum. see Note 3 regarding serum potency and variability.

### 3.2. Behavioral Testing

#### 3.2.1. Von Frey

1. Habituation to testing device and baseline recordings. Mice are habituated to stay in the plexiglass containers for a minimum of an hour (depending upon strains; see Note 4) prior to testing. The experimenter must ensure that mice are calm and are no longer displaying exploratory behavior. We recommend to assess baseline thresholds with the same frequency as used in the experimental design, e.g., every third day, and to have a minimum of three baseline recordings prior to injection of K/BxN serum.
2. Multiple methods of testing mechanical hypersensitivity exist using von Frey filaments. We recommend the up-down method due to the reduced number of hair applications required.

The up-down method was originally developed for assessment of tactile allodynia in rats based upon Dixon (9). The method is described here only briefly.

Filaments are applied to the plantar surface between the tori for 5 s. A response results in clear and rapid lifting, shaking, or licking of the foot. Responses should be recorded from one side of all mice (i.e., left) before testing on the right. In instances where the mouse begins walking, jumping, or exploring, the testing is discontinued and resumed after a period of 5–10 min.

In mice, testing begins with the middle hair (0.4 g) of the following set (0.04 g, 0.07 g, 0.16 g, 0.4 g, 0.6 g, 1.0 g, 2.0 g) and hairs are applied to collect 6 total responses. The first two responses should straddle the threshold (no withdrawal and then a withdrawal, or vice versa) and the following four are recorded according to the idea that (1) if no withdrawal response is recorded a stronger stimulus should be presented and (2) if a withdrawal response is recorded then a weaker stimulus is to be presented. Using the formula published by Chaplan in ref. 10, the 50% g threshold =  $(10^{[x_f + k\delta]})/10,000$ , where  $x_f$  = value (in log units) of the final von Frey hair used;  $k$  = tabular value (see Appendix in ref. 10 for the pattern of positive/negative responses); and  $\delta$  = mean difference (in log units) between stimuli.

Baseline 50% withdrawal values vary between strains but are expected to fall between 1.3 g and the maximum of 2.0 g. A description of relative differences in baseline mechanical hypersensitivity

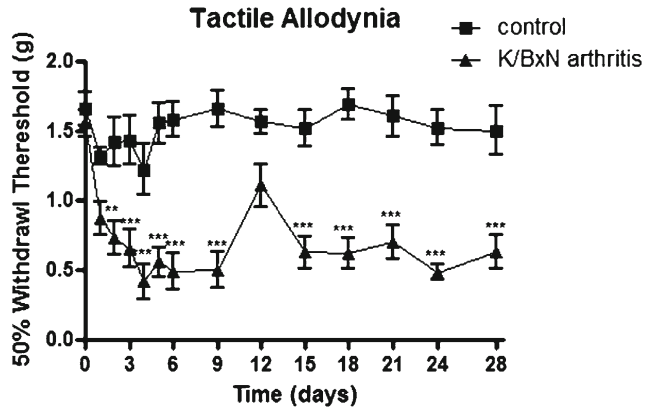


Fig. 2. Characterization of mechanical hypersensitivity in mice subjected to K/BxN serum transfer arthritis. Graph displays 50% tactile thresholds (g) showing tactile allodynia day 2–28 (excluding day 12). Each time point represents mean  $\pm$  SEM ( $n=9$  mice/group), \* $p<0.05$ , \*\* $p<0.01$ , and \*\*\* $p<0.001$  by Bonferroni post-test. Figure 2 has been reproduced from ref. 3 with permission from the International Association for the Study of Pain (IASP).

can be found in 11, with A/J, AKR/J, and BALB/c demonstrating high mechanical sensitivity at baseline and C57Bl/6, CBA/J, and SM/J the lowest baseline sensitivity. Data can be graphed as either (a) 50% threshold values or as (b) percent change from baseline.

Figure 2 shows a representative experiment in which the mechanical hypersensitivity was assessed with the up–down method in control and K/BxN serum transfer arthritic mice over a 28-day time period.

### 3.2.2. Thermal

1. Mice are acclimated in their plexiglass containers for a minimum of an hour (depending upon strains; see Note 4) prior to testing. The experimenter must ensure that mice are calm and are no longer displaying explorative behavior.
2. Here, we assess thermally evoked paw withdrawal responses using a Hargreaves-type testing device (12) (UARDG, Department of Anesthesiology, University of California, San Diego, 92103-0818).
  - (a) Allow the glass surface to reach 30°C.
  - (b) Initiate the thermal nociceptive stimulus (here, a focused projection bulb under the glass surface) coincident with starting the timer.
  - (c) Terminate the stimulus and timer upon a brisk withdrawal of the paw.

Thermal latency is defined as the time required before withdrawal and is measured in seconds. Prior to experimental onset, change in the stimulus intensity can be achieved by altering the amperage of the bulb. Average baseline values typically fall within

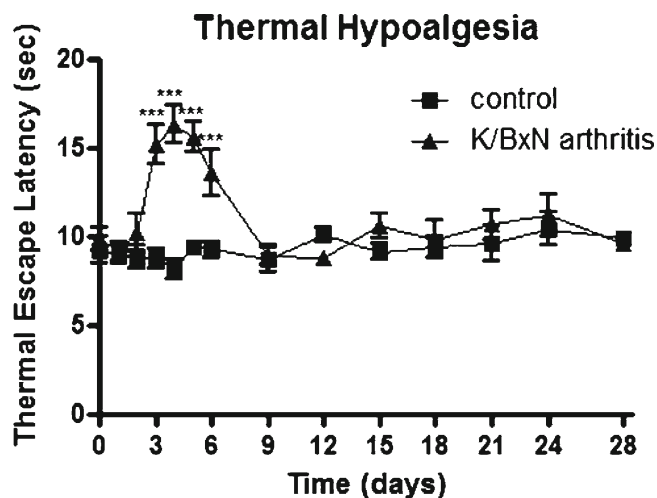


Fig. 3. Characterization of thermal sensitivity induced by K/BxN serum transfer arthritis. Graph displays thermal thresholds (s) demonstrating that arthritic animals display thermal hypoalgesia day 3–6, with no other changes from baseline. Each time point represents mean  $\pm$  SEM ( $n=9$  mice/group), \* $p<0.05$ , \*\* $p<0.01$ , and \*\*\* $p<0.001$  by Bonferroni post-test. Figure 3 has been reproduced from ref. 3 with permission from the International Association for the Study of Pain (IASP).

8–12 s. To prevent thermal exposure damage, a cutoff time of 20 s is recommended. Figure 3 shows representative thermal sensitivity recordings spanning 28 days for control and K/BxN serum transfer arthritic mice. K/BxN serum transfer arthritic mice display hypo-sensitivity during day 3–6 post serum transfer as compared to control mice.

### 3.2.3. Activity

Measurement of mouse activity records a spontaneous index. A loss of activity may be secondary to disability, pain resulting from movement or a combination of both. In Fig. 4, the typical activity count during the dark cycle for control and K/BxN serum transfer arthritic mice is displayed. K/BxN serum transfer arthritic mice have a reduced dark cycle activity during day 2–8 following serum transfer.

1. Habituate mice individually in cages with motion detector attached. Recording should be taken from mice for at least 3–7 days prior to experimental onset to ensure accurate baselines.
2. Initiate arthritis as per instructions in Subheading 3.1. Care should be taken to handle mice as little as possible during activity monitoring experiments. If possible, injections should be given during the beginning of the light cycle (see Note 5).
3. Always dedicate one motion detector to monitor background room activity. It can be particularly useful to have a record of staff entering and exiting the room to correlate to any unexpected activity changes.

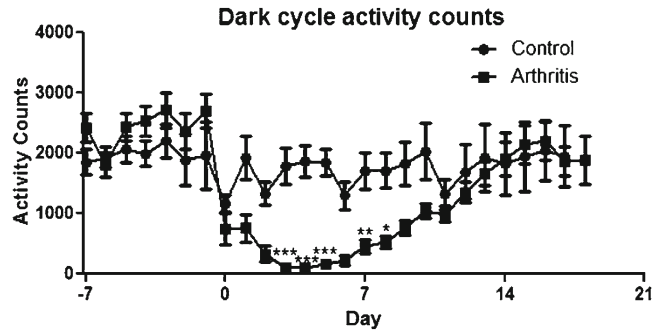


Fig. 4. Activity monitoring in control mice and mice subjected to K/BxN serum transfer arthritis. Graph displays activity counts registered during the 12-h dark cycle. Arthritic mice display significantly reduced activity on days 3, 4, 5, 7, and 8 following K/BxN serum transfer. Each time point represents mean  $\pm$  SEM ( $n=5-10$  mice/group), \* $p < 0.05$ , \*\* $p < 0.01$ , and \*\*\* $p < 0.001$  by Bonferroni post-test.

4. Using the DigSigMon software, monitor activity for desired length of time. We recommend at least 18–28 days with this model in order to see the full drop and resumption of activity from this model.
5. Data can be displayed in a wide variety of manner using manipulations available on the software. We suggest displaying total counts per 12-h period from the nocturnal cycle. Little change is noted during the light cycle as a result of K/BxN serum transfer arthritis. Because food and caging materials are changed during the light cycle, disruptions in counts are minimized with display of the nocturnal cycle. It is important to minimize the bedding and enrichment components which may block the IR beam. Alternative methods of data display and analysis include hourly binning of activity counts or the display of the full diurnal cycle.

---

## 4. Notes

Factors contributing to variability in arthritis severity and potentially also hypersensitivity:

1. Strain selection: Genotypic and phenotypic studies by Ji et al. (6) outline the susceptibility of a variety of inbred strains and F2 generational crosses between responder/nonresponder strains. Pain-like behavior has not been assessed in most of these strains subsequent to induction of K/BxN serum transfer arthritis.
2. Gender: It is recommended that investigators conduct pilot studies with appropriate controls to evaluate gender differences

in pain-like behavior. A lack of sex-linked differences in clinical arthritis indices has been reported (6); however, gender-based pain-like behavioral differences have not been systematically explored.

3. Serum potency: In this protocol, we recommend two 100- $\mu$ L injections for a robust induction of K/BxN serum transfer arthritis with a persistent pain-like state during the inflammatory phase as well as the postinflammatory phase to allow for maximal mechanical hypersensitivity and thus the testing of pharmacologic analgesics. To investigate factors suspected to enhance arthritic indices or mechanical hypersensitivity, it is recommended to reduce the injection volume to 50  $\mu$ L. As the spontaneously arthritic mice produce variable levels of anti-GPI antibodies over their lifetime, it is highly recommended for consistency to pool serum and use one pooled collection for the whole experimental series. Alternatively, the antibody titer level can be measured by ELISA. Protocols for antibody titer measurement are outlined in ref. 8. Maximal plasma anti-GPI antibody concentration is expected around 8–10 weeks of age (5). Serum can be obtained by either sacrifice of the animal at day 60 or by routine bleeding, as specified by local animal use committees.
4. The length of acclimation period is strain dependent. For example, the length of time for acclimation among strains in our experience is C3H < C57Bl/6 < Balb/C.
5. All experiments using activity as a measure of behavior resulting from the K/BxN serum transfer arthritis should incorporate as little handling of the mice as possible. Drugs via implanted pumps or available in the drinking water allow for the best separation between groups and avoid confounding effects due to handling.

## References

1. Sokka, T., Kautiainen, H., Toloza, S., Makinen, H., Verstappen, S. M., Lund Hetland, M., Naranjo, A., Baecklund, E., Herborn, G., Rau, R., Cazzato, M., Gossec, L., Skacic, V., Gogus, F., Sierakowski, S., Bresnihan, B., Taylor, P., McClinton, C., and Pincus, T. (2007) QUEST-RA: quantitative clinical assessment of patients with rheumatoid arthritis seen in standard rheumatology care in 15 countries, *Ann Rheum Dis* 66, 1491–1496.
2. Taylor, P. C. (2010) The importance of the patients' experience of RA compared with clinical measures of disease activity, *Clin Exp Rheumatol* 28, S28–31.
3. Christianson, C. A., Corr, M., Firestein, G. S., Mobargha, A., Yaksh, T. L., and Svensson, C. I. (2010) Characterization of the acute and persistent pain state present in K/BxN serum transfer arthritis, *Pain* 151, 394–403.
4. Kouskoff, V., Korganow, A. S., Duchatelle, V., Degott, C., Benoist, C., and Mathis, D. (1996) Organ-specific disease provoked by systemic autoimmunity, *Cell* 87, 811–822.
5. Matsumoto, I., Staub, A., Benoist, C., and Mathis, D. (1999) Arthritis provoked by linked T and B cell recognition of a glycolytic enzyme, *Science* 286, 1732–1735.
6. Ji, H., Gauguier, D., Ohmura, K., Gonzalez, A., Duchatelle, V., Danoy, P., Garchon, H. J., Degott, C., Lathrop, M., Benoist, C., and Mathis, D. (2001) Genetic influences on the

- end-stage effector phase of arthritis, *J Exp Med* **194**, 321–330.
7. Monach, P., Hattori, K., Huang, H., Hyatt, E., Morse, J., Nguyen, L., Ortiz-Lopez, A., Wu, H. J., Mathis, D., and Benoist, C. (2007) The K/BxN mouse model of inflammatory arthritis: theory and practice, *Methods Mol Med* **136**, 269–282.
  8. Monach, P. A., Mathis, D., and Benoist, C. (2008) The K/BxN arthritis model, *Curr Protoc Immunol Chapter 15*, Unit 15 22.
  9. Dixon, W. J. (1980) Efficient analysis of experimental observations, *Annu Rev Pharmacol Toxicol* **20**, 441–462.
  10. Chaplan, S. R., Bach, F. W., Pogrel, J. W., Chung, J. M., and Yaksh, T. L. (1994) Quantitative assessment of tactile allodynia in the rat paw, *J Neurosci Methods* **53**, 55–63.
  11. Mogil, J. S., Wilson, S. G., Bon, K., Lee, S. E., Chung, K., Raber, P., Pieper, J. O., Hain, H. S., Belknap, J. K., Hubert, L., Elmer, G. I., Chung, J. M., and Devor, M. (1999) Heritability of nociception I: responses of 11 inbred mouse strains on 12 measures of nociception, *Pain* **80**, 67–82.
  12. Dirig, D. M., Salami, A., Rathbun, M. L., Ozaki, G. T., and Yaksh, T. L. (1997) Characterization of variables defining hind-paw withdrawal latency evoked by radiant thermal stimuli, *J Neurosci Methods* **76**, 183–191.

## A New Rat Model of Bone Cancer Pain

Ruixin Zhang and Lixing Lao

### Abstract

Pain is a major symptom of bone cancer. Bone cancer pain significantly affects quality of life, but its underlying mechanisms have not been defined. Because skeletal metastases are particularly common in patients with prostate cancer, a model that mimics bone cancer pain has been established by injecting AT-3.1 prostate cancer cells into the tibia of the male Copenhagen rat. The model shows progressive hyperalgesia and allodynia that are associated with the gradual destruction of the tibia and can be used to study the mechanisms, such as glial activation, of these disorders.

**Key words:** Bone cancer pain, Metastatic bone tumors, Hyperalgesia, Allodynia, Rat, Immunohistochemistry, Immunofluorescence

---

### 1. Introduction

It has been reported that 70–90% of patients with advanced cancer experience intractable pain (1). Metastatic bone tumors are thought to be the most common cause of cancer-related pain (2–4) and are particularly prevalent in patients with breast and prostate cancer.

Prostate carcinoma, one of the most common malignancies affecting males, results in a high rate of morbidity and mortality. Bone is the most frequent site of prostate carcinoma metastasis, and skeletal metastases have been identified at autopsy in up to 90% of patients that die from prostate carcinoma (5, 6). Skeletal metastasis results in significant bone pain, which cannot be well-controlled because its underlying mechanisms are not clear. To clarify these mechanisms, a model that closely mimics the pain caused by prostate cancer-induced skeletal metastasis has been established in the male rat (7).

---

## 2. Materials

### **2.1. Prostate Cancer Cell Culture**

1. The AT-3.1 prostate cancer cell line (American Type Culture Collection, Rockville, MD), stored in liquid nitrogen.
2. RPMI 1640 Medium (Sigma) with L-glutamine supplemented with 250 nM dexamethasone and 10% fetal bovine serum (Sigma).
3. Calcium- and magnesium-free Hank's balanced salt solution (Sigma).
4. Trypsin solution, 0.05% trypsin and 0.02% ethylenediamine tetraacetic acid (EDTA) (Gibco/BRL).
5. T-75 plastic flasks (Corning Glass).

### **2.2. Surgical Implantation of Cancer Cells into Bone**

1. Male Copenhagen rats weighing 200–220 g (Harlan).
2. 7% tincture of iodine.
3. 70% ethanol.
4. Needles, 23 gauge; a Hamilton syringe, 50  $\mu$ l.
5. Bone wax (Ethicon).
6. Triple antibiotic ointment (neomycin–polymixin–bacitracin).
7. Rimadyl (Pfizer).
8. A Deltaphase Isothermal pad (Braintree Scientific, Inc.) for maintaining the body temperature of the rats during and after surgery.
9. Surgical instruments: Scalpel handle, blades, scissors, forceps, needle holder, needles, 3–0 thread.
10. Cotton-tipped applicator (Henry Schein).
11. Hot Glass Bead Dry Sterilizer (Stoelting).

### **2.3. Immuno histochemistry and Immunofluorescence**

1. Paraformaldehyde (4%) in 0.1 M phosphate buffer (PB) at pH 7.4.
2. Sucrose in PB (30%).
3. PB saline (PBS, 0.01 M).
4. Triton X-100 and H<sub>2</sub>O<sub>2</sub> (Sigma).
5. Primary antisera: GFAP, OX-42, and IL-1 $\beta$ .
6. Normal donkey serum.
7. ABC and DAB kits (Vector).
8. CY2-conjugated donkey anti-rabbit and CY3-conjugated donkey anti-mouse antibodies (Jackson ImmunoResearch Laboratories).
9. Alcohol, xylene, and DPX (Electron Microscopy Sciences).

10. Aqueous mounting medium (Biomeda Corp.).
11. Fluorescent microscope (Nikon).
12. Gloves and masks.

---

### 3. Methods

#### 3.1. Cell Culture

1. The AT-3.1 prostate cancer cell line is propagated from frozen stock ( $5 \times 10^6$  cells/vial/ml). Fourteen milliliter of RPMI-1640 Medium is put into a T-75 flask, and the flask is placed into an incubator for at least 15 min to allow the medium to reach its normal pH of 7.0–7.6.
2. A screw-cap vial containing cells in frozen medium is taken from the nitrogen tank, placed immediately into a 37°C water bath, and gently agitated for about 2 min to thaw the frozen contents.
3. As soon as the contents are thawed, the vial is decontaminated by spraying it with 70% ethanol and wiping it with tissues (Kimwipes).
4. The cell suspension is centrifuged at  $125 \times g$  for 5 min, the supernatant is discarded, and the cell pellet is resuspended in 1 ml of RPMI-1640 medium.
5. The cells are transferred to the T-75 flask, and the cells are separated as much as possible by gently drawing up and dispersing the medium with serological pipettes.
6. The T-75 flask is transferred to a water-saturated incubator with an atmosphere of 5% CO<sub>2</sub>:95% air, where the cells are cultured.
7. The medium is changed each day. On the day of surgery, cells are detached by rinsing gently with calcium- and magnesium-free Hank's balanced salt solution and a trypsin solution containing 0.05% trypsin and 0.02% EDTA. The detached cells are collected by centrifuging 10 ml of medium at  $175 \times g$  for 3 min. The resulting pellet is washed twice with 10 ml of calcium- and magnesium-free Hank's solution and recentrifuged at  $175 \times g$  for 3 min. The final pellet is resuspended in 1 ml of Hank's solution, and the cells are counted using a hemocytometer. Cells are diluted to a final concentration of  $3 \times 10^5$  cells/10  $\mu$ l Hank's solution that is kept on ice until injected into the rats.

#### 3.2. Surgical Procedures

Male Copenhagen rats weighing 200–220 g (Harlan) are kept under controlled conditions (22°C  $\pm$  0.5°C, relative humidity 40–60%, 7:00 am to 7:00 pm alternate light–dark cycles, food and water ad libitum). The commonly used Sprague-Dawley rats (Harlan) do not respond well to the AT-3.1 cells (unpublished observations).

1. Following complete induction of anesthesia with sodium pentobarbital (50 mg/kg, i.p.; see Note 1), one leg of the rat is shaved and the skin is disinfected with 7% tincture of iodine and 70% ethanol.
2. A 1-cm-long rostrocaudal incision is made in the skin over the upper medial half of the tibia. The tibia is carefully exposed with minimal damage to the muscle (see Note 2).
3. Using a 23-gauge needle, the bone is pierced 5 mm below the knee joint medial to the tibial tuberosity. The needle is then replaced with a 50- $\mu$ l Hamilton syringe containing the cells to be injected. A 10- $\mu$ l volume of prostate cancer cells ( $3 \times 10^5$  cells) or vehicle (Hank's solution only) is injected into the bone cavity. After a 2-min delay while the cells filled the space in the bone cavity, the syringe is removed and bone wax (Ethicon) is used to close the injection site (see Notes 3–6).
4. The muscle is stitched and the skin wound is closed using 3–0 silk threads. The animal is placed on a heated pad until it regained consciousness, and then returned to its home cage (see Notes 7 and 8). Each rat is monitored during the experiment for general condition and changes in body weight.

### **3.3. Radiology and Histochemical Staining**

To confirm cancer development in the tibia, rats are radiographed on days 7, 13, and 20 following the implantation.

1. Rats are anesthetized with sodium pentobarbital, placed prone on X-ray film (Henry Schein blue sensitive film), and exposed to an X-ray source (Emerald 125) for 1/20 s at 40 KVP. The X-ray film is developed in a film developer (Konica SRX-101).
2. The radiographic images are quantified visually using the scale developed by Schwei et al. (8): 0, normal bone structure with no sign of deterioration; 1, minor loss of medullary bone; 2, substantial loss of medullary bone with erosion of cortical bone; and 3, substantial loss of medullary bone with major cortical destruction of the proximal epiphysis. Figure 1a, b compares a normal tibia to one with scale 3 deterioration and destruction of trabeculae.
3. After demineralizing in EDTA (10%) for 2–3 weeks, the tibiae are embedded in paraffin, and 5- $\mu$ m sections are cut with a microtome and stained with Harris' hematoxylin and eosin (HE) to verify cancer cell infiltration and bone destruction. See Fig. 1b.

### **3.4. Thermal Hyperalgesia**

The cancer and vehicle rats are tested for paw withdrawal latency (PWL) using a previously described method (9, 10).

1. The rat is placed under an inverted clear plastic chamber on the glass surface (30°C) of a Paw Thermal Stimulator System (UCSD, San Diego) and allowed to acclimatize for 30 min before the test (see Note 9).

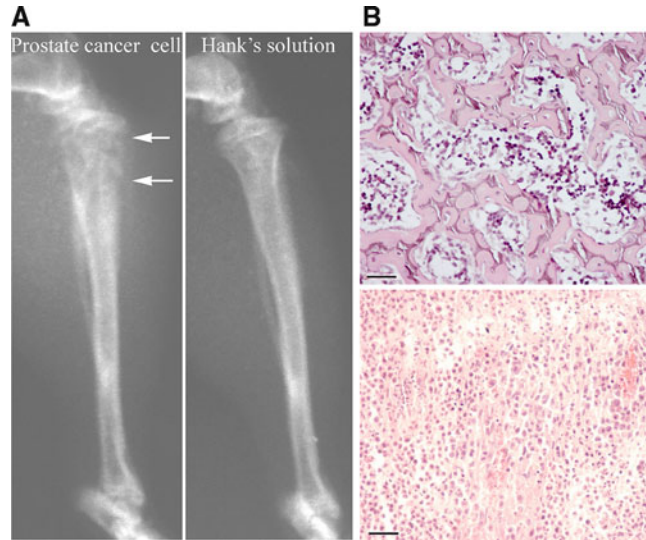


Fig. 1. (a) Radiographs of tibiae 20 days after inoculation with AT-3.1 prostate cancer cells ( $3 \times 10^5$ , left panel) and Hank's solution (right panel). Arrows indicate structural destruction of the proximal cortical bone (score = 3). (b) HE staining of normal proximal tibial epiphysis (upper panel) and cancer-inoculated epiphysis (lower panel). Note that the tumor cells are densely packed in the marrow cavity and have induced the destruction of trabeculae. Bar = 40  $\mu\text{m}$ . The animal protocols were approved by the Institutional Animal Care and Use Committee at the University of Maryland School of Medicine. Reproduced from ref. 7 with permission from International Association for the Study of Pain, IASP.

2. A radiant heat stimulus is applied to the plantar surface of each hind paw with a projector lamp bulb placed underneath the glass floor (CXL/CXR, 8 V, 50 W).
3. PWL to the nearest 0.1 s is automatically recorded when the rat withdraw its paw from the stimulus. Stimulus intensity is adjusted to derive an average baseline PWL of approximately 10.0 s in naive animals. Paws are alternated randomly to preclude "order" effects. A 20-s cutoff is used to prevent tissue damage.
4. Mean PWL is established by averaging the latency of four tests with a 5-min interval between each test. It is measured at baseline and on days 8, 12, 15, and 19 after injection. It may progressively decrease on days 12, 15, and 19 in rats inoculated with prostate cancer cells but not in those that received Hank's solution, as shown in Fig. 2. The investigator who performed the behavioral tests should be blinded to group assignment.

### 3.5. Mechanical Hyperalgesia (Paw Pressure)

The rats are tested for mechanical hyperalgesia with a Paw Pressure Analgesia Instrument (Ugo Basile, Italy) that determined the nociceptive hind paw withdrawal pressure threshold (PWPT) (11).

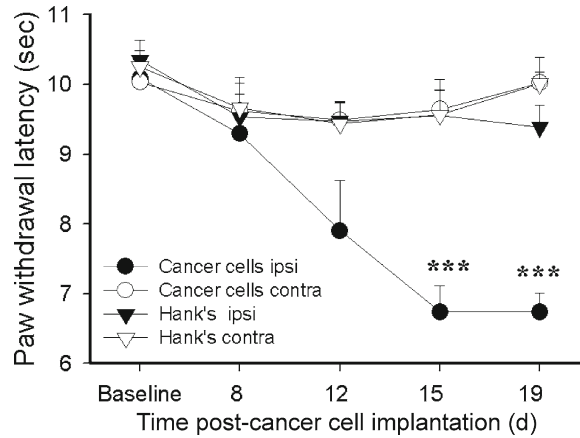


Fig. 2. Cumulative effects on hind paw withdrawal latency (PWL) of AT-3.1 prostate cancer cells ( $3 \times 10^5$  cells/ $10 \mu\text{l}$ ) injected into the cavity of the right tibia. PWL progressively decreased on days 12, 15, and 19 after inoculation with prostate cancer cells ( $n=8$ ) but not after inoculation with Hank's solution ( $n=8$ ). \*\*\* $P < 0.001$  compared to the Hank's-injected side. Contralateral paws showed no change in PWL. Reproduced from ref. 7 with permission from International Association for the Study of Pain, IASP.

1. The animals are gently held in the hand and the hind paws are placed between the hard surface and the motor-driven levered piston.
2. When the foot pedal is pushed to start the motor, an incremental pressure, measured by means of an automated gauge, is applied to the dorsal surface of the hind paw with a blunt, wedge-shaped, 1.75-mm<sup>2</sup> piston.
3. The end point is paw withdrawal. The minimum paw pressure (in grams) that elicits paw withdrawal is defined as PWPT. Paws are alternated to preclude "order" effects. A cutoff of 250 g is employed.
4. Mean PWPT is established by averaging the values of four consecutive tests, separated by intervals of 30 s. It is measured before surgery and on days 9, 13, and 20 after injection. It decreases on days 13 and 20 in rats injected with prostate cancer cells but not in those that received Hank's solution, as shown in Fig. 3. Contralateral PWPT should show no changes.

### 3.6. Mechanical Allodynia (Von Frey Filaments)

For mechanical allodynia, hind paw withdrawal threshold (PWT) is determined using von Frey filaments, as described by Ren (12).

1. The rat is habituated to stand on its hind paws on a soft pad while leaning against the gloved hand of the experimenter.
2. The test begins with filament No. 10 (4.31 marking), which is applied to the lateral edge of the hind paw.

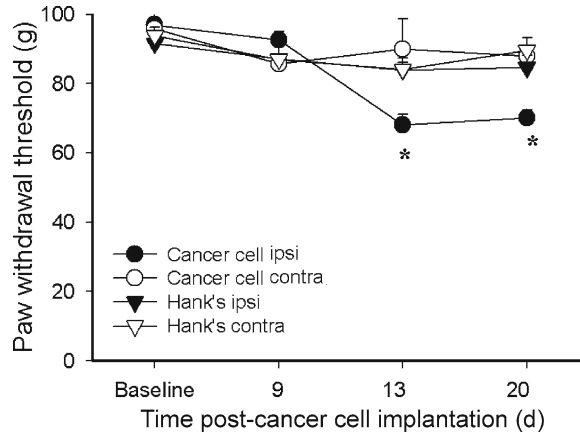


Fig. 3. Effects on hind paw withdrawal pressure threshold (PWPT) of an AT-3.1 prostate cancer cell ( $3 \times 10^5$  cell/ $10 \mu\text{l}$ ) inoculation of the right tibia. PWPT decreased on days 13 and 20 after prostate cancer cell inoculation ( $n=8$ ) but not after inoculation with Hank's solution ( $n=8$ ). Contralateral PWPTs showed no changes. \* $P < 0.05$  compared to the Hank's-injected side. Reproduced from ref. 7 with permission from International Association for the Study of Pain, IASP.

3. A decreasing series of filaments is used if the rat responds to the starting filament; an increasing series of filaments is used if the rat does not respond to the starting filament.
4. Each filament is applied ten times at intervals of a few seconds. If paw withdrawal is observed at least six times to probing with a given filament, the rat is considered responsive to that filament. PWT is defined as the lowest filament force that produced at least six withdrawal responses out of ten tests. It is expressed as the median force in grams because the results yielded by different filaments are nonlinearly dispersed. PWT of the inoculated paws shows progressive decrease over the testing period as shown in Fig. 4a while that of the noninoculated paws remained unchanged as shown in Fig. 4b.

### 3.7. Immuno histochemistry

Immunostaining is carried out to investigate the central mechanisms of bone cancer pain.

1. After the behavioral test, cancer rats are deeply anesthetized with sodium pentobarbital (60 mg/kg, i.p.) and perfused transcardially with 500 ml of 4% paraformaldehyde (Sigma) in 0.1 M PB at pH 7.4 (see Note 10).
2. The lumbar 4–5 spinal cord is removed, immersed in the same fixative for 2 h at  $4^\circ\text{C}$ , and transferred to 30% sucrose (w/v) in PB for overnight cryoprotection.
3. Thirty micron-thick sections are cut on a cryostat and rinsed first in PBS with 0.75% Triton X-100 and 1%  $\text{H}_2\text{O}_2$  for 1 h and then in PBS with 3% normal serum (NS) for 30 min.



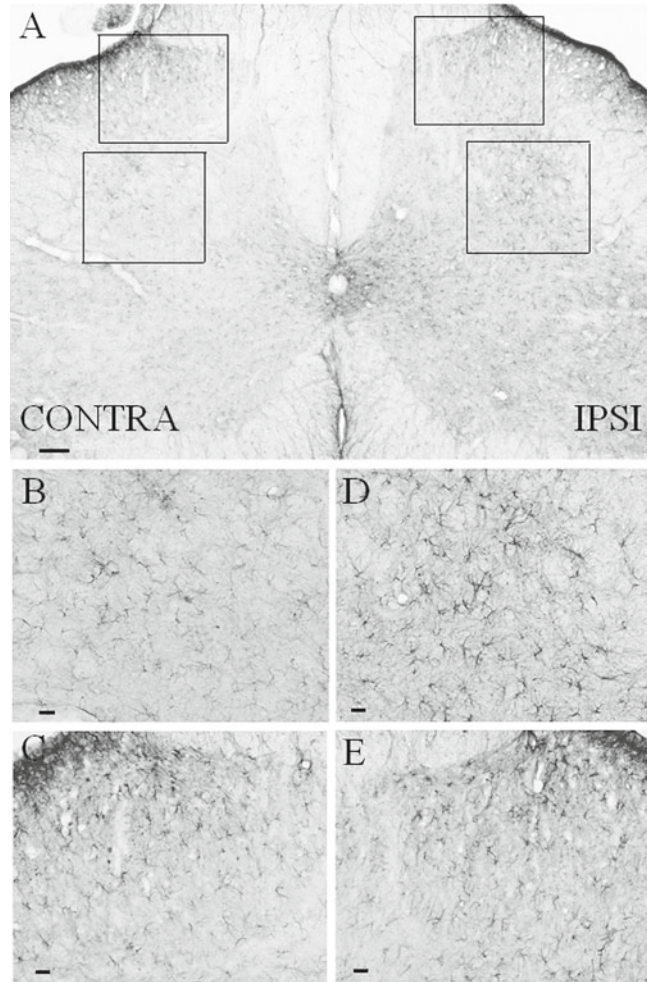


Fig. 5. GFAP staining of the lumbar (L4–L5) spinal cord 20 days after AT-3.1 cell injection into the tibia. (a) A low-power microphotograph of the spinal cord; (b–e) high-power microphotographs of contralateral (b, c) and ipsilateral (d, e) laminae V–VI (b, d) and superficial dorsal horns (c, e). Note that GFAP staining was enhanced in the ipsilateral spinal cord (d, e) compared to that on the contralateral side (b, c) and that astrocyte cell bodies of the ipsilateral side increased in size (d) compared to contralateral astrocytes (b). Scale bars are 100  $\mu\text{m}$  in (a) and 20  $\mu\text{m}$  in (b)–(e). Reproduced from ref. 7 with permission from International Association for the Study of Pain, IASP.

(1:1,000, Chemicon), OX-42 (1:1,000, Biosource), or NeuN (1:1,000, Chemicon).

- After three 10-min washings in PBS, sections are incubated in a mixture of CY2-conjugated donkey anti-rabbit (1:500, Jackson ImmunoResearch Laboratories) and CY3-conjugated donkey anti-mouse (1:1,000) for 1 h at room temperature. Control sections are similarly processed, except that the primary antisera are omitted.

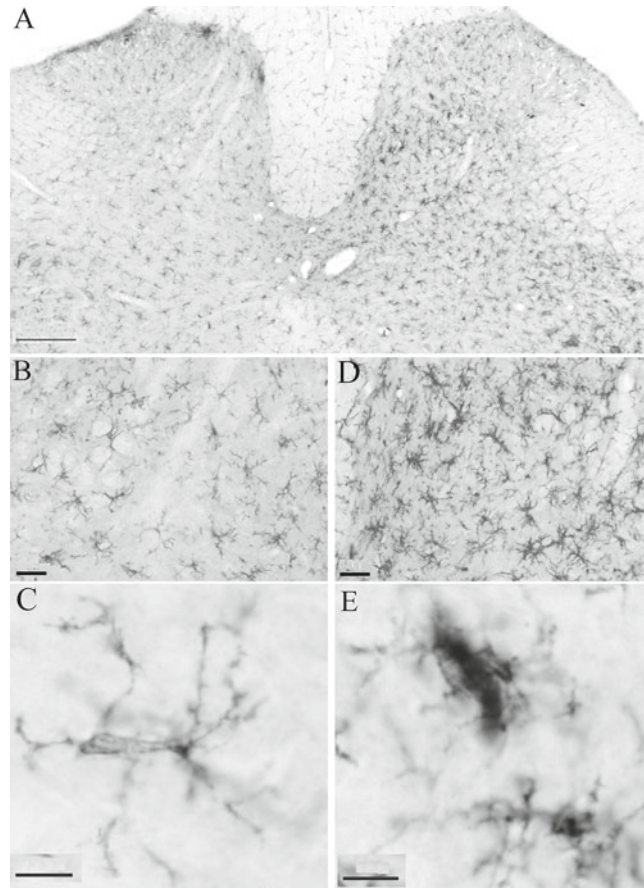


Fig. 6. OX-42 staining of the lumbar (L4–L5) spinal cord 20 days after AT-3.1 cell injection into the tibia. (a) A low-power microphotograph of the spinal cord; (b and d) high-power microphotographs of contralateral (b) and ipsilateral (d) dorsal horns. Note that spinal cord OX-42 staining was enhanced ipsilaterally (d) compared to that of the contralateral side (b). (c and e) Activated microglia (e) are hypertrophied compared to resting microglia (c). Scale bars are 200  $\mu\text{m}$  in (a), 40  $\mu\text{m}$  in (b) and (d), and 10  $\mu\text{m}$  in (c) and (e). Reproduced from ref. 7 with permission from International Association for the Study of Pain, IASP.

4. The stained sections are mounted on gelatin-coated slides and coverslipped with aqueous mounting medium. Examination under a Nikon fluorescent microscope reveals colocalization of IL-1 $\beta$  and GFAP in astrocyte cell bodies, as shown in Fig. 8.

---

## 4. Notes

1. The depth of anesthesia is determined every 5 min by inducing the toe pinch (pedal withdrawal) and eye blink (palpebral) reflexes. Neither of these reflexes can be induced during anesthesia.

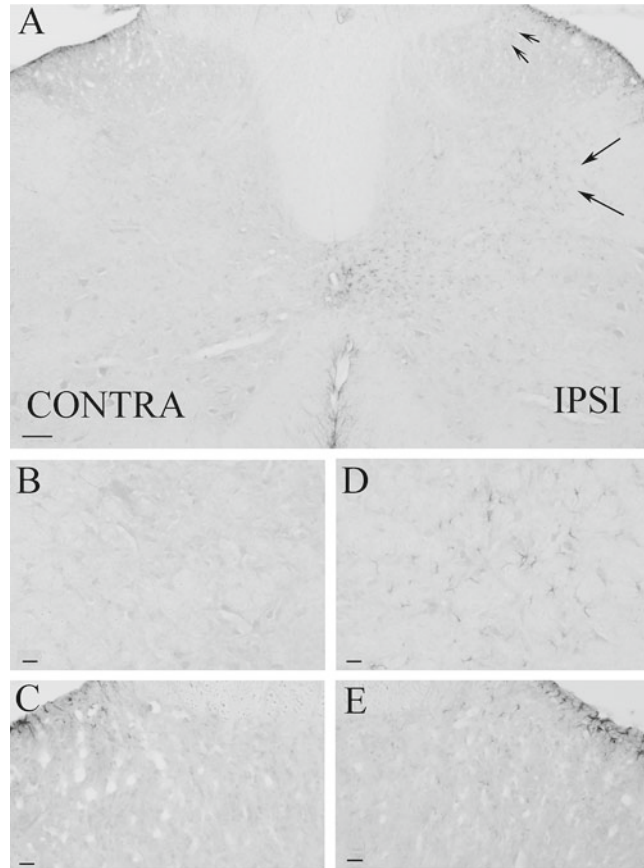


Fig. 7. IL-1 $\beta$  staining of the lumbar (L4–L5) spinal cord 20 days after AT-3.1 cell injection into the tibia. (a) A low-power microphotograph of the spinal cord; (b–e) high magnification of contralateral (b, c) and ipsilateral (d, e) laminae V–VI (b, d) and I–II (c, e), respectively. Note that there are many IL-1 $\beta$  immunostained cells on the ipsilateral side and few on the contralateral side. Scale bars are 100  $\mu$ m in (a) and 20  $\mu$ m in (b–e). Reproduced from ref. 7 with permission from International Association for the Study of Pain, IASP.

2. All surgical instruments are sterilized with a Hot Glass Bead Dry Sterilizer (Stoelting).
3. The bone is pierced by gently turning the 23-gauge needle several times.
4. The cell line is determined to be pathogen free by Veterinary Resources.
5. The bone wax is placed into the injection holes with the beveled end of a wooden applicator stick (Henry Schein) that should be autoclaved in advance.
6. The area around the hole is washed with saline using a cotton-tipped applicator (Henry Schein).

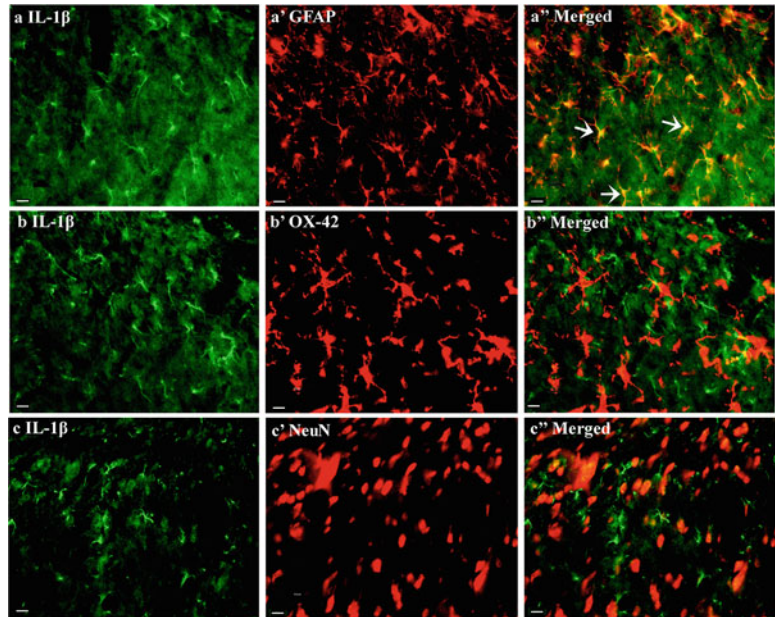


Fig. 8. (a–c) Micrographs showing colocalization of IL-1 $\beta$  and GFAP in the lumbar spinal superficial laminae 20 days after AT-3.1 cell injection into the tibia. Sections are double labeled with anti-IL-1 $\beta$  (green) and anti-GFAP, anti-OX-42 or anti-NeuN (red). The first column shows IL-1 $\beta$  immunostaining. The second column shows immunostaining with three cell markers GFAP, OX-42, and NeuN, respectively, for astrocytes, microglia, and neurons. The third column shows the merged graphs. Note that IL-1 $\beta$  is localized in astrocytes (yellow cells) as indicated by arrows. Scale bars represent 10  $\mu$ m. Reproduced from ref. 7 with permission from International Association for the Study of Pain, IASP.

7. Triple antibiotic ointment is applied to the wound.
8. Rimadyl (Pfizer) at 5 mg/kg is given subcutaneously before recovery from anesthesia and repeated after 24 h for pain control.
9. Rats are habituated and handled gently for two 30-min periods beginning 2 days before the baseline behavioral test.
10. Paraformaldehyde is toxic and should be manipulated with gloves and mask in a fume hood to prevent contact with skin and inhalation.
11. Antibodies are stored in  $-20^{\circ}\text{C}$  freezer and made to final dilution on the day that the immunohistochemistry is performed.
12. Washing time can be longer if the background is too dark.
13. The dehydration and xylene clearance are performed under a hood.

## Acknowledgments

The author would like to thank Dr. Lyn Lowry for her editorial support. This work was funded by NIH grant R21 CA102383-01.

## References

1. Foley, K. M. (2000) Controlling cancer pain. *Hospital Practice* **35**, 101–108.
2. Mercadante, S. (1997) Malignant bone pain: pathophysiology and treatment. *Pain* **69**, 1–18.
3. Reale, C., Turkiewicz, A. M., and Reale, C. A. (2001) Antalgic treatment of pain associated with bone metastases. *Crit Rev Oncol Hematol* **37**, 1–11.
4. Banning, A., Sjogren, P., and Henriksen, H. (1991) Treatment outcome in a multidisciplinary cancer pain clinic. *Pain* **47**, 129–134.
5. Bubendorf, L., Schopfer, A., Wagner, U., Sauter, G., Moch, H., Willi, N., Gasser, T. C., and Mihatsch, M. J. (2000) Metastatic patterns of prostate cancer: an autopsy study of 1,589 patients. *Hum Pathol* **31**, 578–583.
6. Rana, A., Chisholm, G. D., Khan, M., Sekharjit, S. S., Merrick, M. V., and Elton, R. A. (1993) Patterns of bone metastasis and their prognostic significance in patients with carcinoma of the prostate. *Br J Urol* **72**, 933–936.
7. Zhang, R.-X., Liu, B., Wang, L., Ren, K., Qiao, J.-T., Berman, B. M., and Lao, L. (2005) Spinal glial activation in a new rat model of bone cancer pain produced by prostate cancer cell inoculation of the tibia. *Pain* **118**, 125–136.
8. Schwei, M. J., Honore, P., Rogers, S. D., Salak-Johnson, J. L., Finke, M. P., Ramnaraine, M. L., Clohisey, D. R., and Mantyh, P. W. (1999) Neurochemical and Cellular Reorganization of the Spinal Cord in a Murine Model of Bone Cancer Pain. *J Neurosci* **19**, 10886–10897.
9. Hargreaves, K., Dubner, R., Brown, F., Flores, C., and Joris, J. (1988) A new and sensitive method for measuring thermal nociception in cutaneous hyperalgesia. *Pain* **32**, 77–88.
10. Zhang, R. X., Lao, L., Qiao, J. T., and Ruda, M. A. (2004) Effects of aging on hyperalgesia and spinal dynorphin expression in rats with peripheral inflammation. *Brain Res* **999**, 135–141.
11. Stein, C., Millan, M. J., and Herz, A. (1988) Unilateral inflammation of the hindpaw in rats as a model of prolonged noxious stimulation: alterations in behavior and nociceptive thresholds. *Pharmacol Biochem Behav* **31**, 445–451.
12. Ren, K. (1999) An improved method for assessing mechanical allodynia in the rat. *Physiol Behav* **67**, 711–716.

# Chapter 21

## Exposure of the Dorsal Root Ganglion to Pulsed Radiofrequency Current in a Neuropathic Pain Model of Peripheral Nerve Injury

Danielle Perret, Doo-Sik Kim, Kang-Wu Li, and Z. David Luo

### Abstract

The spinal nerve ligation model of neuropathic pain in rats, as originally described by Kim and Chung (Pain 50:355–363, 1992), provides an excellent venue to study the antinociception and modulation effects of pulsed radiofrequency (PRF) current in pain processing. We describe the procedure of application of PRF current near the exposed L5 dorsal root ganglion (DRG) in rats with L5 spinal nerve ligation injury-induced behavioral hypersensitivity. This method employs the direct visualization of the L5 DRG, allowing for confirmation of the location of the PRF probe adjacent to the DRG.

**Key words:** Pulsed radiofrequency current, Pain processing, Neuropathic pain, Dorsal root ganglion

---

### 1. Introduction

The use of pulsed radiofrequency (PRF) current for the clinical treatment of neuropathic pain is widespread. PRF is documented in the treatment of trigeminal (1, 2) and other peripheral neuralgias (3–9) and in the treatment of radicular pain (1); it is also frequently applied in the treatment of facet joint pain (1). Novel applications continue to be described and span the treatment of discogenic pain to the treatment of articular pain (10–18). This large accumulation of clinical observational data, accompanied by few prospective controlled study data (19–22), supports that PRF can provide an analgesic effect. Several animal studies are available to confirm antinociception (23–26). The precise mechanism of PRF analgesic action, however, is not clear. It may include reversible disruption of impulse transmission in small, unmyelinated, nociceptive fibers (27, 28);

ultrastructural damage to mitochondria and microtubules that may impede the transmission of pain impulses (29); and early (30) and late (31) changes in cellular activity in the spinal dorsal horn associated with the dorsal root ganglion (DRG) receiving adjacent PRF current. Both basic and clinical studies show a greater and more sustained effect when PRF is applied adjacent to the DRG as opposed to a peripheral nerve (5, 32, 33). It is believed that long-term modulation of DRG cellular function derives from alterations in gene expression, which may play a critical role in the PRF-induced antinociception. To further explore this mechanism, there is a need for studying the direct effect of PRF on regulation of DRG gene expression. In this chapter, we describe the procedure for applying PRF adjacent to exposed DRG in a rat neuropathic pain model.

---

## 2. Materials

### 2.1. Rats

1. Adult male Harlan Sprague–Dawley rats (Harlan Industries, Indianapolis, IN, USA) weighing 140–180 g should be housed with a 12-h light–dark cycle and with access to food and water ad libitum.
2. Rats should be kept in a similar environment for at least 2 days for acclimation.

### 2.2. Surgery Materials

1. Isoflurane Anesthesia Vaporizer (Surgivet Isotec 4, Surgivet Inc., Waukesha, WI).
2. Isoflurane (Western Medical Group: Phoenix Pharmaceutical Inc., St., Joseph, MD).
3. Oxygen tank (Airgas, Inc., Lakewood, CA).
4. Anesthesia induction box (Surgivet Veterinary Surgical Products, Waukesha, WI).
5. Electrical razor (Oster “Fast Feed” Blade: 913-50, Boca Raton, FL).
6. Betadine solution (Perdue Frederick, Stamford, CT).
7. 75% EthOH (Goldshield Chemical Co., Hayward, CA).
8. Stereo microscope (MZ9s, Leica Microsystems Inc., Bannockburn, IL).
9. Number 10 surgical blade (Feather Surgical Blade, Safety Razor Co., Osaka, Japan).
10. Surgical retractors.
11. Surgical hemostats, Adson forceps, needle holders (Fine science Tools, Foster City, CA).

12. Small rongeur (Fine science Tools, Foster City, CA).
13. Bead sterilizer (Inotech Steri 350, Inotech Biosystems International, Inc., Rockville, MD).
14. Sterile cotton gauze and cotton-tipped sticks (Fisher Scientific, Waltham, MA).
15. Sterile cotton towels for surgical field preparation (Fisher Scientific, Waltham, MA).
16. Small electrocautery device (Advanced Meritech International, CAT #CH-H1, 86-38 53rd Avenue, Suite 100, Flushing NY 11373, USA) (see Note 1).
17. Needle holders.
18. 6.0 silk suture for spinal nerve ligation (Harvard Apparatus, Holliston, MA).
19. 4–0 chromic suture for muscle, fascia, and subcutaneous suture closure (Ethicon G181H, Somerville, NJ).
20. Rat staples for skin closure (EZ Clips, Stoelting Co., Wood Dale, IL).
21. Heating pad, maintained at 37°C by a temperature controller (Sunbeam Products, Inc., Fontana, CA).
22. Heating lamp.
23. Sterile saline (0.9% NaCl, autoclaved).
24. 5 mL syringe; 25 g (1.5 in. length) needles (Becton Dickinson, NJ).

### **2.3. Behavioral Testing Materials**

1. Touch Test Sensory Evaluator Kit/von Frey filaments (Stoelting Company #58011).
2. Allodynia testing apparatus (see Note 2).
3. Transparent enclosures with dimensions approximately 30 (height) × 10 (width) × 22 (depth) cm (see Note 3).

### **2.4. PRF Application Materials**

1. Radiofrequency (RF) lesion generator machine (RFG-3C Plus, Radionics, Burlington, MA, USA) and RF electrode with build-in thermocouple for temperature monitoring.
2. RF probe (Radionics, Burlington, MA, USA); a standard 5-cm-length SMK RF probe modified for a 2-mm active exposed tip (see Note 4).
3. Small precise ruler.
4. Cutting edge or sharp scissors to modify the RF probe.
5. RF needle housing (a pipette tip; see Note 4).
6. Small grounding electrode clip.
7. Electrical outlet.
8. Stop watch or stop clock.

9. Pen and paper for notes (or digital recording device) for logging electrode impedance, DRG tissue temperature, and current during PRF application.

---

### 3. Methods

#### 3.1. Spinal Nerve Ligation Surgery

Detail procedure for the spinal nerve ligation (SNL) injury model is described in Chapter 4, First Edition of this book (34) (see Note 5).

1. All surgical tools should be sterilized prior to use. We use a bead sterilizer for our operations. Surgery time is approximately 15 min per rat.
2. Induction of anesthesia is performed in an induction box with 5% isoflurane in O<sub>2</sub> in a ventilation hood.
3. The back fur of the anesthetized rats is shaved between the thoracic and lumbar region and the animal is placed prone in a surgical table and anesthesia is maintained with 2% isoflurane in O<sub>2</sub> during the operation.
4. Upon confirmation of adequate anesthesia by pinching the paws, the skin is scrubbed with betadine, and then 70% EtOH.
5. A longitudinal incision about 3 cm in length extending approximately from the L5 to S1 vertebra level is made in the left paraspinal under a surgical microscope. The landmark for the incision is the L5 spinous process identified at the level of the iliac crest. The left L5 spinal nerve is exposed after blunt separation of the L5–S1 paraspinal muscles from the spinal processes and removal of the L6 transverse process.
6. The L5 spinal nerve is tightly ligated with a 6–0 silk suture distal to the dorsal root ganglion.
7. Muscle, fascia, and subcutaneous layers are sutured with a 4–0 chromic suture and skin closure can be done with rat staples or 6–0 silk sutures.
8. Warm sterile saline (5 mL) is injected intraperitoneally for volume replacement post operation (see Note 6).
9. During the recovery from anesthesia, core body temperature is maintained at 37°C by using a heat lamp regulated by a temperature controller.
10. Rats should be allowed to recover after the spinal nerve ligation surgery for at least 1 week before exposing the DRG for PRF stimulation. During this period, behavioral tests should be performed to monitor the development of behavioral hypersensitivities at the injury side as described below.

### 3.2. DRG Exposure Surgery

1. All surgical tools should be sterilized prior to use. Surgery time is approximately 30 min per rat.
2. Rats are anesthetized via induction with 5% isoflurane in oxygen and via maintenance with 2% isoflurane in oxygen.
3. The lumbrosacral area of the rat is shaved with an electrical razor.
4. The operative field is prepped with betadine, and then 75% EthOH solutions.
5. A 2-cm skin incision is made in the posterior lumbrosacral junction with a number 15 blade under a surgical microscope.
6. The left L4–S1 paraspinal muscles are bluntly dissected from the spinous processes.
7. The spinous process of L5 is identified at the level of the iliac crest.
8. The interspinous muscles at this level are retracted laterally.
9. The plates of the vertebral arch are exposed at the L6 level.
10. L5–6 articular processes are removed on the left side (spinal nerve-ligated side) with a small rongeur to expose the L5 DRG.
11. Bleeding is controlled with the application of direct pressure or with a small electrocautery device (see Note 1).
12. The L5 DRG location is verified by tracking the L5 spinal nerve proximal to the ligature (Fig. 1).

### 3.3. PRF Application

1. The RF probe is modified as described (see Note 4). The RF probe is placed adjacent to the exposed L5 DRG.
2. The electrode is then connected to the radiofrequency lesion generator machine.

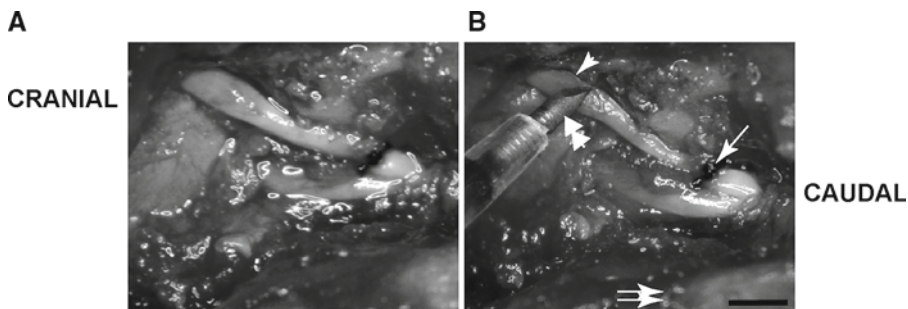


Fig. 1. Placement of a radiofrequency electrode adjacent to the left L5 dorsal root ganglion in a rat. Images showing the relative locations of L5 DRG, L5 spinal nerve ligation site (a) and placement of a radiofrequency electrode adjacent to the L5 DRG (b). The images were designed to show the location and size relationships for the L5 spinal nerve ligation site, L5 DRG, and PRF probe in a wider surgical view from a postmortem mock-up. Both images are from a similar view, so labels and scale bar are presented on panel b only. *Arrow*—L5 spinal nerve ligature. *Arrowhead*—L5 DRG. *Double arrowheads*—PRF probe tip. *Double arrows*—tip of the iliac crest. *Scale bar*=2 mm. Reproduced from Perret et al. (26) with permission from Lippincott Williams & Wilkins.

3. The grounding clip is placed on adjacent exposed tissue (muscle or fascia).
4. Electrode impedance is checked. For values above 1,000  $\Omega$ , irrigation of the field with a few drops of normal saline is provided.
5. To mimic common clinical parameters, the RF machine is set to 25 V (peak voltages) and delivers 500 kHz, 20-ms RF pulses at a rate of 2 Hz for a duration of 120 s. As discussed recently in detail by Perret et al. (2011), these parameters may be altered (26). For sham-PRF application, the RF machine is set to deliver pulses at a rate of 2 Hz for a period of 120 s; however, the current is set to zero.
6. The RF temperature should be set to be limited to 42°C to avoid a thermal lesion.
7. When the RF machine is on and PRF current is delivered, electrode impedance, DRG tissue temperature, and current should be recorded in 15-s intervals throughout the period of PRF exposure (see Note 7).
8. The RF machine stops when the period is complete; the RF probe is removed from the needle housing and both RF probe and needle housing should be wiped clean with cotton gauze soaked with 75% EthOH. The RF machine can be left on (no current is flowing) so that the settings do not have to be reentered for the next rat.
9. At the end of treatment, muscle and deep fascia layers are closed with a 4–0 chromic suture.
10. Subcutaneous layers are closed with a 4–0 chromic suture.
11. Skin closure is done via rat staples.
12. The animal is allowed to recover from anesthesia on a heating pad maintained at 37°C by a temperature controller.
13. During recovery, 5 mL of warm sterile saline is injected intraperitoneally into the rat (using a 25-gauge needle) for volume replacement (see Note 6).

### **3.4. Behavioral Testing**

Depending on the experimental design, behavioral hypersensitivity to different types of modality testing can be studied in this neuropathic pain model. Similar procedures are used to test hind paw sensitivities to von Frey filament stimulation (mechanical stimulation) pre- and post-SNL and -PRF procedures as described briefly below and in more detail in Chapter 8, First Edition of this book (35). For testing thermal hyperalgesia, the detail procedure is described in Chapter 2, First Edition of this book (36). Both tactile allodynia and thermal hyperalgesia should be peaked within 1 week post surgery as shown by different laboratories (26, 37–40) (see Note 8).

1. An individual rat is placed in a clear plastic enclosure on top of the wire mesh floor on the testing apparatus for at least 15-min acclimation.
2. To determine the 50% paw withdrawal thresholds to von Frey filament stimulation, a series of filaments of varying buckling weights (0.4, 1.0, 1.4, 2.0, 4.0, 6.0, 8.0, and 15.0 g), starting with one that has a bending force of 2.0 g, is applied perpendicularly in consecutive order to the hind paw plantar surface of L5 dermatome distribution with a pressure causing the filament to buckle. A positive response, such as paw lifting or licking, within 5 s leads to the use of the next weaker filament. An absence of a positive response after 5 s prompts the use of the next higher weight filament. The process continues until the completion of evaluation according to the up-down method or until five consecutive negative responses (record a maximum value of 15 g) or four consecutive positive responses (record a minimum value of 0.25 g) have been reached (41).
3. The resulting scores derived from six consecutive recordings, starting with the one before any change in response (positive versus negative), are used to calculate the 50% paw withdrawal thresholds using the formula,  $50\% \text{ gm threshold} = (10^{(X_f + kd)}) / 10,000$ , where  $X_f$  is the value (in log units) of the final von Frey filament used,  $k$  is the value of the pattern of positive versus negative responses from a Table in Chaplan et al. (41), and  $d$  is the mean difference (in log units) between stimuli (41).
4. After PRF stimulation to the L5 DRG, SNL rats display faster and better recovery of tactile allodynia compared with the sham-treated SNL rats as shown in our recent study (26).

---

## 4. Notes

1. Electrocauterization may help to stop bleeding, which could be severe upon removal of articular processes (see Subheading 3.2). However, electrocautery may add electrical stimulation near the DRG, thus causing artifacts for PRF stimulation. We recommend avoiding electrocauterization if other means can be used to stop bleeding successfully.
2. We have the allodynia testing apparatus made by a mechanical shop in our University. The dimensions are approximately 69 (height)  $\times$  76 (width)  $\times$  40 (depth) (cm) (see Fig. 1 in Chapter 13 of this book). These dimensions can be changed based on the sizes of the transparent enclosures (see Note 3). Usually, the size of the grid in the top of the apparatus is 1.2  $\times$  1.2 cm for rat testing, which can be changed based on the sizes of the animals to be tested.

3. The size of the transparent enclosure is for an individual compartment, and it should be adjusted based on the size of the animal to be used. The enclosure should be made with thick plastic boards and two to three compartments can be divided with dividers in the same enclosure so that they are heavy enough to prevent being knocked down by the rat. The enclosure should be tall enough so that the rat inside cannot escape. In addition, the interior dimensions should be just big enough for the rat to relax comfortably without excessive extra room for the rat to move around and explore, which would make the behavioral testing more difficult.
4. The RF probe (Radionics, Burlington, MA, USA) is a standard SMK RF (5 cm length) probe (for a needle with a 5-mm active tip), which is modified as follows. The 5-mm active end is removed. 2 mm of the distal insulation material is then removed to provide a 2-mm exposed active distal end. The 5-cm RF electrode is then placed into the RF needle housing, a pipette tip with the cut-end allowing for exposure of the distal 2 mm of the electrode to be used for PRF treatment (Fig. 1b).
5. We selected this model for our studies. A similar procedure can be applied to study PRF effects on DRG modulation in other animal models.
6. Sterile saline should be warmed in a syringe under the heating pad before injection to minimize further heat loss upon injection of cold saline.
7. The DRG tissue temperature should not increase significantly and current should be near zero throughout the period of sham-PRF exposure.
8. The same person, who should be blinded to the surgery and treatment of the animals, should perform the behavioral testing to avoid any interpersonal variations and objective bias, respectively.

---

## Acknowledgments

This work was supported in part by pilot grants from the Committee on Research and Graduate Academic Programs and the Department of Anesthesiology & Perioperative Care, University of California Irvine Medical Center (D. Perret). The authors would like to thank Mr. Joshua Lee for his technical assistance in preparing the figure.

## References

1. von Boxem K, van Eerd M, Brinkuize T, Patijn J, van Kleef M, van Zundert J. (2008) Radiofrequency and pulsed radiofrequency radiofrequency treatment of chronic pain syndromes: the available evidence. *Pain Practice* 8, 385–93.
2. Orlandini, G. (2004) Pulsed percutaneous radiofrequency treatment of the Gasserian ganglion for therapy of trigeminal neuralgia: technical notes, validity of the method and selection of the patients. *Pain* 108, 297–8.
3. Haider, N., Mekasha, D., Chiravuri, S., and Wasserman, R. (2007) Pulsed radiofrequency of the median nerve under ultrasound guidance. *Pain Physician* 10, 765–70.
4. Navani, A., Mahajan, G., Kreis, P., and Fishman, S. M. (2006) A case of pulsed radiofrequency lesioning for occipital neuralgia. *Pain Med* 7, 453–6.
5. Cohen, S. P., Sireci, A., Wu, C. L., Larkin, T. M., Williams, K. A., and Hurley, R. W. (2006) Pulsed radiofrequency of the dorsal root ganglia is superior to pharmacotherapy or pulsed radiofrequency of the intercostal nerves in the treatment of chronic postsurgical thoracic pain. *Pain Physician* 9, 227–35.
6. Rhame, E. E., Levey, K. A., and Gharibo, C. G. (2009) Successful treatment of refractory pudendal neuralgia with pulsed radiofrequency. *Pain Physician* 12, 633–8.
7. Mitra, R., Zeighami, A., and Mackey, S. (2007) Pulsed radiofrequency for the treatment of chronic ilioinguinal neuropathy. *Hernia* 11, 369–71.
8. Rozen, D., and Ahn, J. (2006) Pulsed radiofrequency for the treatment of ilioinguinal neuralgia after inguinal herniorrhaphy. *Mt Sinai J Med* 73, 716–8.
9. Shah, R. V., and Racz, G. B. (2003) Pulsed mode radiofrequency lesioning to treat chronic post-tonsillectomy pain (secondary glossopharyngeal neuralgia). *Pain Pract* 3, 232–7.
10. Tamimi, M. A., McCeney, M. H., and Krutsch, J. (2009) A case series of pulsed radiofrequency treatment of myofascial trigger points and scar neuromas. *Pain Med* 10, 1140–3.
11. Sluijter, M. E., Teixeira, A., Serra, V., Balogh, S., and Schianchi, P. (2008) Intra-articular application of pulsed radiofrequency for arthrogenic pain – report of six cases. *Pain Pract* 8, 57–61.
12. Rohof, O. J. (2002) Radiofrequency treatment of peripheral nerves. *Pain Pract* 2, 257–60.
13. Shah, R. V., and Racz, G. B. (2003) Pulsed mode radiofrequency lesioning of the suprascapular nerve for the treatment of chronic shoulder pain. *Pain Physician* 6, 503–6.
14. Liliang, P. C., Lu, K., Liang, C. L., Tsai, Y. D., Hsieh, C. H., and Chen, H. J. (2009) Pulsed radiofrequency lesioning of the suprascapular nerve for chronic shoulder pain: a preliminary report. *Pain Med* 10, 70–5.
15. Kane, T. P., Rogers, P., Hazelgrove, J., Wimsey, S., and Harper, G. D. (2008) Pulsed radiofrequency applied to the suprascapular nerve in painful cuff tear arthropathy. *J Shoulder Elbow Surg* 17, 436–40.
16. Wu, H., and Groner, J. (2007) Pulsed radiofrequency treatment of articular branches of the obturator and femoral nerves for management of hip joint pain. *Pain Pract* 7, 341–4.
17. Teixeira, A., and Sluijter, M. E. (2006) Intradiscal high-voltage, long-duration pulsed radiofrequency for discogenic pain: a preliminary report. *Pain Med* 7, 424–8.
18. Vallejo, R., Benyamin, R. M., Kramer, J., Stanton, G., and Joseph, N. J. (2006) Pulsed radiofrequency denervation for the treatment of sacroiliac joint syndrome. *Pain Med* 7, 429–34.
19. Tekin, I., Mirzai, H., Ok, G., Erbuyun, K., and Vatansver, D. (2007) A comparison of conventional and pulsed radiofrequency denervation in the treatment of chronic facet joint pain. *Clin J Pain* 23, 524–9.
20. Kroll, H. R., Kim, D., Danic, M. J., Sankey, S. S., Gariwala, M., and Brown, M. (2008) A randomized, double-blind, prospective study comparing the efficacy of continuous versus pulsed radiofrequency in the treatment of lumbar facet syndrome. *J Clin Anesth* 20, 534–7.
21. Simopoulos, T. T., Kraemer, J., Nagda, J. V., Aner, M., and Bajwa, Z. H. (2008) Response to pulsed and continuous radiofrequency lesioning of the dorsal root ganglion and segmental nerves in patients with chronic lumbar radicular pain. *Pain Physician* 11, 137–44.
22. Van Zundert, J., Patijn, J., Kessels, A., Lame, I., van Suijlekom, H., and van Kleef, M. (2007) Pulsed radiofrequency adjacent to the cervical dorsal root ganglion in chronic cervical radicular pain: a double blind sham controlled randomized clinical trial. *Pain* 127, 173–82.
23. Ozsoylar, O., Akcali, D., Cizmeci, P., Babacan, A., Cahana, A., and Bolay, H. (2008) Percutaneous pulsed radiofrequency reduces mechanical allodynia in a neuropathic pain model. *Anesth Analg* 107, 1406–11.
24. Aksu, R., Ugur, F., Bicer, C., Menku, A., Guler, G., Madenoglu, H., Canpolat, D. G.,

- and Boyaci, A. (2010) The efficiency of pulsed radiofrequency application on L5 and L6 dorsal roots in rabbits developing neuropathic pain. *Reg Anesth Pain Med* 35, 11–5.
25. Hagiwara, S., Iwasaka, H., Takeshima, N., and Noguchi, T. (2009) Mechanisms of analgesic action of pulsed radiofrequency on adjuvant-induced pain in the rat: roles of descending adrenergic and serotonergic systems. *Eur J Pain* 13, 249–52.
  26. Perret, D. M., Kim, D.-S., Li, K.-W., Sinavsky, K., Newcomb, R. L., Miller, J. M., and Luo, Z. D. (2011) Application of Pulsed Radiofrequency Currents to Rat Dorsal Root Ganglia Modulates Nerve Injury-Induced Tactile Allodynia. *Anesthesia & Analgesia* 113, 610–16.
  27. Sluijter, M. E., Cosman, E. R., Rittman, W. B., and van Kleef, M. (1998) The effects of pulsed radiofrequency fields applied to the dorsal root ganglion. A preliminary report. *Pain Clin* 11, 109–17.
  28. Hildebrandt, J. (2001) Relevance of nerve blocks in treating and diagnosing low back pain – is the quality decisive?. *Schmerz* 15, 474–83.
  29. Erdine, S., Bilir, A., Cosman, E. R., and Cosman, E. R., Jr. (2009) Ultrastructural changes in axons following exposure to pulsed radiofrequency fields. *Pain Pract* 9, 407–17.
  30. Higuchi, Y., Nashold, B. S., Jr., Sluijter, M., Cosman, E., and Pearlstein, R. D. (2002) Exposure of the dorsal root ganglion in rats to pulsed radiofrequency currents activates dorsal horn lamina I and II neurons. *Neurosurgery* 50, 850–5; discussion 6.
  31. Van Zundert, J., de Louw, A. J., Joosten, E. A., Kessels, A. G., Honig, W., Dederen, P. J., Veening, J. G., Vles, J. S., and van Kleef, M. (2005) Pulsed and continuous radiofrequency current adjacent to the cervical dorsal root ganglion of the rat induces late cellular activity in the dorsal horn. *Anesthesiology* 102, 125–31.
  32. Podhajsky, R. J., Sekiguchi, Y., Kikuchi, S., and Myers, R. R. (2005) The histologic effects of pulsed and continuous radiofrequency lesions at 42 degrees C to rat dorsal root ganglion and sciatic nerve. *Spine (Phila Pa 1976)* 30, 1008–13.
  33. Hamann, W., Abou-Sherif, S., Thompson, S., and Hall, S. (2006) Pulsed radiofrequency applied to dorsal root ganglia causes a selective increase in ATF3 in small neurons. *Eur J Pain* 10, 171–6.
  34. Chung, J. M., Kim, H. K., and Chung, K. (2004) Segmental spinal nerve ligation model of neuropathic pain. *Methods Mol Med* 99, 35–45.
  35. Higuera, E. S., and Luo, Z. D. (2004) A rat pain model of vincristine-induced neuropathy. *Methods Mol Med* 99, 91–8.
  36. Allen, J. W., and Yaksh, T. L. (2004) Assessment of acute thermal nociception in laboratory animals, in *Pain Research: Methods and Protocols* (Luo, Z. D., Ed.), pp 11–23, Humana Press Inc., Totowa.
  37. Kim, S. H., and Chung, J. M. (1992) An experimental model for peripheral neuropathy produced by segmental spinal nerve ligation in the rat. *Pain* 50, 355–63.
  38. Luo, Z. D., Chaplan, S. R., Higuera, E. S., Sorkin, L. S., Stauderman, K. A., Williams, M. E., and Yaksh, T. L. (2001) Upregulation of dorsal root ganglion (alpha)2(delta) calcium channel subunit and its correlation with allodynia in spinal nerve-injured rats. *J Neurosci* 21, 1868–75.
  39. Wang, R., Guo, W., Ossipov, M. H., Vanderah, T. W., Porreca, F., and Lai, J. (2003) Glial cell line-derived neurotrophic factor normalizes neurochemical changes in injured dorsal root ganglion neurons and prevents the expression of experimental neuropathic pain. *Neuroscience* 121, 815–24.
  40. Takeda, K., Sawamura, S., Tamai, H., Sekiyama, H., and Hanaoka, K. (2005) Role for cyclooxygenase 2 in the development and maintenance of neuropathic pain and spinal glial activation. *Anesthesiology* 103, 837–44.
  41. Chaplan, S. R., Bach, F. W., Pogrel, J. W., Chung, J. M., and Yaksh, T. L. (1994) Quantitative assessment of tactile allodynia in the rat paw. *Journal of Neuroscience Methods* 53, 55–63.

# INDEX

## A

- After-hyperpolarization (AHP) .....87
- Animal models ..... 1, 4, 5, 99, 109, 110, 122, 154,  
172, 213, 224, 225, 237, 239, 240, 282
- Avulsion spinal cord injury .....172

## C

- Capacitance .....69–71, 86
- CCI. *See* Chronic constriction injury (CCI)
- Central sensitization ..... 110, 233
- Chronic constriction injury (CCI).....160–163
- Clinical pain management.....4
- Cold allodynia .....209
- Complex traits .....38–39
- Conditional reward..... 160, 162, 166–167
- Copy number variation (CNV) .....15
- Culture of isolated sensory neurons .....78–82
- Current
  - Ca<sup>2+</sup> .....76–77, 85–86, 88, 93, 94
  - Ca<sup>2+</sup>-modulated K<sup>+</sup> .....85
  - current-clamp .....66, 69–71
  - evoked..... 83, 91, 93
  - fast. ....83, 84, 93
  - high-threshold activating.....85
  - inactivation .....83–86
  - K<sup>+</sup>.....71, 76–78, 84–86, 93, 94
  - low threshold activating .....85
  - Na<sup>+</sup> ..... 71, 76–77, 82–86,  
90, 92, 93
  - persistent ..... 82–85, 93, 94
  - rectifier .....84–85, 93
  - reversal potential..... 83, 94
  - separation .....84
  - slow.....83–84, 93
  - tail.....83, 94
  - threshold..... 82, 83, 85, 87
  - transient..... 84, 93, 94
  - TTX resistant ..... 82–84, 92, 93
  - TTX sensitive.....82–84
  - voltage-gated ..... 76–77, 82–86,  
88, 92–94
- Cutaneous allodynia ..... 110, 116

## D

- Degenerative joint disease .....239
- Dorsal root ganglia ..... 3, 78–79, 232
- Dural cannula .....115
- Dural inflammation.....119

## E

- Electrode capacitance transients .....69, 71
- Electrode placement .....69
- Electrophysiology .....4, 138
- Evoked nociceptive behavior .....160
- Extracranial allodynia .....110

## F

- Facial cancer model ..... 150, 151, 154–156
- Feeding disorder .....150
- First-dimension gel electrophoresis .....52
- FlashDixon .....115
- Fractionation of synaptosome-associated  
proteins .....51

## G

- Gene polymorphisms .....9
- Genetic variants.....2
- Genetically modified mice.....5
- Genome-wide association study .....10–30
- Genotype.....41, 253
- Genotype-phenotype associations .....2
- Gigaseal .....69, 71
- Global gene expression analysis ..... 13–14, 30–38
- Grip strength .....240–242,  
244–247

## H

- Headache.....4, 109–119
- Hematoxylin and eosin (H&E) staining ..... 154, 155,  
217, 225, 227, 234–235, 253, 264
- High threshold ..... 82, 85, 93, 143
- High-throughput..... 2, 4, 12, 14, 39
- Hindpaw mechanical allodynia ..... 176, 178, 180, 181
- Horizontal slices .....66

Human genetic variation .....10  
 Human genomic DNA..... 15, 20, 41  
 Hydraulic extrusion .....66, 68

**I**

Individualized pain medications.....2  
 Inflammatory arthritis.....250  
 Infraorbital nerve.....160–163  
 In-gel digestion of protein.....55–56  
 Input resistance.....86  
 Intra-articular injection .....241, 242, 246  
 Intracellular recording .....65, 82  
 Intrinsic membrane properties.....65  
 Ionic currents.....66, 75  
 Isolated sensory neurons.....4, 74, 78–86

**L**

Laminectomy.....66, 68, 70, 78, 175–177,  
 186–192, 198–199  
 Longitudinal cutting.....66  
 Low threshold .....82, 83, 85, 94, 101,  
 104–105, 143  
 Lumbosacral ventral root avulsion injury.....185–192

**M**

Mass spectrometry.....3, 48, 50  
 Mechanical allodynia.....100, 104–106, 150,  
 164–165, 172, 176, 178, 180, 181, 185–187, 190,  
 209, 210, 212, 215, 218, 219, 250, 266–267  
 Mechanical hyperalgesia.....209, 241–245, 265–266  
 Membrane capacitance.....69, 86  
 Meninges.....99, 100, 110, 125  
 Microarray.....10  
 Migraine.....2, 99, 109, 110  
 Motor assessment.....174, 178

**N**

Neuronal excitability.....74, 87  
 Neurons  
     C1/C2 .....141–146  
     cultured.....4, 81  
     dissociated .....73, 75, 81  
     dorsal horn.....48, 65  
     dorsal root ganglia (DRG).....78–79, 88, 94  
     healthy.....71, 90  
     isolated.....4, 73–96  
     large diameter .....82, 95  
     nociceptive.....138, 210  
     nociceptive specific .....138  
     nucleus caudalis .....100, 128  
     primary .....48, 73–96  
     sensory.....3–5, 73–96  
     small diameter .....82, 88

substantia gelatinosa .....65  
 superficial lamina.....69  
 trigeminal ganglia (TG) .....78, 79, 128  
 unhealthy.....71  
 Vi/Vc.....141–146  
 wide dynamic range.....138

**O**

Osteoarthritis .....239–248

**P**

Pain  
     above-level.....202  
     arthritis.....4, 259  
     articular.....275  
     at-level.....181, 202  
     below-level.....172  
     bone cancer .....4, 261–272  
     cancer.....2, 4, 160, 166  
     discogenic .....275  
     facet joint.....275  
     facial cancer .....4, 149–156  
     genetic mechanisms of.....10  
     headache-related.....4, 109–119  
     inflammatory .....3, 4, 10, 133, 134, 160, 250, 259  
     intractable .....223, 224, 261  
     joint .....134, 249–259, 275  
     neuropathic.....1, 3, 4, 47–62, 121, 160,  
         171–182, 185–192, 205–212, 220, 275–282  
     orofacial .....4, 159–168  
     orofacial deep.....134  
     osteoarthritis.....239–248  
     pancreatic.....223–225  
     parotid .....134  
     peripheral ischemic.....213  
     peripheral nerve injury.....3, 4, 185, 275–282  
     persistent .....259  
     radicular.....275  
     somatic.....224  
     thrombus-induced ischemic.....219  
     visceral .....4, 134, 223–225, 227, 237  
 Pancreatitis .....223–237  
 Parasagittal slices .....66  
 Parotid gland distension .....133–147  
 Parotid gland inflammation.....134, 139, 140, 142  
 Parotitis model .....134, 135, 139  
 Paw withdrawal thresholds.....115, 200, 201, 281  
 Peptide mass fingerprinting.....50  
 Peptide purification .....50, 56–57  
 Perforated patch recording .....77–78, 88, 95, 96  
 Perfusion systems.....74–76, 90  
 Peri-oral sensitivity assessment.....123  
 Peripheral neuralgias.....275  
 Phenotype .....2, 10, 39, 41

Post-translational modifications ..... 3, 48

Potential

- action ..... 86–88, 94, 95
- hyperpolarized ..... 84, 85, 93
- membrane ..... 69, 73, 86, 87, 93–95
- pre-pulse ..... 83–86, 93, 94
- resting membrane ..... 69, 86, 93
- test ..... 83–85, 93, 94

PRF. *See* Pulsed radiofrequency (PRF)

Primary afferent ..... 5, 110, 147, 185, 186

Proteomics ..... 3

Protocol

- activation ..... 84
- inactivation ..... 83–86
- input resistance ..... 86
- steady-state inactivation ..... 83, 85
- time locked ..... 86–88, 94
- voltage ..... 84, 85

PsychoFit ..... 101, 102, 104

Pulsed radiofrequency (PRF)

- current ..... 275–282
- probe ..... 277, 279, 280, 282

**R**

Recording chambers ..... 75–76

Rheobase ..... 87, 95

Rheumatoid arthritis ..... 10, 249, 250

Run-down ..... 88

**S**

Salivary gland ..... 133, 134

Second dimension gel electrophoresis ..... 49, 52, 53, 62

Secondary heat hyperalgesia ..... 209

Series resistance ..... 70, 71, 91

Serum transfer arthritis ..... 249–259

Single nucleotide polymorphism (SNP) ..... 2, 10

Size fractionation ..... 47

SNL. *See* Spinal nerve ligation (SNL)

SNP. *See* Single nucleotide polymorphism (SNP)

Somatosensation ..... 74

Spared nerve injury (SNI) model ..... 205–212

Spinal cord contusion injury model ..... 195–202

Spinal cord injury ..... 47, 171, 172, 176

Spinal dorsal horn ..... 48, 65, 66, 206, 276

Spinal nerve ligation (SNL) ..... 277–279

Spontaneous nociceptive behavior ..... 160

Square pulse ..... 88, 95

Superficial laminae ..... 141, 272

Supradural catheterization ..... 100

Supradural injection ..... 100

Suprathreshold stimulation ..... 87, 95

Sustained depolarization ..... 87

Synaptic interactions ..... 65

Synaptic transmission ..... 67

Synaptosomal fraction ..... 48, 51

Synaptosomal membrane fractionation ..... 48, 51

Synaptosome-associated proteins ..... 48, 51, 54

**T**

Tactile withdrawal thresholds ..... 115–117

Testing

- air puff ..... 124
- allodynia ..... 105, 123–124, 127, 164–165, 218, 277, 281
- behavioral ..... 99–104, 110, 112, 114–118, 126–127, 136–137, 145, 182, 186, 187, 190, 199–201, 226–228, 231, 237, 251–252, 255–258, 277, 280–282
- conditional reward ..... 162, 166–167
- face rubbing ..... 161
- facial allodynia ..... 99–106
- facial sensory testing ..... 114–115
- formalin ..... 160, 161, 163–164, 166
- hindpaw sensory ..... 115
- locomotor function ..... 202
- mechanically evoked withdrawal reflex ..... 161
- sensory ..... 39, 114–115, 186, 190, 192, 206, 209–211
- spontaneous eye closures ..... 161
- thermal hyperalgesia ..... 200–202

Thermal hyperalgesia ..... 150, 200–202, 214, 215, 218–219, 264–265, 280

Thrombosis ..... 213, 216–218, 220

Transverse slices ..... 66, 70

Trigeminal

- fibers ..... 110
- ganglia ..... 78, 79, 128, 129
- nerve ..... 121, 122, 126–128, 159
- neuralgia ..... 121–129
- nuclei ..... 110
- root compression ..... 122, 124–127, 129
- spinal subnucleus caudalis ..... 137
- system ..... 110, 159

Trigeminovascular system ..... 110

Two-dimensional gel electrophoresis ..... 3, 47–62

**V**

Voltage-clamp ..... 66, 69–71, 76–77, 83, 89, 93

Voltage-gated ion channels ..... 74, 84

**W**

Weight bearing ..... 240–244, 246

Whole-cell

- configuration ..... 66, 69–71
- patch-clamp recording ..... 65–71
- recording ..... 66, 68, 73–96
- voltage-clamp ..... 66

Whole-genome sampling analysis (WGSA) ..... 14